PL–TR–92–3018
Vol. 2 of 3

PL–TR–92–3018
Vol. 2 of 3

PROCEEDINGS OF THE SECOND ANNUAL ADVANCED POLYMER COMPONENTS SYMPOSIUM. VOL. II.

John J. Rusek

PHILLIPS LABORATORY
OLAC PL/RKCP
Edwards AFB CA 93523–5000

July 1992

Interim Report

PHILLIPS LABORATORY
Propulsion Directorate
AIR FORCE MATERIEL COMMAND
EDWARDS AIR FORCE BASE CA 93524–7001

NOTICE

When U.S. Government drawings, specifications, or other data are used for any purpose other than a definitely related Government procurement operation, the fact that the Government may have formulated, furnished, or in any way supplied the said drawings, specifications, or other data, is not to be regarded by implication or otherwise, or in any way licensing the holder or any other person or corporation, or conveying any rights or permission to manufacture, use or sell any patented invention that may be related thereto.

FOREWORD

The work reported in this Phase I Interim report was performed under JON: 573000R9 with the OLAC PL/RKFE Branch at the Phillips Laboratory, Edwards AFB CA 93523–5000. OLAC PL Project Manager was Dr. John J. Rusek.

The report has been reviewed and is approved for release and distribution in accordance with the distribution statement on the cover and on the SF Form 298.

John J. Rusek

DR. JOHN J. RUSEK
Project Manager

Stephen L. Rodgers

STEPHEN L. RODGERS
Chief, Emerging Technologies Branch

94-105

RANNEY G. ADAMS
Public Affairs Director

REPORT DOCUMENTATION PAGE

Form Approved
OMB No 0704-0188

1. AGENCY USE ONLY (LEAVE BLANK)	2. REPORT DATE	3. REPORT TYPE AND DATES COVERED
	July 1992	Interim

4. TITLE AND SUBTITLE
Proceedings of the Second Annual Advanced Polymer Components Symposium

5. FUNDING NUMBERS
C:
PE: 62302F
PR: 5730
TA: 00R9

6. AUTHOR(S)
John J. Rusek

7. PERFORMING ORGANIZATION NAME(S) AND ADDRESS(ES)
Phillips Laboratory
OLAC PL/RKFE
Edwards AFB CA 93523-5000

8. PERFORMING ORGANIZATION REPORT NUMBER
PL-TR-92-3018

9. SPONSORING/MONITORING AGENCY NAME(S) AND ADDRESS(ES)

10. SPONSORING/MONITORING AGENCY REPORT NUMBER

11. SUPPLEMENTARY NOTES
COSATI CODE(S):21/06; 21/08/01; 21/09/01; 21/08/02; 21/09/02; 07/05; 07/06

12a. DISTRIBUTION/AVAILABILITY STATEMENT
Distribution approved for public release; Distribution is unlimited.

12b. DISTRIBUTION CODE
A

13. ABSTRACT (MAXIMUM 200 WORDS)

Advanced propulsion concepts rely on advanced propulsion materials. The Phillips Laboratory is aggressively pursuing advanced polymeric materials for use in Solid, Liquid, and Nuclear propulsion component applications. Traditional composite materials have high specific strengths, but suffer from high cost and labor intensive processing. The APC program is currently exploring thermotropic liquid crystal polymers; these materials have high specific strength and can be economically processed by traditional high volume routes such as injection molding and blow molding. Applications envisioned for these materials include rocket nozzles, pressure cases, propellant tanks and conduits, nuclear propulsion containment, fairings, high pressure tanks and orbit-processed habitats for interplanetary voyages. These proceedings contain the papers given at the Second Annual Advanced Polymer Components Symposium, which was held at the United States Air Force Academy at Colorado Springs CO.

14. SUBJECT TERMS
Liquid Crystal Polymers; Liquid Propulsion Synchrotron Radiation; Advanced Materials; Solid Propulsion; Neutron Diffraction; Thermotropic Polyester; Nuclear Propulsion; Polyester Synthesis

15. NUMBER OF PAGES

16. PRICE CODE

17. SECURITY CLASSIFICATION OF REPORT	18. SECURITY CLASSIFICATION OF THIS PAGE	19. SECURITY CLASSIFICATION OF ABSTRACT	20. LIMITATION OF ABSTRACT
Unclassified	Unclassified	Unclassified	SAR

DISCLAIMER NOTICE

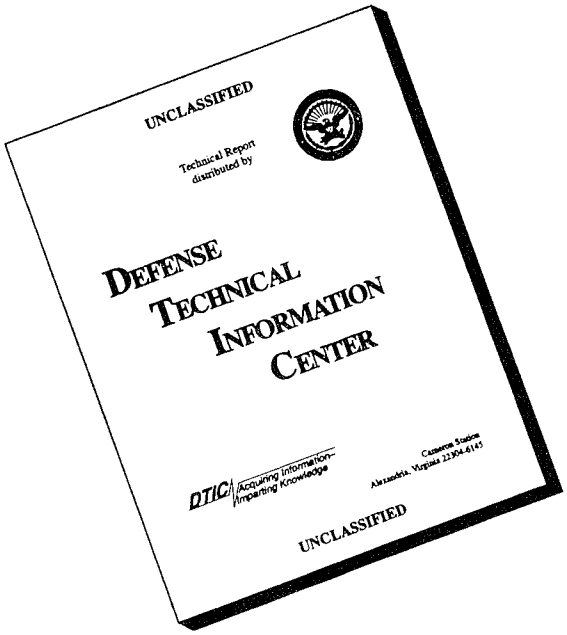

THIS DOCUMENT IS BEST QUALITY AVAILABLE. THE COPY FURNISHED TO DTIC CONTAINED A SIGNIFICANT NUMBER OF PAGES WHICH DO NOT REPRODUCE LEGIBLY.

TABLE OF CONTENTS
Volumes 1–3

Volume 1

Volume 2

Volume 3

EXAFS OF HALOGENATED LIQUID CRYSTAL POLYMERS

K.P. Chaffee, J. J. Rusek
Phillips Laboratory, Fundamental Technologies Division
Edwards AFB, CA 93524

Abstract

Extended X-ray Absorption Fine Structure (EXAFS) measurements were conducted on poly (1-Chloro-p-phenylene terephthalate) and poly (1-Bromo-p-phenylene terephthalate) in order to determine the utility of using this technique to study the 'physico-chemical annealing' phenomenon shown by thermotropic liquid crystal polymers. The reduced EXAFS spectra of the monomer and the as-synthesized polymer were compared to spectra obtained from samples that had undergone shear in the melt, and also shear followed by a thermal treatment cycle. Significant differences are evident in the absorption fine structure of the aforementioned samples. Qualitatively, the amount of 'structure' present (as shown in the transforms) peaks in the shear oriented samples. Possible chain conformations that are consistent with the data are presented.

Introduction

Commercially available thermotropic liquid crystal polymers have been shown to possess physical and chemical properties that make them attractive candidate materials for space and missile applications.[1] Also present however, is a large dependence of these properties on the microstructure and, therefore, processing parameters. A task was established as part of the Advanced Polymer Initiative to determine the feasibility of using a site specific technique, Extended X-ray Analysis Fine Structure, to study the microstructure, and microstructural changes, of an appropriate model system. In principle, EXAFS should be quite sensitive to microstructural changes.

The chi function, $\chi(k)$, which describes the single scattering EXAFS process, is given by:

$$\chi(k) = (2\pi m/h^2k^2)\Sigma_i\Sigma_a\, N_a[t_a(2k)/R_i^2]\exp[-2k^2\sigma_a{}^2-2R_i/\lambda]\sin[2kR_i+\delta_a(k)]$$

where the sum is over nearest neighbor shells i of N_a atoms of type a, located at R_i, with static and thermal disorder σ_a and backscattering amplitude t_a.[2] 'k' is the photoelectron wavenumber in inverse angstroms. It was anticipated that the disorder term would be quite large for the monomer

and as-synthesized polymer, especially for atoms in a shell that were located outside of the absorbing molecule. The net result is a greatly reduced $\chi(k)$ for a given shell (and also a different phase shift). As the sample becomes more oriented through shear and/or thermal treatments, the chi function should change accordingly. This was indeed the case.

The following paper describes the experiments and the results in the context of the goal of this task of the APC Initiative. It will conclude by recommending what further courses of action are appropriate.

Sample Preparation

The model systems chosen were based on the bromine and chlorine substituted poly (phenylene terephthalate) thermotropic polyesters. The synthesis and purification of these polymers are described in detail elsewhere in this document.[3] The Bromo-hydroquinone and chloro-hydroquinone monomers (both solids at ambient conditions) were selected as the reference compounds for the EXAFS analysis. Shear orienting of the polymer was easily accomplished by heating the as-synthesized polymer to its melting point on a hot plate and then shearing the molten polymer between glass slides (the polymer was heated and sheared in air). The polymer was subsequently removed from the glass by scraping with a razor blade. Reasonable caution was taken to not heat the polymer to degradation. After shear orienting and removal from the glass slide, some of this polymer was placed in a N_2 purged oven at 160 degrees C for 24 hours.

The Br and Cl k edge EXAFS were measured in a transmission geometry on beamlines X-19A (Cl) and X-11A (Br) at NSLS, and at E4 (Cl) and ROEMOII (Br) at HASYLAB at DESY. The Br samples were comprised of pressed pellets of the Br containing molecules mixed with medium molecular weight polyethylene glycol (PEG, approximately 3400) in a ratio to yield a pellet approximately 1 mm. thick with an absorption edge ($\Delta\mu x$) of between 1 and 1.5 (bulk densities were assumed). For example, the ratio of poly(1-bromo-p-phenylene terephthalate) to PEG was, by weight, 20 mg/54 mg. It was discovered that under approximately 1000 psi, the PEG would flow, yielding a consolidated pellet free from voids. Where necessary, the polymer powders were gently ground before mixing with the PEG in order to insure that the individual Br containing powder particles were sufficiently small (thin). The Br EXAFS measurements were made at LN_2 temperatures and ambient. A typical Br edge spectrum is shown in Figure 1.

The Cl edge measurements are inherently complicated by two factors. First, the low energy of the Cl k edge (2822 eV) makes the measurement difficult due to the relatively strong absorption of air (and all light elements), specifically Ar. At the time the experiments were conducted at X-19A, the X-19A I0 chamber suffered from an air leak; thereby introducing an Ar absorption edge into the middle ($k \cong 10.5$ inverse angstroms) of the EXAFS

region and greatly complicating analysis. Secondly, it is not possible to press pellets thin enough for transmission samples and yet thick enough to withstand handling. A pellet of the chlorine substituted polymer with an edge absorption of unity would be 85 μm thick. The first difficulty can be minimized by dropping the effective x-ray beam path through air to near zero by either good preventative maintenance on the part of the beamline PRT, or by conducting the measurements under vacuum. The latter approach was used at E4. Since the fluorescent yield for Cl is fairly small (less than 10% of the Auger dominated de-excitation events are by this mechanism), this complimentary measurement technique was not deemed feasible at the time. Therefore as a compromise, the Cl containing samples were 'sprinkled' onto a thin polyethylene sheet for transmission measurements. By doing this, one does not have great control over either the total thickness of the sample, or its uniformity. A typical Cl edge spectrum is shown in Figure 2. The remainder of the discussion will be concerned with the Br edge data.

Results and Discussion

The raw absorption spectra were reduced to the chi function in the prescribed way.[4] All data sets were treated in the same manner and normalized at the same energy (point normalization) in order to facilitate direct comparison. Most of the data shown are the result of averaging three to four raw data files. Edge shifts due to monochromator drifts eliminated files for averaging; this was not common.

Figures 3-6 display the k-weighted chi functions for the monomer, as-synthesized polymer, shear oriented polymer, and the shear oriented and thermally treated polymer respectively. Note the increased structure at high k for the shear oriented polymer. The changes in these data are readily apparent. Not only are there other frequencies (shells of atoms) entering into the data for the polymers, but the relative amplitudes and phases of the frequency components are changing as well. From the previous discussion, the latter can be attributed to either an increase in the number or type of atom in a given shell, or a decrease in the disorder term.

Figures 7-10 show the magnitude of the fast fourier transforms of the k-weighted chi functions of Figures 3-6 (note that the transforms are not phase corrected). Figure 11 is an overlay of the FFTs. Note the changes in the region of 4-10 angstroms. Figure 12 is the FFT of a simulation generated by the program FEFF version 5.05 of the Br hydroquinone monomer molecule (sungle molecule) using the atom locations as determined by the ab-initio quantum chemistry program GAMESS.[5,6] The input atom locations for the FEFF program are given in Table 1.

Table 1.
FEFF 5.05 Atom locations

atom	location	distance from Br
Br	0.0, 0.0,0.0	
C1	1.90190, 0.0,0.0	1.902
C2	2.56641,-1.24894,0.0	2.854
C2	2.61264, 1.20273,0.0	2.876
C3	4.01959, 1.19322,0.0	4.192
C4	4.68892,-0.04666,0.0	4.689
C3	3.97528,-1.24224,0.0	4.165
O	1.91179,-2.47480,0.0	3.127
O	4.66667, 2.42901,0.0	5.261
H1	5.77927,-0.06555,0.0	5.779
H2	4.50095,-2.19696,0.0	5.009
H	0.94372,-2.23248,0.0	2.424
H	2.08424, 2.15591,0.0	2.999
H	5.63800, 2.20647,0.0	6.054

A comparison of the simulation of Figure 12 with the actual data shown in Figure 7 reveals fairly reasonable agreement for the first two peaks in the transform. These are for the carbons labeled C1 and C2 respectively. However, the agreement beyond the second shell is poor.

Figure 13 shows a similar simulation, but with a second Br hydroquinone monomer located in the orientation shown near the figure. This orientation is reasonable considering the electrostatic interaction of the two molecules. The peaks in the data match the simulation in Figure 13 in location but not amplitude. The FEFF simulation calculates the thermal disorder term for each path using the correlated Debye model. The static disorder must be added by the user. The value of this term, the importance (and unimportance) of various multiple scattering pathways, and the effects of focusing (forward scattering) complicate the complete analysis.

If one may use the simulation as a starting point to speculate as to the nature of the polymer FFTs, the following conjecture may be made. As the transition is made from monomer to as-synthesized polymer, the neighboring chain is 'pushed out' from the absorbing Br. This may result in the peak at approximately four angstroms in the monomer splitting into two peaks (remember that in the monomer simulation of Figure 13, the nearest carbon atoms on the neighboring ring are 4.3 angstroms away). When the polymer is shear oriented in the melt, the chain-chain orientation changes in a complicated way, resulting in much more ordered system (hence the peaks at higher R increasing in size). After the shear oriented polymer is heated, the highly ordered microstructure relaxes, yielding a structure

somewhat midway between the as-synthesized and the shear oriented polymer in terms of static disorder. This last observation may explain the loss in anisotropy observed in SAXS data when skin samples of injection molded specimens are subjected to a similar thermal treatment.

Conclusions

The result of the series of experiments for this task of the APC Initiative is the conclusion that EXAFS is indeed very sensitive to the microstructural changes of the model thermotropic polyester. It is believed that there is a great deal of information in these data sets. However, the analysis is incomplete. Since there are differing atoms comprising a given shell (O and C in the second shell, for example), peak isolation and the related curve fitting techniques are extremely difficult, if not impossible, to complete. A sophisticated approach to modeling of the system with better control over and feeling for the static and thermal disorder terms should provide more illumination on the structure out to approximately 8-10 angstroms. A comparison of the data collected under room temperature and that of the above is in progress.

Acknowledgments

The authors wish to thank the following individuals from Case Western Reserve University and Wright Patterson AFB for their assistance at NSLS and the many helpful discussions that followed; Dr. R.W. Hoffman, Dr. J.A. Mann, Dr. C.A. Zorman, and Dr. G.A. Derose (WPAFB). Mr. Dave Cooke of PL/RKFE manufactured the rotary sample holder without which many of these measurements would not have been made.

References

1. Proceedings of the First Annual Advanced Polymer Components Symposium, John J. Rusek ed., Phillips Laboratory Propulsion Directorate, July 1992.

2. Edward A. Stern, *X-Ray Absorption: Principles, Applications, Techniques of EXAFS, SEXAFS and XANES*, D.C. Koningsberger and R. Prins eds., John Wiley & Sons, 1988.

3. J.J. Rusek and Paul Jones, "Synthesis and Thermal Analysis of Thermotropic Polyesters"

4. D.E. Sayers, *X-Ray Absorption: Principles, Applications, Techniques of EXAFS, SEXAFS and XANES*

5. J.J. Rehr, J. Mustre de Leon, S.I. Zabinsky, and R.C. Albers, "Theoretical X-ray Absorption Fine Structure Standards", Phys. Rev. B44, 4146 (1991).

6. M.W. Schmidt et. al., QCPE Bulletin, 10, 52-54 (1990).

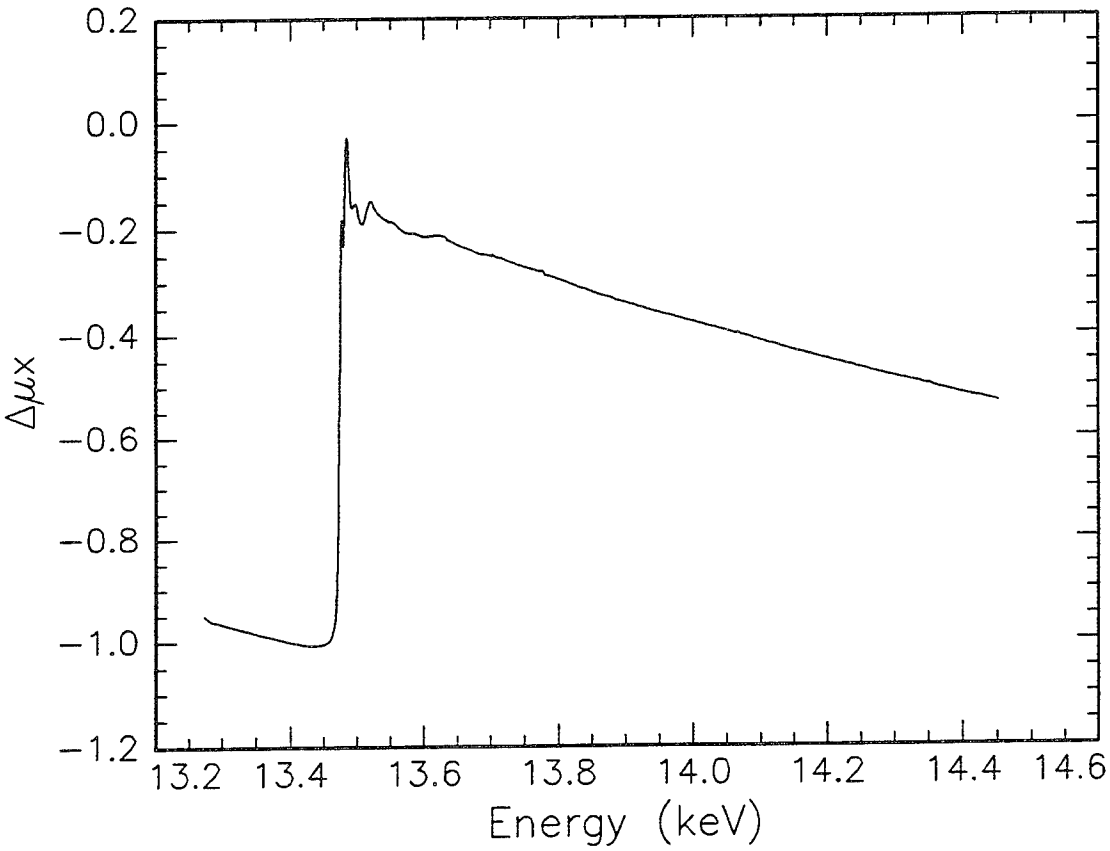

Figure 1. Typical Br edge raw data (Shear oriented polymer)

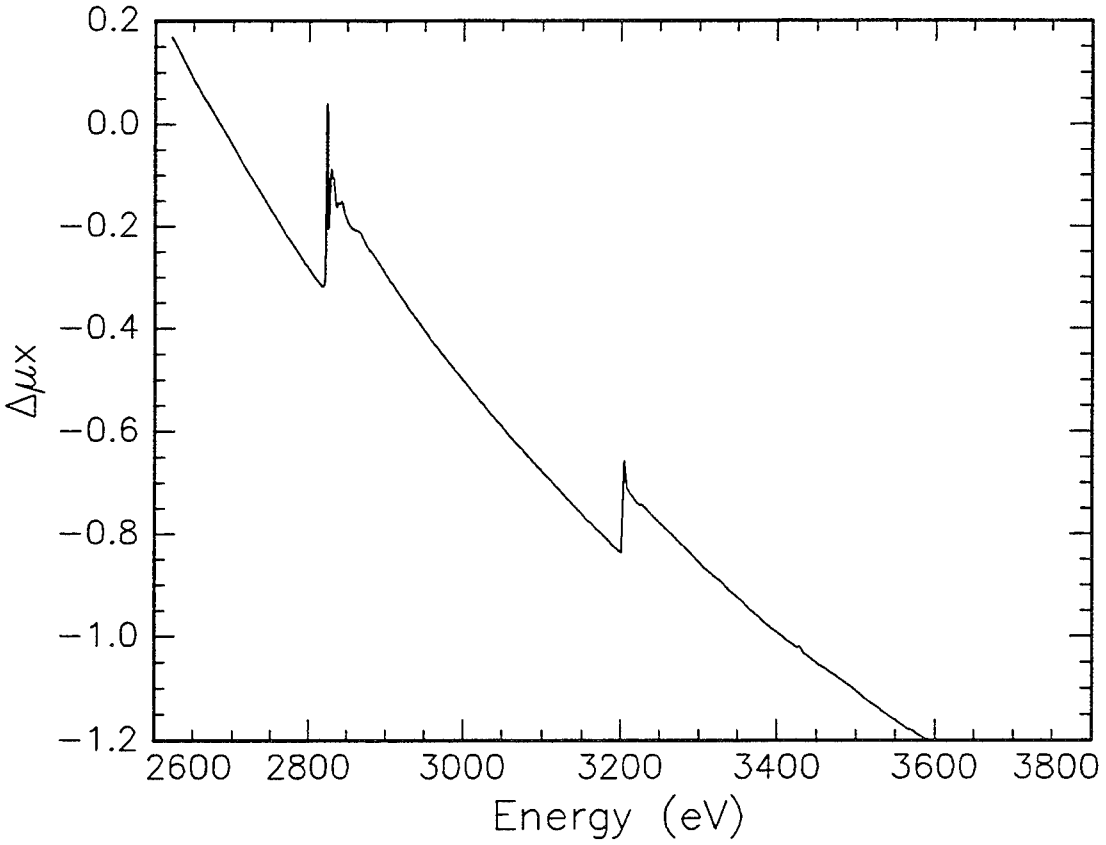

Figure 2. Typical Cl edge raw data (Cl hydroquinone monomer)

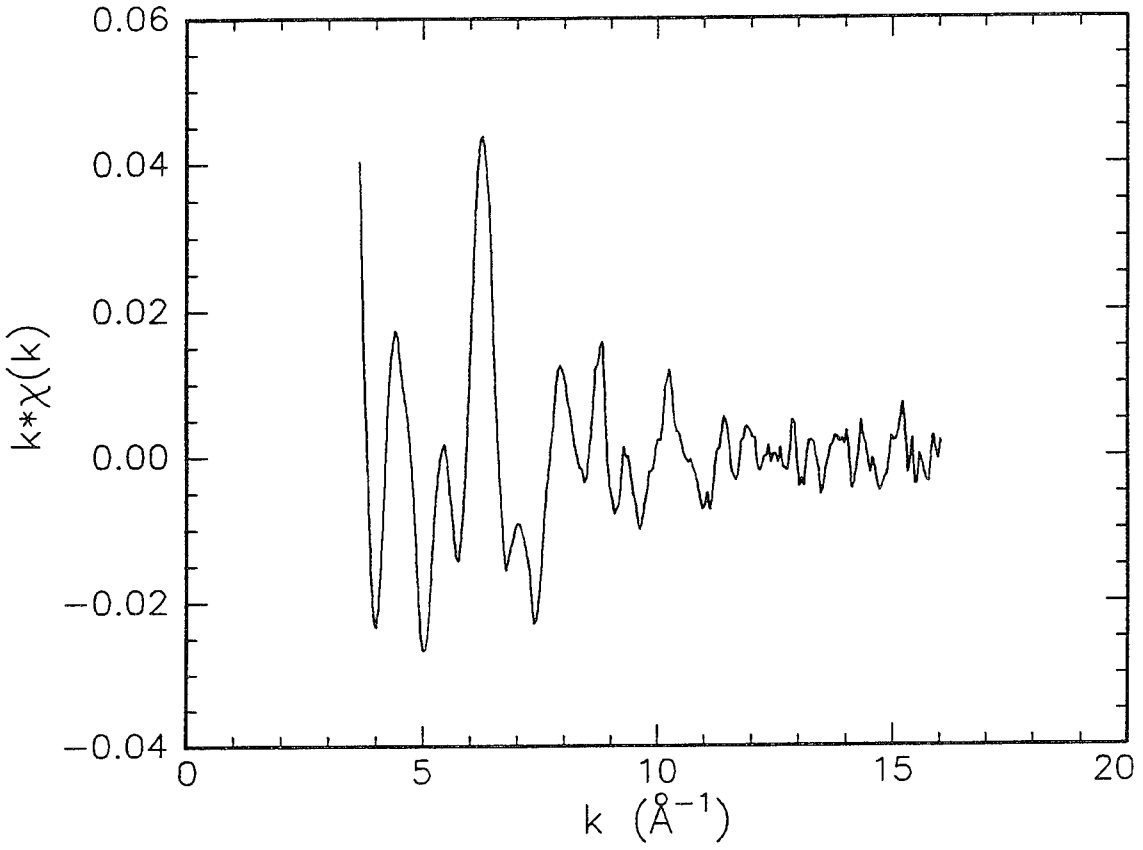

Figure 3. Br hydroquinone monomer

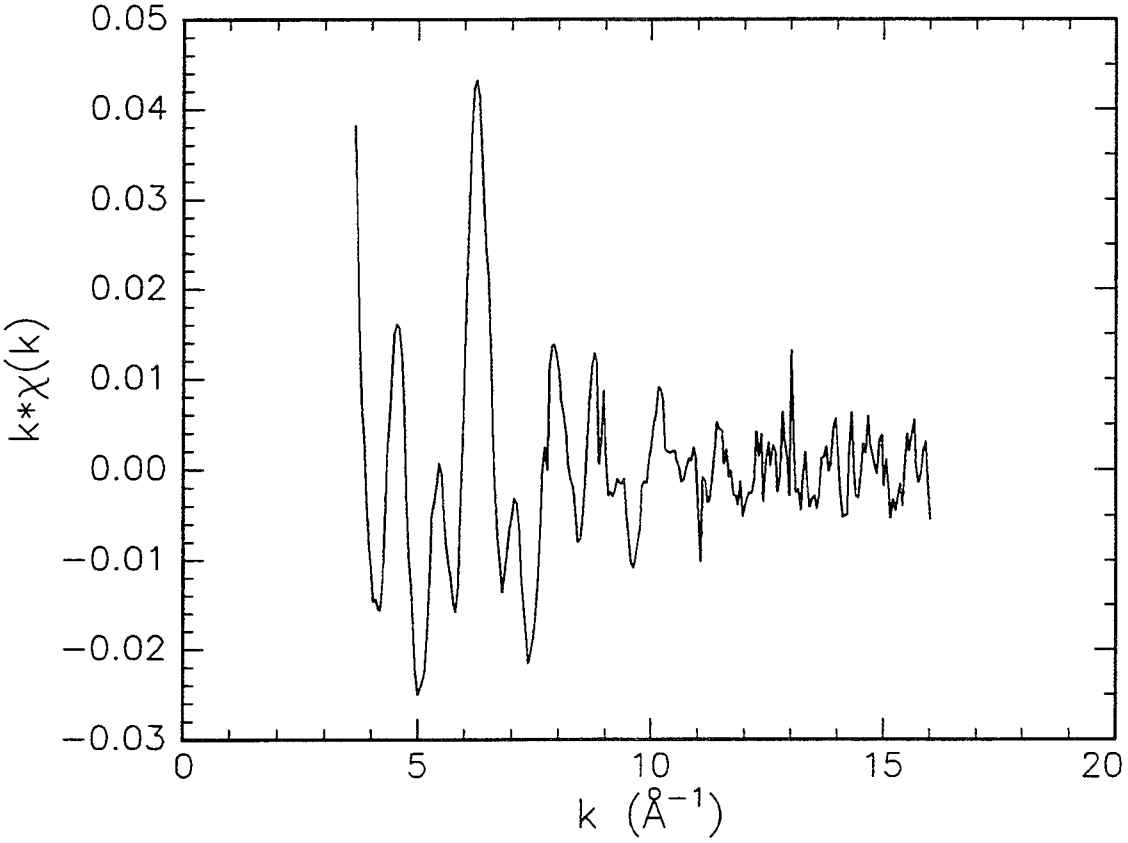

Figure 4. As−synthesized poly (1−Br−p−phenylene terephthalate)

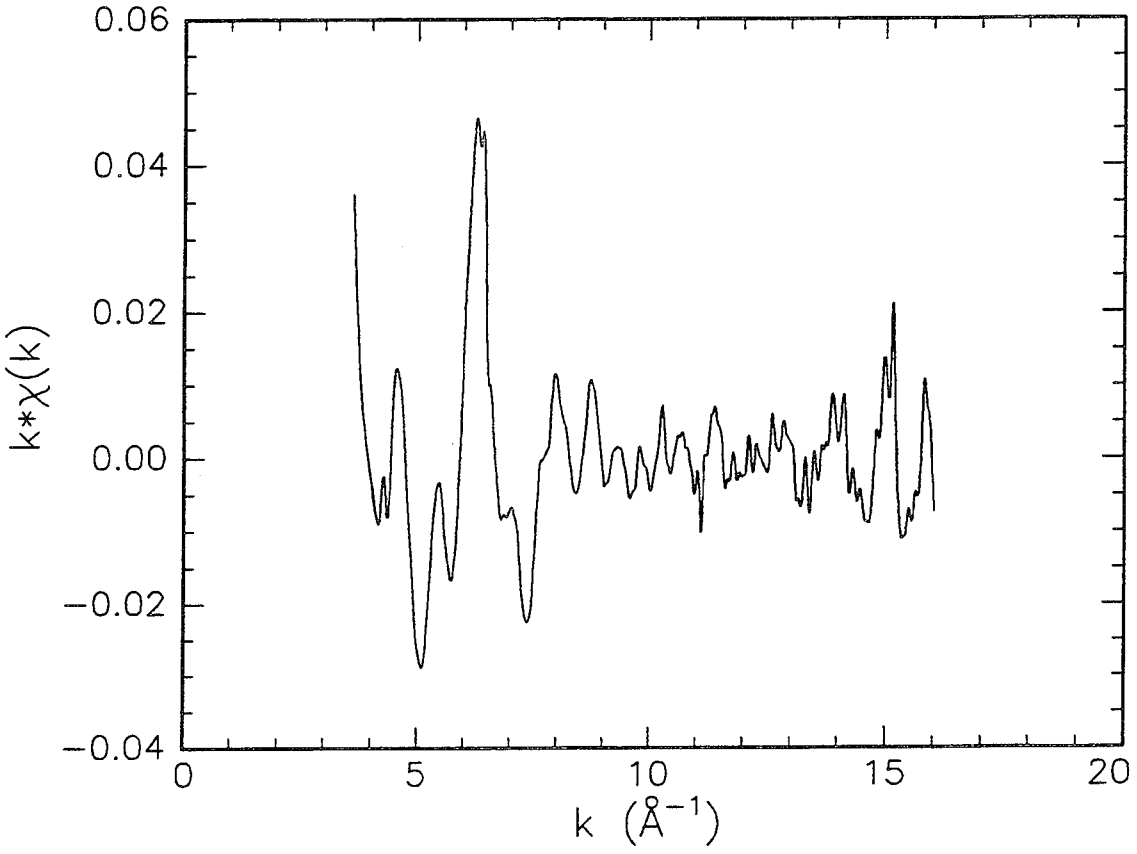

Figure 5. Shear oriented poly (1−Br−p−phenylene terephthalate)

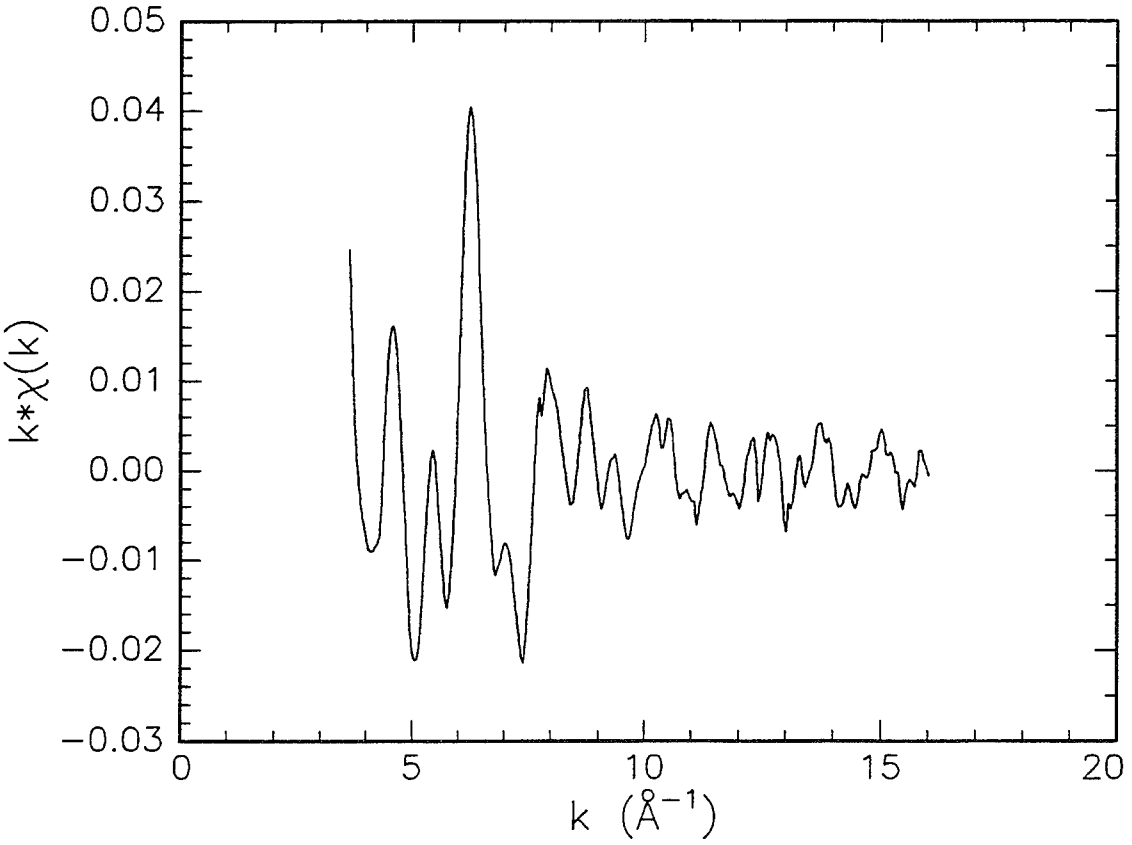

Figure 6. Shear oriented and heat treated Br substituted polymer

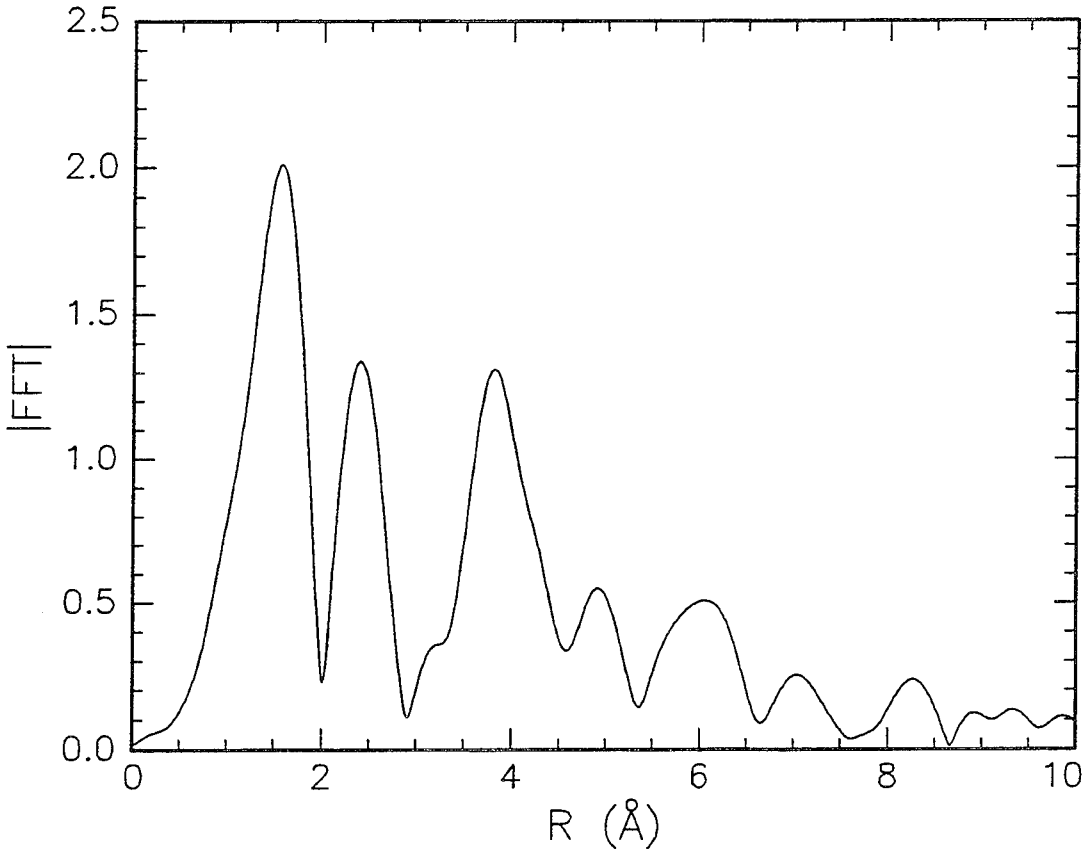

Figure 7. |FFT| of Br hydroquinone monomer

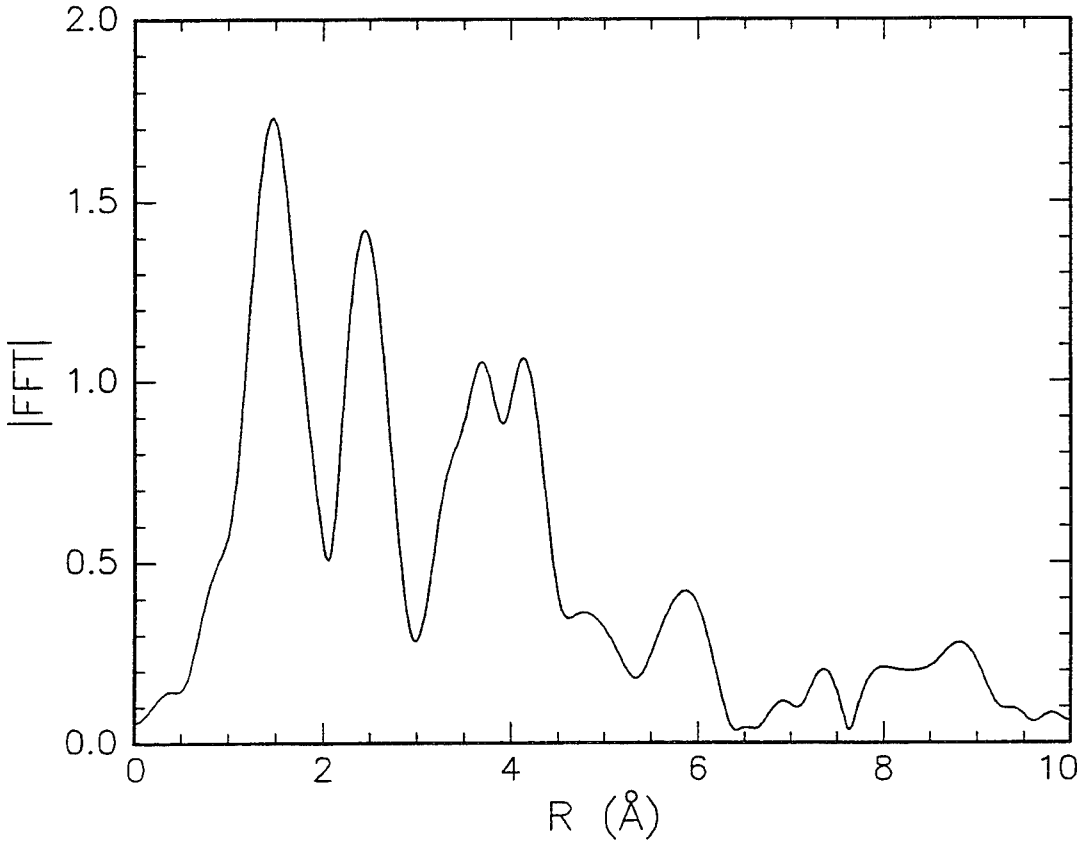

Figure 8. |FFT| of as-synthesized Br substituted polymer

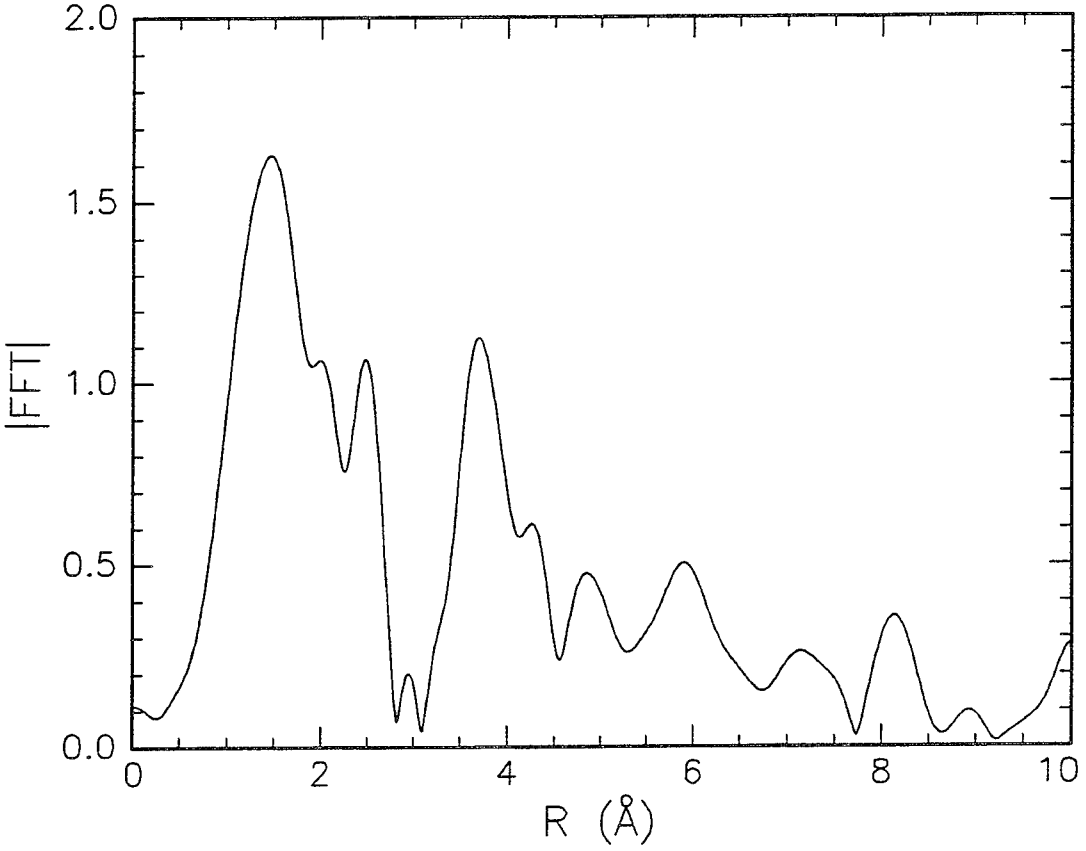

Figure 9. |FFT| of shear oriented Br substituted polymer

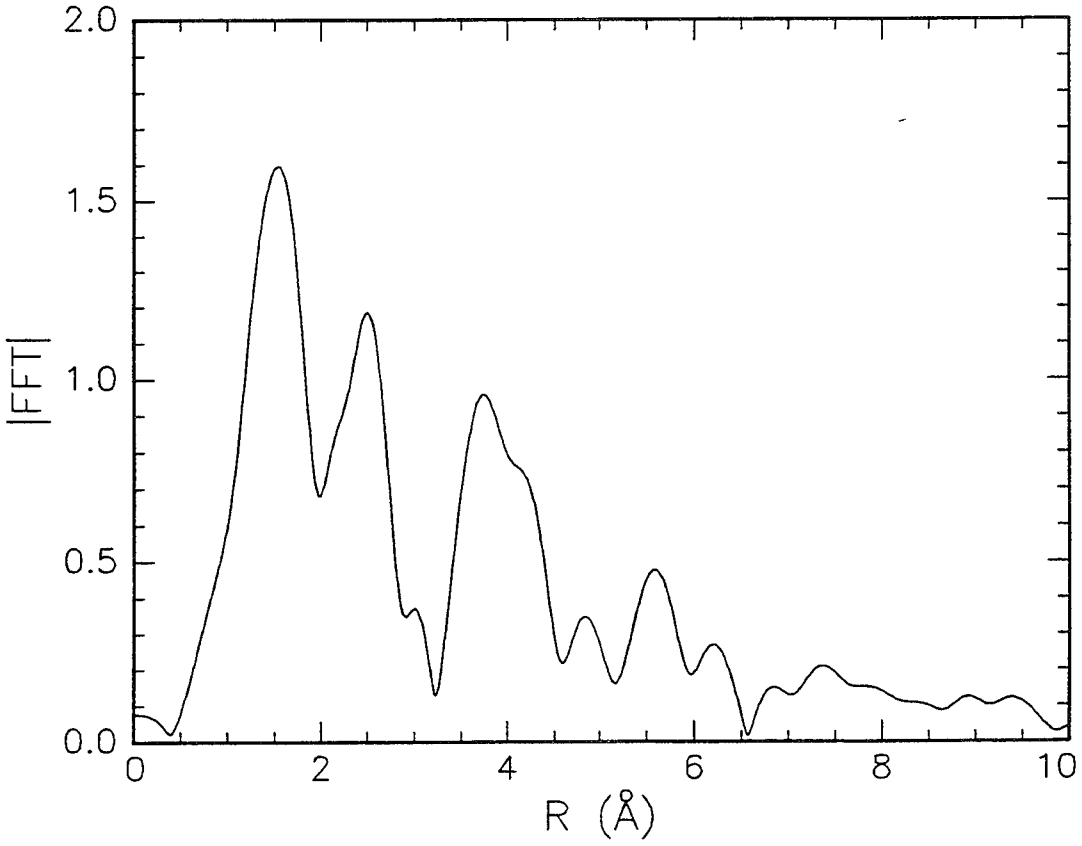

Figure 10. |FFT| of shear oriented and heat treated Br substituted polymer

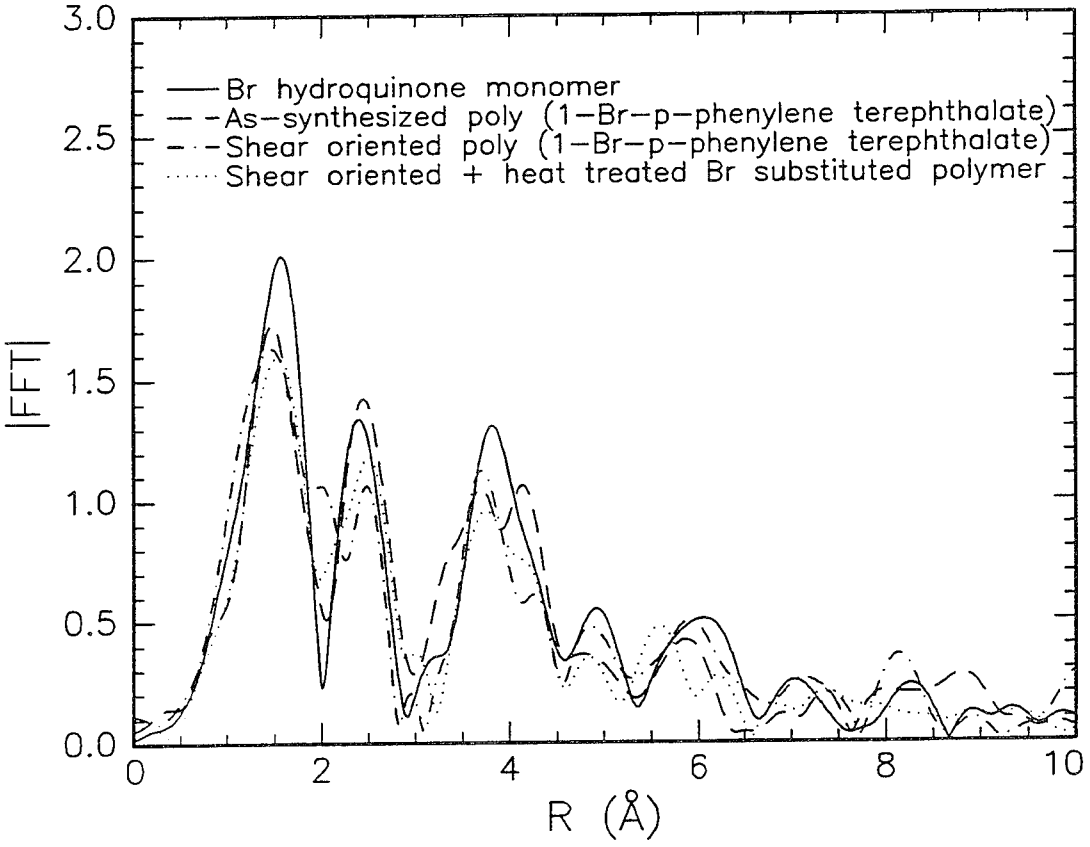

Figure 11. Overlay of |FFT|

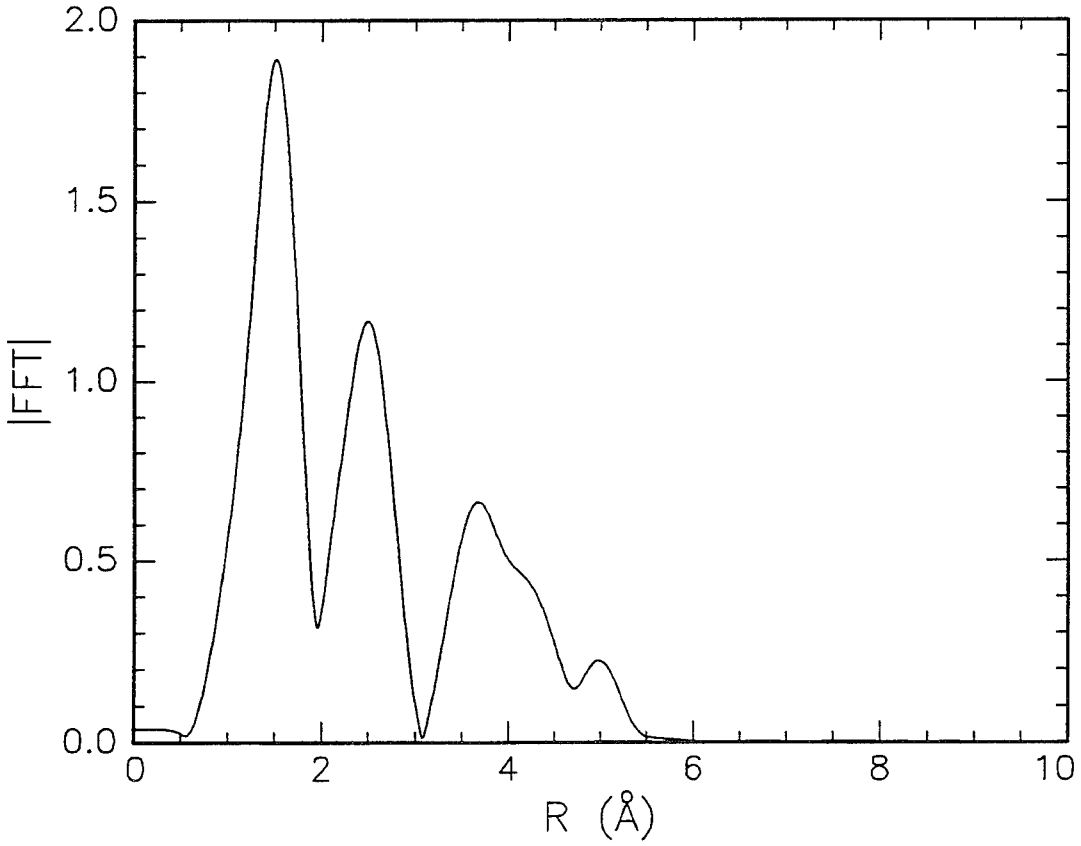

Figure 12. |FFT| of simulation generated by FEFF 5.05

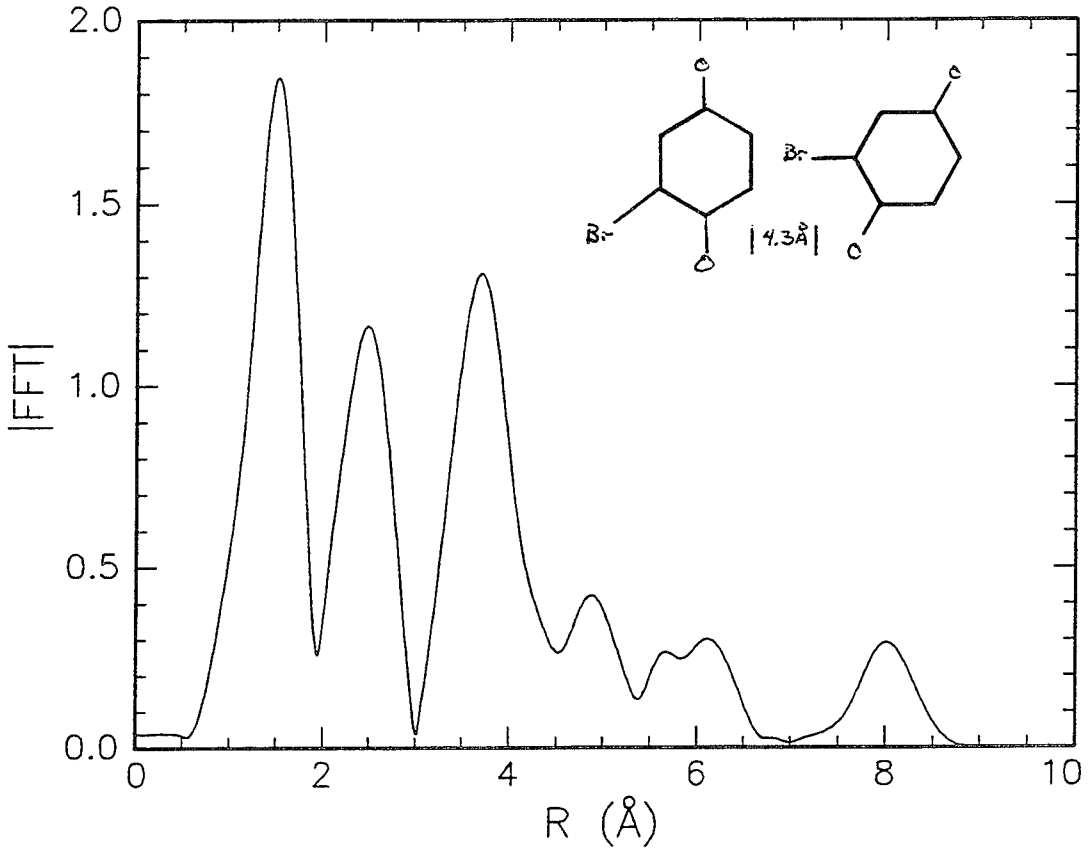

Figure 13. |FFT| of simulation of pair of Br hydroquinone monomers

DEVELOPMENT AND TESTING OF A CURVED MICA X-RAY FOCUSSING SPECTROMETER FOR EXTENDED X-RAY ABSORPTION FINE STRUCTURE STUDIES

Christian A. Zorman, Guy A. DeRose* and Richard W. Hoffman
Department of Physics
Case Western Reserve University
Cleveland, Ohio 44106

Extended x-ray absorption fine structure (EXAFS) is a spectroscopy used to determine the local structure of materials. The data may be collected in transmission or fluorescence modes, the latter requiring filters to eliminate unwanted background signals. For high Z materials the standard practice is to use an elemental filter with an atomic number (Z) one or two less than the element being probed. For low Z materials, however, few elemental filters exist, leaving the experimentalist little recourse but to collect data without a filter.

In response to this need, we have been developing and testing a curved mica x-ray focussing spectrometer which will not only focus diverging x-rays but also filter out all but the wavelength selected by the operator. This is accomplished by Bragg diffraction of the x-rays from the crystal planes of the mica. This paper will report on the background, development and testing of the spectrometer, including data collected on Beamline X-11A at the National Synchrotron Light Source at Brookhaven National Laboratory.

I. INTRODUCTION

With the advent of high intensity continuous wavelength x-ray sources like the National Synchrotron Light Source at Brookhaven National Laboratory, techniques such as extended x-ray

absorption fine structure (EXAFS) have become popular tools for researchers in many disciplines to probe the local structure of materials. Where it used to take days using x-ray tube sources, data can now be collected in minutes. Dilute as well as concentrated species can be studied. This spectroscopy yields quantitative information about the number, types and nearest neighbor distances of the atom being probed. Because x-rays cause very little if any damage to a sample, EXAFS has applications in fields ranging from materials science to biology, including polymer science and engineering.

EXAFS data can be collected in both transmission and fluorescence modes. Each requires the use of some kind of x-ray detector, the most common being the gas ionization chamber. A complete description of an EXAFS experimental setup as well as details concerning transmission EXAFS has been given by many authors, most notably Koningsberger and Prins[1]. Data collection of fluorescence EXAFS differs from that of transmission EXAFS in that filters are commonly used in fluorescence EXAFS to eliminate unwanted background noise. The two most common components of background noise are scattering of incident radiation by the sample and fluorescence radiation from other elements in the sample. Filters are chosen such that the absorption edge of the filter material is between the desired fluorescence emission line energy and the absorption edge energy of the element being probed. The desired radiation then passes through the filter while the unwanted radiation is absorbed. This is best accomplished by choosing a filter with an atomic number (Z) one less than the element under study. For elements above Ru, the filters can be either Z - 1 or Z - 2, consistent with the above energy criterion. The best filters are made of single element foils, but only if they can be made thin enough to pass

the desired radiation without too much attenuation. This works well for most elements, but poses a problem for light elements because no thin, free-standing single element foils exist. Some researchers have made filters out of a slurry of oxides, Duco[tm] cement and acetone deposited on a Mylar[tm] foil[2]. However, for some elements no such oxides are available.

II. BACKGROUND AND DEVELOPMENT

It has been known for many years that large single crystals could be used to separate different wavelengths of x-rays. This can be done by application of Bragg's Law of x-ray diffraction, which relates the wavelength of incident x-radiation to the interplanar spacing of the crystal and the angle of incidence of the incoming x-rays. Bragg's Law can be expressed in the following form:

$$n\lambda = 2d\sin(\theta)$$

where: n is the order of diffraction
λ is the wavelength of the incident x-ray
d is the spacing between crystal planes
θ is the angle of incident radiation

From Bragg's Law one can see that a crystal can be used as an wavelength discriminator, thus functioning as an x-ray filter in an EXAFS experiment. However, in such an experiment, the fluorescence x-rays emanate from the source in all directions. A flat crystal would only diffract a very small portion of the x-rays, the rest being lost because they were not incident at the appropriate angle.

In order to use a crystal as a filtering device for an EXAFS experiment, the crystal would not only have to be wavelength dispersive but would also have to be oriented such that the Bragg condition is met for fluorescence radiation emanating from the sample. The proper orientation would focus the x-rays into a detector. Wanting the same qualities but for a different purpose, Johann made a x-ray focussing, wavelength dispersive device made by curving a flat mica crystal[3]. He desired to photograph the K-α lines emanating from a copper target. Using an instrument represented schematically in Figure 1, he was able to photograph the fifth order K-α doublet. His device was based on the Rowland circle geometry, where the radius of curvature of the crystal is twice that of the focal circle. For the device to work, the source and detector must both lie on the focal circle. The device does not provide a perfectly focussed image, but it was sufficient for Johann to get a sharp photograph of the K-α doublet. Since a gas ionization chamber does not require that the incoming x-rays be sharply focussed but only to the extent that they enter the window of the detector, the Johann design can be adapted for EXAFS work. In fact Hastings et al used an adaptation of the Johann device to collect EXAFS on dilute concentrations of Fe in a Cu matrix[4]. But their design utilized a mosaic of graphite crystals held in place by an intricate and obviously somewhat costly mounting device. Others have also tried focusing divergent x-rays using Johann's design with Si and Ge crystals[5]. These devices focus well but suffer from the fact that Si and Ge are not very flexible, resulting in extremely large focal circles (diameters on the order of 100 cm). Since hutches at most synchrotrons are very space limited, these devices would not work well for routine EXAFS at most facilities. Also the mechanisms used to bend the Si and Ge crystals accurately are expensive and not easy to construct.

The Johann design with a mica crystal was selected for a number of reasons. By photographing the Cu K-α lines, Johann showed that a curved mica crystal could provide adequate focussing and filtering. Mica is readily available and its cleavage planes, oriented perpendicular to the surface normal, are good diffractors of x-rays. Most importantly, mica is highly flexible, permitting a focal circle small enough to fit in a typical EXAFS experiment. For these reasons mica is the most cost and space efficient crystal for this purpose.

Figure 2 shows schematically how the Johann design was adapted for use in fluorescence EXAFS. The crystal was curved to a radius of 20 cm, resulting in a focal radius of 10 cm. The mica was aligned so that diffraction would take place between crystal planes with a spacing of 19.96 angstroms. The position of the sample and detector along the focal circle was determined by the Bragg equation. To maximize the intensity of the radiation reaching the detector, the lowest possible order of diffraction was chosen. Due to the size of the crystal, Bragg angles less than 10 degrees were not available. To insure that only diffracted x-rays reached the detector, a Pb x-ray stop was used to eliminate line of sight between the sample and the detector. The samples were positioned in the standard fluorescence EXAFS configuration, which is 45 degrees with respect to the incident beam.

III. RESULTS AND DISCUSSION

Figures 3 and 4 show representative spectra using the Johann design. Figure 3 is an EXAFS spectrum from an Fe foil while Figure 4 is that from a Mn foil. The data were collected at

beamline X-11A at the National Synchrotron Light Source under less than normal EXAFS operating conditions. Usually the storage ring operates in a 25 electron bunch mode, but when these spectra were collected the ring was in a one bunch mode. Thus the current in the ring was reduced by about a factor of 2.5. Regardless, the x-ray intensity was sufficient to test the device by looking for edge shifts in EXAFS spectra. Such shifts would indicate that fluorescence radiation was reaching the detector by Bragg diffraction from the mica crystal. Figures 3 and 4 clearly show such shifts, although the magnitudes are relatively small. Also it is quite apparent that no analyzable EXAFS was collected using this instrument.

As is apparent from the data, this device is not ready for routine fluorescence EXAFS work. Quite possibly the low current in the storage ring led to a reduction in signal at the detector. More likely, the problem can be found with the setup. Factors limiting the amount of signal measured by the detector include the small solid angle subtended by the ionization chamber window, the position of the Pb beam stop, the accuracy at which the mica was curved and the intensity of the diffracted beam itself. Due to a lack of available ionization chambers at the beamline, the ionization chamber used in this experiment had a solid angle about 12 times less than the standard fluorescence chamber detector.

Because of the energies and angles available, the optimum order of diffraction for Fe EXAFS with this geometry was n = 8. Due to this relatively high order, the intensity of the diffracted beam is somewhat low, accounting for the diminished signal. Fortunately, this device is being developed for use with light elements like Cl, where the optimum order of diffraction would be

n = 3. Because the lowest available x-ray energy at beamline X-11A is 4.5 keV, too high for EXAFS on elements with an atomic number less than 22 (Ti), such tests with low Z samples could not be performed.

IV CONCLUSIONS AND FUTURE WORK

At this point the curved mica x-ray focussing spectrograph is not ready for low energy fluorescence EXAFS. Fluorescence radiation can be filtered and directed into a detector, however, the intensity of the detected radiation is not sufficient to extract any EXAFS information from the spectra. Detectors with larger solid angles and devices that curve the mica more accurately must be developed and tested before such a system can be routinely used.

V ACKNOWLEDGMENTS

The authors would like to thank Dr. John Rusek and Dr. Kevin Chaffee of Phillips Laboratory, Edwards AFB for their help and support on this project. This work was supported by the US Air Force Office of Scientific Research and RDL under grant number 92-99. The National Synchrotron Light Source is supported by the US Department of Energy Office of Basic Energy Sciences under contract number DE-AC02-76CH00016.

REFERENCES

1. D. C. Koningsberger and R. Prins, eds., "X-ray Absorption: Principles, Applications and Techniques of EXAFS, SEXAFS and XANES", John Wiley, New York, 1988.

2. "Fluorescent Ion Chamber Detector", **X-11A Beamline Instruction Manual**, March 1982, p. 1.

3. H. H. Johann, Z. Phys. **69**, 185 (1931).

4. J. B. Hastings, P. Eisenberger, B. Lengeler and M. L. Perlman, Physical Review Letters, **43**, 24, (1979) p. 1807.

5. P. Stephens, P. Eng and T. Tse, Rev. Sci Instru. **64**, 2 (1993) p. 374.

*Present address: Wright Laboratory, Hardened Materials Branch, WL/MLPJ, Wright-Patterson AFB, OH 45433-7702.

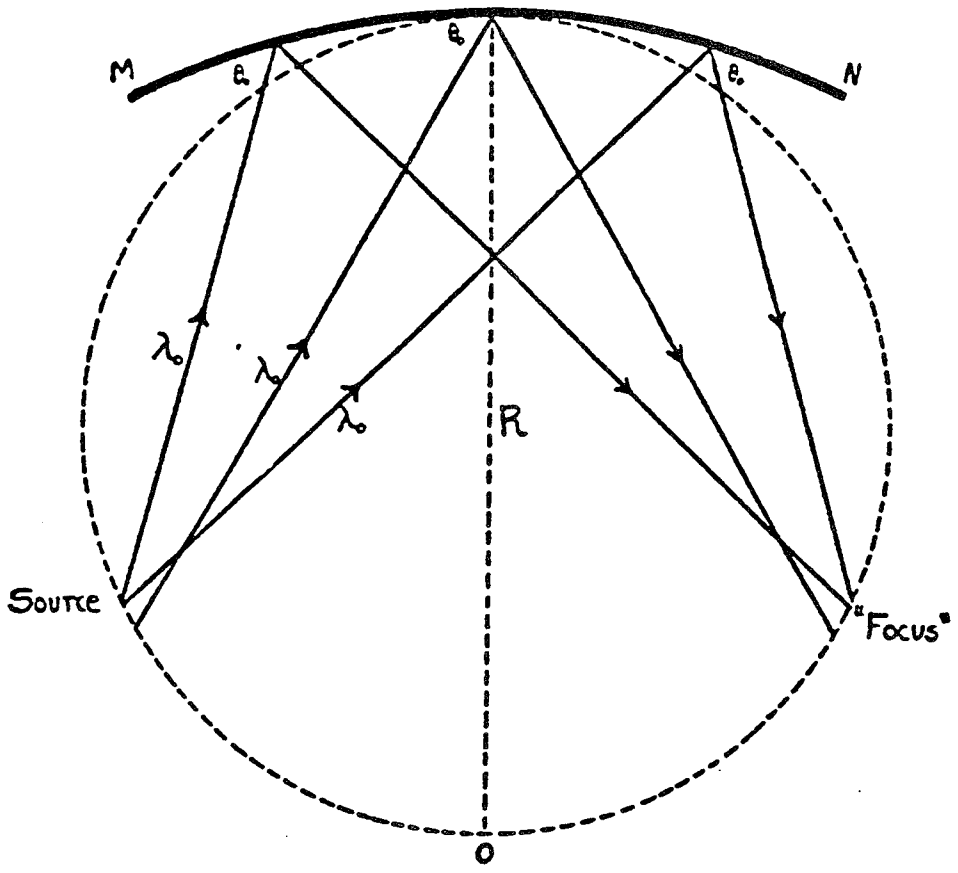

FIGURE 1. The Johann X-ray focussing design.

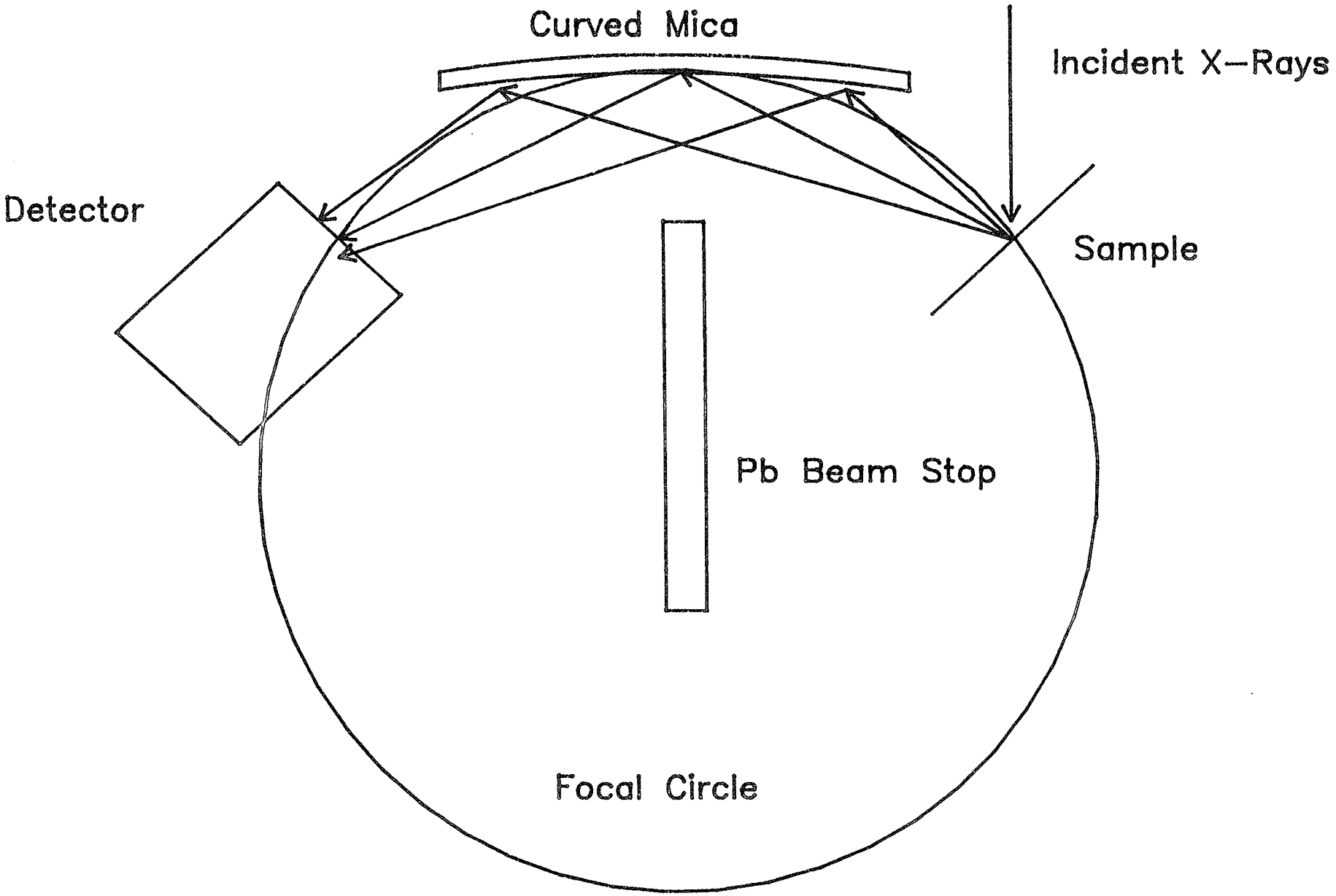

FIGURE 2. The Johann design adapted for EXAFS

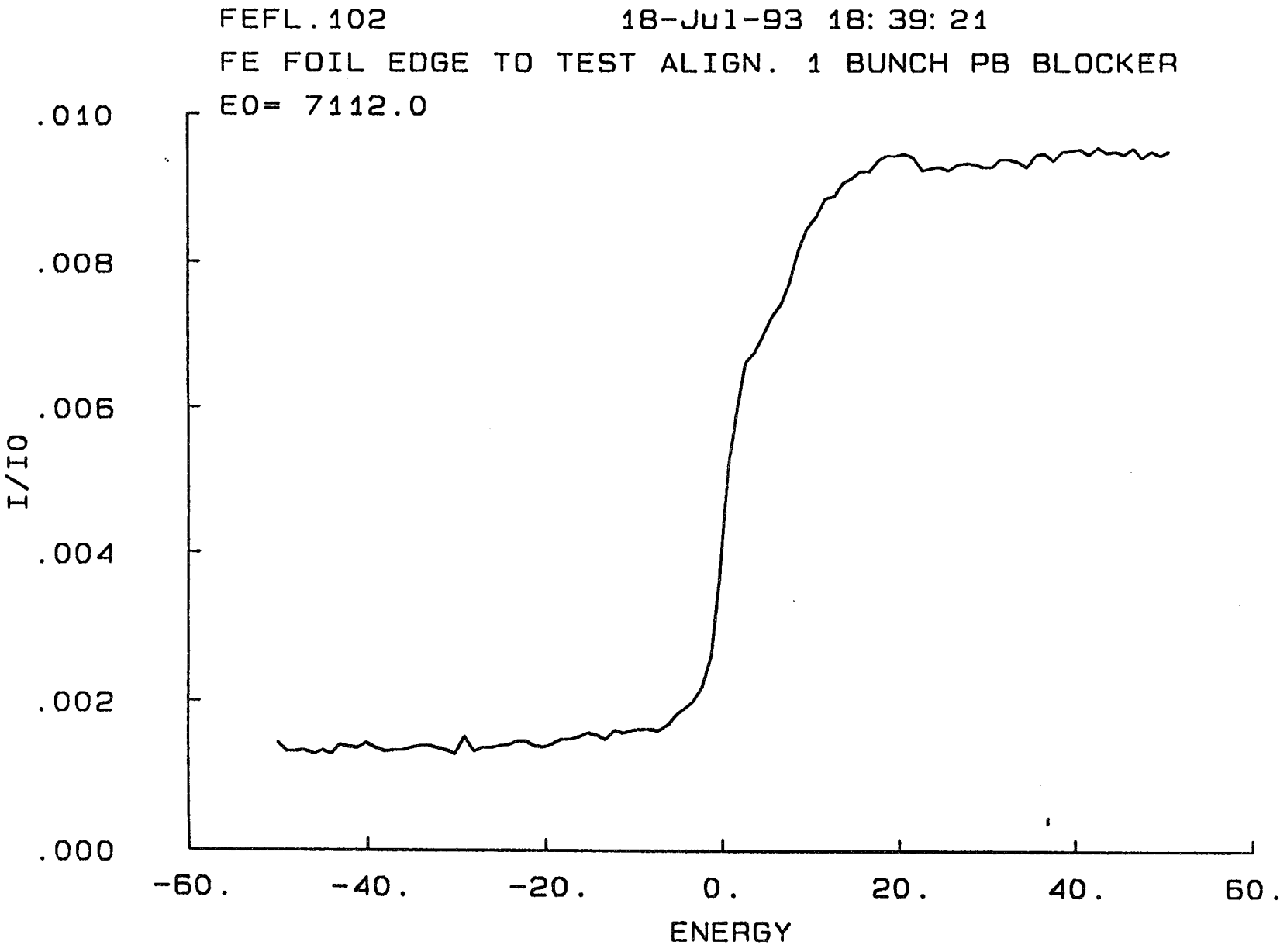

FIGURE 3. EXAFS spectrum from an Fe foil using the curved mica x-ray focusser.

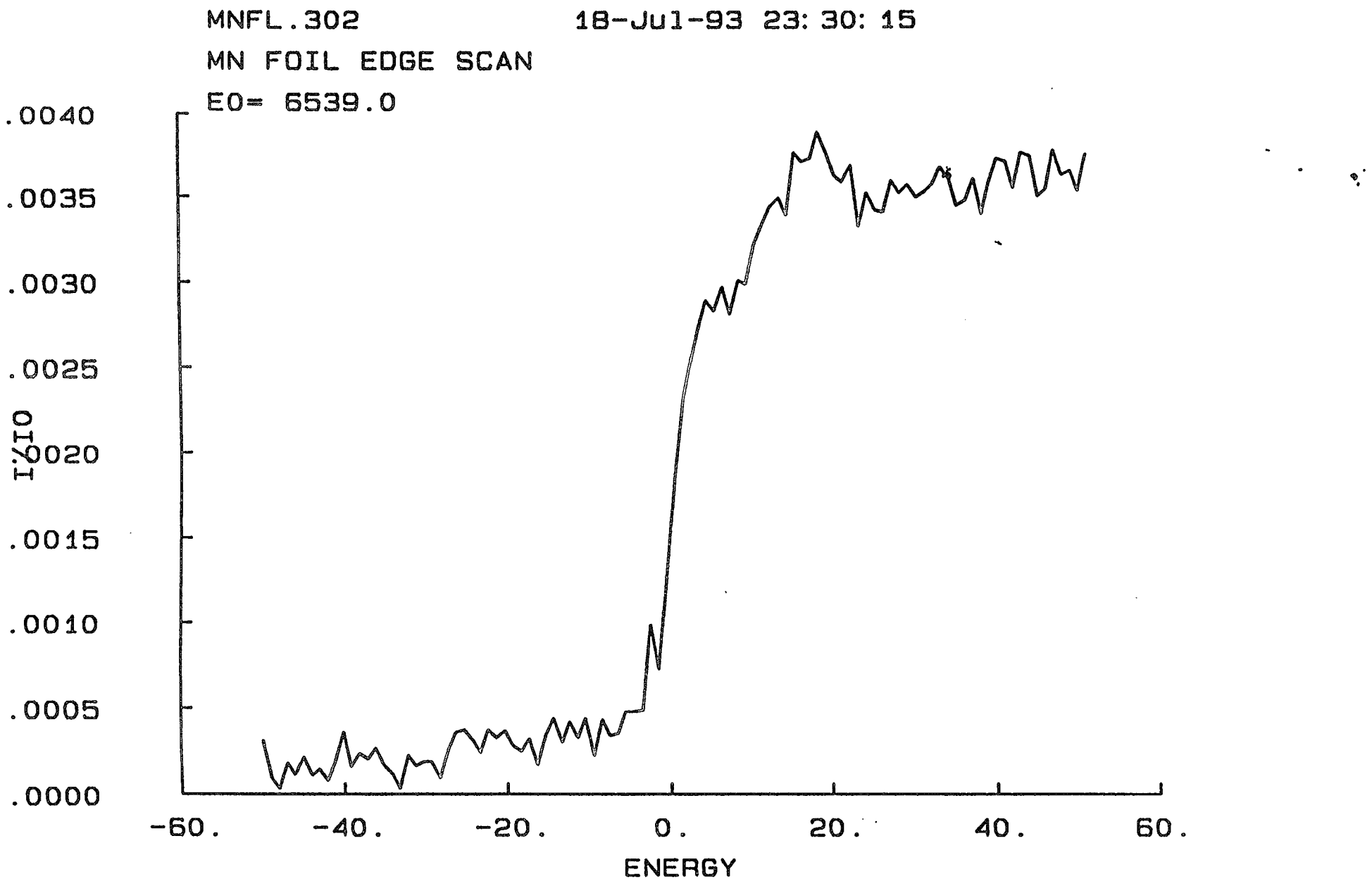

FIGURE 4. EXAFS spectrum from a Mn foil using the curved mica x-ray focusser.

Final Report

Characterization, FDEMS Sensing and In situ Process Monitoring of the Physical Changes Occurring with Time and Temperature During Cure of High Temperature Liquid Crystal Thermotropes

to

Dr. John J. Rusek
Phillips Laboratory
Bldg. 8351
OLAC PL/RKCP
Edwards, CA 93523-5000

from

David E. Kranbuehl and Brian Kipp
Chemistry and Applied Science
The College of William and Mary
Williamsburg, VA 2387-8795

June 1, 1992

Contract #FO4611-91-C-0131

Introduction

This final report on characterization, FDEMS sensing and in situ process monitoring of the physical changes occurring with time and temperature during cure of high temperature thermotropic polymers consists of 3 parts: an executive summary, a detailed report of the past 10 months' work, and a report of the initial 12 month's work dated 9/15/92. In summary, we have verified the following conclusions regarding the SYN-9 resin system prepared at the Air Force Phillips Laboratory in Edwards, California.

- This hydroquinoneterephthaloyl polyester is a thermotropic liquid crystal
- Hold cycles at 300C, 340C, and 380C created more ordering with a wider distribution of melting temperatures and a higher average melting temperature
- 380C holds for 30 minutes or longer displayed the most significant ordering
- Changes observed were physical and not chemical
- An additional pressure is required to cause a large increase in the mechanical properties
- The hydroquinoneterephthaloyl polyester can be molded under pressure in the flow state and allowed to cool to achieve a strong molded product with greatly enhanced mechanical properties.

Executive Summary

The objectives of this project were to:

- To find out whether SYN-9 is a thermotropic liquid crystal
- To determine the effects of various time/temperature hold cycles on the chemistry and morphology
- To determine which time/temperature combinations enhance mechanical properties the most
- To relate curing effects to physical or chemical processes
- To develop and demonstrate the ability of frequency dependent electromagnetic sensors (FDEMS) to monitor in situ the changes in state of the SYN type thermotropic polymer systems continuously during processing.

All of these objectives were addressed. The positive results achieved in this study should be used in future work in which FDEMS sensors and the knowledge base developed in the work are transitioned to the fabrication of prototype parts, to monitor-optimize the cure process in the fabrication mold, for on line quality verification-certification during processing and for intelligent closed loop process control.

After investigating a number of commercially available thermotropic resin systems and a variety of laboratory synthesized hydroquinoneterephthaloyl polyester resins, the project focused on the polyester resin SYN-9 shown in Figure 1. The SYN-9 resin is a compromise between the very high melting point of a non-substituted phenyl backbone with the lower easier to process softening properties of bulky side groups, Figure 2. The final months' work emphasized 4 experimental approaches to characterizing and monitoring of the cure process: differential scanning calorimetry (DSC); frequency dependent electromagnetic sensing (FDEMS) for in situ on-line sensor monitoring; fourier-transform infrared (FT-IR) and thermal mechanical analysis (TMA). See Figure 3. In addition, a high temperature polarizing microscope was used to further verify the thermotropic liquid crystal transition.

A synopsis of the differential scanning calorimetry DSC results is shown in Figures 4-9 and in Figure 10, which tabulates these results. In summary, the SYN-9 resin melts at 312°C with a heat of transition of approximately 10 J/g. Heat treatment of the resin at temperatures of 300°C or higher moves the melting temperature Tm to a higher value, see Table in Figure 10, along with Figures 4-9. Further, the melting endotherm broadens. An annealing temperature of 300°C for

4 hours and annealing temperatures of 340°C for 1 hour, the value of Tm increases to around 330°, a 20° increase. Thirty minutes at 380°C pushes the peak and broadens it to the point where it disappears. This trend is clearly seen in Figure 5. In Figure 5 the SYN-9 is ramped to 340° and held for 45 minutes 3 times. Each ramp shows a gradual increase in Tm and a broadening into multiple peaks. Figures 6, 7 and 8 show a similar effect as the SYN-9 is ramped to 380° and held for 15 minutes. On the third ramp after two 15 minute holds at 380° the Tm broadens and increases to the point where it disappears.

Figure 9 shows a multiple ramp on a representative simple liquid crystal which shows a crystal to smectic transition at 75°, scmetic to nematic at 90°, and nematic to isotropic transition at 120°. Since the isotropic transition is about 1/10 as large as the crystal to liquid crystal transition, it would be very hard to detect. We also believe it would occur at a very high temperature, perhaps over 400°. Thus to verify the presence of the liquid crystal ordered state above 315°, observations were made on a high temperature polarizing microscope stage at the University of North Carolina. The results are shown in Figure 11. A crystal nematic transition occurs at 315° and a nematic to isotropic transition occurs at 415°.

Overall, these results suggest the SYN-9 hydroquinoneterephthaloyl polyesters are a semicrystalline solid with amorphous and crystalline regions. Holding the resin above Tg, but below the nematic-isotropic transition temperature, increases ordering. Particularly in the 340° to 380° range, the ordered regions of the polymer grow into higher melting regions, higher Tm, and a greater breadth in the melting region due to variation in the ordered domains.

The FDEMS sensors were used to monitor in situ during processing in the mold the changing physical state of the SYN-9 resin under the same conditions as the DSC study. The very significant advantage of the FDEMS sensors is that they can not only monitor the SYN-9 resin during fabrication in a laboratory press, but also in a tool on the manufacturing floor. Figures 12-15 discuss the essential principle of the FDEMS sensor's operation, the ability to monitor the changes in rotational mobility of dipoles and the translational mobility of ions in the resin during processing. These two molecular mobilities are an extremely sensitive means of monitoring and detecting changes in the state and properties of the resin during fabrication in situ in the mold.

Demonstration and verification of the FDEMS sensors' ability to monitor the effects of annealing and the changing state of the resin is discussed in detail in the first 12 month report, part III of this final report. Figures 16 and 17 are a clear demonstration of the sensor's sensitivity and in situ monitoring capabilities. In Figure 16 the SYN-9 is ramped to 380°, cooled to 90°, reramped to 380°, held for 15 minutes and then cooled. The continuous uninterrupted output from the sensor is shown in Figure 16. The dark overlapping lines at the lower frequencies trace the

increasing and decreasing value of the ionic translational mobility. This mobility is directly related to the changing viscosities and modulus of the resin. In the 100 to 140 minute region of the first cool down, dipolar peaks at increasingly lower frequencies track the decrease in the rotational mobility of the polymers in the amorphous region.

It is important to note after the 15 minute hold at 380° during the second ramp, these dipolar mobility peaks are greatly suppressed in magnitude. This suggests there are few polymers in the amorphous state and/or their mobility is greatly decreased. In other words, the presence or absence of the amorphous regions dipolar mobility peaks reflects the increased ordering during annealing in the 380° hold. Second, the reduced translational mobility of the ions, *i.e.* $\log \varepsilon'' x \omega$ is now equal to 4.4 in the second hold and decreasing compared to 5.0 in the first 380° hold indicates increasing ordering and resistance to translational mobility. Both effects show the sensor's ability to monitor the effects of annealing on ordering in the resin.

Figure 17 shows even more clearly the sensors' monitoring of translational mobility which is decreasing with time during a 2 hour 380° hold. Further, once again the dipolar mobility peaks seen after the first ramp up and down and on the second ramp up, disappear after a hold at 380° on the last ramp down.

Figures 16 and 17 indicate through the FDEMS sensor's output that the SYN-9 resin is undergoing physical changes during the 380° hold which result in a decrease in translational mobility with time at the molecular level and a decrease in the rotational mobility in the amorphous portion of the polymer. Both of the changes in molecular mobility strongly demonstrate both the SYN-9 system is ordering during the hold and that the FDEMS provide an in situ on-line sensor for monitoring this ordering-annealing during processing.

As part of this study FT-IR spectra were taken to determine if the effects observed in this report could be due to chemical reactions or crosslinking, rather than physical changes in state, morphology, *i.e.* increased ordering. Figures 18, 19, and 20 summarize the FT-IR spectra taken after a variety of thermal treatments. In summary, no detectable changes were observed except for a small shift in a carbonyl peak from 1800 to 1680 cm^{-1}. It is known that the position of carbonyl peaks depend on the environment. The softening temperatures of SYN-9 as noted by the FDEMS sensor and the TMA results, to be discussed, is around 150°. Above this temperature residual methylene chloride solvent can leave and more importantly the carbonyl groups would begin to rotate and move into an orientation of higher order. This type of orientation of the carbonyl groups would cause a shift in the carbonyl peak from one position such as 1800 cm^{-1} to 1690 cm^{-1} as observed in the sample after annealing 5 hours at 280°. Above 300° the sample turns brown, the sensitivity decreases, and no major changes in the FT-IR spectra are observed.

Last we turn to the thermal mechanical analysis TMA results, Figures 21-25. The thermal mechanical analyzer was used to determine the temperature at which penetration of a needle point into the sample occurred and the depth of the penetration. The 300° cured sample, Figure 22, shows slight penetration, softening, at 150° and large penetration, 100% at 258°. The 380° oven cured sample shows similar behavior, Figure 23. But two samples from the FDEMS sensor in the press cured sample, Figures 24 and 25, show penetration at over 400° and then only 20% penetration as compared to 100% in the samples above. The TMA results strongly support the conclusion that annealing at 380° under pressure induces "coordinated ordering" such that the softening temperature increases by over 100° as monitored by TMA.

In summary, the conclusions of the 20 month project are:

- This hydroquinoneterephthaloyl polyester is a thermotropic liquid crystal;
- Hold cycles at 300C, 340C, and 380C created more ordering with a wider distribution of melting temperatures and a higher average melting temperature;
- Changes observed were physical and not chemical;
- An additional pressure is required to cause a large increase in the mechanical properties;
- The hydroquinoneterephthaloyl polyester can be molded under pressure in the flow state and allowed to cool to achieve a strong molded product with greatly enhanced mechanical properties.

Syn 9

- Condensation polymerization of three monomer units

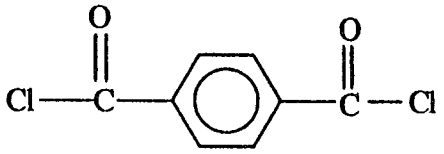

terephthaloyl chloride

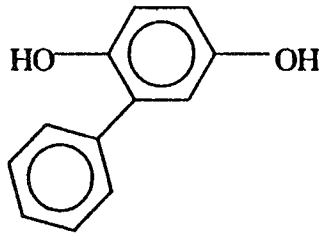

phenylhydroquinone

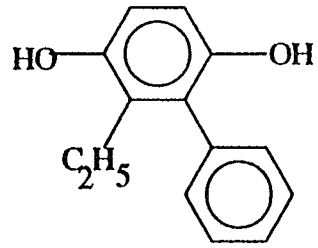

ethylphenylhydroquinone

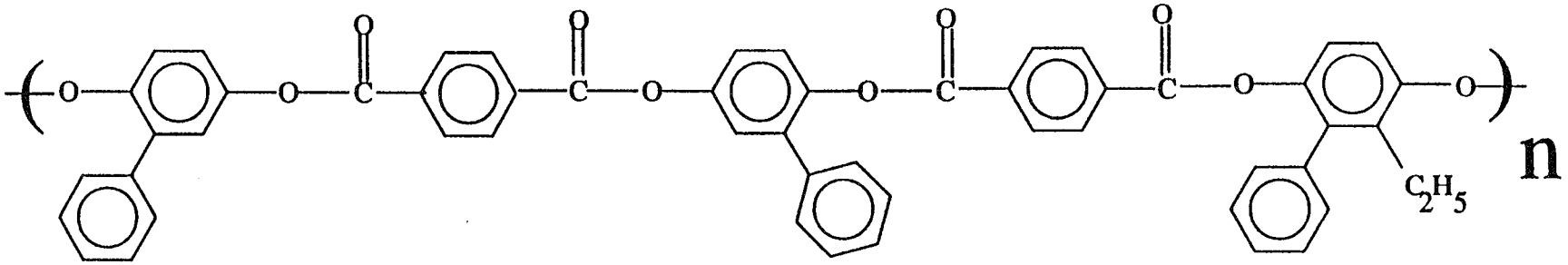

- The molecular structure of syn9 allows it to achieve a rod-like orientation
- Methods used to make syn9 thermotropic :

  1) Random Copolymerization

  2) Bulky Side Groups

T_m(C)

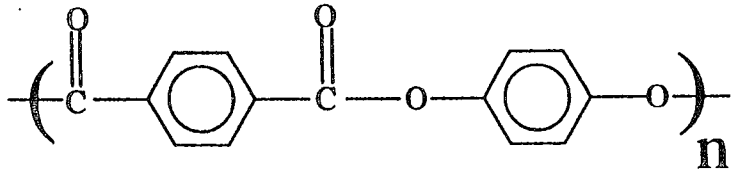

>600

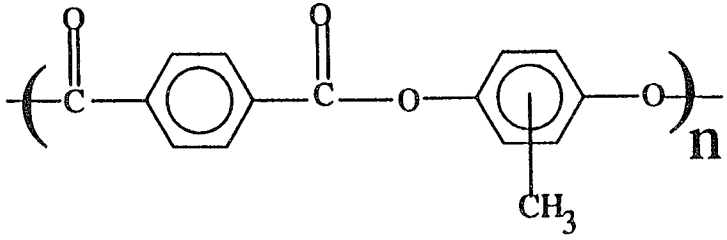

>400

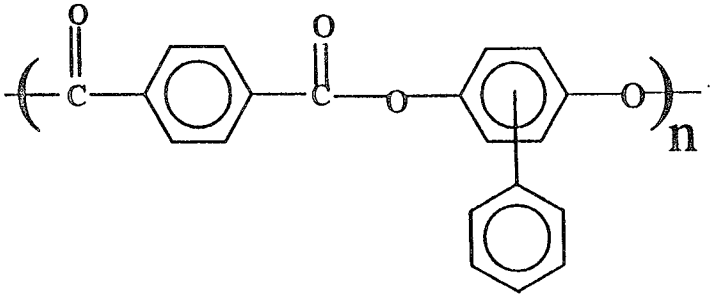

≈340

Experimentation

Four Main Instruments Used:

1) DSC
- locates phase transitions (Tm and Tg) and calculates enthalpy
- used to observe the effects of high temperature holds on size and location of phase transitions

2) FDEMS
- moniters molecular mobility of ions and dipoles
- used to determine if high temperature holds lock up this molecular mobility

3) FT-IR
- gives IR spectra for different degrees of cure
- used to determine whether changes were physical or chemical

4) TMA
- displays penetration of sample upon heating
- used to determine physical property enhancement due to the curing cycle

Differential Scanning Calorimetry (DSC)

- Melting, crystallization, vaporization, and simple heating all involve heat flow
- Two aluminium pans (only one with the sample) are rigorously kept in line with a precise temperature program
- An adjusted amount of electrical energy must be supplied to keep the sample pan in accordance with the temperature program
- This energy is related to heat flow in mW

DSC Data File: ey919
Sample Weight: 5.590 mg
Tue Feb 02 16:26:10 1993
ey9 (fresh); empty ref.

PERKIN-ELMER
7 Series Thermal Analysis System

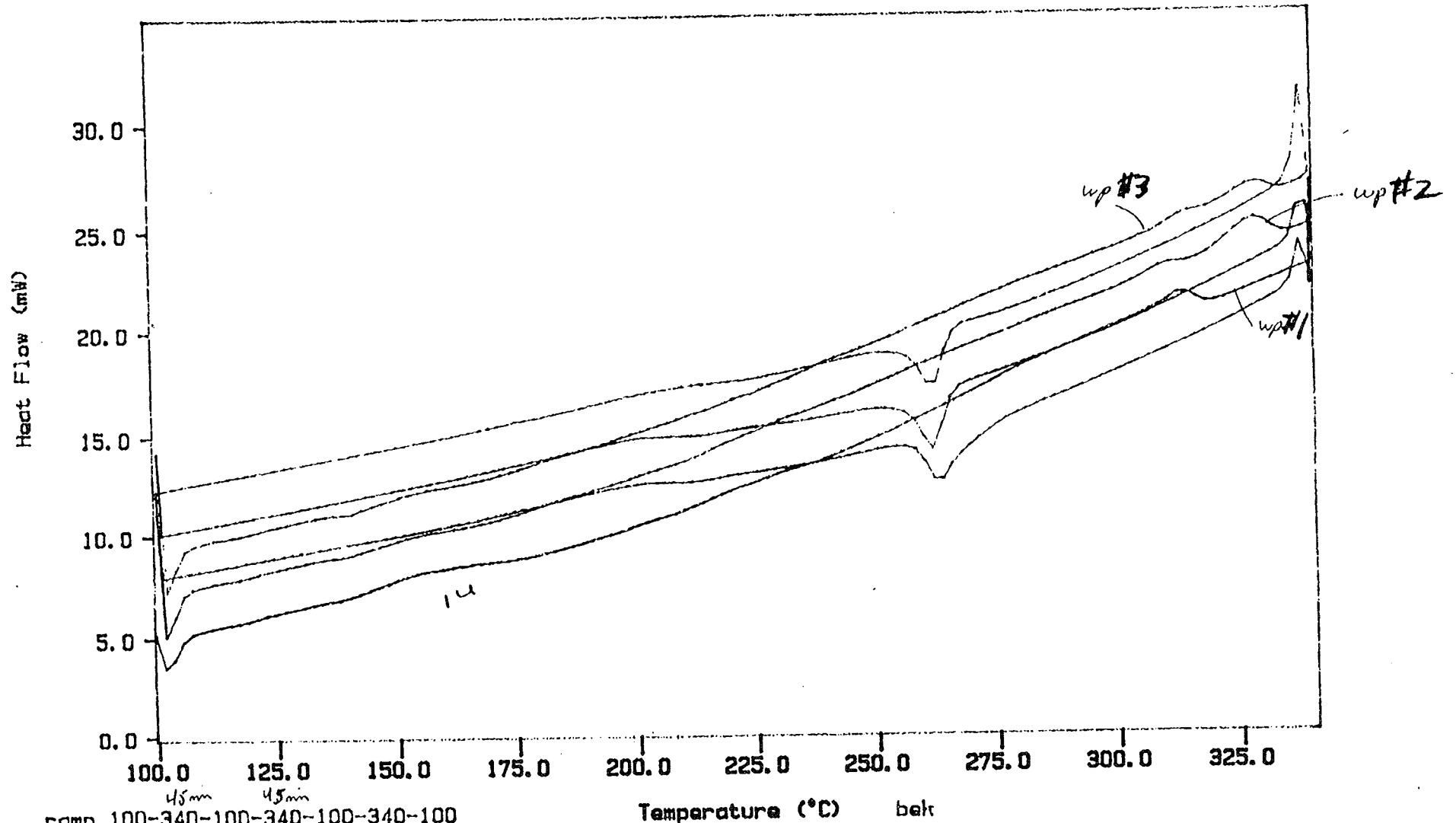

ramp 100-340-100-340-100-340-100

TEMP 1:	100.0 C	TIME 1:	0.0 min	RATE 1:	20.0 C/min
TEMP 2:	340.0 C	TIME 2:	45.0 min	RATE 2:	20.0 C/min
TEMP 3:	100.0 C	TIME 3:	0.0 min	RATE 3:	20.0 C/min
TEMP 4:	340.0 C	TIME 4:	45.0 min	RATE 4:	20.0 C/min
TEMP 5:	100.0 C	TIME 5:	0.0 min	RATE 5:	20.0 C/min
TEMP 6:	340.0 C	TIME 6:	0.0 min	RATE 6:	20.0 C/min
TEMP 7:	100.0 C				

DSC Data File: ey918
Sample Weight: 5.540 mg
Mon Feb 01 14:49:31 1993
ey9 (fresh); empty ref

PERKIN-ELMER
7 Series Thermal Analysis System

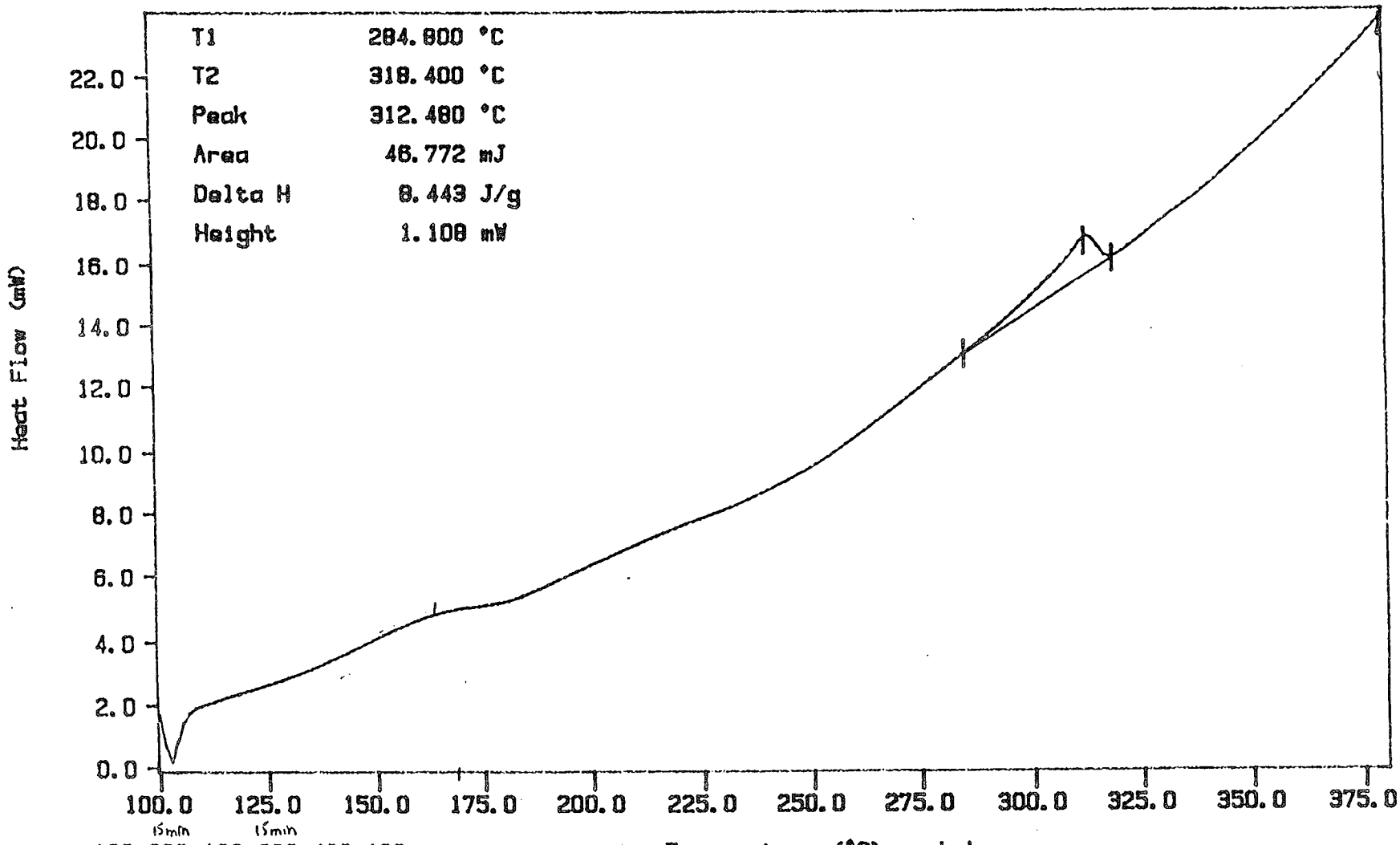

DSC Data File: ey918
Sample Weight: 5.540 mg
Mon Feb 01 14:48:31 1993
ey9 (fresh); empty ref

PERKIN-ELMER
7 Series Thermal Analysis System exp # 2

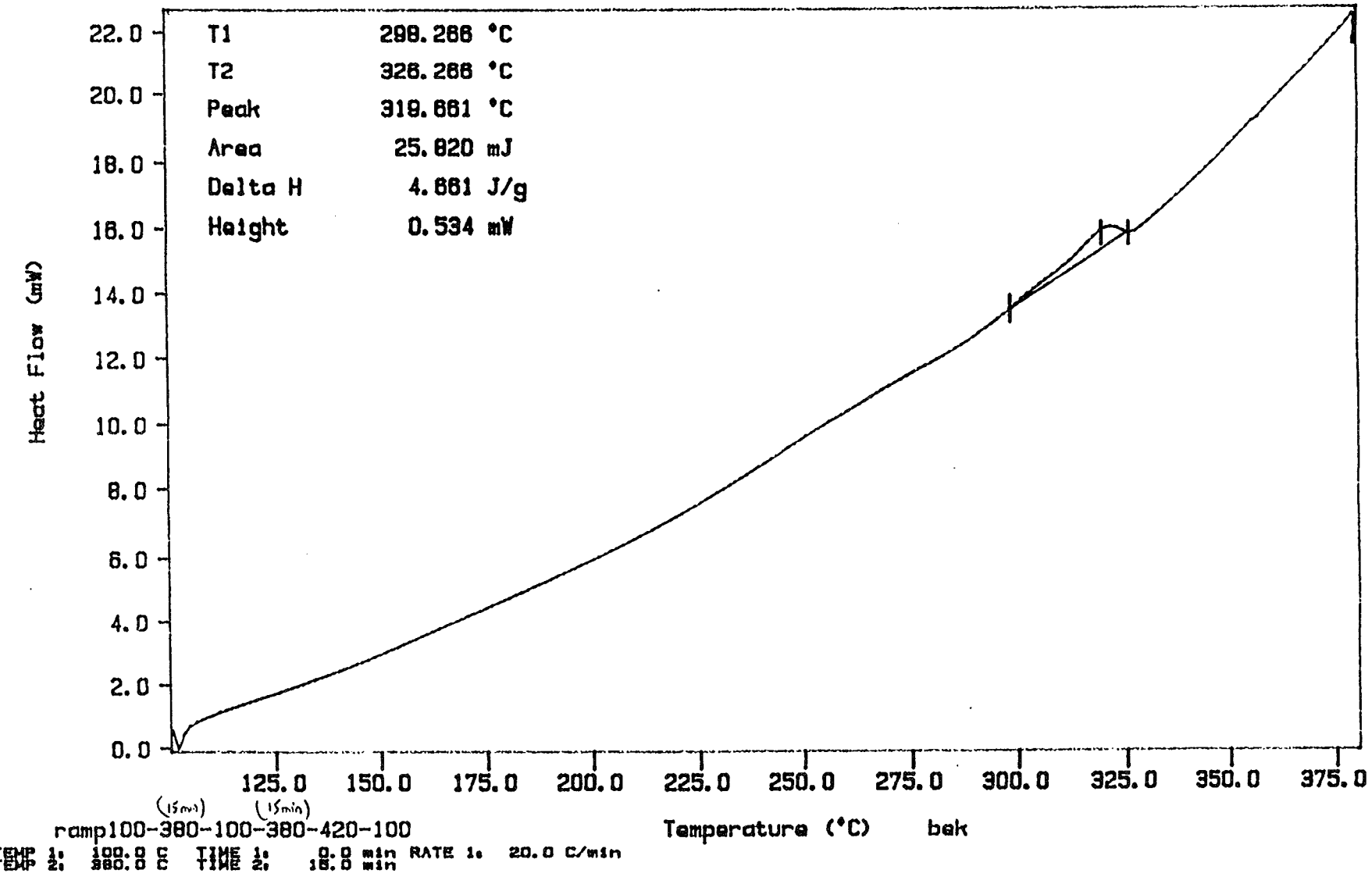

TEMP 1: 100.0 C TIME 1: 0.0 min RATE 1: 20.0 C/min
TEMP 2: 380.0 C TIME 2: 15.0 min

DSC Data File: ey918
Sample Weight: 5.540 mg
Mon Feb 01 14:49:31 1993
ey98 (fresh): empty ref

PERKIN-ELMER
7 Series Thermal Analysis System

yp #3

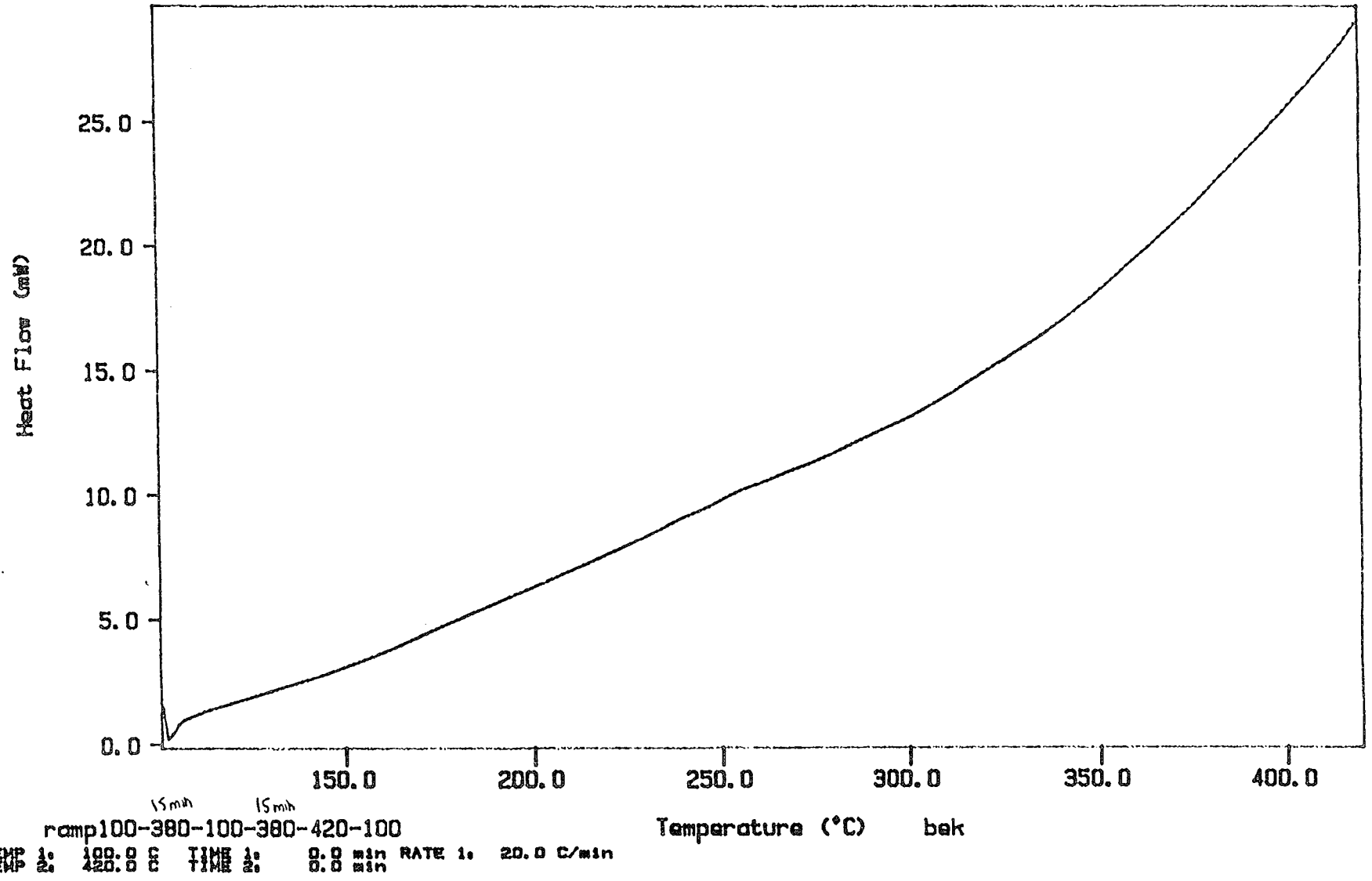

TEMP 1: 100.0 C TIME 1: 0.0 min RATE 1: 20.0 C/min
TEMP 2: 420.0 C TIME 2: 0.0 min

DSC Data File: tlqcr
Sample Weight: 5.200 mg
Sun Jun 21 21:56:35 1992
True Liquid Crystal (fresh); empty ref.

PERKIN-ELMER
7 Series Thermal Analysis System

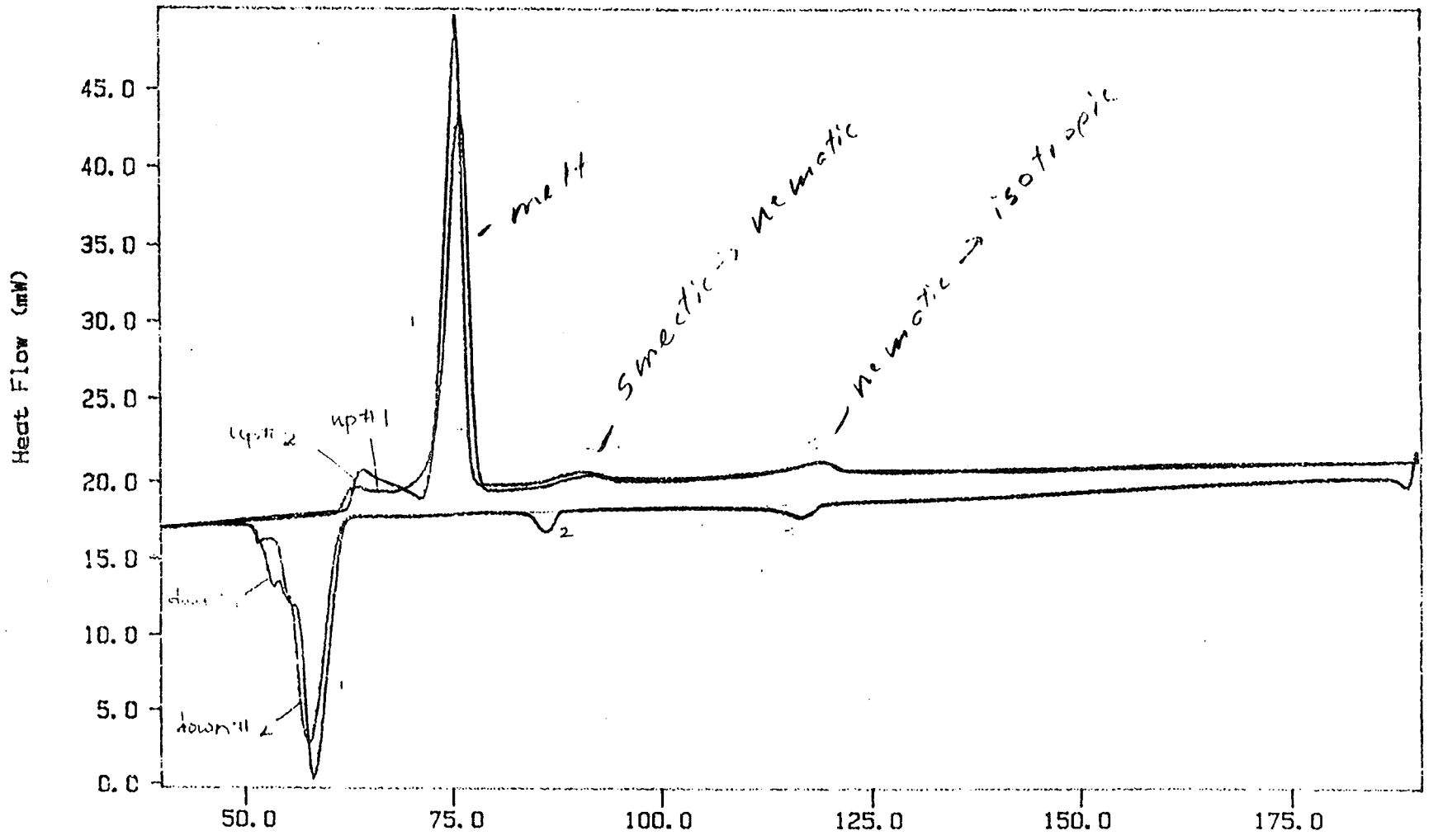

Ramp 40-190-40-190-40C 10C/min

TEMP 1:	40.0 C	TIME 1:	0.0 min	RATE 1:	10.0 C/min
TEMP 2:	190.0 C	TIME 2:	0.0 min	RATE 2:	10.0 C/min
TEMP 3:	40.0 C	TIME 3:	0.0 min	RATE 3:	10.0 C/min
TEMP 4:	190.0 C	TIME 4:	0.0 min	RATE 4:	10.0 C/min
TEMP 5:	40.0 C				

Temperature (°C) cke

down #1 → 3.2 J/g peak 2
2.803 J/g peak 3
78.956 J/g peak 1
down #2 → 78.193 J/g peak 1
3.229 J/g peak 2
3.062 J/g peak 3

up #1 → 102.423 J/g peak 1
2.529 J/g peak 2
4.505 J/g peak 3
up #2 → 97.31 J/g peak 1
3.15 J/g peak 2
3.10 J/g peak 3

DSC DATA

Hold Time & Temp	Fresh Peak (C)	New Peak (C)	Tg
240 min @ 236C	312	313	
240 min @ 274C	312 (7.2 J/g)	314 (16.9 J/g)	
240 min @ 274C	305 (10.1 J/g)	306 (22.0 J/g)	
60 min @ 300C	313 (6.1 J/g)	321 (8.5 J/g)	
240 min @ 300C	304 (18.5 J/g)	334 (18.9 J/g)	
240 min @ 300C	312	331	
45 min @ 340C	313 (5.0 J/g)	328 (5.8 J/g)	150
90 min @ 340C	313 (5.0 J/g)	328 (6.2 J/g)	160
15 min @ 380C	312 (8.4 J/g)	319 (4.7 J/g)	165
30 min @ 380C	312 (8.4 J/g)	no peak	

Polarizing Microscope

- Glass Transition 150C
- "Softening" observed (birefringent) 260C
- Fluid, nematic, and birefringent melt 315C
- melt becomes isotropic 415C

FDEMS

- Frequency Dependent Electromagnetic Sensing
- Every molecule is polarizable
- Measurement can be modeled by a parallel plate capacitor
- Dipoles will attempt to allign with the electric field

Two Molecular Probes

Ionic - free charge σ

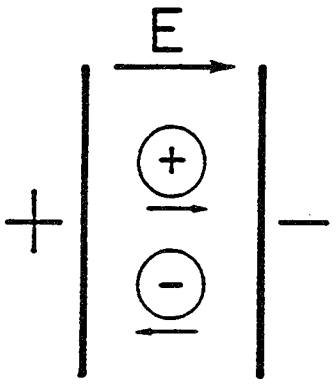

translational diffusion of ions

$$\rho_T \frac{dx}{dt} = \text{force}$$

sphere: $\rho_T = 6\pi\eta r$

Dipolar - bound charge τ

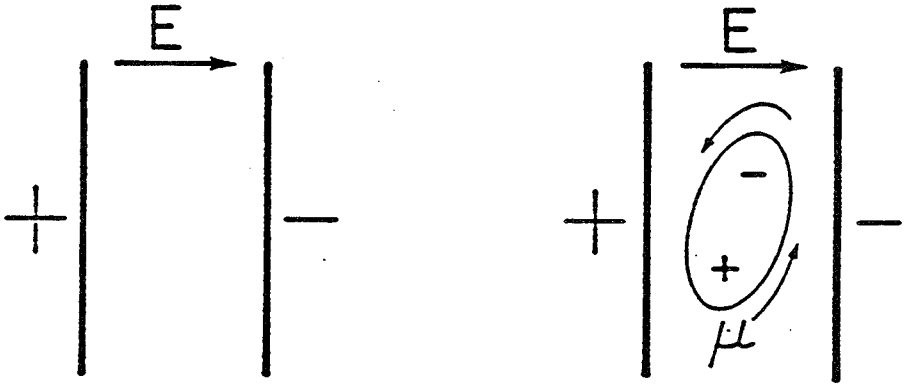

rotational diffusion of dipoles

$$\rho_R \frac{d\theta}{dt} = \text{torque}$$

sphere: $\rho_R = 8\pi\eta r^3$

Capacitor model gives rise to the dielectric permitivity, ε' and the dielectric loss factor, ε''

$$\varepsilon' = C / C_0 \qquad \varepsilon'' = G / (C_0 2\pi f)$$

- Each has a dipolar and ionic component

$$\varepsilon' = \varepsilon'_D + \varepsilon'_I \qquad \varepsilon'' = \varepsilon''_D + \varepsilon''_I$$

- The dipolar term expresses the individual molecular dipole moments
- The ionic term rises from mobile ions in fluid samples

Focus on log$\varepsilon'' * \omega$

- Frequencies from 5Hz to 1MHz
- Overlap indicates ionic translation dominates
- Peaks represent rotational contribution
- Decrease during constant temperature reflects a loss of mobility

Probe: 1 (syn 9)

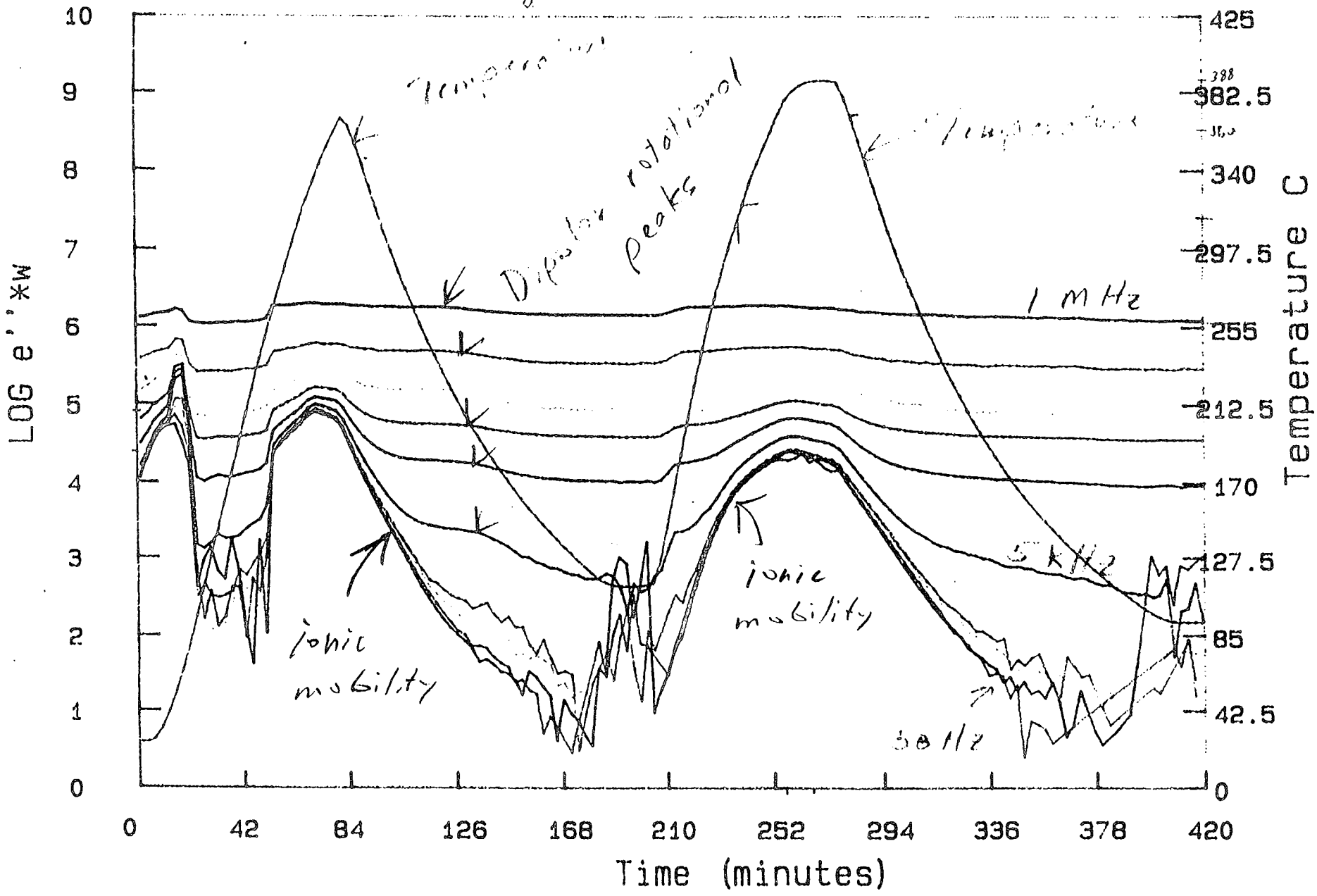
LOG e'' *w
Temperature C
Time (minutes)
1 MHz
5 kHz
60 Hz
ionic mobility
ionic mobility
Dipolar rotational peaks
0
42
84
126
168
210
252
294
336
378
420
0
1
2
3
4
5
6
7
8
9
10
42.5
85
127.5
170
212.5
255
297.5
340
382.5
425

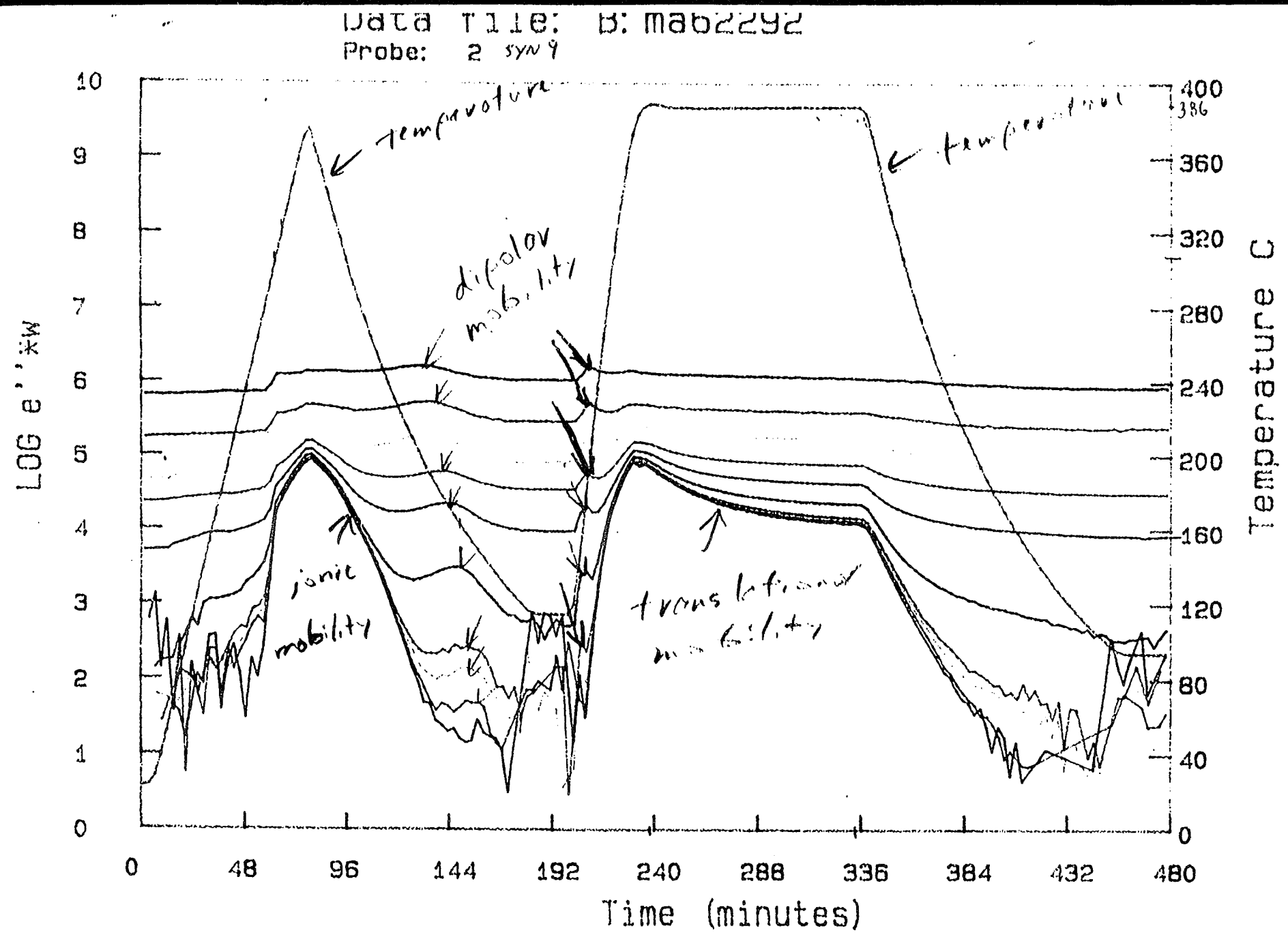
Data Title: B: mab2292
Probe: 2 syn 9
LOG e'' *w
Temperature C
Time (minutes)
0
48
96
144
192
240
288
336
384
432
480
0
1
2
3
4
5
6
7
8
9
10
0
40
80
120
160
200
240
280
320
360
400
386
dipolar mobility
ionic mobility

FT-IR Results

Heat treatment	Change in Spectra
fresh	
30 min @ 100C	No change
30 min @ 200C	Distinct peak at 1680cm-1 Decrease in 1800cm-1 peak
30 min @ 280C	Strong peak at 1680cm-1 No peak at 1800cm-1
30 min @ 320C	Low resolution

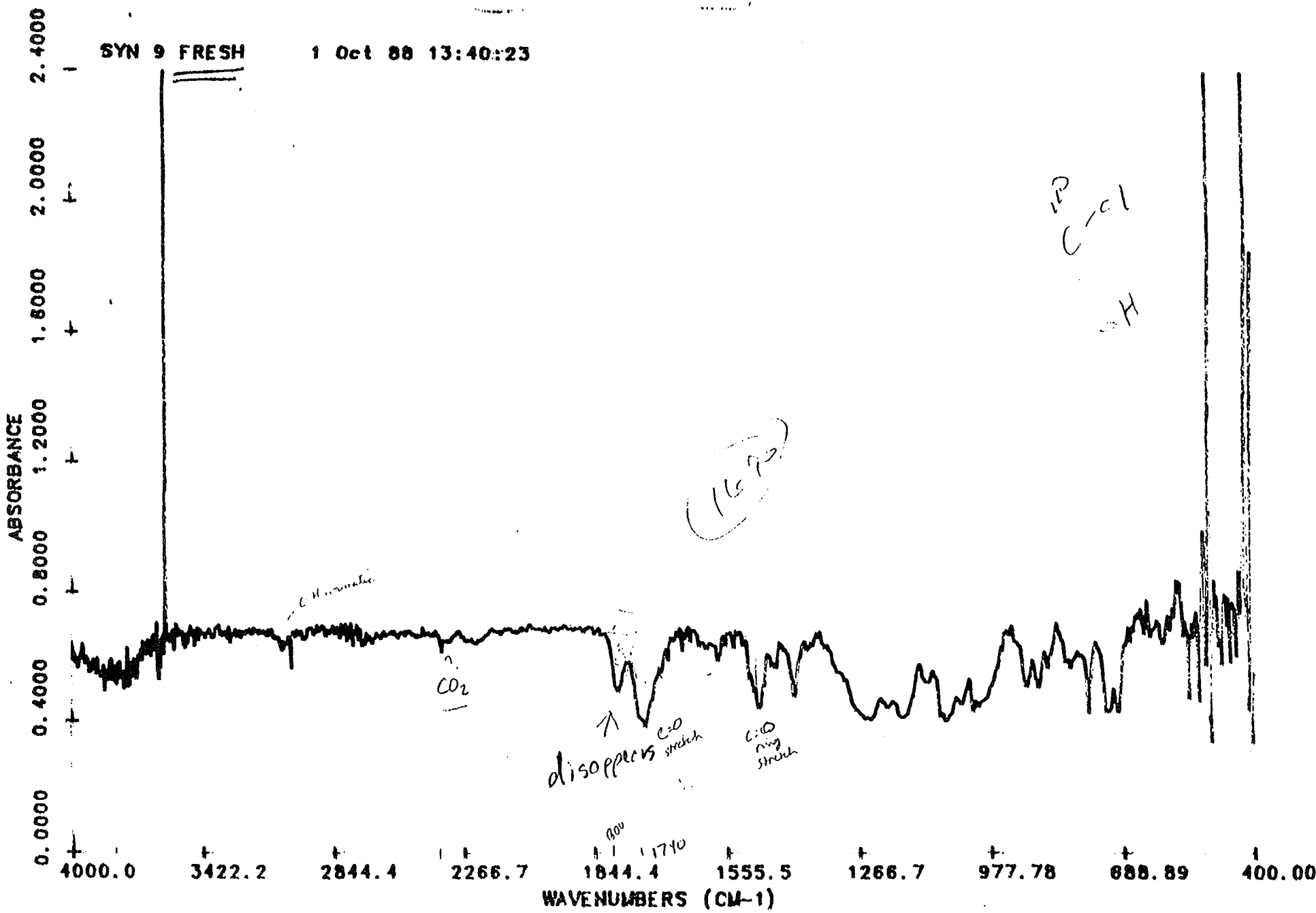
SYN 9 FRESH
1 Oct 88 13:40:23
ABSORBANCE
2.4000
2.0000
1.8000
1.2000
0.8000
0.4000
0.0000
4000.0
3422.2
2844.4
2266.7
1844.4
1555.5
1266.7
977.78
688.89
400.00
WAVENUMBERS (CM-1)
1800
1740
CO_2
disappears
C=O stretch
C=O ring stretch
C-Cl
H

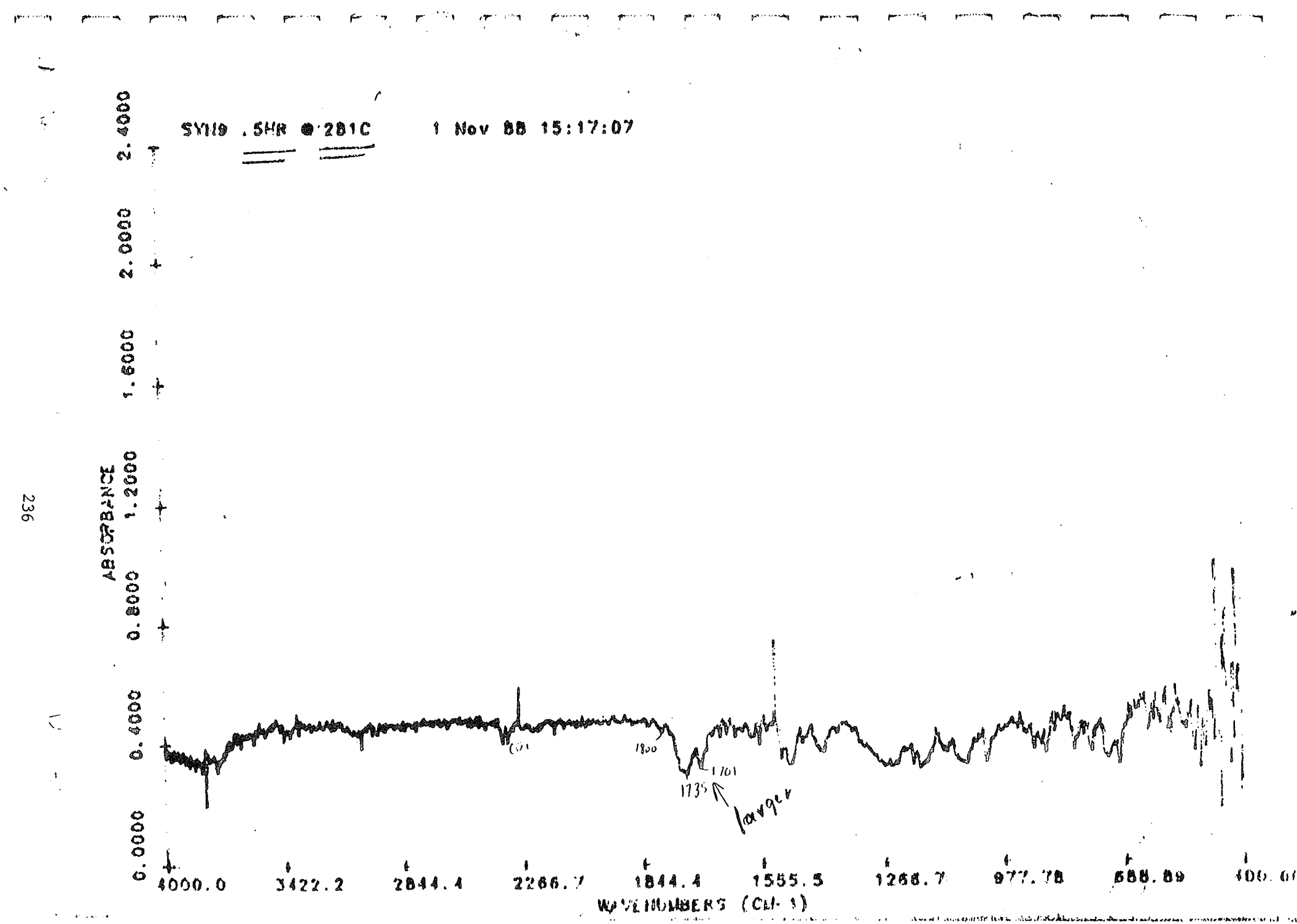
SYN19 .5HR @ 281C
1 Nov 88 15:17:07
ABSORBANCE
2.4000
2.0000
1.6000
1.2000
0.8000
0.4000
0.0000
1800
1735
1701
larger
4000.0
3422.2
2844.4
2266.7
1844.4
1555.5
1266.7
977.78
688.89
WAVENUMBERS (CM-1)

Thermal Mechanical Analysis (TMA)

- Measures penetration of a pin with constant load into the sample during an increasing temperature program

Hold Time & Temperature	Tm (C)	Tg (C)
Pre-Cured Sample		
60 min @ 380C	263	159
60 min @ 340C	254	
60 min @ 300C	258	158
From Dielectric Run		
240min @ 274C	261	144
10 min @ 380C	220	
90 min @ 380C	410 (14%)	

TMA ANALYSIS OF LIQUID CRYSTAL

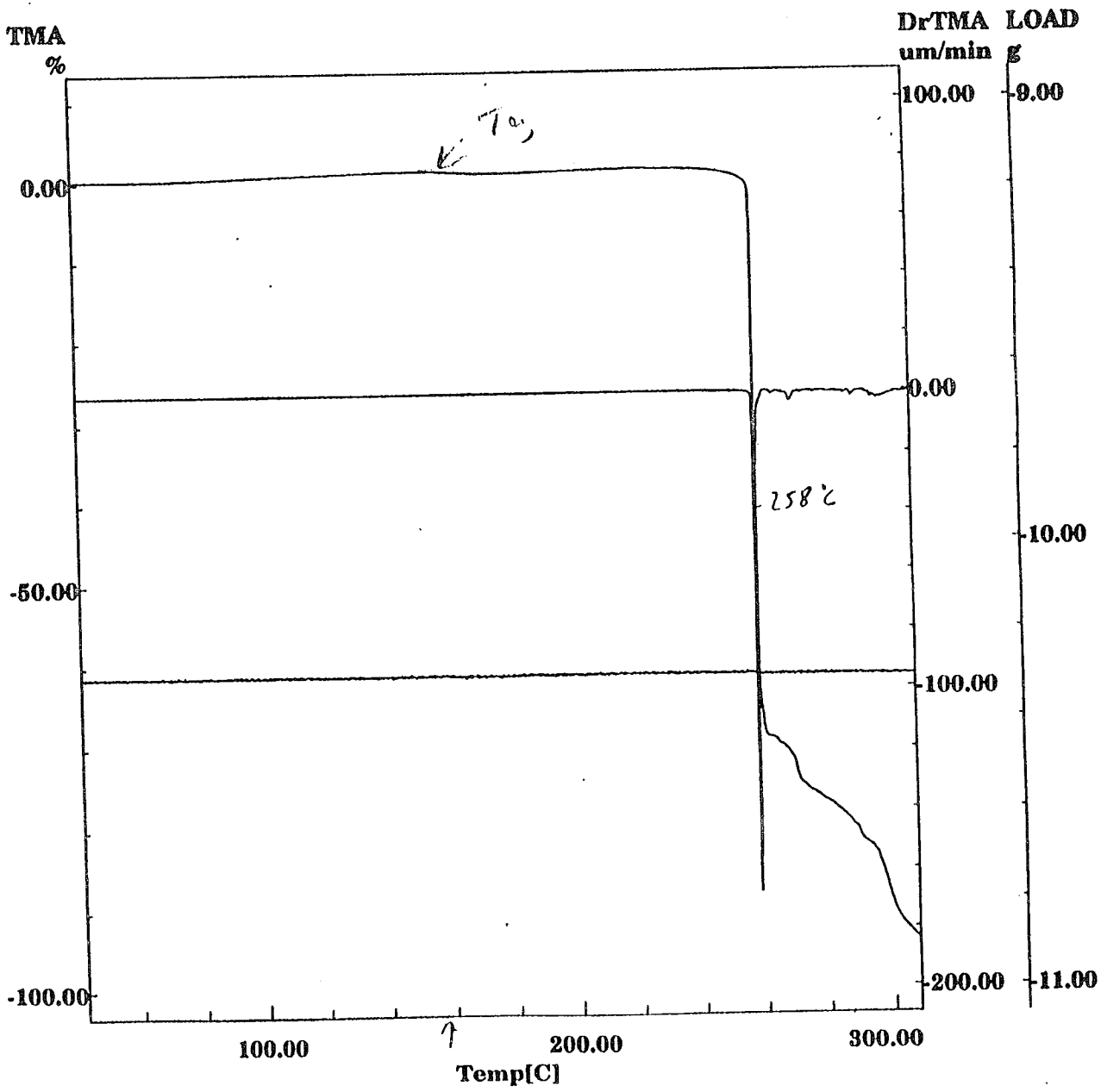

Temp Program

Rate [C/min]	Hold Temp [C]	Hold Time [min]
10.0	320.0	0.0

File Name: SYN9-300.D00
Sample Name: syn9 cured hr @ 300
Length: 1.092[mm]

TMA ANALYSIS OF LIQUID CRYSTAL

File Name: syn9-380
Sample Name: syn9 cured hr @ 380
Length: 0.8240[mm]

Temp Program

Rate [C/min]	Hold Temp [C]	Hold Time [min]
10.0	420.0	0.0

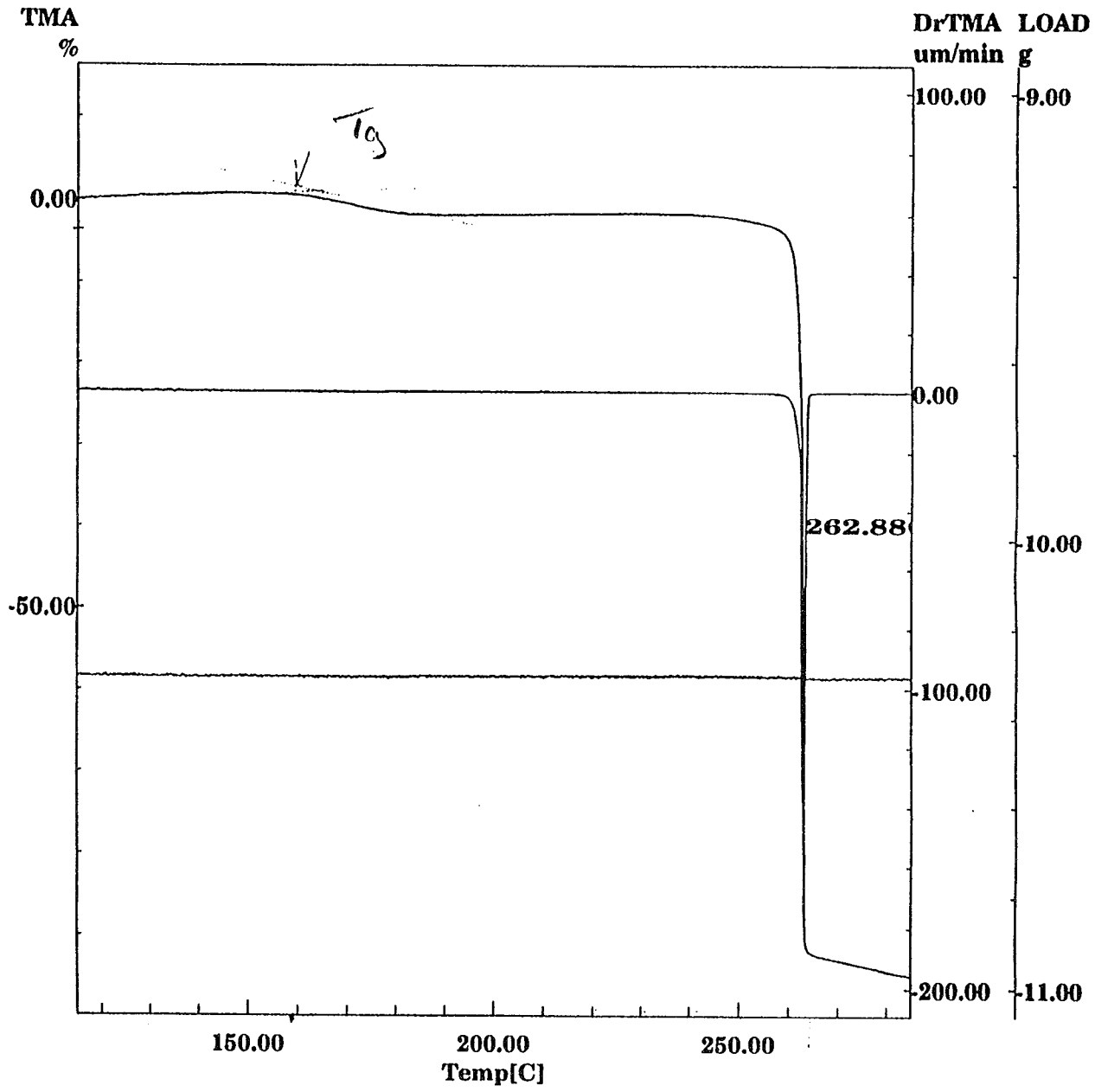

THERMAL ANALYSIS DATA

DATE 92/08/03

FILE NAME A803L49.000 [TMA]

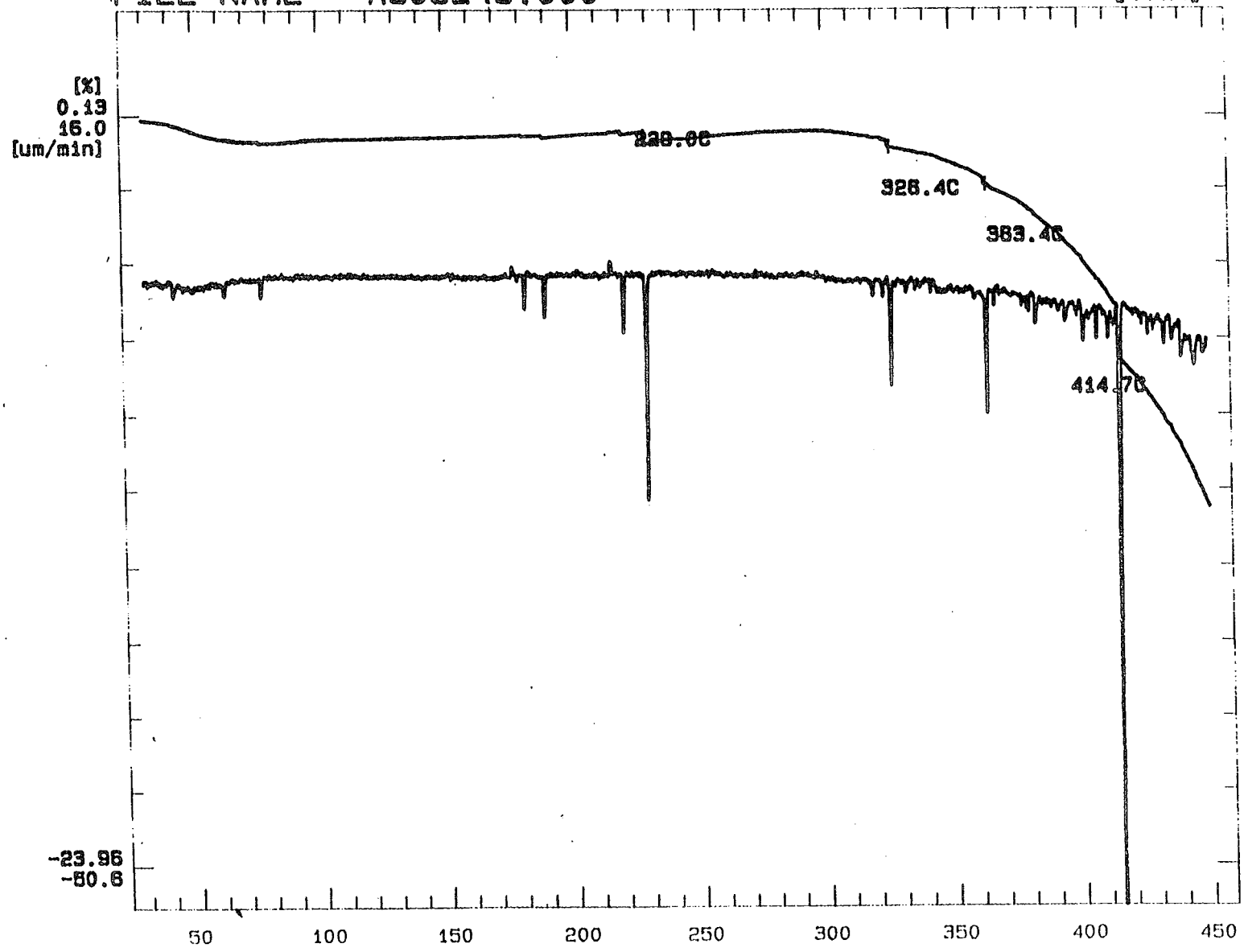

MEASURING CONDITIONS

SAMPLE NAME	syn9
SAMPLE SIZE	0.830
SAMPLING INT	1.0
ACQ. DATE	92/08/

COMMENT

syn9 remprt-460cured

HEATING PROGRAM

	RATE	TEMP	TIM
1	5.0	460.0	

syn 9 - previously held for 1 hr at 380

SHIMADZU

240

THERMAL ANALYSIS DATA

DATE 92/08/05

FILE NAME A806J41.000 [TMA]

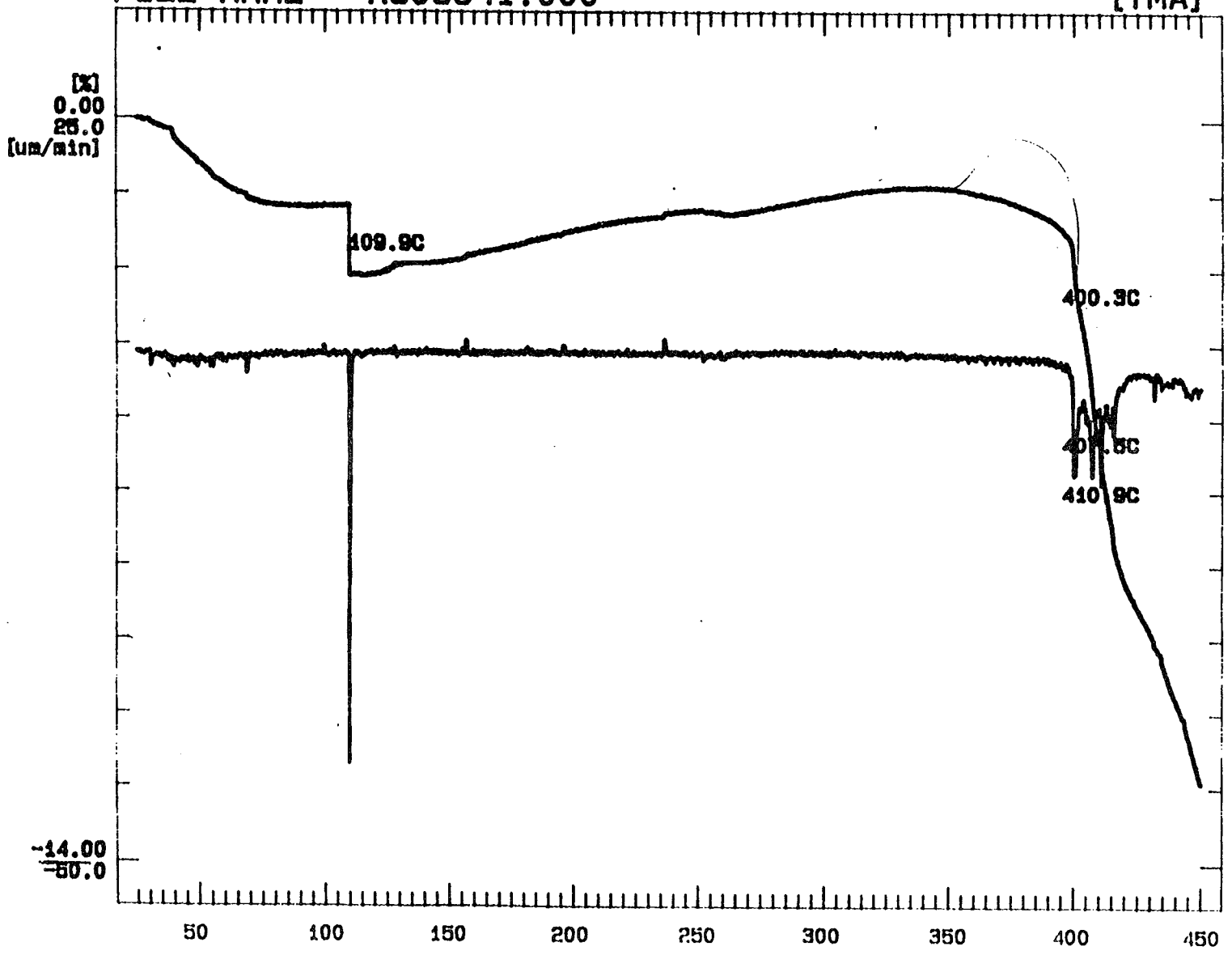

MEASURING CONDITIONS

SAMPLE NAME	syn9h1
SAMPLE SIZE	0.520
SAMPLING INT	1.0
ACQ. DATE	92/08/
COMMENT	
ramp rt-450, 5C/min	

HEATING PROGRAM

	RATE	TEMP	TIM
1	5.0	450.0	

SYN9
hr hold @
380°C

WILLIAM

Time/Temperature Dependence of the Physical Properties in SYN-9 A Thermotropic Liquid Crystal

to

Dr. John J. Rusek
Phillips Laboratory
Bldg. 8351
OLAC PL/RKCP
Edwards, CA 93523-5000

from

Brian Kipp and David E. Kranbuehl
Chemistry and Applied Science
The College of William and Mary
Williamsburg, VA 23187-8795

May 30, 1993

Contract #FO4611-91-C-013

Time/Temperature Dependence of the physical Properties in Syn9 A Thermotropic Liquid Crystal

Chapter 1

Introduction

An aromatic copolyester, labeled syn9, which may exhibit liquid crystalline thermotropic properties has been studied. Various hold cycles were implemented in the attempt to induce ordering in the polymer. This paper will examine if ordering does occur and which time/temperature cycles will be the most effective. The objective is that increased ordering will lead to enhanced mechanical properties upon return to the solid state. Hopefully some high performance properties, as one might find in a thermoset, will be present in the cured syn9. However, syn9 will still have the capability of being molded like a traditional thermoplastic.

Liquid Crystals

In order to understand the behavior of syn9 as it undergoes various cure cycles, one must know the properties of a thermotropic liquid crystal. Liquid crystal is an appropriate term for these compounds because they have phases

that are somewhat ordered but still fluid between the crystalline and the disordered fluid states. This ordering by definition is only in one or two dimensions but not in three, as in a crystal. The disordered liquid is referred to as being isotropic, and the array of ordered phases preceding the isotropic melt are mesophases. There are four major types of mesophases: smectic, nematic, cholesteric, and discotic[1]. Smectic mesophases have two ordered dimensions (ie. planar orientation) while nematic mesophases exhibit only one dimensional order (ie. linear and parallel). Cholesteric mesophases resemble a two dimensional twisted nematic mesophase. Discotic mesophases stack like coins although coin formation seems unlikely for this system[1] (see figure 1).

Figure 1[1]

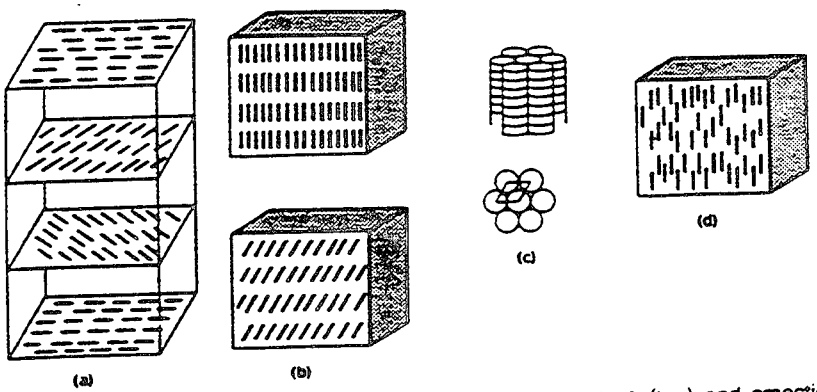

Liquid crystal structures: (*a*) cholesteric (*b*) smectic A (top) and smectic (c) (bottom), (*c*) discotic, and (*d*) nematic (2).

Although a liquid crystal polymer (LCP) may exhibit multiple mesophases, one liquid crystalline mesophase and an isotropic melt are necessary conditions that must be met for

liquid crystallinity. Once a clearing temperature is reached the polymer system will only exist as an isotropic melt[2].

LCP's can be classified as being lyotropic, thermotropic, and as having mesogenic side groups. Lyotropic LCPs display ordered states in concentrated solutions. They typically have such high melting points that lyotropic LCPs would decompose before becoming liquid crystalline[2]. Therefore, concentrated solutions are needed to observe any liquid crystalline behavior. Thermotropic LCPs are simply those which can exist as ordered melts. Their melting points are lower than lyotropic LCPs and are therefore easier to work with. Thus, in order to get a thermotropic LCP, one must lower the melting point of a lyotropic LCP.

The Syn9 System

Syn9 is an aromatic copolyester formed by a condensation polymerization with terephthaloyl chloride (Figure 2) and two different substituted hydroquinone monomer units. The hydoquinones in Syn9 are phenylhydroquinone and ethylphenylhydroquinone (Figure 2).

Figure 2

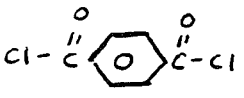

terephthaloyl chloride

phenylhydroquinone

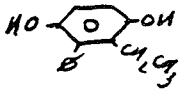

ethylphenyl-hydroquinone

These monomer units polymerize in a random copolyester fashion resulting in the atactic polymer shown below (fig. 3).

Figure 3

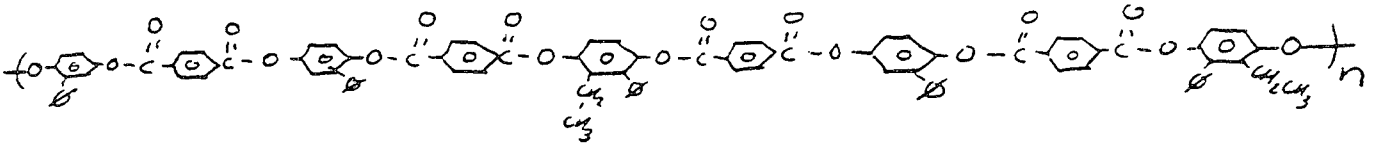

Both terephthaloyl chloride and hydroquinone are primarily aromatic para-disubstituted molecules which would form strictly rod-like segments[1]. One can visualize that a stiff rod-like polymer chain could orient itself in a liquid crystalline mesophase, and therefore it is possible that syn9 is an LCP.

Many Liquid Crystals have such extreme melting temperatures that they are not easily processed in the liquid state. The melting point must be lowered so the system does not decompose before flow occurs. Two of the methods of lowering the melting point are used in syn9. The first method is by random copolymerization which is shown by the two different substituted hydroquinones. This random arrangement would inhibit syn9 from packing as tightly as some lyotropic polymers. The second method consists of the addition of bulky side groups such as the phenyl substitutions on the hydroquinones in syn9[3]. The different effects of substitution on melting points of related polymers are shown in table I.

Table I

Melting Points for Thermotropic LCPs

Bulky Side Group	T (Melting) °C
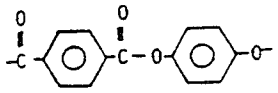	> 600
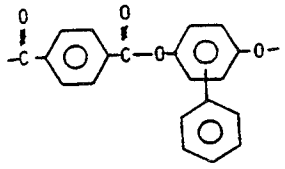	= 340

Flexible Group	T (Melting) °C
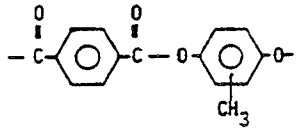	> 400

Chapter 2

Experimentation

Most thermotropic liquid crystal polymers are aromatic, heteromonomer copolyesters[1]. If syn9 is a thermotropic liquid crystalline polymer, then more order may be induced in the solid state upon a heat treatment of the liquid crystal mesophase. In addition, this could result in enhanced physical solid state properties. If the physical properties can be enhanced, at what temperature, for how long, and to what extent can the mechanical properties be increased? In attempt to answer this question four main methods were used: Differential Scanning Calorimetry (DSC), FDEMS dielectric sensing, Thermal Mechanical Analysis (TMA), and FT-IR.

The DSC allows one to determine the temperature of phase transitions and the enthalpy of that change. In addition the shifting of these transitions can be studied as a result of various cure cycles. FDEMS can monitor the molecular mobility of the ions and dipoles within the polymer system. Also the effects of the temperature holds can be studied on a molecular level. The TMA measures the mechanical properties of different pre-cured samples. Finally the FT-IR can help determine if the changes observed are chemical or physical in nature.

Chapter 3

Differential Scanning Calorimetry

The DSC measurements are based on two basic principles. The first is that all samples contain stored energy in the form of thermal movement. Secondly, when the state of the system is changed, an input or output of energy must accompany it. This energy is usually in the form of heat. Melting, crystallization, vaporization, and simple heating are all processes which involve a flow of heat[4]. In conducting a DSC run, the sample is first placed in an aluminum pan, which only need contain 5-10 mg of the sample. Both the sample pan and an empty reference pan are heated according to an accurately controlled temperature program. When the sample undergoes a transition, power is adjusted to the sample pan in order to keep the temperature in accordance with the reference pan[5]. These adjustments are converted into heat flow in mW and plotted versus either time or temperature.

A major focus of these measurements was the effects of various temperature holds on the endothermic phase transition observed in the "up" ramps. Up ramps refer to a period of increasing temperature and down ramps to decreasing temperature. The endothermic phase transition is observed as a peak in the DSC plot. This peak first occurs while heating the amorphous polymer and is observed around 313°C. Since this initial temperature up ramp has been performed many times

and is part of virtually every run, the confidence of this value is very high. It is necessary to extend past this phase transition because it is presumably a melting temperature. Thus, when going beyond this temperature the polymer is in some form of liquid mesophase, though the type of phase remains to be seen. Hold temperatures of 380°C, 340°C, 300°C, 274°C, and 236°C were used and the effects of these temperatures on the initial endothermic peak were observed. Each of the hold temperatures were above the regularly occurring, corresponding exothermic peak on the down ramp, so presumably some part of the system is in a supercooled, liquid mesophase during the hold. The temperature hold at 274°C was preformed for four hours to allow sufficient time for any changes to occur. When the first ramp was taken to 340°C the endothermic peak of interest occurred at 312°C with a peak size of 7.2 J/g. The four hour hold occurred in the supercooled region below the initial melting endotherm (274°C), but presumably in the liquid crystalline state. After this hold the sample was again heated to see the effect on this phase transition. The peak shifted upward a minimal 2°C but the integrated area of the peak grew from 7.2 J/g to 16.9 J/g.

Two similar runs were conducted for a 300°C hold, with one lasting 60 minutes and the other was 4 hours (See Figure 4 and 5). In contrast to the run at 274°C, the two holds had a much greater shifting effect on the endothermic peak. Although the 60 minute hold caused an 8 degree increase, an

additional 3 hours moved this peak to 334°C. The heat flow was significantly exothermic during the hold with a decrease of 2.1 mW. The exothermic nature during the hold is evidence of some physical change that occurs at 300°C and not seen at 274°C.

The runs at 340°C were conducted using two 45 minute holds with complete down ramps in between (see Figure 6). The peak again shifted to a higher temperature but with a less clearly defined peak. Though the most prominent part of the peak occurs at 328°C, a less defined doublet remains near the original melting peak. This would suggest that there are two different crystalline portions of the polymer. This is important in demonstrating that one polymer system can have different crystalline areas with different melting points. Eventually, if this trend continues, this phase transition would appear to be "smeared". This observation is critical in understanding the data from the 380°C holds.

Two 15 minute holds at 380°C first reduced the peak size and then appeared to eliminate this peak (see Figure 7 a,b, and c). The elimination of this peak could represent a distribution over many melting points such that a single peak would not be distinguishable from the baseline. Although this cured sample was taken to 420°C in an effort to find an observable peak, none was forthcoming. In addition, the corresponding exothermic peak was significantly reduced and smeared. This exothermic peak on the first down ramp after a 15 minute hold was not smeared but shifted significantly to

248°C. This shift was at least 10°C greater than any other experiment. The data for all relevant DSC runs are presented in table 2.

Table 2

Hold Time & Temp	Fresh Peak (°C)	New peak (°C)	Tg
240min @ 236°C	312	313	
240min @ 274°C	312 (7.2 J/g)	314 (16.9 J/g)	164
240min @ 274°C	305 (10.1 J/g)	306 (22 J/g)	
240min @ 274°C	313	314	
60 min @ 300°C	313 (6.1 J/g)	321 (8.5 J/g)	
240min @ 300°C	304 (18.5 J/g)	334 (18.9 J/g)	204
240min @ 300°C	312	331	211
45 min @ 340°C	313 (5.0 J/g)	328 (5.8 J/g)	200
90 min @ 340°C	313 (5.0 J/g)	328 (6.2 J/g)	198
20 min @ 340°C	313	315	
40 min @ 340°C	313	321	
15 min @ 380°C	312 (8.4 J/g)	319 (4.7 J/g)	200
30 min @ 380°C	312 (8.4 J/g)	no peak	

The column titled "fresh peak" represents the temperature and size of the endothermic peak on the initial ramp of a fresh sample. These should be the same since each sample was not previously heat treated and was then heated from 100°C to at least 340°C in the same manner every time. Differences could result from variances of crystallinity in the uncured fresh sample, but most occurred as predicted at 313°C. The new peak column shows the endothermic phase transition after the given hold to exemplify the effects of that hold. The enthalpy in J/g for the phase transition at that temperature are given in parentheses. This value is achieved by integrating the peak to find its area, and then dividing by the sample's mass.

The glass transition temperature was difficult to determine since it was not very pronounced. Some values on the down ramps could be estimated and are presented in the Tg column. This is easily explained because several truly rigid polymer systems ordinarily do not have a glass transition. Even if they occur these second order phase transitions are difficult to observe. The Tg values on the up ramps are even less clear, but an estimated value of 160°C can be obtained. If this value can be believed, the various hold temperatures of 300°C or greater caused a shift in the Tg to over 200°C. However, on successive up ramps the transition remained in the 160°C region. This splitting of Tg values can be explained easily if the rates of heating were different. These samples were run at the same rate, therefore this explanation can not be valid. The different glass transition temperatures could be due to the complex mixture of amorphous and various crystalline states. The only clear result of the glass transition studies was that the 380°C hold eliminated the softening point. This again supports a high degree of crystallinity in the solid after this hold.

An unfortunate result of this data is that only one endothermic peak occurred. By definition an LCP must have two or more first order phase transitions, which should be observable by a DSC trace. A known liquid crystal was run in the DSC which gave the output in figure 8. The large transition around 75°C is the melting peak and if significant is size due heat required to change the solid to a liquid

crystalline state. The next, much smaller peak (≈90°C) shows the transition from one liquid crystalline state to another. A logical assumption would be that this peak represents a smectic to a nematic mesophase transition. The last peak (≈122°C) would be the clearing temperature to isotropic melt which is a necessary transition that all LCPs must have. The heat of transition values for the second and third peaks are roughly 5% as large as the melting endotherm. The melting endotherm for syn9 averaged around 9 J/g. If the assumption of relative heats of transition holds, then one might expect these following transitions to be on the order of 0.5 J/g. This very small value may not appear as a peak due to the peak being indistinguishable from the background noise.

It is also possible that the DSC ramps were being run at too rapid a pace to detect multiple phase transitions. Three simple temperature ramps (200-350°C) were run at varying rates (Figures 9 a,b, and c). The first was at the standard rate of 20°C/min , and a strong endothermic peak (312°C) was observed. Next the rate was slowed to 10°C/min and the same peak became more spread out, but still in the same position. Lastly, the syn9 sample was heated at 5°C/min and the peak in question was distributed over many temperatures, and did not resemble a typical first order transition any longer. This endothermic peak was still centered around 312°C, but started to resemble a Tg transition. Therefore the rate did not elicit any new peaks, but the individual transitions may not be separable. This could help explain the smearing in this case, if there

were more than one transition represented there.

Polarizing Microscope

Most of the DSC data correlated well with the findings of Dr. Edward T. Samulski at The University of North Carolina at Chapel Hill. A sample of syn9 was sent in order to be run in a polarizing microscope which is an instrument not available at William and Mary. A polarizing microscope has the ability to heat the sample while being carefully viewed through a microscope. Using this instrument, a glass transition was detected at 150°C along with a clear transition to a fluid, birefringent melt at 315°C. Dr. Samulski believes that this liquid crystalline phase is nematic and also unusually fluid. Most importantly the elusive isotropic phase transition was finally observed. This transition to an unordered state occurred around 415°C although some decomposition had begun. In addition, a return to the LC phases was difficult. Finally, this study also reported an arbitrary "softening" temperature at 260°C where the sample first became birefringent. From this additional data it is clear that syn9 is a LCP, and the holds are operating on a very fluid, nematic mesophase.

DSC Data File: sy820
Sample Weight: 5.860 mg
Sun Feb 07 14:47:00 1993
syn9 (fresh); empty ref.

PERKIN-ELMER Figure 4
7 Series Thermal Analysis System

ramp 100-340-300(hr)-340-100

TEMP 1:	100.0 C	TIME 1:	0.0 min	RATE 1:	20.0 C/min
TEMP 2:	340.0 C	TIME 2:	0.0 min	RATE 2:	20.0 C/min
TEMP 3:	300.0 C	TIME 3:	60.0 min	RATE 3:	20.0 C/min
TEMP 4:	340.0 C	TIME 4:	0.0 min	RATE 4:	20.0 C/min
TEMP 5:	100.0 C				

DSC Data File: ey922
Sample Weight: 5.170 mg
Tue Mar 16 15:20:31 1993
ey99 empty ref.

PERKIN-ELMER
7 Series Thermal Analysis System

Figure 5

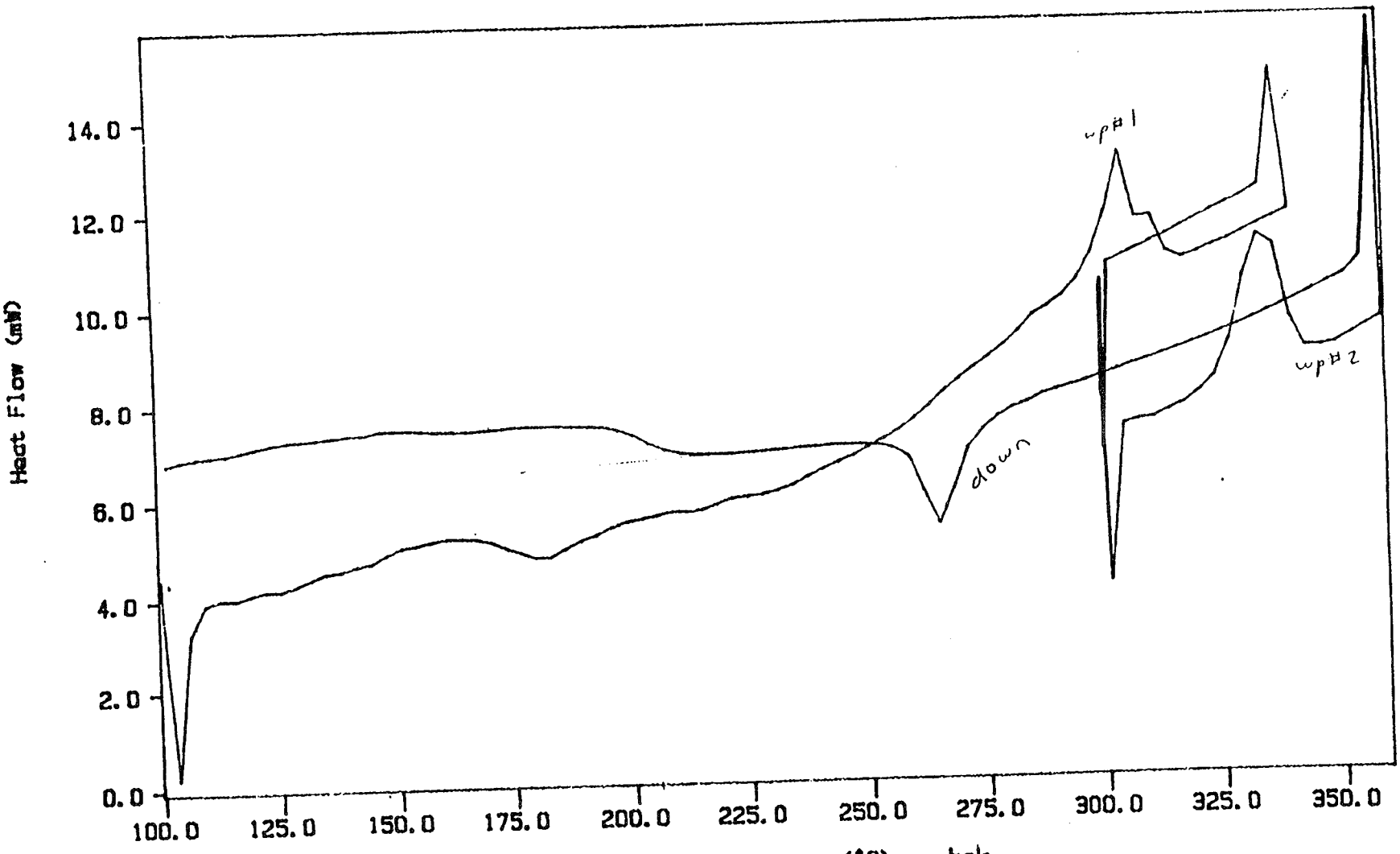

ramp 100-340-300(4hr)-360-100

TEMP 1:	100.0 C	TIME 1:	0.0 min	RATE 1:	20.0 C/min
TEMP 2:	340.0 C	TIME 2:	0.0 min	RATE 2:	20.0 C/min
TEMP 3:	300.0 C	TIME 3:	240.0 min	RATE 3:	20.0 C/min
TEMP 4:	360.0 C	TIME 4:	0.0 min	RATE 4:	20.0 C/min
TEMP 5:	100.0 C				

DSC Data File: sy919
Sample Weight: 5.590 mg
Tue Feb 02 16:26:10 1993
syn9 (fresh); empty ref.

PERKIN-ELMER

Figure 6

7 Series Thermal Analysis System

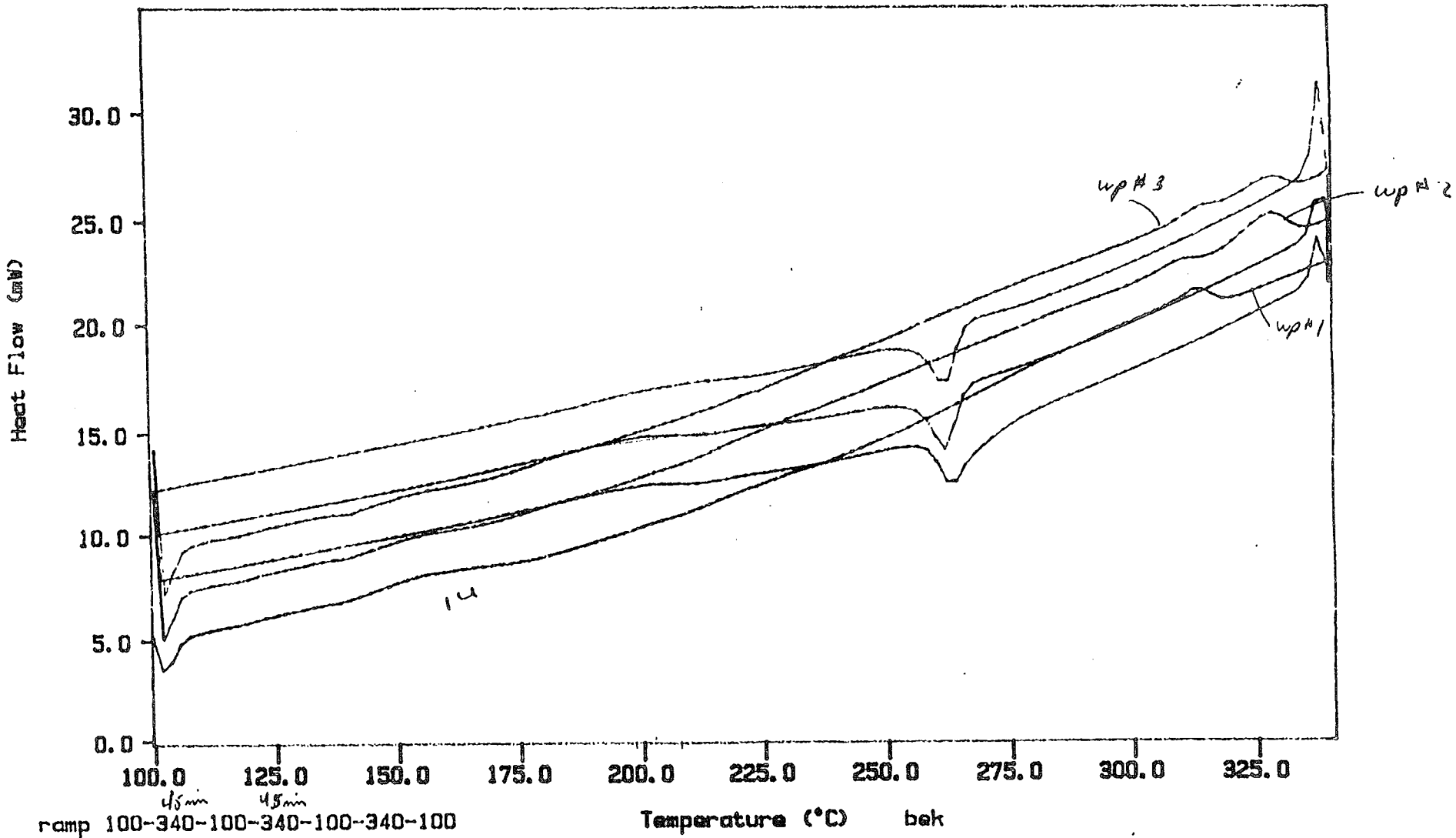

ramp 100-340-100-340-100-340-100

TEMP 1:	100.0 C	TIME 1:	0.0 min	RATE 1:	20.0 C/min
TEMP 2:	340.0 C	TIME 2:	45.0 min	RATE 2:	20.0 C/min
TEMP 3:	100.0 C	TIME 3:	0.0 min	RATE 3:	20.0 C/min
TEMP 4:	340.0 C	TIME 4:	45.0 min	RATE 4:	20.0 C/min
TEMP 5:	100.0 C	TIME 5:	0.0 min	RATE 5:	20.0 C/min
TEMP 6:	340.0 C	TIME 6:	0.0 min	RATE 6:	20.0 C/min
TEMP 7:	100.0 C				

DSC Data File: ey818
Sample Weight: 5.540 mg
Mon Feb 01 14:49:31 1993
ey18 (fresh); empty ref

PERKIN-ELMER Figure 7a
7 Series Thermal Analysis System exp #1

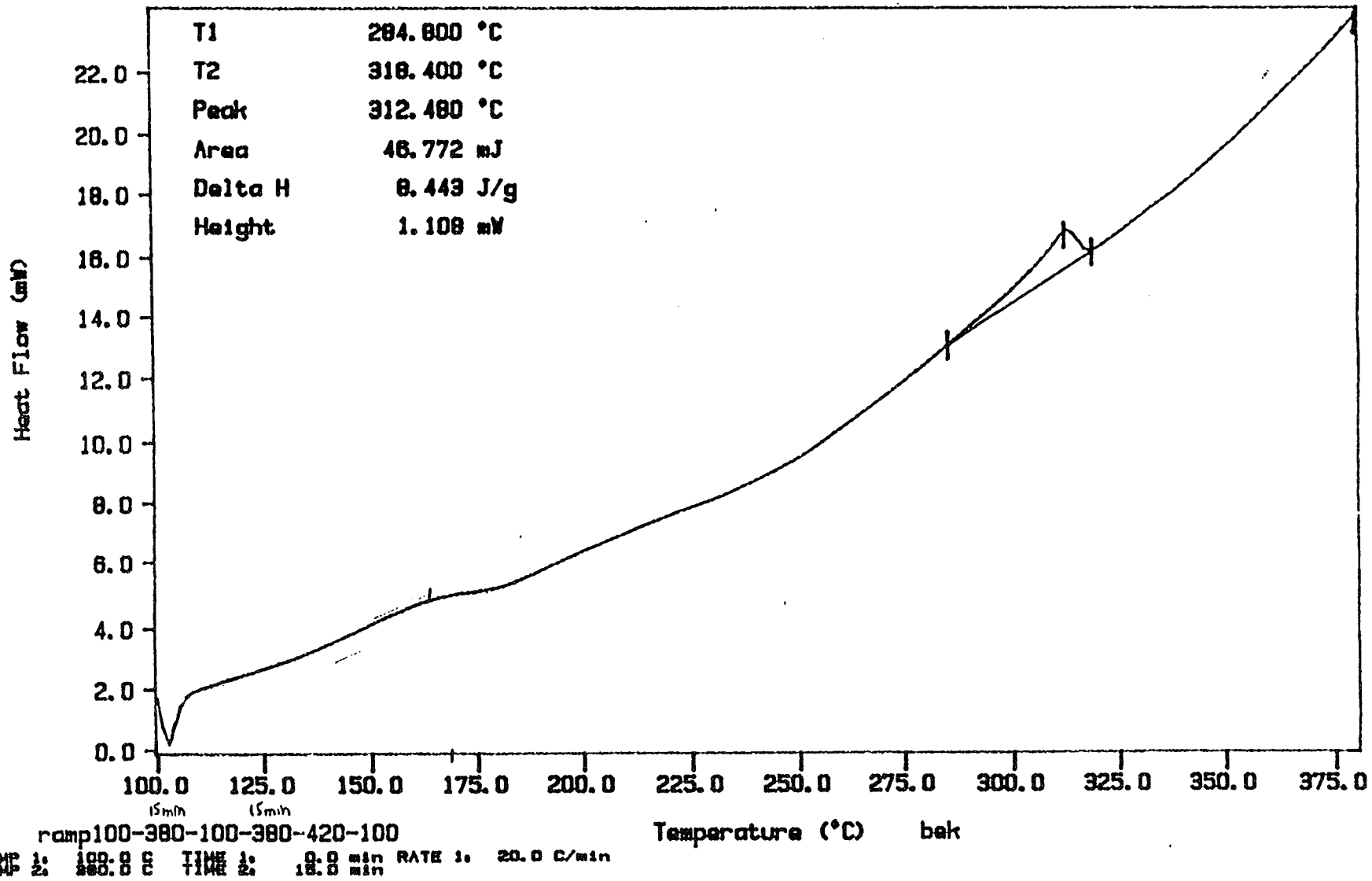

DSC Data File: ey918
Sample Weight: 5.540 mg
Mon Feb 01 14:49:31 1993
ey9 (fresh); empty ref

PERKIN-ELMER Figure 7b
7 Series Thermal Analysis System exp # 2

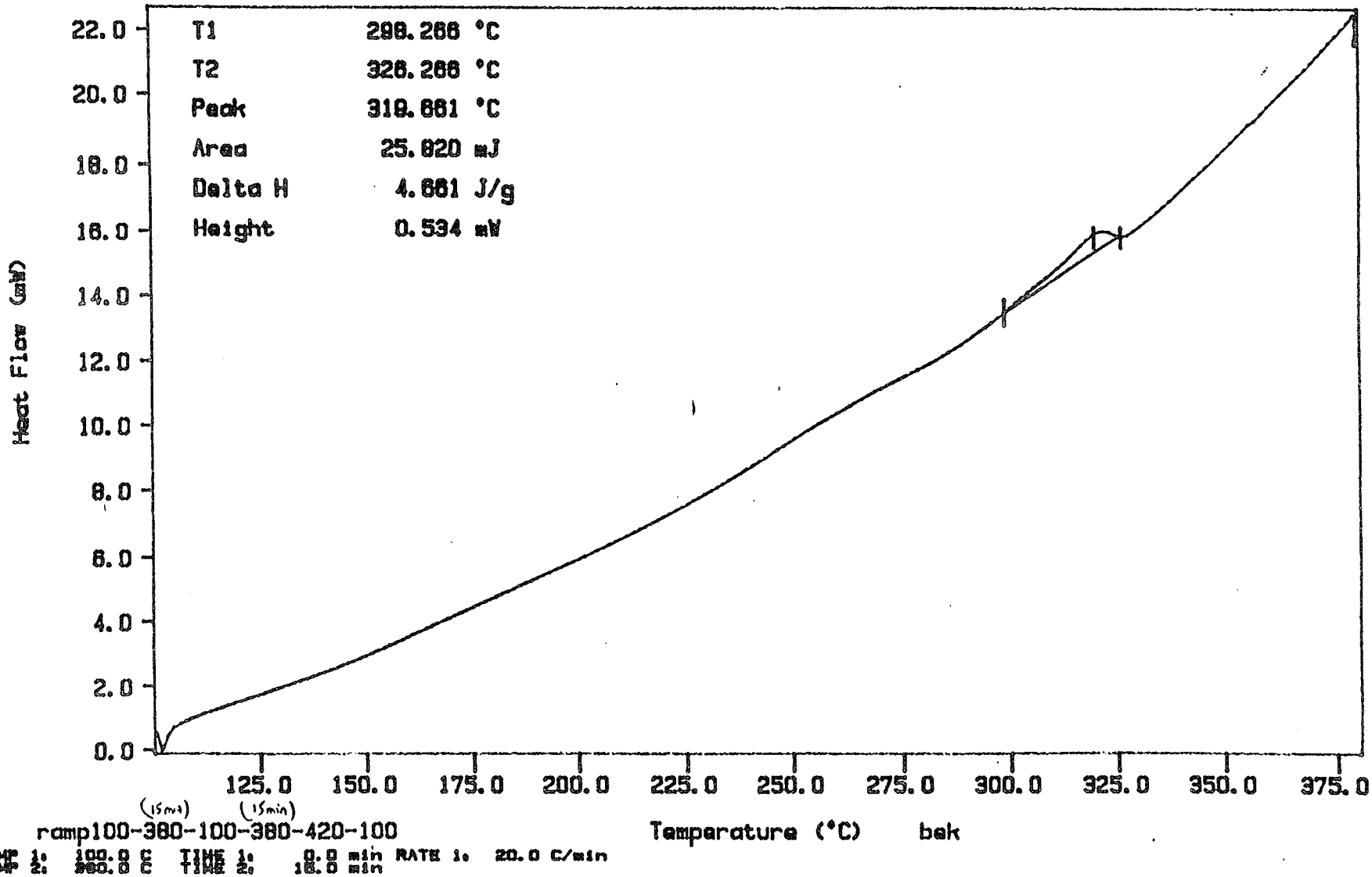

DSC Data File: ey918
Sample Weight: 5.540 mg
Mon Feb 01 14:49:31 1993
eyn9 (fresh); empty ref

PERKIN-ELMER Figure 7c
7 Series Thermal Analysis System wp#3

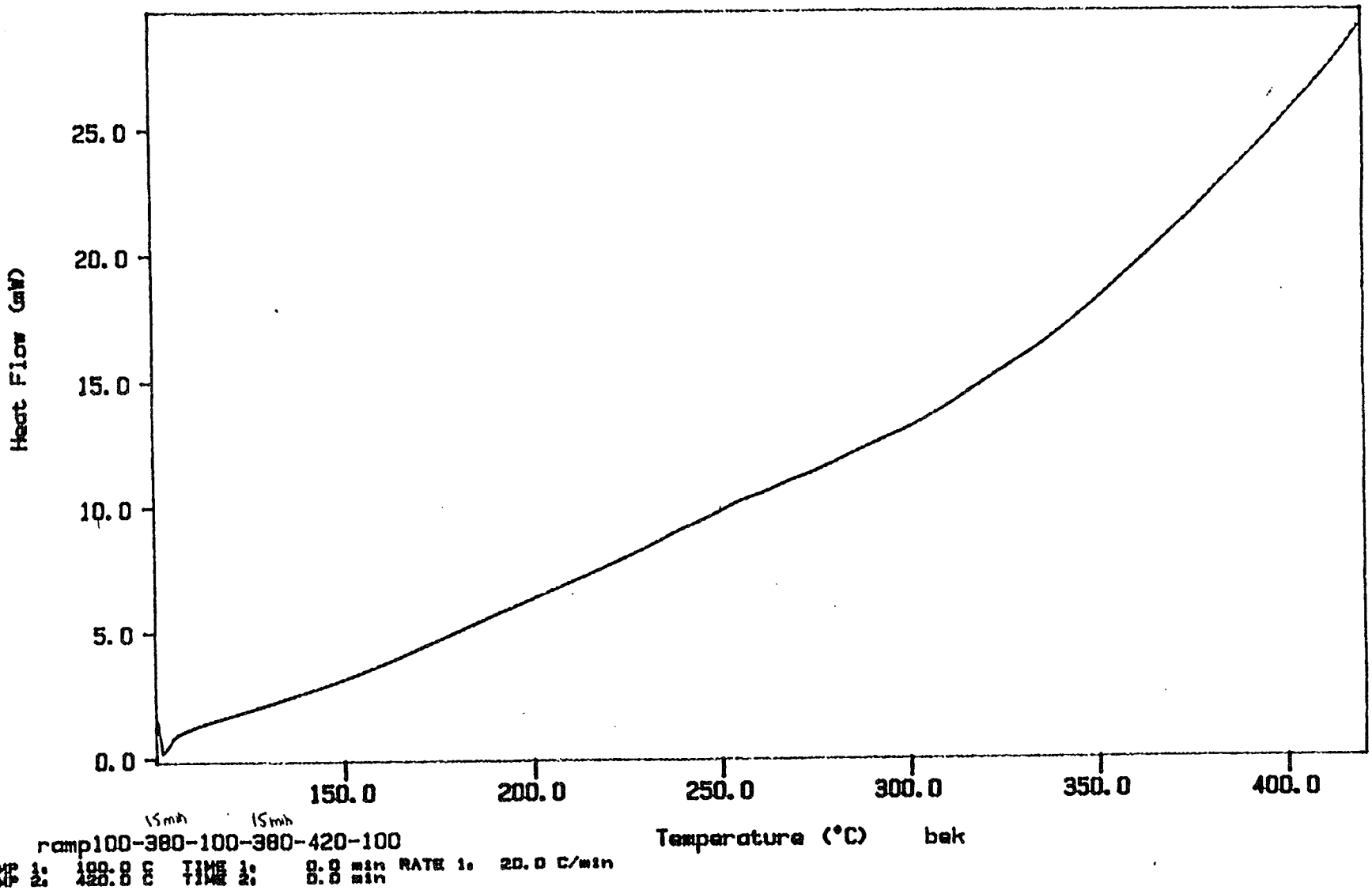

40 40 40 10°C/min

DSC Data File: tlqcr
Sample Weight: 5.200 mg
Sun Jun 21 21:56:35 1992
True Liquid Crystal (fresh); empty ref.

PERKIN-ELMER Figure 8
7 Series Thermal Analysis System

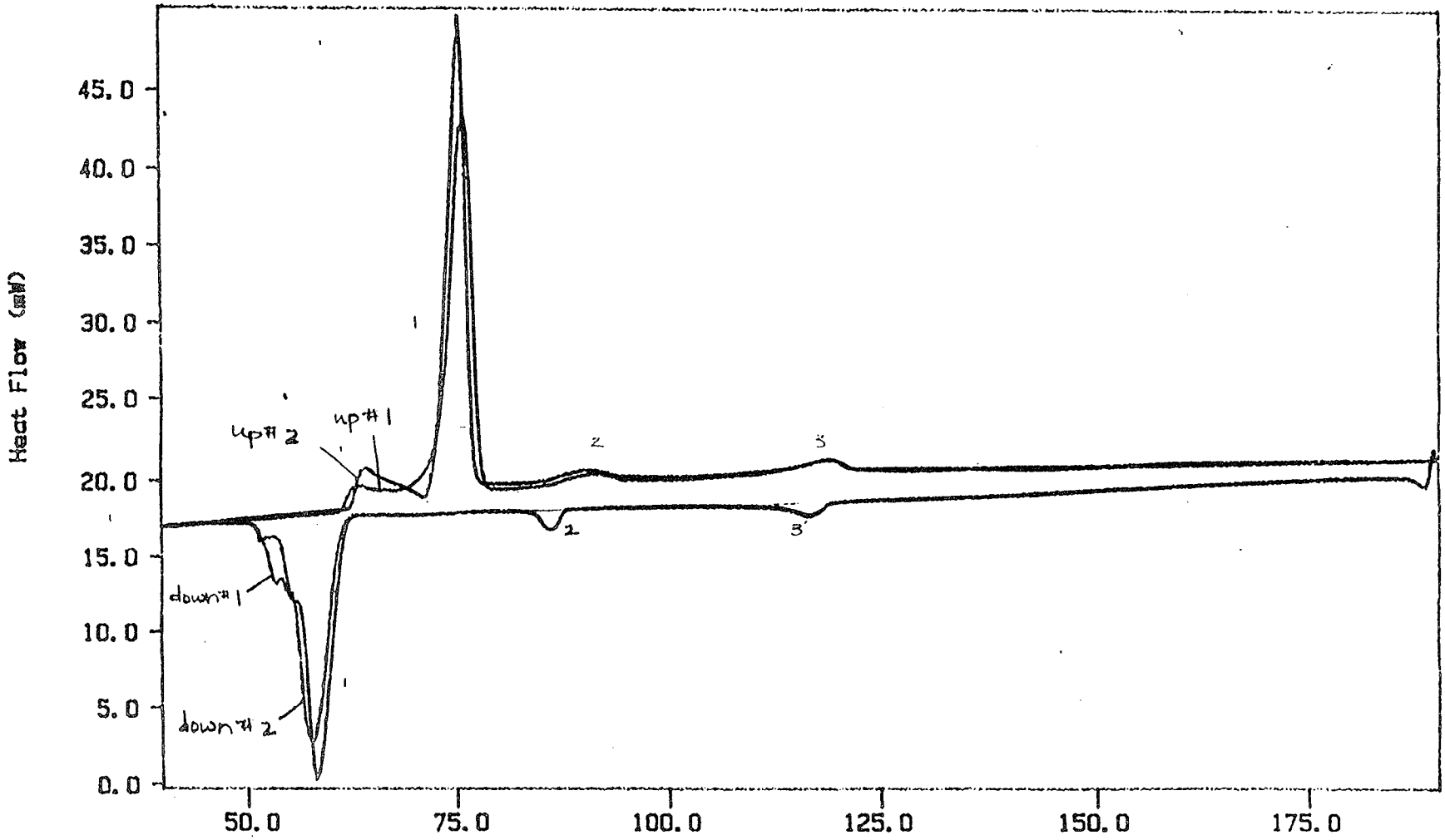

Ramp 40-190-40-190-40C 10C/min

TEMP 1:	40.0 C	TIME 1:	0.0 min	RATE 1:	10.0 C/min
TEMP 2:	190.0 C	TIME 2:	0.0 min	RATE 2:	10.0 C/min
TEMP 3:	40.0 C	TIME 3:	0.0 min	RATE 3:	10.0 C/min
TEMP 4:	190.0 C	TIME 4:	0.0 min	RATE 4:	10.0 C/min
TEMP 5:	40.0 C				

Temperature (°C) cke

down #1 → 3.2 J/g peak 2
2.803 J/g peak 3
78.956 J/g peak 1

down #2 → 78.193 J/g peak 1
3.229 J/g peak 2

up #1 → 102.423 J/g peak 1
2.579 J/g peak 2
4.505 J/g peak 3

up #2 → 97.395 J/g peak 1
3.180 J/g peak 2

DSC Data File: ey924
Sample Weight: 5.310 mg
Fri Apr 02 15:12:57 1993
ey#9 (fresh); empty ref

PERKIN-ELMER Figure 9a
7 Series Thermal Analysis System

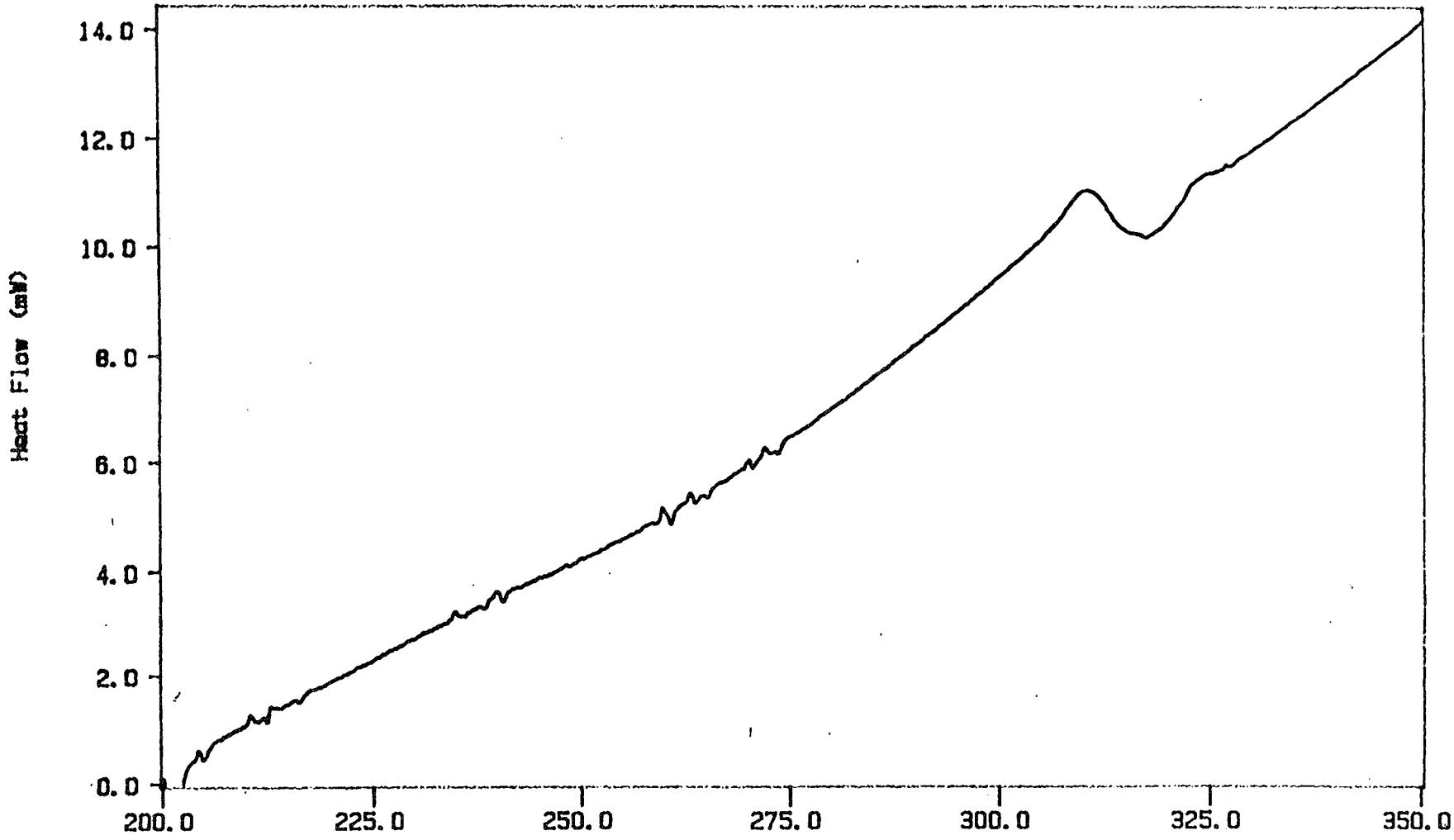

ramp 200-350 20C/min
TEMP 1: 200.0 C TIME 1: 0.0 min RATE 1: 20.0 C/min
TEMP 2: 350.0 C

DSC Data File: ey925
Sample Weight: 5.100 mg
Fri Apr 02 15:38:31 1993
ey9 (fresh); empty ref

PERKIN-ELMER

Figure 9b

7 Series Thermal Analysis System

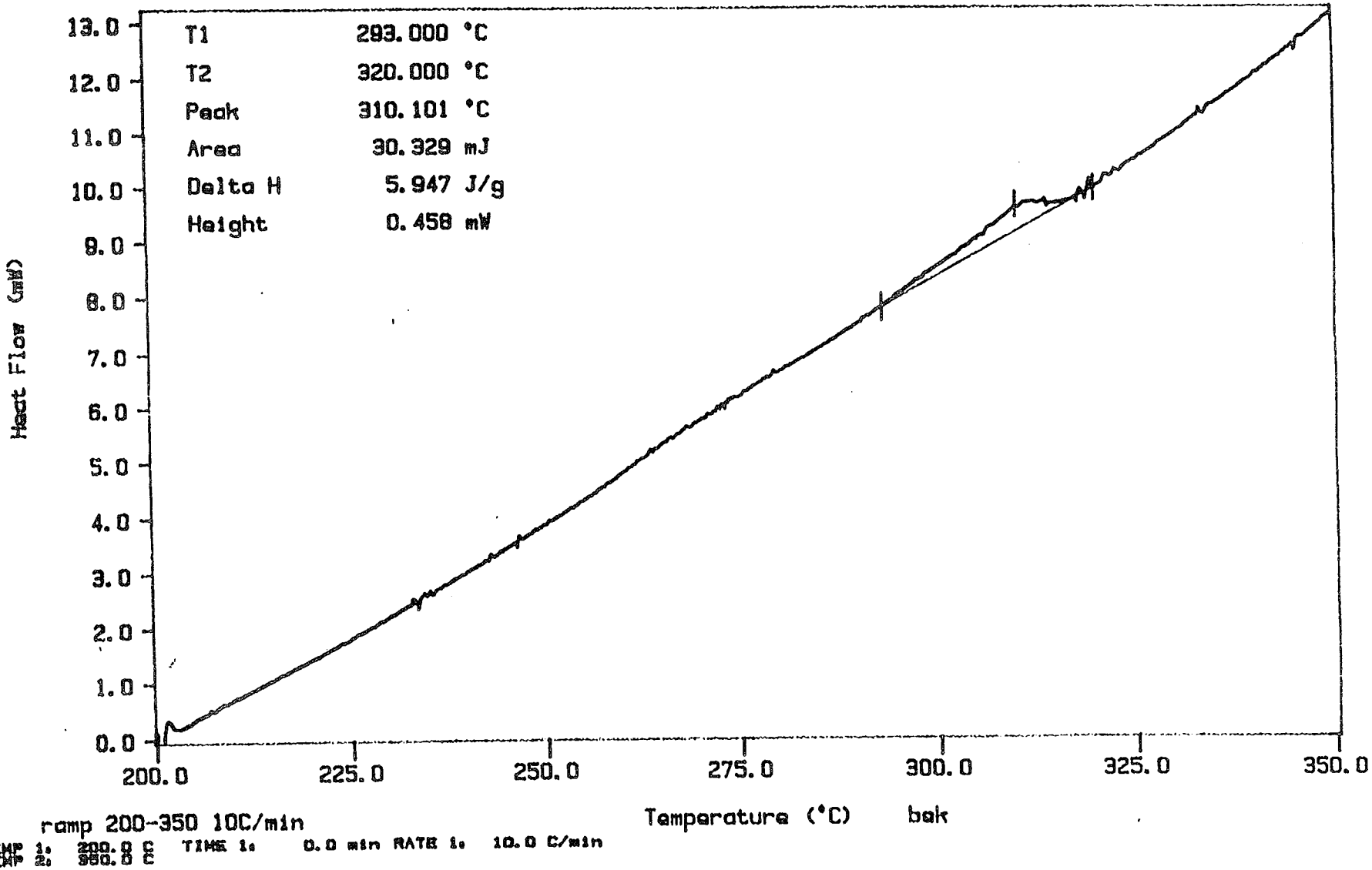

ramp 200-350 10C/min

TEMP 1: 200.0 C TIME 1: 0.0 min RATE 1: 10.0 C/min
TEMP 2: 350.0 C

DSC Data File: ey928
Sample Weight: 5.000 mg
Fri Apr 02 16:20:53 1993
ey99 (fresh): empty ref

PERKIN-ELMER

7 Series Thermal Analysis System

Figure 9c

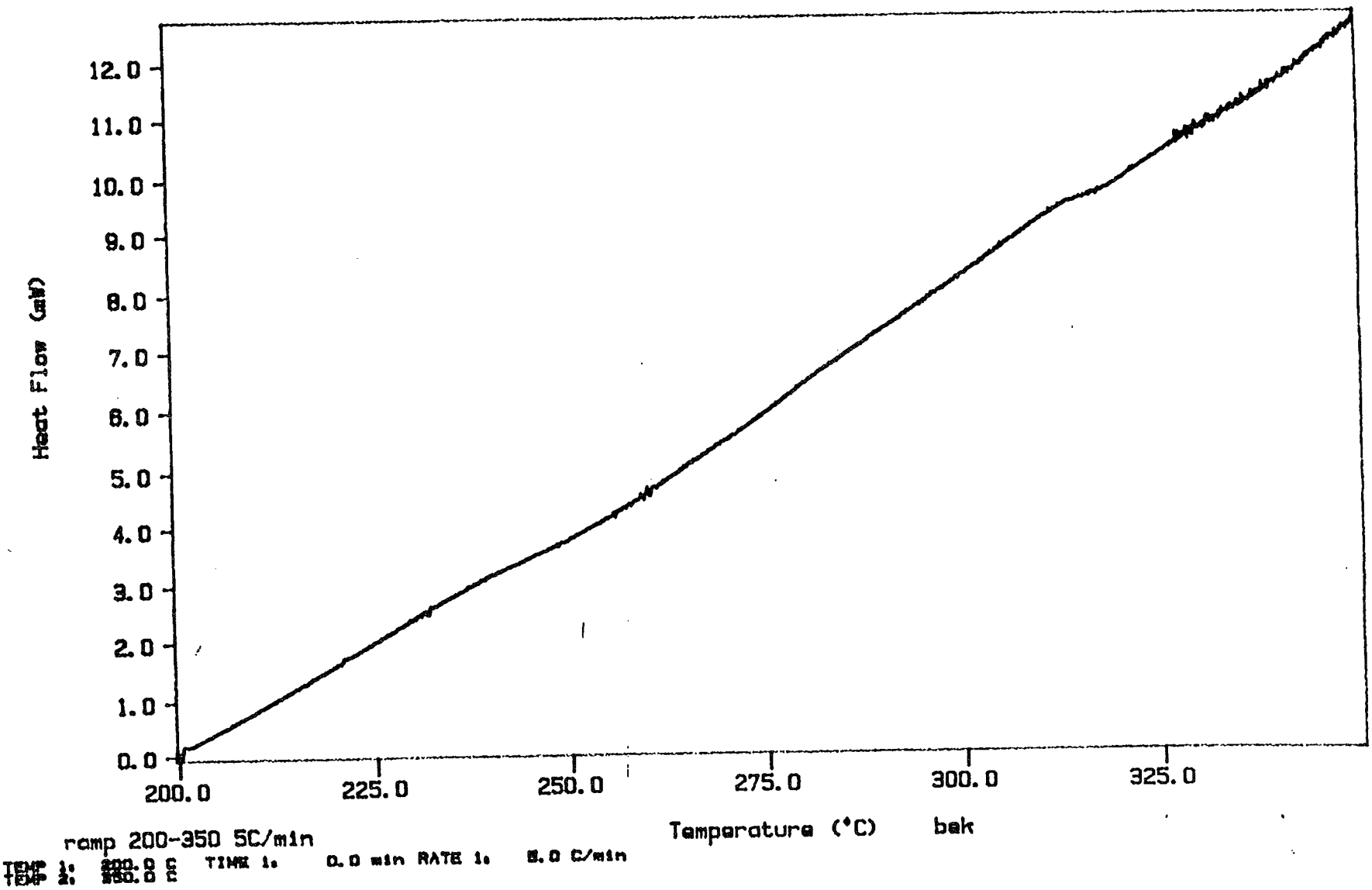

Chapter 4

FDEMS

The second major technique that was employed to characterize syn9 was FDEMS. FDEMS stands for Frequency Dependent Electromagnetic Sensing. This is a method by which cure processes can be monitored on a molecular level. FDEMS is based on the fact that any molecule is either polar or is capable of having an induced dipole. Polarization is a term which describes this separation of positive and negative charge within a molecule[6]. If a material is placed in an alternating electric field, the dipoles of the molecules in that dielectric material will attempt to line themselves up with the field. A simple parallel plate capacitor can be used to model FDEMS measurements. In this representation one of the plates carries a positive charge while the other is negative. Between these parallel plates an electric field will exist. When a dielectric material is placed between the plates it becomes polarized in the manner described above. Each material will obviously have a differing extent to which it can be polarized. In addition the polarizability is dependent on the state of that system. The polarizability of a molecule can be defined as the average molecular polarized dipole induced by an electric field of unit strength[7]. When an alternating electric field is applied to the capacitor, the polarizable material will attempt to change its orientation to

one that aligns with the given field (figure 10).

Figure 10

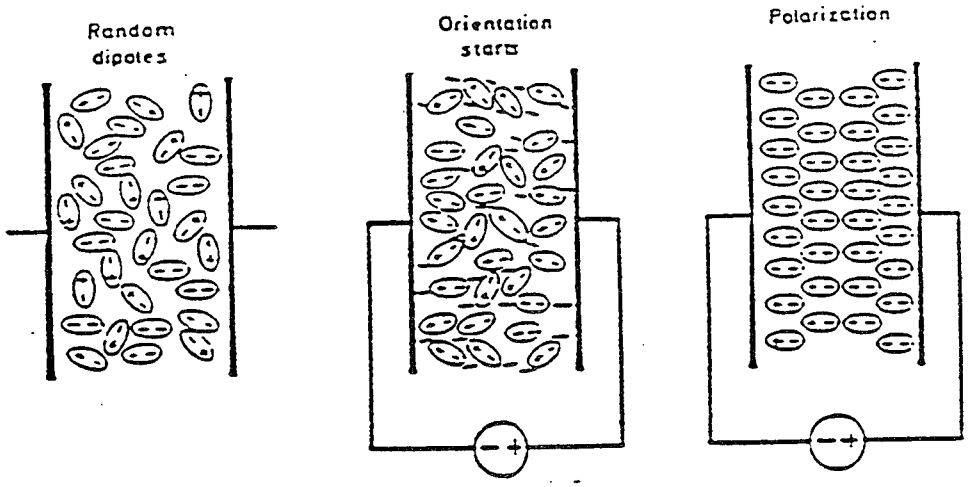

There are two dielectric components that arise from the capacitor model. The first relates the initial capacitance (C_o) with the capacitance impeded by the dielectric material (C). This relationship is given by equation 1.

$$(1)\quad \epsilon' = C/C_o$$

The second similarity relates the conductance which is frequency dependent as well. The frequency arises from the alternating applied electric field. This equation is given by equation 2.

$$(2)\quad \epsilon'' = G/(C_o 2\pi f)$$

In equation 2 the conductance is given by G and the frequency

by f.

ϵ' expresses the dielectric permitivity and ϵ'' represents the dielectric loss factor. The loss represented in ϵ'' is due to the time dependent nature of the polarization and conduction. Both ϵ' and ϵ'' have dipolar and ionic components[6] shown by equations 3 and 4.

$$(3)\quad \epsilon' = \epsilon_D' + \epsilon_I'$$

$$(4)\quad \epsilon'' = \epsilon_D'' + \epsilon_I''$$

The dipolar term results from individual molecular dipole moments. The ionic term dominates in fluid samples that give rise to mobile ions. These ions can migrate towards the charged plates and produce localized layers of charge. Therefore the ionic term will dominate during periods of low viscosity, low frequencies, and high temperatures. The two graphs of interest plot $\log\epsilon''*w$ and ϵ' with frequencies ranging from the Hz to the MHz regions. This plot is made verses time and has a temperature axis as well. An overlap of the ϵ'' values of differing frequencies in the $\log\epsilon''*w$ graph implies that ionic translational diffusion is the dominant physical process affecting the loss term[7]. On a macroscopic level the sample is becoming fluid and the sample is said to have "wet out" the sensor. An approximate melting temperature can be derived from this overlapping of $\log\epsilon''*w$ values.

Peaks in the $\log\epsilon''*w$ frequencies represent when dipolar rotational diffusion process contribute to ϵ''. These peaks will be referred henceforth simply as dipolar peaks. A

decrease in the logϵ"*w values for a given frequency infers a decreased mobility of the ions[7]. This obviously accompanies the decreasing temperatures in the down ramps but is a particularly interesting occurrence during a steady temperature hold.

The values for ϵ' and ϵ" are acquired from measurements of conductance and capacitance throughout a range of frequencies from 5 Hz to 1 MHz. Conductance and capacitance are converted to ϵ' and ϵ" by DekDyne Data Acquisition Software. FDEMS measurements are made with an impedance analyzer. Both the Hewlett-Packard 4192 A LF and the Solartron 1260 were used in data collection, and each was controlled by an IBM compatible 386 personal computer. The key to the data collection however lies in the sensors developed by Dr. Kranbuehl. Each sensor has an array of interdigitated electrodes (figure 11) made of gold on a ceramic plate. These sensors are designed to withstand temperatures incurred during cure cycles of over 400°C.

Figure 11
Interdigitated Electrodes

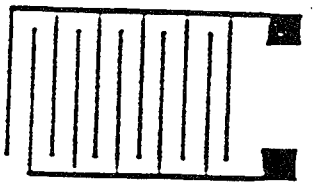

In this experiment the sample of syn9, which has yet to be heat treated, was ground finely and placed on the sensor. Enough sample was used in order to insure that the entire

sensor was covered. The syn9 comes in a very granular form and was ground to make certain that an even pressure would be applied. An uneven pressure could cause the sensor to break. The sample and mounting apparatus was then placed in a Model C Carver Thermal Laboratory Press and ramped through the desired temperature cycles.

An effort was made to correlate the FDEMS runs with certain DSC ramps. Just as in the DSC, a 4 hour hold at 274°C was preformed (figure 12). Similarly, the sample was ramped to 340°C in order to "wet out" the sensor, and then allowed to stabilize at the desired temperature for 4 hours. A careful study of the logϵ"*w data shows most of the various frequency dependent values remain steady throughout the hold. Therefore the ionic mobility is constant in this range of cure. Once the hold is completed, the sample is allowed to cool. Upon cooling the characteristic dipolar peaks are observed. These dipolar peaks show the rotational diffusion process contributing to ϵ". One would say the 274°C sample of syn9 has a considerable amorphous portion because there is still much rotational diffusion of the dipoles. An elimination of the dipolar peaks would express an increased percent crystallinity or perhaps even a complete elimination of the amorphous portion of the polymer. This effect is due to the dipoles rotation being hindered by a tight packing or an increased crystalline ordering. The dielectric permitivity, ϵ', also remained very steady for the lower frequencies of interest.

The next FDEMS run followed an initial ramp to 366°C with a second to 388°C (figure 13). The first ramp clearly had dipolar peaks along the down ramp. These were mirrored in the up ramp of the second temperature cycle. It is important to note the second ramp stalled for approximately 10 minutes above 380°C. In any case this second ramp was sufficient to eliminate the dipolar peaks. This might relate back to the phenomena observed in the DSC holds (see figure 7).

A corresponding 340°C hold run was then conducted (figure 14). The initial melting ramp elicited the same results, although a higher temperature was reached (376°C). The second ramp was intended to hold at 340°C, but instead showed a drop of 20°C during the hold. The ϵ'' values during this hold were clearly decreasing. Unfortunately, one cannot be sure if this decreased mobility was a function of the decreasing temperature or due to some ordering effect. After the hold it is useful to note that the dipolar peaks, while still present have been significantly diminished in intensity.

Finally the effects of a 90 minute hold at 380°C were studied (figure 15). As before two ramps were preformed, and the first one showed the same results as the previous runs. Fortunately, this hold was very steady at 386°C and the ϵ'' values behavior during the hold are now relevant. The ϵ'' values were noticeably decreasing which implies a decreased mobility of the dipoles. Since the temperature was constant, another factor must be contributing to this decrease. Most likely this liquid state is becoming more ordered while being

held at this temperature. Two runs of this nature were preformed, but the second displayed a much less consistent hold. Unfortunately, a temperature hump again occurred so their was a temperature dependence playing a role in the reduced mobility. In both cases it is clear however that these holds were sufficient to eliminate the dipolar peaks that typically occur with decreasing temperatures. This would contribute to the conclusion that these LCP's are now more ordered, and perhaps a higher percent crystallinity upon returning to the solid form. A summary of all FDEMS data is presented in Table III. The Tg values were calculated by taking the highest point of the dipolar peaks and finding the temperature at that point. The melting point was found by approximating the point where all the loge"*w values come together. This is only an approximate value because many factors can effect this point. This sample might melt unevenly, it may not evenly cover the sensor, and the point of overlap is difficult to determine from the graph.

Table III

Hold Time &Temperature	Before Hold Dipolar Peak (Tg)	Tm	Tm(DSC)	After Hold DipolarPeak(Tg)
240min @274°C	-	283	312	192
10 min @380°C	179	295	312	None
60 min @340°C	173	312	312	173
90 min @380°C	177	306	312	None

HP kinetics
RTMP45

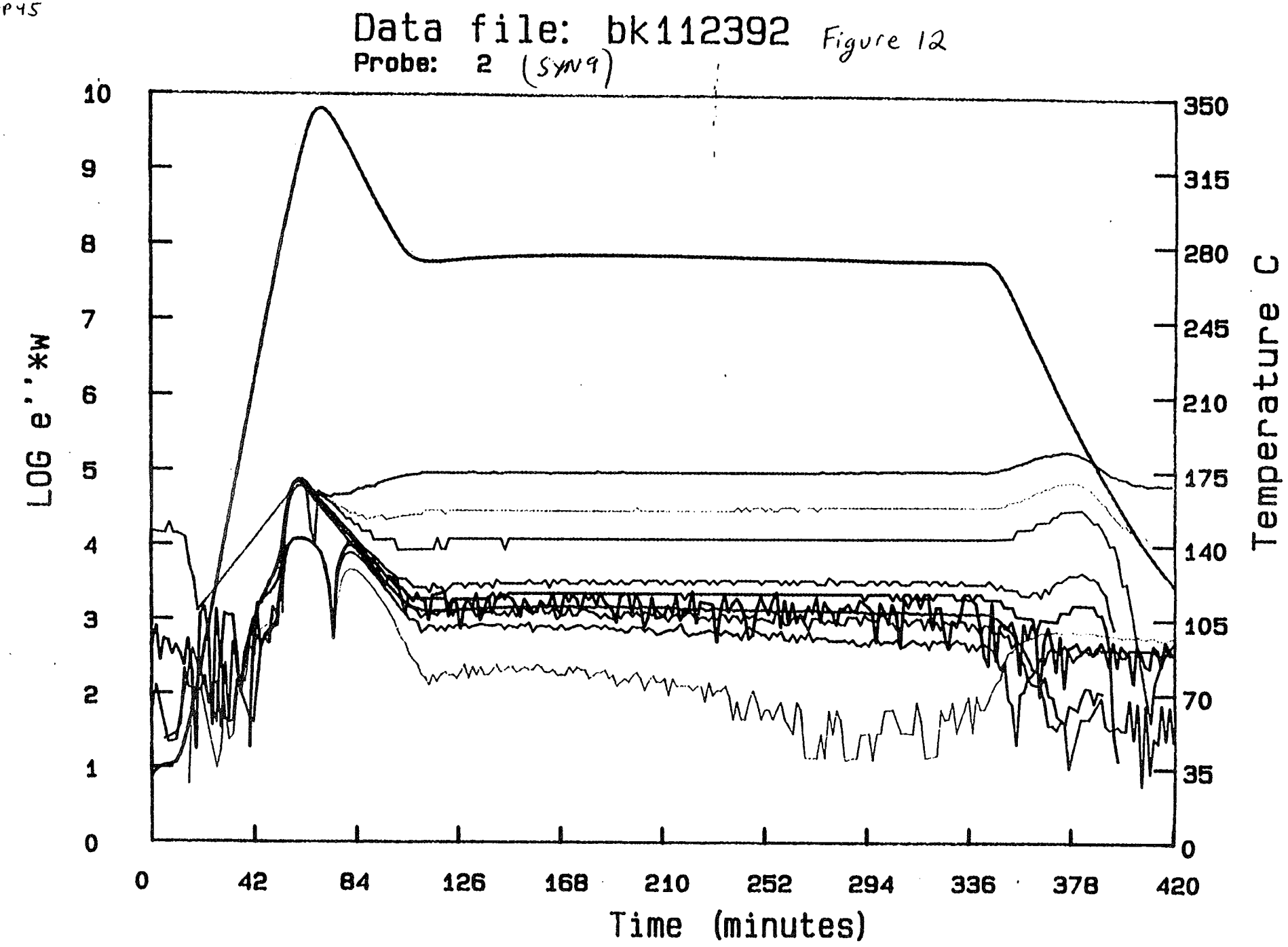

Figure 12

Data file: b:bk7992 Figure 13

Probe: 1 (sym 9)

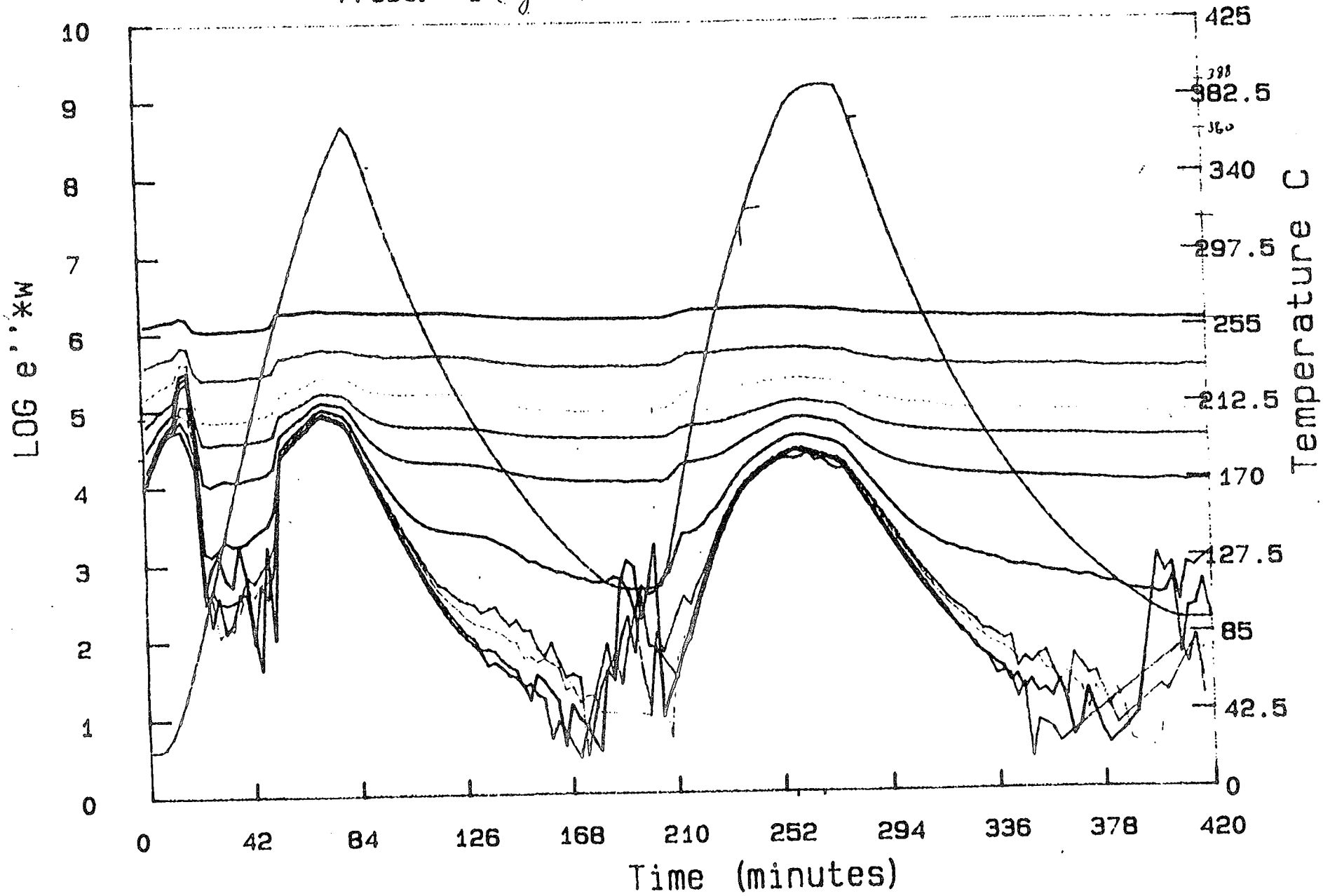

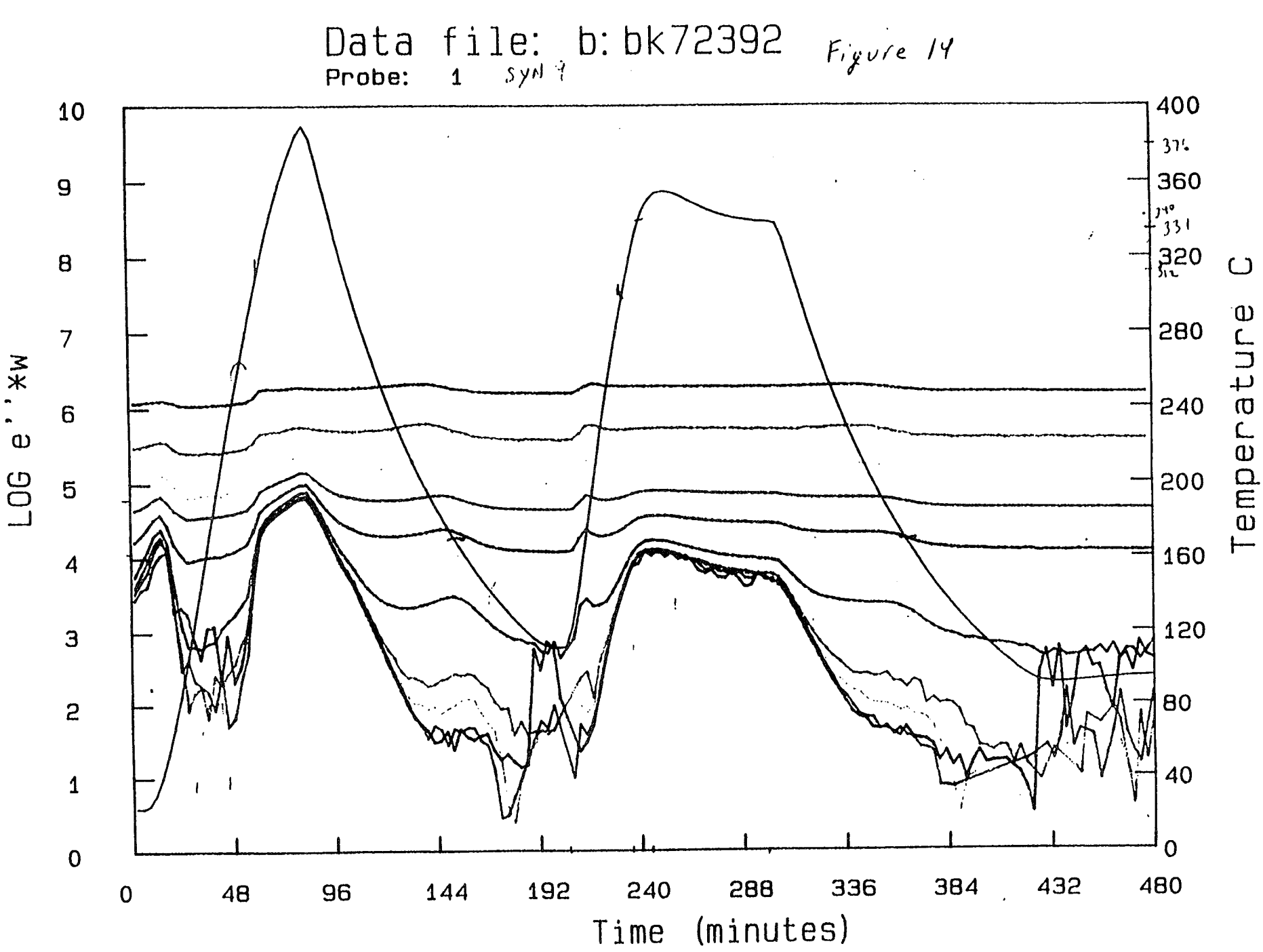
Data file: b:bk72392
Probe: 1
LOG e''*w
Temperature C
Time (minutes)
0
1
2
3
4
5
6
7
8
9
10
0
40
80
120
160
200
240
280
320
360
400
0
48
96
144
192
240
288
336
384
432
480

Figure 14

Data file: B: ma62292 Figure 15

Probe: 2 syn 9

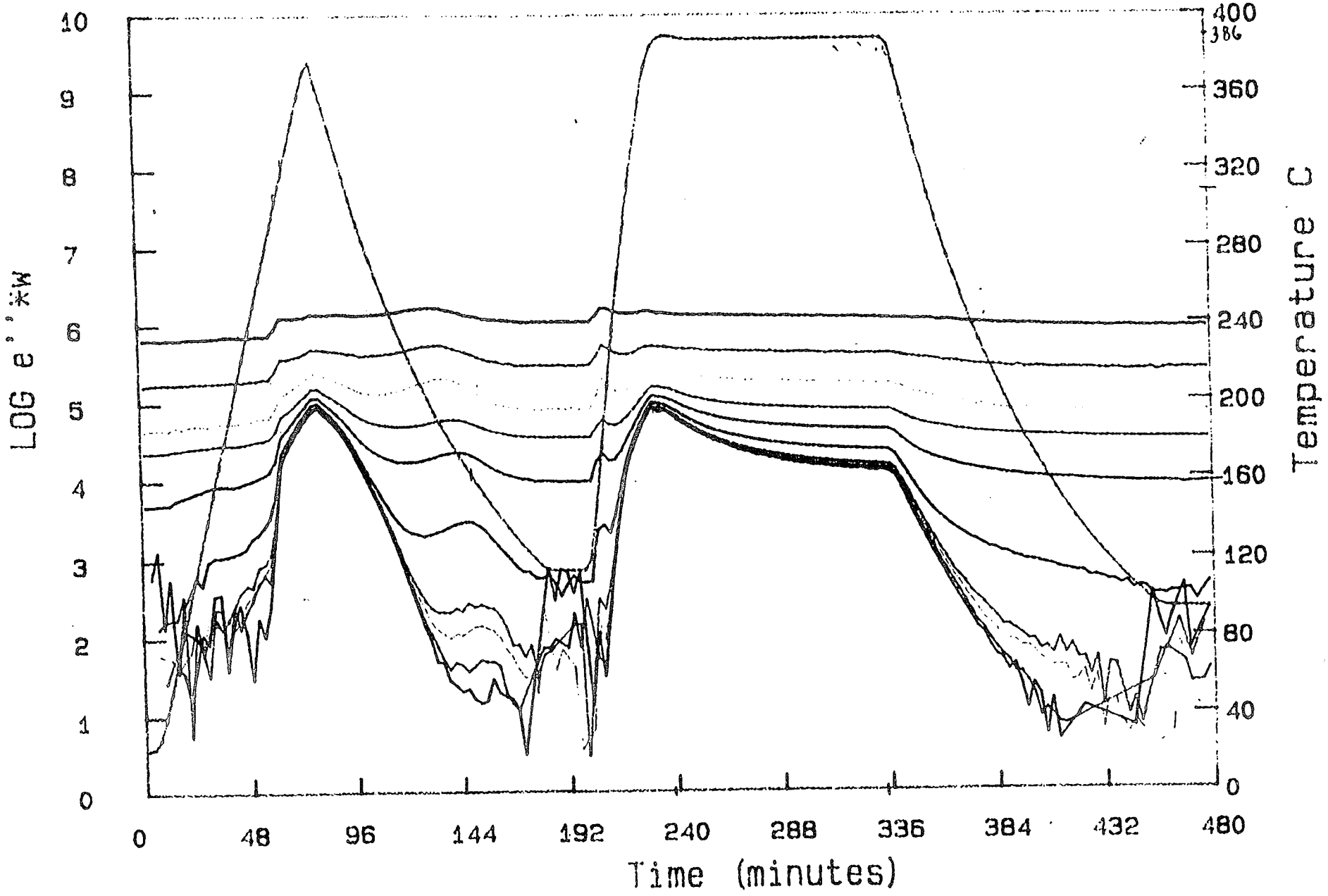

Chapter 5

FT-IR

The changes noted in the dielectric and DSC data were clear and have been documented, but the nature of these changes has not been determined. The differences could be a result of chemical or physical changes. The FT-IR was employed to determine which of these two options was the case. The FT-IR is an infrared spectral analyzer formally known as the Fourier Transform Infrared Spectrometer. This device generates an infrared spectra (4000-400 cm-1) just as a typical dispersive instrument, but has a number of advantages. First, all of the frequencies are measured simultaneously which would allow for a rapid scan. An average number of scans can be used to create the spectra rather than only using a single scan. The frequency scale used is generated by a very accurate and stable Ne-He laser. The energy throughput is greater with the FT-IR and the problem of stray light is almost negligible. The gratings or filters found in dispersive IR instruments must be changed causing discontinuities on the spectra. The problem is avoided through FT-IR measurements. Finally, due to the simultaneous frequencies a constant resolution is guaranteed.

The process of producing an FT-IR spectra begins with the stable Ne-He laser beam. This beam is split in two and a path difference is introduced. The beam is then combined through

the use of mirrors and directed into the sample. When the beams are recombined an interference pattern is obtained as the path difference is varied. An interferogram is generated which represents this path difference and is measured by recording the detector signal as a function of that path difference of the two beams. Typically a background interferogram is run and then is subtracted from the sample interferogram to give the sample's true spectra. The absorbance/transmittance plots that are customary for IR spectra are a result of the Fourier Transformation. The process analysis the interferogram as a sum of sine and cosine waves with discrete frequencies[6]. The set of frequencies is chosen such that the exact number of complete cycles matches the length of the interferogram from zero path difference to maximum path difference. These frequencies will produce the data points in the final spectra, which are typically reported as wavenumbers (cm-1). The sample cell was a Model 6003 Photoacoustic Sample call and detection is through a small microphone located within the cell. A carbon black background was first run and then the sample was placed on this black soot-like material in the cell. The syn9 sample was run in a Nicolet 20DXB FT-IR Spectrometer.

The effects of heat treatment on the sample's spectra were observed in order to determine if changes noted earlier were chemical or physical. Presumably if the spectra's bands appeared to stretch at the same frequencies after heat treatment, then no chemical rearrangement was occurring. A

similar spectra would support the argument that the polymer remains intact and undergoes a physical reordering, but not chemical reactions. A fresh sample was placed in the sample chamber and the resulting spectra serves as a basis of comparison for the heat treated samples. A fresh sample was then heated for thirty minutes at only 100°C and returned to the analyzer. This heated sample showed no change in any of the spectral bands. Next the sample was heated up to 200°C for another half hour. In the bending region of the spectra (low wavenumbers; below 1000 cm-1) no change occurred, but in the carbonyl stretching region a small trend was beginning. On the previous two spectras, a pronounced ester peak at 1740 cm-1 was accompanied by another at 1800 cm-1. The 1740 cm-1 peak tailed off slowly to the 1700 cm-1 region but no distinctive peak could be seen there. The 200°C spectra showed a clear peak at 1680 cm-1, and a clear decrease in the relative size of the 1800 cm-1 peak. Next the sample was taken to approximately 280°C. This was still below the flow temperature, but the first visually observable changes were taken place. The tan color of the sample darkened to a deep brown. This might refer to the observable "softening" that Dr. Samulski reported. The spectra for this sample reemphasized the trends noted above. The peak at 1800 cm-1 was completely eliminated while the one at 1700 cm-1 began to rival the 1740 cm-1 peak in intensity. Secondly, another trend is that the absorbance of the bands is occurring at reduced values. Unfortunately, this second trend becomes a debilitating factor

once flow has occurred, because the intensity of the signal is so reduced that it is difficult to compare with the fresh spectra. An uncured sample just past flow was just legible and confirmed the new carbonyl stretch rearrangement. Many of the cured samples from dielectric runs provided no useful information.

It is known that the chemical environment effects the position of the carbonyl stretches. This environment includes the surrounding molecules nonbonded interactions. Hydrogen bonding of adjacent molecules would have such an effect. It is likely that the amorphous fresh polymer would have some solvent trapped within its framework. In this case the solvent for syn9 was methylene chloride (CH_2Cl_2). The heating of the polymer to 200-300°C for physical rearrangement since no flow had occurred, but would be sufficient for the liberation of trapped solvent. This would alter the environment of the carbonyls and would cause the observed shifting. Another possibility is that since the sample is above Tg, some ordering may be causing the carbonyl shift.

Chapter 6

Thermal Mechanical Analysis

The last apparatus measured the extent of increased mechanical properties through these hold cycles. The Thermal Mechanical Analyzer (TMA) accomplishes this through a penetration measurement. These experiments were fundamentally the most elementary but the results were some of the more perplexing. The pre-cured sample of syn9 was placed on a level platform in the analyzer. This sample was either chipped off of a dielectric sensor or similarly removed from an aluminum pan that was cured in a temperature controlled press. A smooth, flat sample was the ideal, but that could rarely be obtained. A probe, which can be adjusted for different types of mechanical measurements, consisted of simply a pin for a penetration run. This pin was lowed and placed on most uniform portion of the sample. A reading of the sample's thickness was then taken and the position of the sample's surface was then taken to be zero. The TMA is a penetration run measures the pin position relative to this initial setting. The amount of penetration (or expansion) is the plotted versus temperature (or time) as the sample is heated inside the TMA's furnace. The temperature is ramped in a preselected program. Typically the sample was heated until the temperature was reached that allowed the probe, which carried a load of -10.0 g, to penetrate the sample completely.

This point is typically a sharp drop-off and easily detected as the point at which the sample is fluid enough to allow full penetration. A glass transition can be seen if one watches the run take place. It is easier to see during the run because the penetration scale is smaller. It can be read off of the final graph, but because of the penetration axis being full scale makes it much more difficult.

The TMA experiments involved two different sets of samples: pre-cured without pressure and dielectric samples. The each of these sets involve three samples, the pre-cured samples without pressure were cured at temperatures of 380°C, 340°C, and 300°C.

The first sample was held at 380°C for 60 minutes, and then transferred to the TMA upon cooling to room temperature (Figure 16). This plot did show a clear glass transition around 159°C, and the sample was rapidly and completely penetrated at 262°C. By comparison another fresh sample of syn9 was cured in the same fashion, but at 340°C. The pin fully penetrated around 254°C, although the drop-off was not nearly as sharp. The 300°C sample resulted in an intermediate value of 258°C (Figure 17). One should note that the 300°C hold was preformed in the same manner as the DSC and the FDEMS runs, that is the sample was ramped above its melting temperature (to about 329°C) and then allowed to cool to the desired hold temperature.

The other TMA runs preformed from samples previously used in FDEMS data collection. After an FDEMS run the syn9 polymer

is cured and flattened on the sensor. One should note that a slight pressure was applied to these systems (see pg. 26). Now the sample must be chipped off and a flat sample must be obtained. The TMA runs were preformed in the same manner described above on these portions of cured syn9. The sample from the 240 minute hold at 274°C resulted in a complete penetration at 261°C. There was however a clear continual penetration long before this starting at the glass transition value (Tg) of 144°C. Between the Tg and the melting temperature (Tm) the pin already had penetrated almost 25% of the sample. This would support the concept of the sample being considerably amorphous due to the extent of penetration before the melt, that is the point at which the crystalline portion flows. By contrast the 380°C run described above that had a similar Tm was only 4% penetrated before the melting point. The 300°C and 340°C also showed very little penetration between Tg and Tm. It seems clear that the cured samples at 300°C, 340°C, and 380°C are considerably higher percent crystallinity than the 274°C sample.

The next run was a dielectric sample that was ramped to 380°C but allowed to solidify without any hold. This resulted in a long, gradual, but complete penetration starting at 134°C and continuing till almost 230°C. This sample would be considered to have both low crystallinity and mechanical properties. Finally, two runs were preformed on dielectric samples that were cured for one hour at 380°C (Figures 18 a and b). These experiments produced the most spectacular

results. In each case the sample was ramped to 450°C in the TMA but the pin did not penetrate the sample completely. In fact each showed a transition around 400°C but only about 14% of the sample was penetrated! See Table IV for a summary of all TMA data. If this data is to be believed, then it is obvious that the mechanical properties were greatly enhanced for the dielectric 380°C/60 min. hold. The question is why would these results be so different than the 380°C hold mentioned above. The only difference is the added pressure particularly during the melt phase. Enhancement of ordering through extruding or applied pressure is common for LCPs. Therefore, the slight pressure placed the this system would cause syn9 to align in such a manner as to vastly increase the mechanical properties in the solid state.

Table IV

Hold Time & Temperature	Tm (°C)	Tg (°C)
Pre-Cured Sample		
60 min @380°C	263	159
60 min @340°C	254	
60 min @300°C	258	158
From Dielectric Run		
240min @274°C	261	144
10 min @380°C	220	
90 min @380°C	410 (only 14% penetration)	

Figure 16

TMA ANALYSIS OF LIQUID CRYSTAL

File Name: syn9-380
Sample Name: syn9 cured hr @ 380
Length: 0.8240[mm]

Temp Program

Rate [C/min]	Hold Temp [C]	Hold Time [min]
10.0	420.0	0.0

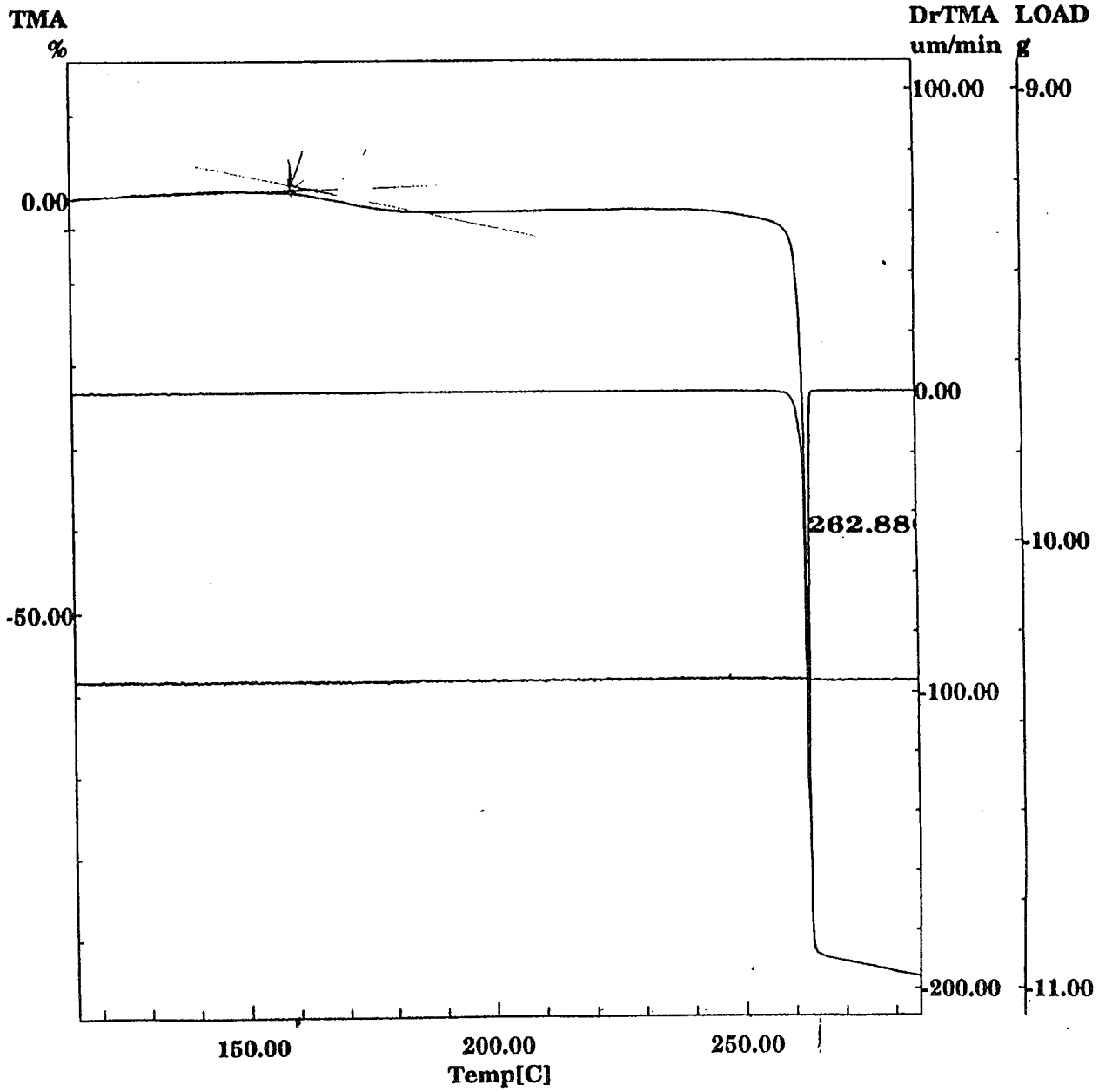

Figure 17

TMA ANALYSIS OF LIQUID CRYSTAL

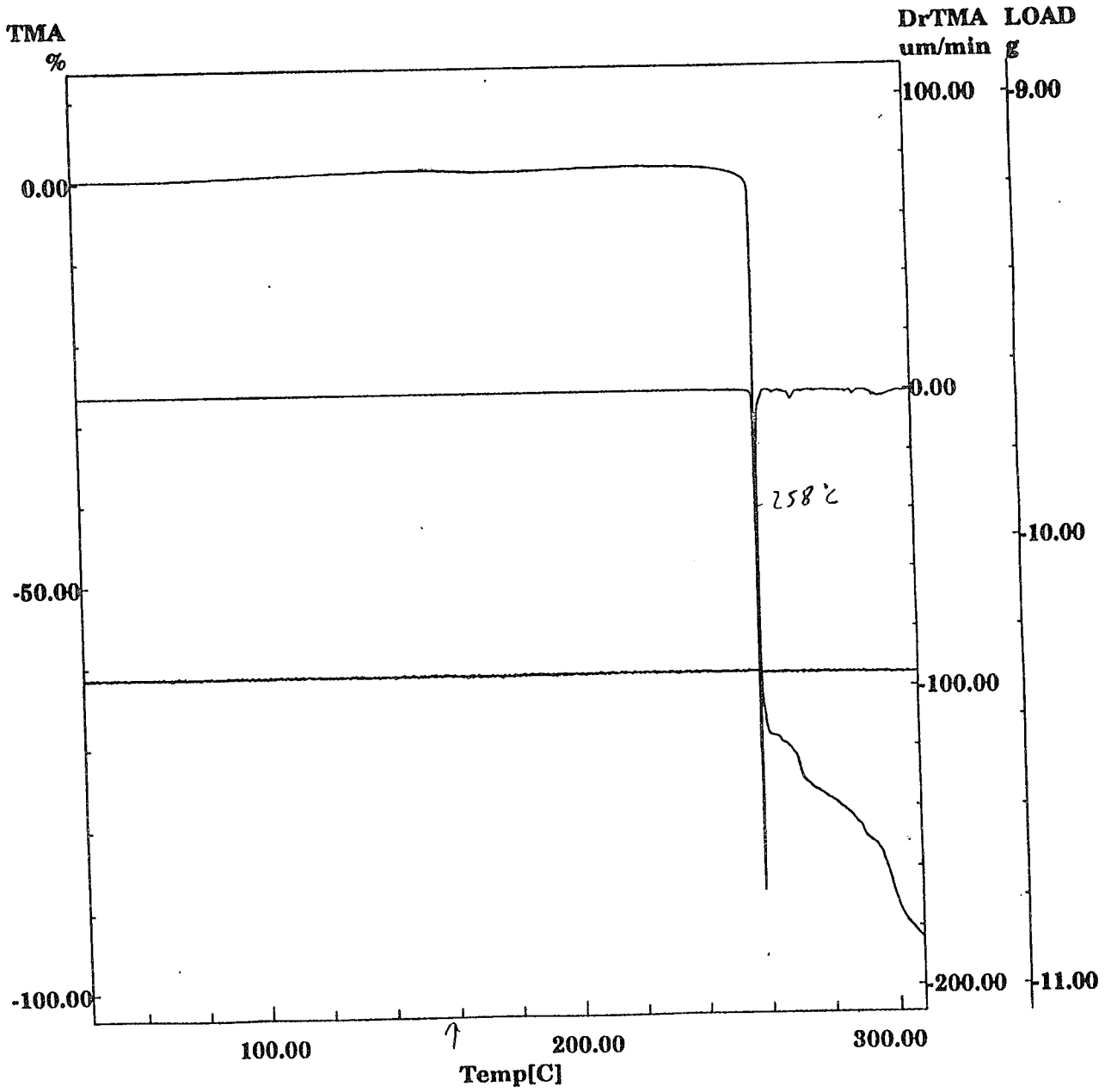

Temp Program

Rate [C/min]	Hold Temp [C]	Hold Time [min]
10.0	320.0	0.0

File Name: SYN9-300.D00
Sample Name: syn9 cured hr @ 300
Length: 1.092[mm]

Figure 18a

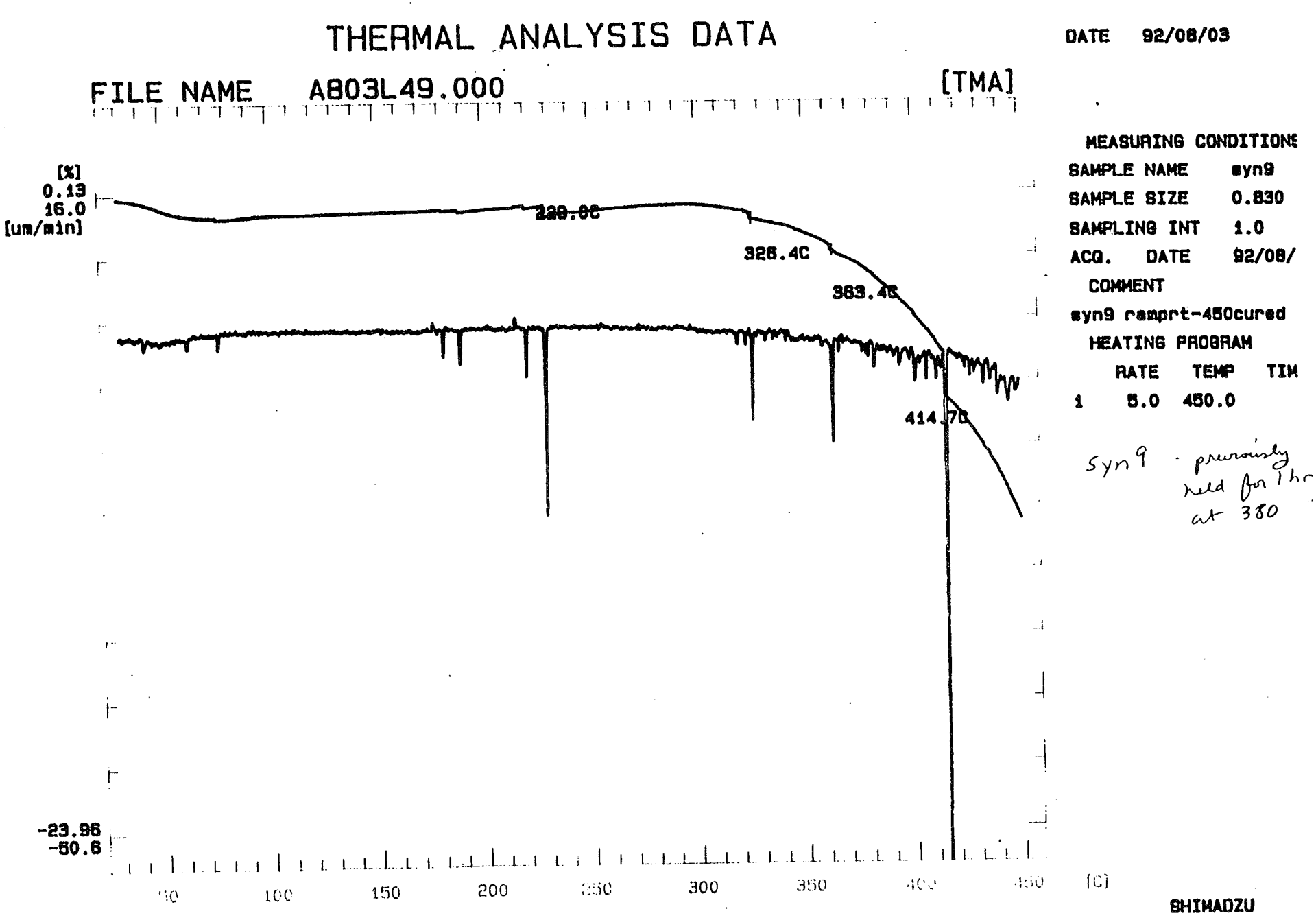

syn9 - previously held for 1hr at 380

Figure 18b

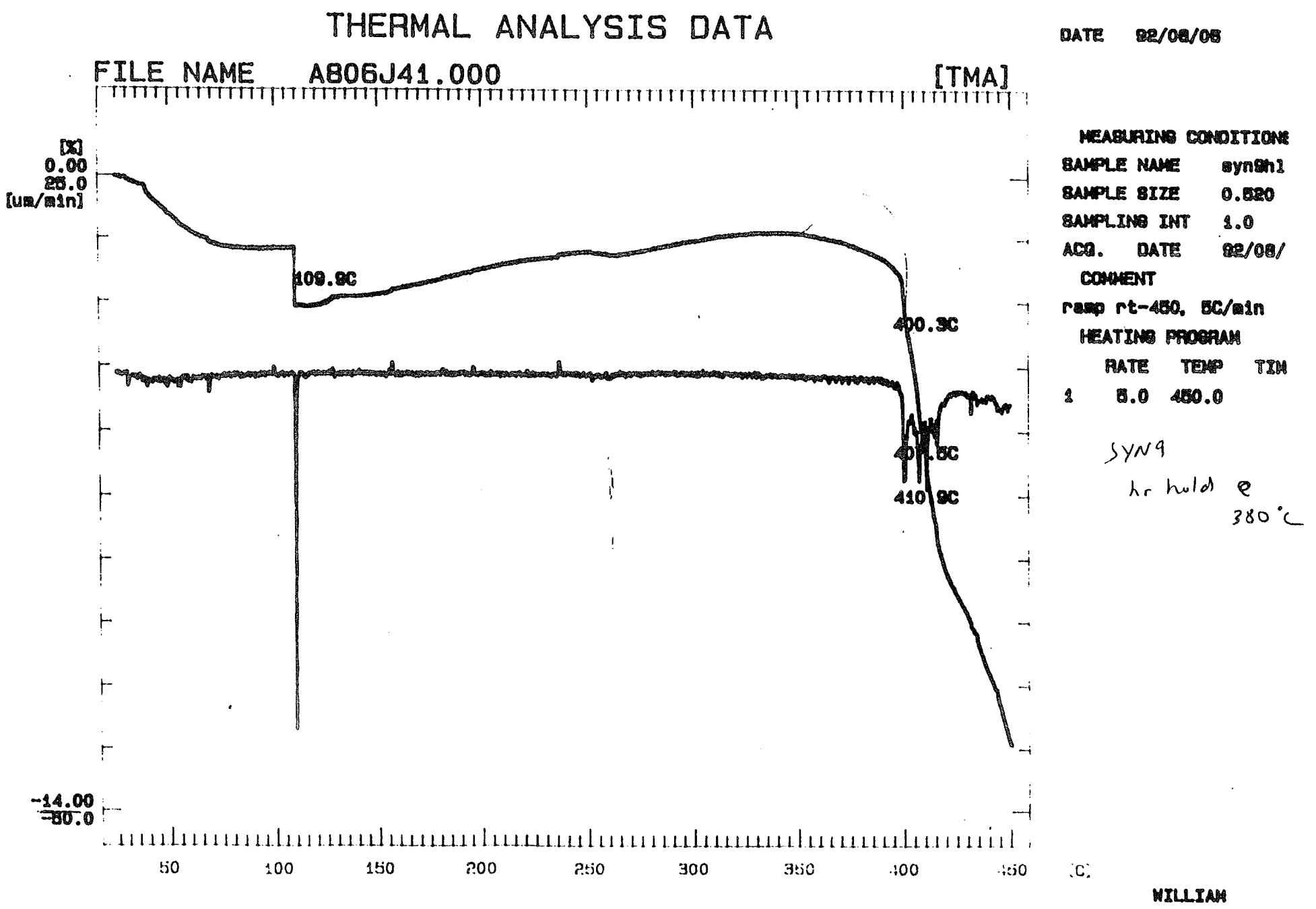
THERMAL ANALYSIS DATA
DATE 92/08/08
FILE NAME A806J41.000
[TMA]
[%]
0.00
25.0
[um/min]
109.9C
400.3C
410.9C
-14.00
-50.0
50
100
150
200
250
300
350
400
450
[C]
MEASURING CONDITION
SAMPLE NAME synSh1
SAMPLE SIZE 0.520
SAMPLING INT 1.0
ACQ. DATE 92/08/
COMMENT
ramp rt-450, 5C/min
HEATING PROGRAM
RATE TEMP TIM
1 5.0 450.0
SYN9
hr hold @
380°C
WILLIAM

Chapter 7

Conclusion

The syn9 system has proven to be a fairly complex one. First of all it seems reasonable from syn9's molecular structure that it could exhibit some liquid crystalline properties. Syn9 consists of a primarily aromatic backbone that does not allow for much flexibility. This rigid backbone should line-up in a rod-like fashion, and would correlate well with common liquid crystalline models.

The Differential Scanning Calorimeter was useful in observing the polymer's melting endothermic phase transition and how various heat treatments effected that endotherm. When a low temperature hold was chosen (236°C or 274°C), no shifting of the peak occurred. A 300°C hold produced the first interesting results. The endothermic peak shifted significantly and would thereby imply a higher degree of crystallinity. In addition, a Tg can be observed so the LCP is still partly amorphous. Upon treatment at higher temperatures (340°C and 380°C) the melting peak is spread out over many temperatures. Presumably, the many different crystalline regions of the polymer are melting at different temperatures. The Tg is also no longer seen after a 30 minute hold at 380°C, and would suggest a high degree of crystallinity. The polarizing microscope also confirmed the initial belief that syn9 is an LCP. This instrument labeled

the initial melt as one to a nematic mesophase, and found the isotropic melt around 415°C.

Next the FDEMS technique was employed to observe the ionic and dipolar mobility of syn9 during various temperature holds. Again the data was uninteresting during a 274°C hold, but higher temperatures produced significant results. The 380°C holds (10 and 90 minutes) both eliminated the dipolar peaks, while the 340 hold reduced them considerably. In addition, the ionic mobility was clearly decreasing during the 90 minute hold. Both results would support the conclusion of a higher percent crystallinity as a result of the heat treatment at 380°C. Crystallinity results in a more structured array, and therefore less ionic mobility and rotational diffusion would be observed in a crystalline sample.

FT-IR was used to observe whether the changes occurring were either physical or chemical. Unfortunately, the sample's signal was greatly reduced after flow. The only change upon heat treatment up to the melting point was in the carbonyl stretching region. A stretch at 1800 cm-1 was reduced and replaced by one at 1700 cm-1. This change is probably due to the loss of trapped solvent from the fresh sample, or possibly some glassly ordering. The only noteworthy conclusion from this data is that no chemical reactions are taking place below the melting temperature.

Finally, the TMA was used to measure the mechanical properties of syn9. The samples cured at 300°C, 340°C, and

380°C displayed no major differences in their mechanical properties. Although, as one would expect, the 380°C hold did produce a slightly higher degree of enhanced physical properties. The surprising result came from dielectric samples that were previously held at 380°C. The only difference in these samples was the existence of an external pressure applied during the melt. The effect was astounding. Not only did the temperature of penetration increase from 263°C to 410°C, but the sample was only partially penetrated (14%).

In conclusion, syn9's mechanical properties can be enhanced through temperature holds. Temperatures below 300°C showed to be ineffective in increasing the percent crystallinity. Intermediate temperatures of 300°C and 340°C did produce an increased crystallinity but still had enough amorphous regions to exhibit a Tg. Finally 380°C holds of 30 minutes or more produced highly crystalline structures. These structures have many different ordered segments which result in many different melting temperatures for different regions of the polymer. If a small, even pressure is applied to the sample the mechanical properties are greatly increased. The obvious area for additional work in this project is with the TMA. More samples should be run under pressure to confirm this hypothesis. In addition, the pressure needs to be quantified to determine exactly how much pressure is most effective. Once both the ideal temperature and pressure are known, then this compound can be a very useful material. Syn9

can be molded in the flow state at 380°C and placed in a mold at that temperature. Then, a pressure can be applied while the system is allowed to cool. Ideally, the end result will be a molded product with greatly enhanced mechanical properties.

Bibliography

1 Sperling, L. H. Introduction to Physical Polymer Science, 2nd Ed. Wiley & Sons, New York, 1992.

2 Ober, C.K. and R.A. Weiss. "Current Topics in Liquid Crystalline Polymers", Liquid-Crystalline Polymers, R.A. Weiss and C.K. Ober Ed. American Chemical Society, Washington D.C., 1990.

3 Huynh-Ba, Gia and E.F. Cluff. "Structure and Properties of Rigid and Semi-rigid Liquid Crystalline Polyesters", Polymeric Liquid Crystals, Alexandre Blumstein, Ed. Plumum Press, New York, 1985.

4 Munk, Petr. Introduction to Macromolecular Science. Wiley & Sons, New York, 1989.

5 Billmeyer, Fred W. Jr. Textbook of Polymer Science. Wiley & Sons, New York, 1984.

6 Hart, S. "Intelligent processing of PMR-15", Masters Thesis. The College of William and Mary, 1992.

7 Williamson, A.S. "Dielectric Sensor In-Situ Control of the RTM Composite Fabrication Process", Masters Thesis. The College of William and Mary, 1990.

8 Perkin-Elmer. Introduction to Fourier Transform Infrared Spectroscopy Instrumentation Selected Applications.

Twelve Month Report

Characterization, FDEMS Sensing and Insitu Process Monitoring of the Physical Changes Occurring with Time and Temperature During Cure of High Temperature Liquid Crystal Thermotropes

to

Dr. John J. Rusek
Phillips Laboratory
Bldg. 8351
OLAC PL/RKCP
Edwards, CA 93523-5000

from

David E. Kranbuehl
Chemistry and Applied Science
The College of William and Mary
Williamsburg, VA 23187-8795

September 15, 1992

Contract #F04611-91-C-0131

Since the February 1992 presentation at the First Annual Advanced Polymer Components Research Symposium in Indianapolis, we have focused of our attention on HX-4000 and the SYN 1, 3, 5 9, and 10 samples you sent us in March. In particular, we have conducted extensive time-temperature process cure cycle experiments using FDEMS (frequency dependent electromagnetic sensor measurements), DSC (differential scanning calorimetry), and thermal mechanical measurements. The work has focused on the following objectives.

- characterizing the time-temperature process cycle dependence of the macroscopic states and phase transitions in these thermotropic liquid crystal polymers.

- developing and demonstrating the ability of FDEMS sensors to monitor in situ the changes in state of the thermotropic polymer continuously during the processing cycle.

Together these two objectives should lead in future work to monitoring and optimizing the cure process in the fabrication mold, to online quality assurance monitoring, and to intelligent automated closed loop process control.

At the February meeting, we reported on some of the initial work demonstrating the ability of the DSC and FDEMS sensing to monitor thermotropic cure. First we will summarize our work on the HX-4000 ystem and then describe the work on the SYN systems. Figure 1 is a DSC scan of HX-4000 in a 100°C to 360° up down up down cycle. The output shows the endothermic melting at 310° shifting slightly to a higher temperature on the second ramp up. The second down cycle shows the exothermic peak broadening and shifting to a lower temperature. Figures 2 and 3 show the FDEMS output ε' and $\varepsilon''x\omega$ ($\omega = 2\pi$ x frequency). The output clearly shows the softening-flow at 310°, onset of a cooling transition around 260°, a dipolar peak over the 5 x 10^5 hertz to 5 x 10^1 hertz frequency range. These peaks are monitoring the mobility of the dipolar groups perpendicular to the chain backbone and/or in the amorphous region of the polymer in the 140° to 200° temperature range. We will observe and use these DSC and FDEMS affects throughout our work on different materials and differing time-temperature process cycles.

Next we turn to the effects of a 320° hold and then the effects of a 380° hold on HX-4000. Figure 4 is an isothermal 320° hold in DSC. The heat flow is exothermic on the Perkin Elmer DSC-7 system. Either additional reaction, perhaps crosslinking, or melting of ordered regions is occurring. Most likely the answer is the former. A subsequent series of ramps after the 320° hold 320-100-360-100 is shown in Figure 5. A slight downward shift in the exothermic melt peak at 280° occurs. One hour at 320° has a modest effect, as an exothermic reaction, probably slightly increasing the MW and some crosslinking.

Next we examined the effects of a 380° hold for 1 hour. The DSC shows a slight endothermic effect, perhaps degradation or ordering. The ramp hold sequence, Figure 7, on the HX-4000 sample after the 380° hold shows a small broad exothermic deflection on cooling as opposed to a sharp exotherm prior to the 380° hold. Further, the exotherm has shifted to the 260-270° region.

Figures 8 and 9 show the FDEMS sensor output of $\varepsilon''x\omega$ and ε' on a log scale. The $\varepsilon''x\omega$ plot shows a clear drop in the ionic mobility with time during the 380° hold. A similar affect is seen in the drop in ε' at the low frequencies. Further, in the region of 320° to 220° the value of ε' increases as the temperature drops. Normally as in Figure 3 or the other temperature regions one would expect ε' to remain stable or drop as the temperature increases. The position of the dipolar peaks in Figure 8 are similar to Figure 2. The dipolar peaks remain sharp and large. This suggests retention of molecular mobility for this system on cure, an observation which often correlates with improved toughness.

The mechanical property consequences of these thermotropic annealing effects are shown in the mechanical property results sent to us in April by Paul Jones. He did a considerable amount of work using hold at 240° to 320°. The results can be seen by comparing the static and dynamic mechanical properties of a fresh sample and a sample held at 320° for 1.9 hours, Figures 10, 11, 12 and 13. Clearly annealing at a temperature above 300° increases the softening temperatures as seen by the changes observed in our FDEMS and DSC output. Second, the 300° plus hold retains the mobility of segmented motion in the 100 to 150° range mechanically. Observe the shoulder peak in Figure 13 and 12 at 120°C. Note the mechanical peak will be at slightly lower temperatures than the dielectric peaks since the frequency is near 1.0 hertz as opposed to 50 to $5x10^5$ hertz in the FDEMS sensor output. Clearly annealing affects are occurring and the FDEMS sensor output can monitor the time temperature dependence of this process, both with considerable sensitivity and also in situ in the mold when thermal heat transfer affects on large samples will produce very different affects from work on small samples in the laboratory. Overall, the correlation between both laboratories' work appears to be extremely good.

fresh 1/2/3/4

DSC Data File: hx410
Sample Weight: 10.000 mg
Fri Feb 14 07:57:35 1992
hx-4000 freef

PERKIN-ELMER
7 Series Thermal Analysis System

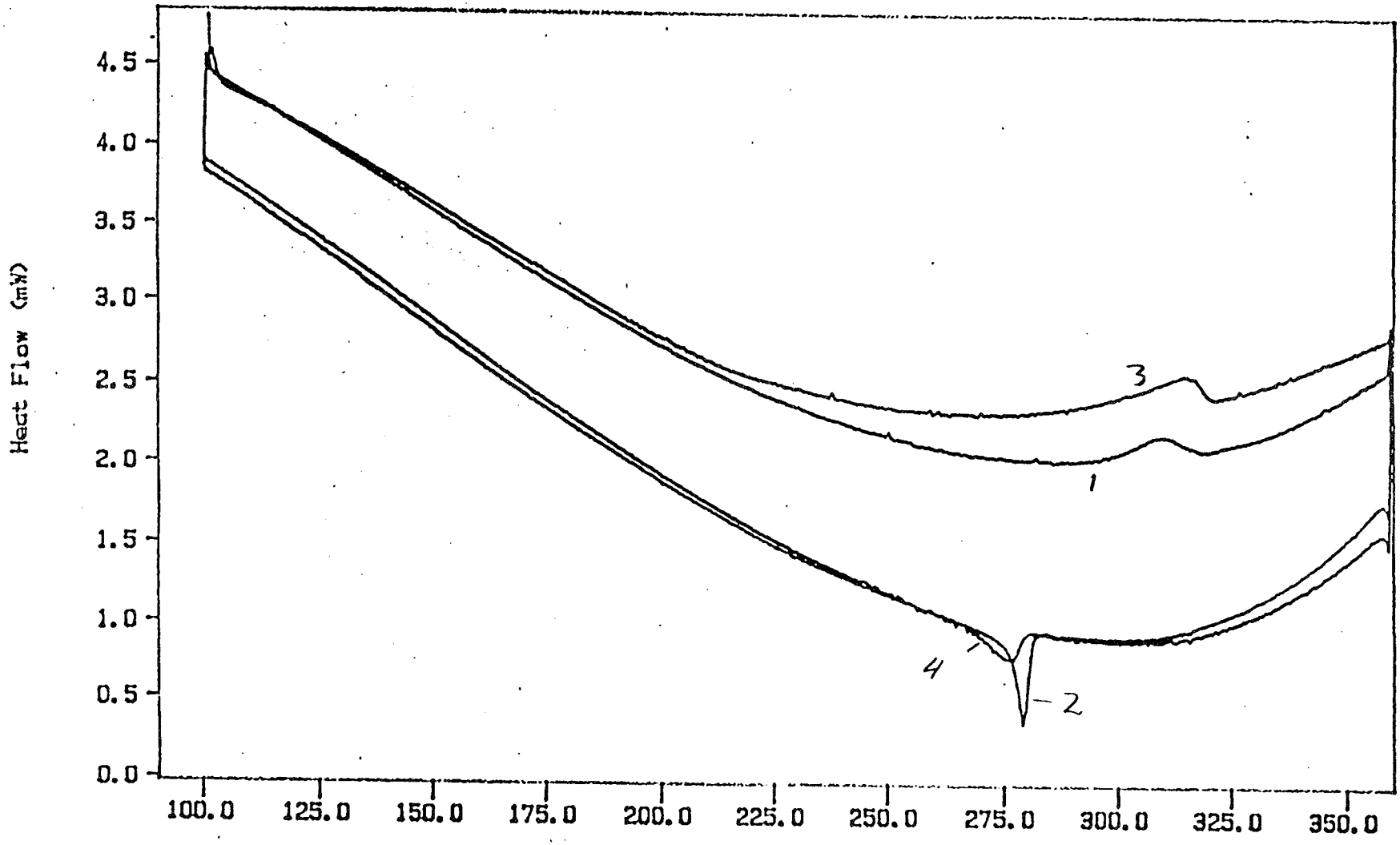

ramp 100c-360c-100c-360c-100c

TEMP 1:	100.0 C	TIME 1:	0.0 min	RATE 1:	2.0 C/min
TEMP 2:	360.0 C	TIME 2:	0.0 min	RATE 2:	2.0 C/min
TEMP 3:	100.0 C	TIME 3:	0.0 min	RATE 3:	2.0 C/min
TEMP 4:	360.0 C	TIME 4:	0.0 min	RATE 4:	2.0 C/min
TEMP 5:	100.0 C				

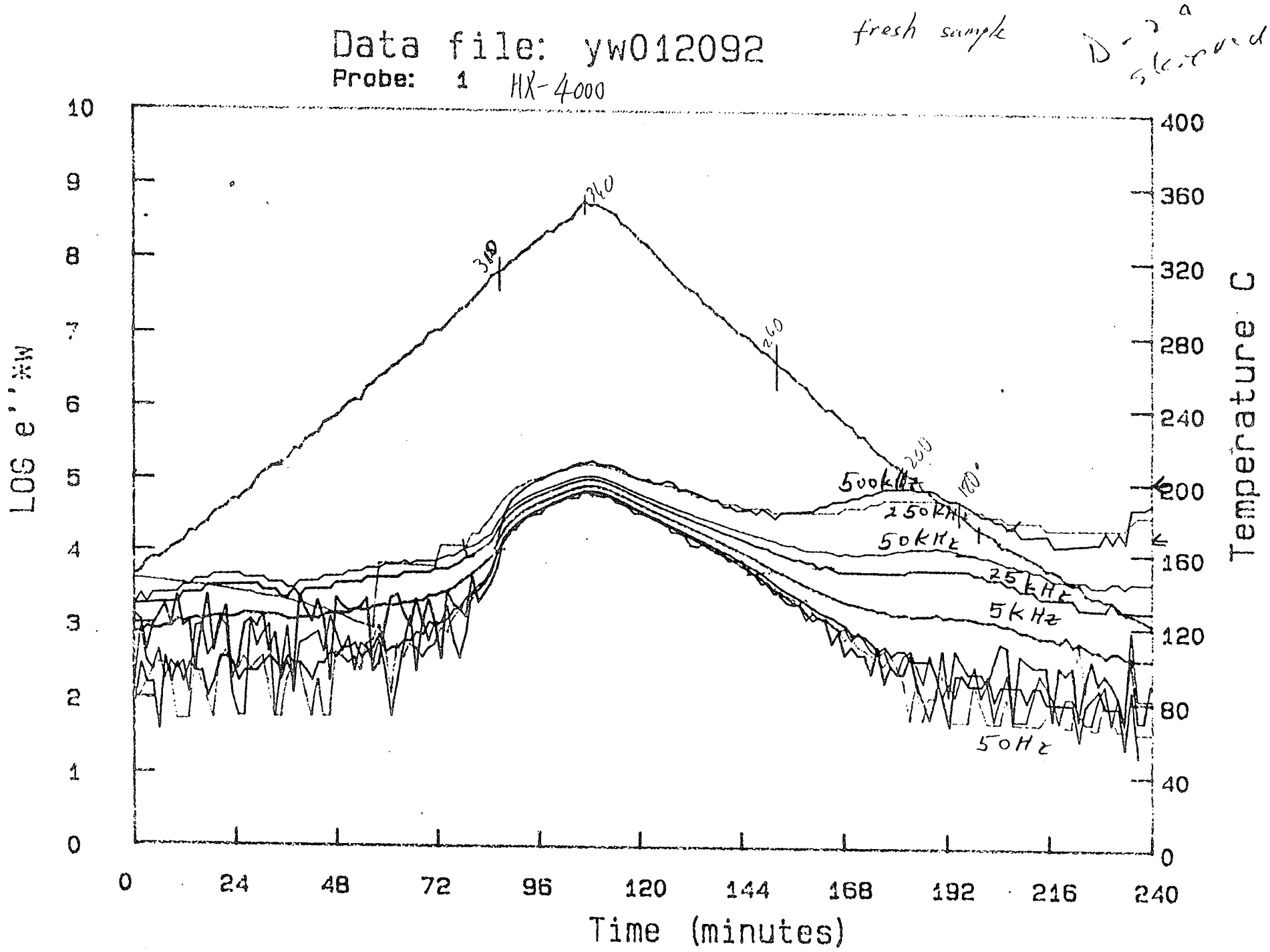
Data file: yw012092
Probe: 1 HX-4000
fresh sample
LOG e'' *W
Temperature C
Time (minutes)
0
24
48
72
96
120
144
168
192
216
240
0
1
2
3
4
5
6
7
8
9
10
40
80
120
160
200
240
280
320
360
400
340
310
260
200
180
500kHz
250kHz
50kHz
25kHz
5kHz
50Hz

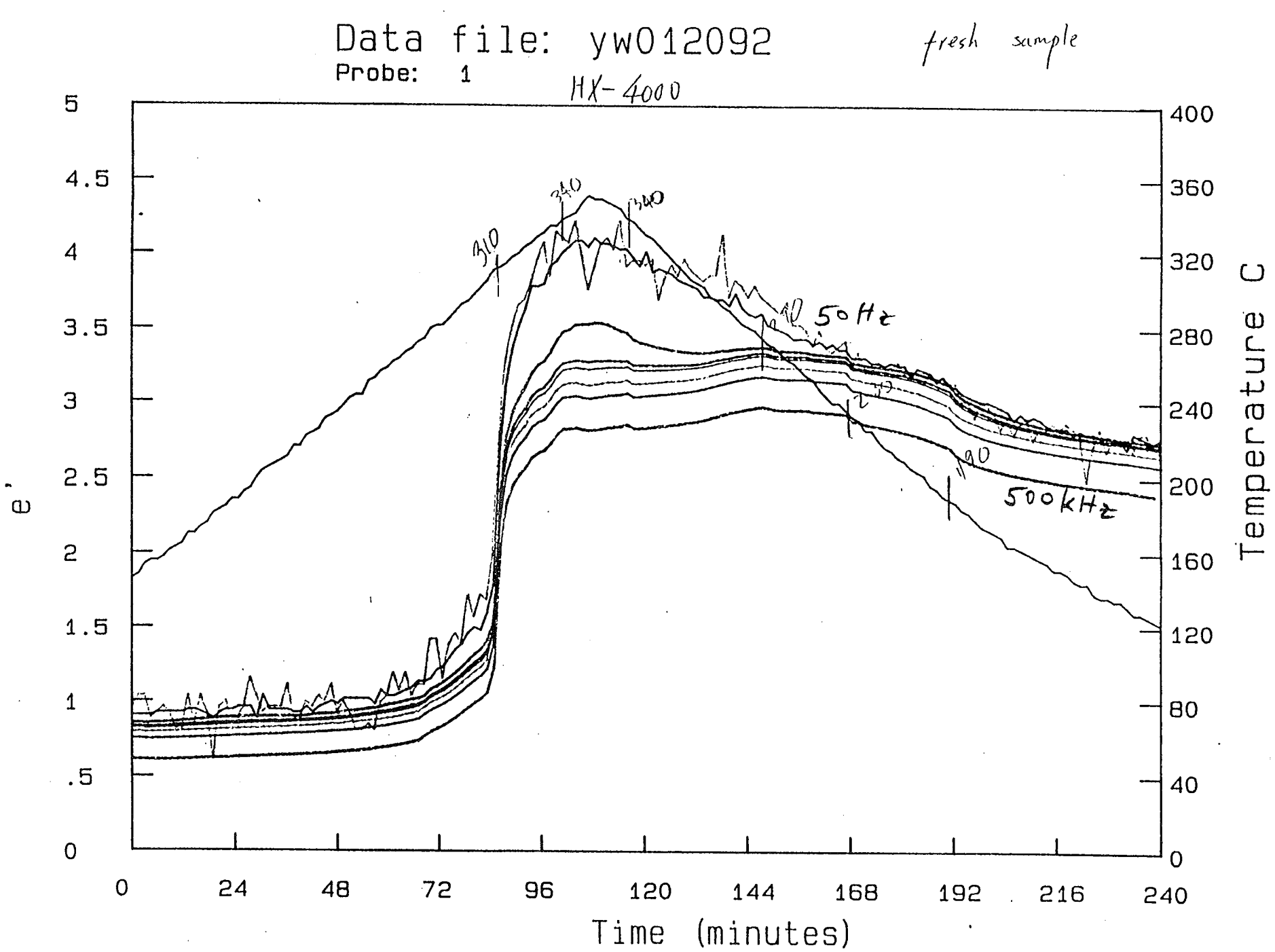
Data file: yw012092
Probe: 1
fresh sample
HX-4000
310
340
340
50 Hz
90
500kHz
e'
Temperature C
Time (minutes)
0
.5
1
1.5
2
2.5
3
3.5
4
4.5
5
0
40
80
120
160
200
240
280
320
360
400
0
24
48
72
96
120
144
168
192
216
240

Iso 320°C 60 min

DSC Data File: hx411
Sample Weight: 8.100 mg
Fri Feb 14 15:28:35 1992
HX-4000 fresh

PERKIN-ELMER
7 Series Thermal Analysis System

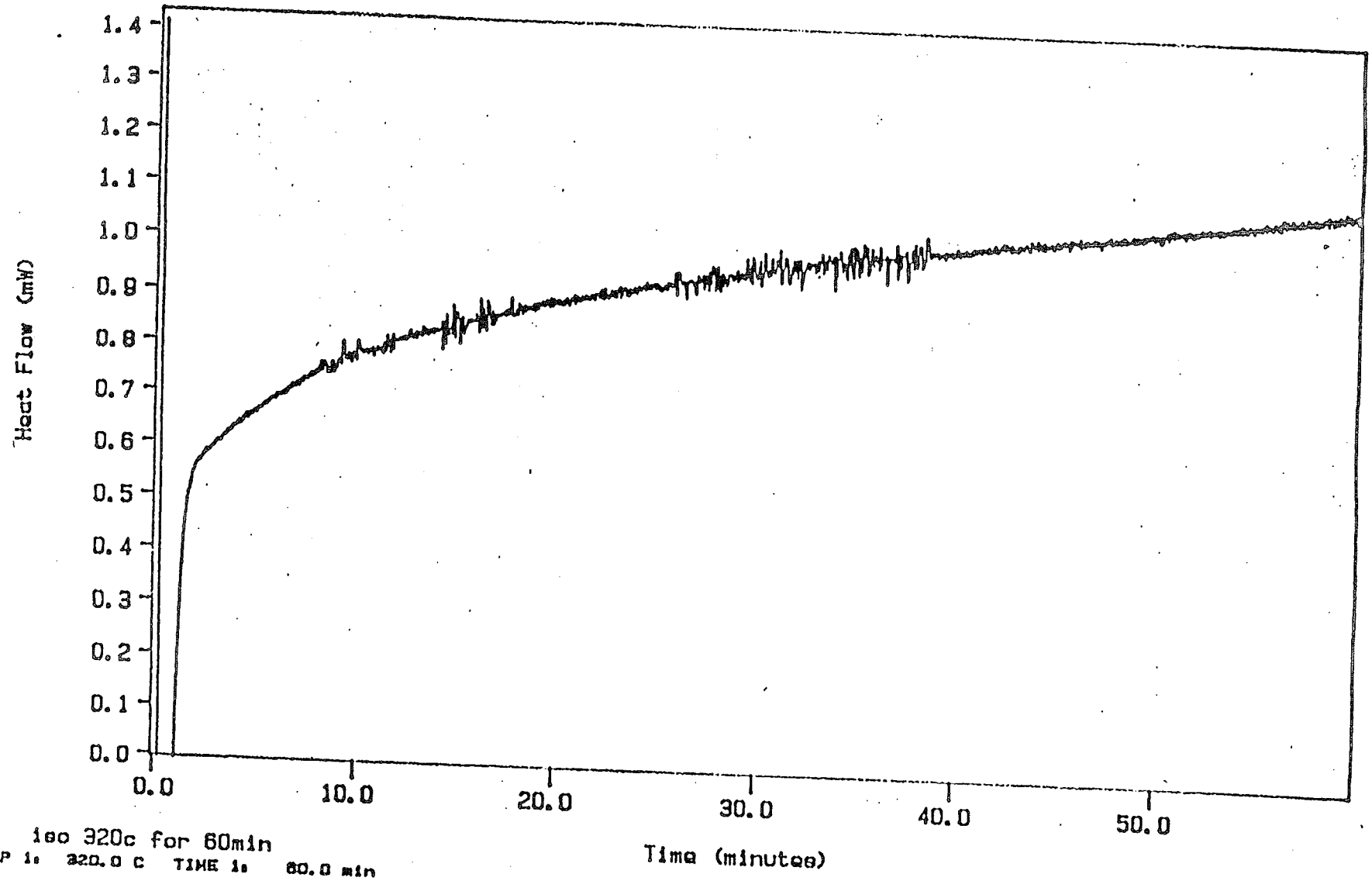

iso 320c for 60min
TEMP 1: 320.0 C TIME 1: 60.0 min

300

DSC Data File: hx412
Sample Weight: 8.100 mg
Fri Feb 14 21:42:52 1982
hx-4000 after iso 320o 60min

PERKIN-ELMER
7 Series Thermal Analysis System

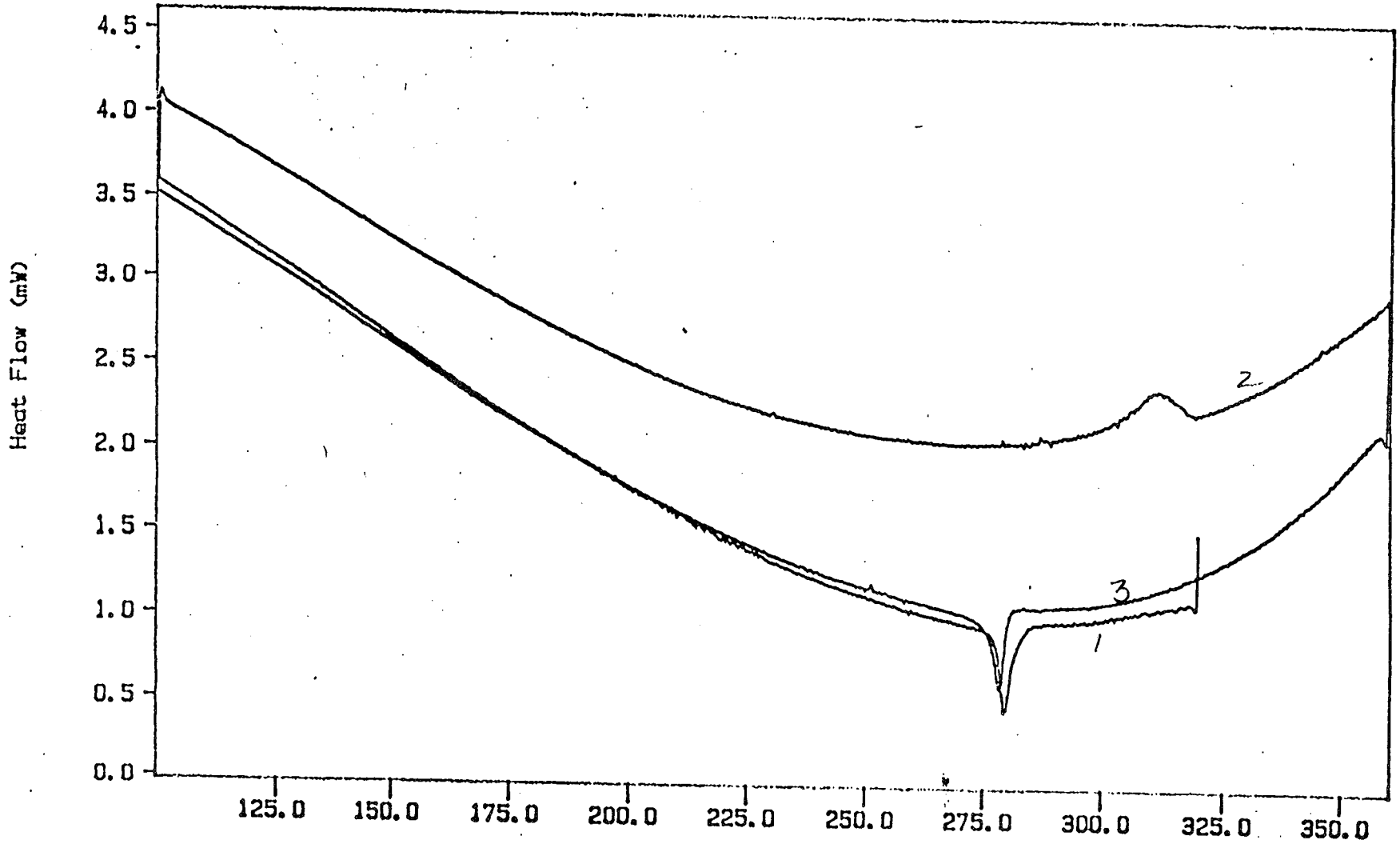

ramp
TEMP 1: 320.0 C TIME 1: 0.0 min RATE 1: 2.0 C/min
TEMP 2: 100.0 C TIME 2: 0.0 min RATE 2: 2.0 C/min
TEMP 3: 260.0 C TIME 3: 0.0 min RATE 3: 2.0 C/min
TEMP 4: 100.0 C

730 380°C 60 min

DSC Data File: hx413
Sample Weight: 10.000 mg
Sun Feb 16 22:24:28 1992
HX-4000m fresh sample

PERKIN-ELMER
7 Series Thermal Analysis System

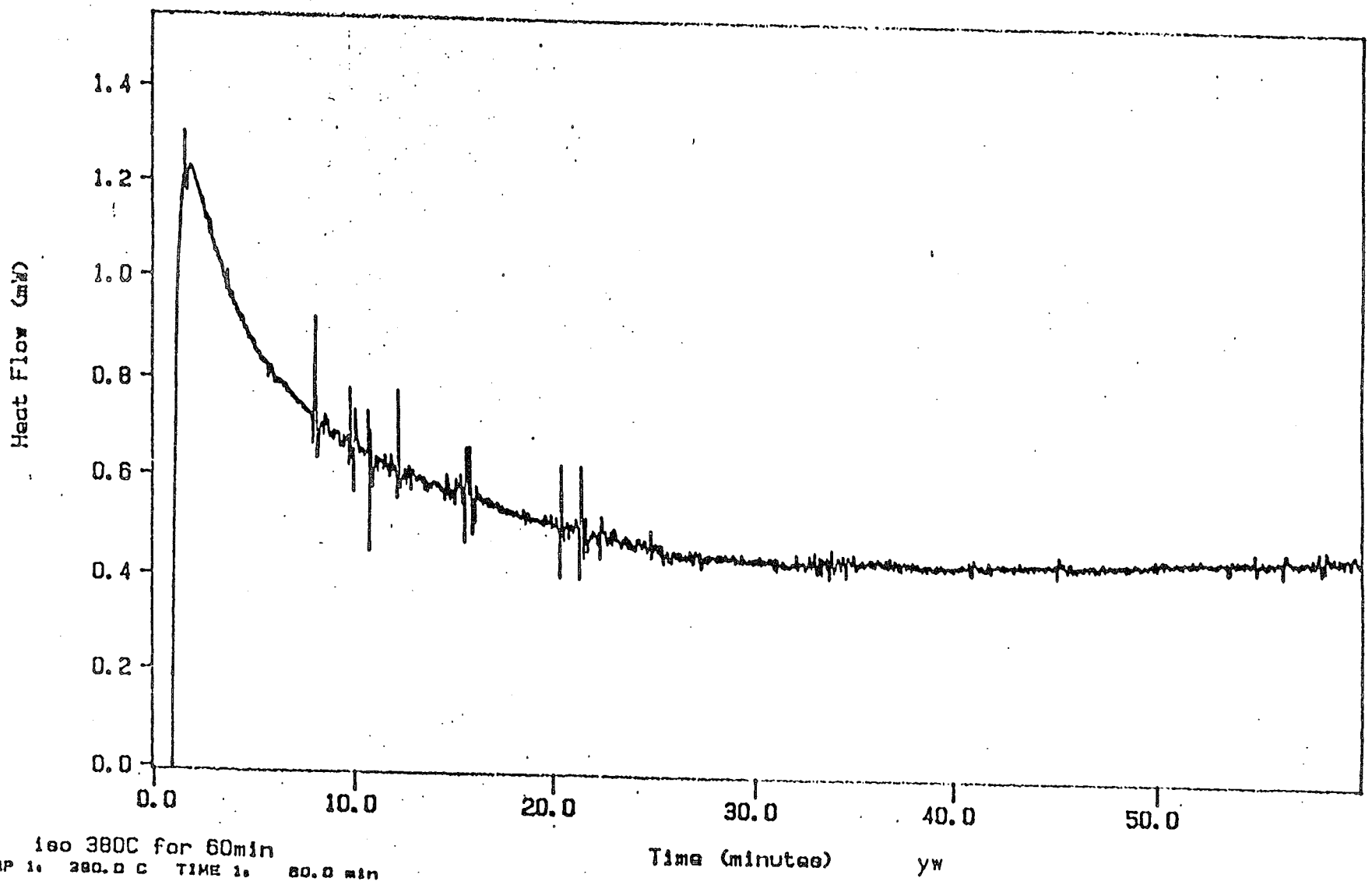

iso 380C for 60min
TEMP 1: 380.0 C TIME 1: 60.0 min

DSC Data File: hx414
Sample Weight: 10.000 mg
Mon Feb 17 05:08:24 1992
hx4000, after iso 380c for 60min

PERKIN-ELMER
7 Series Thermal Analysis System

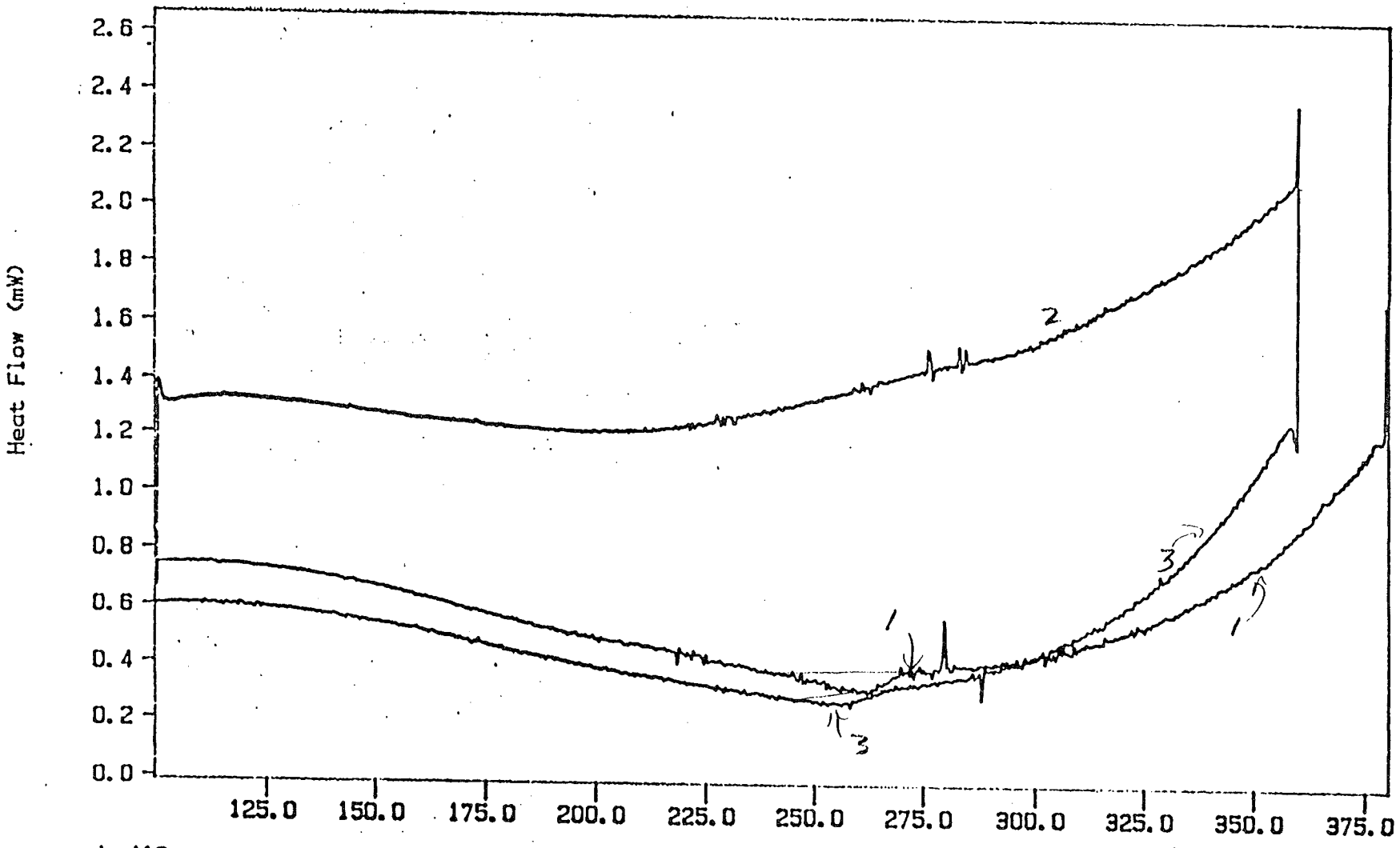

ramp hx413

TEMP 1:	380.0 C	TIME 1:	0.0 min	RATE 1:	2.0 C/min
TEMP 2:	100.0 C	TIME 2:	0.0 min	RATE 2:	2.0 C/min
TEMP 3:	380.0 C	TIME 3:	0.0 min	RATE 3:	2.0 C/min
TEMP 4:	100.0 C				

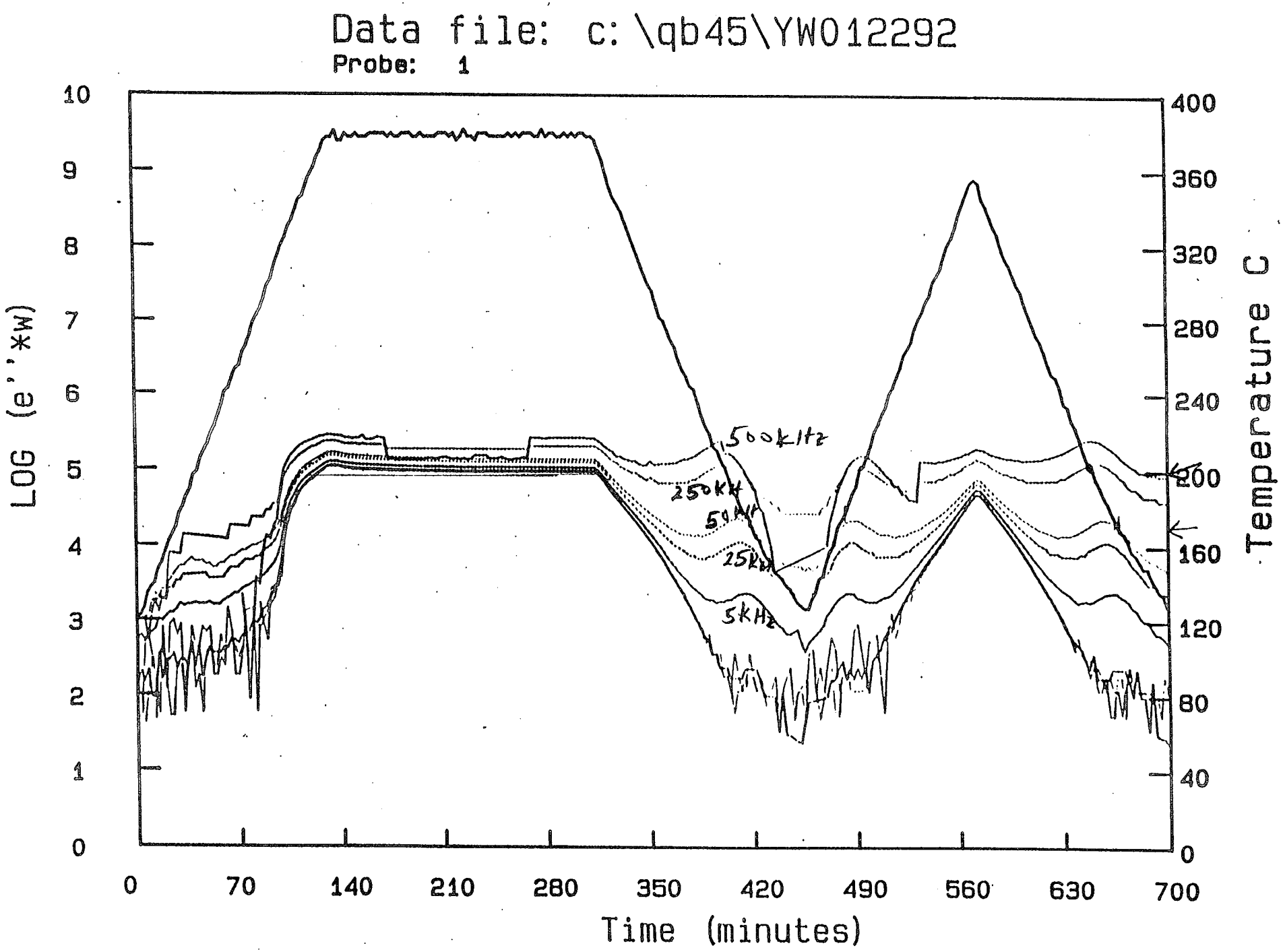
Data file: c:\qb45\YW012292
Probe: 1
LOG (e''*w)
Temperature C
Time (minutes)
500kHz
250kHz
50kHz
25kHz
5kHz
0
70
140
210
280
350
420
490
560
630
700
0
1
2
3
4
5
6
7
8
9
10
40
80
120
160
200
240
280
320
360
400

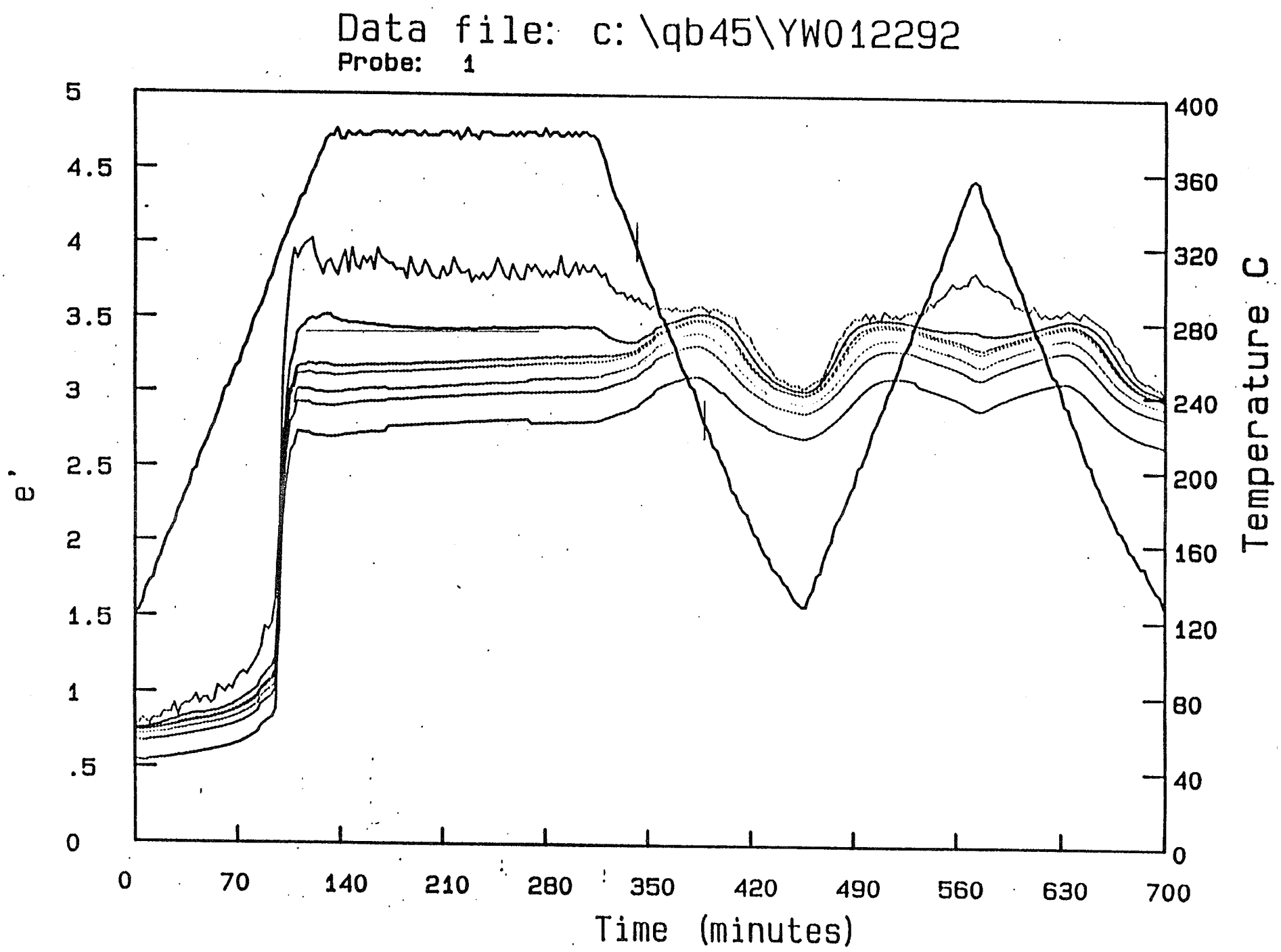
Data file: c:\qb45\YW012292
Probe: 1
e'
Temperature C
Time (minutes)
0
.5
1
1.5
2
2.5
3
3.5
4
4.5
5
0
40
80
120
160
200
240
280
320
360
400
0
70
140
210
280
350
420
490
560
630
700

Sample: HX 4000 UNANNEALED
Size: 3.0500 mm
Method: TMA ON LCP
Comment: 3.0°C/MIN. HELIUM PRUGE 40 ML/MIN, 10 GRAMS WEIGTH USED

TMA

File: A:TMAJOHN.05
Operator: PAUL JONES
Run Date: 8-Aug-91 13:17

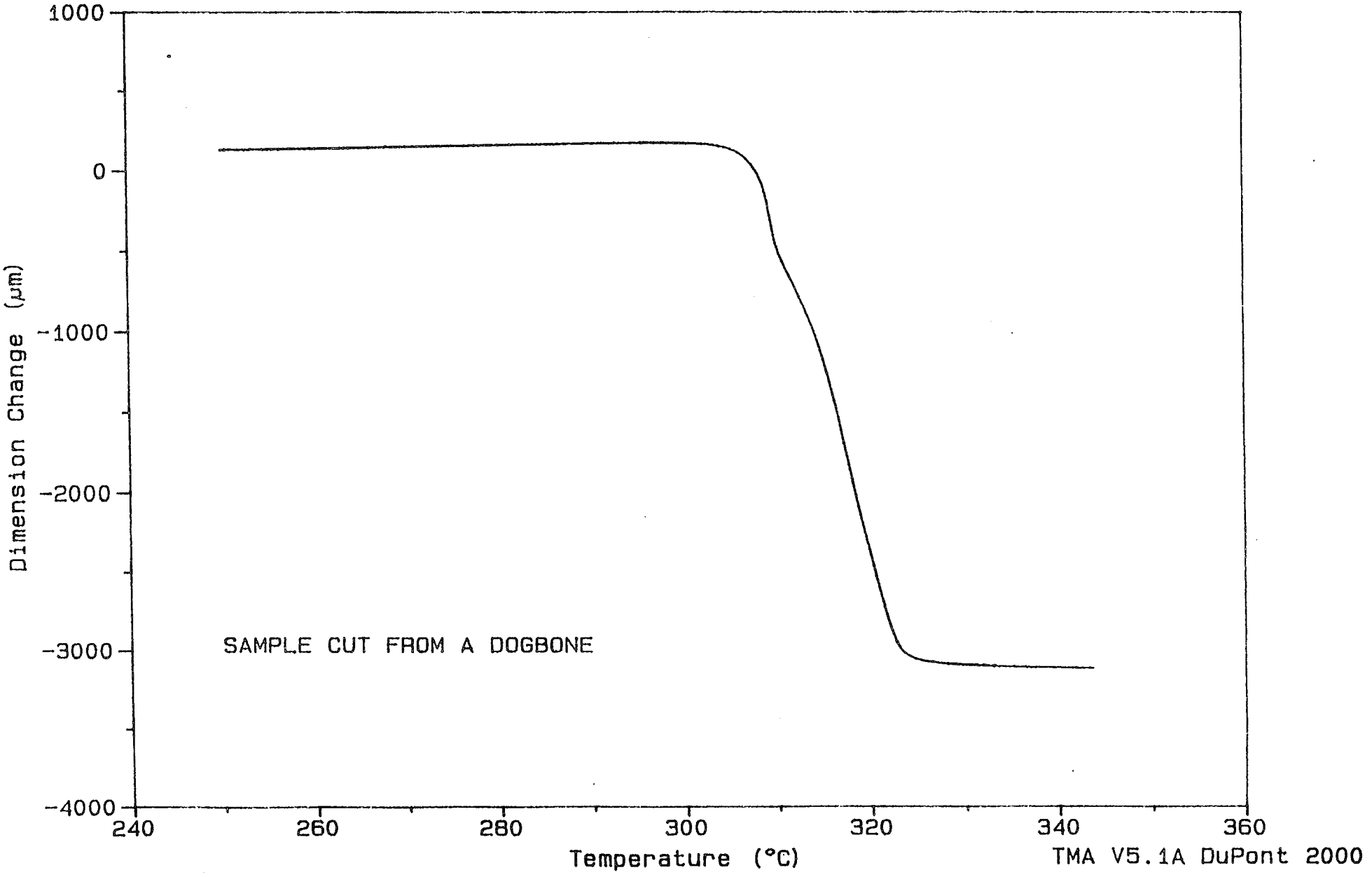

Sample: HX 4000 320°C 1.9 HOURS
Size: 3.1690 mm
Method: TMA ON LCP
Comment: 3.0°C/MIN. HELIUM PRUGE 40 ML/MIN, 10 GRAMS WEIGTH USED

TMA

File: A:TMAJOHN.03
Operator: PAUL JONES
Run Date: 8-Aug-91 11:50

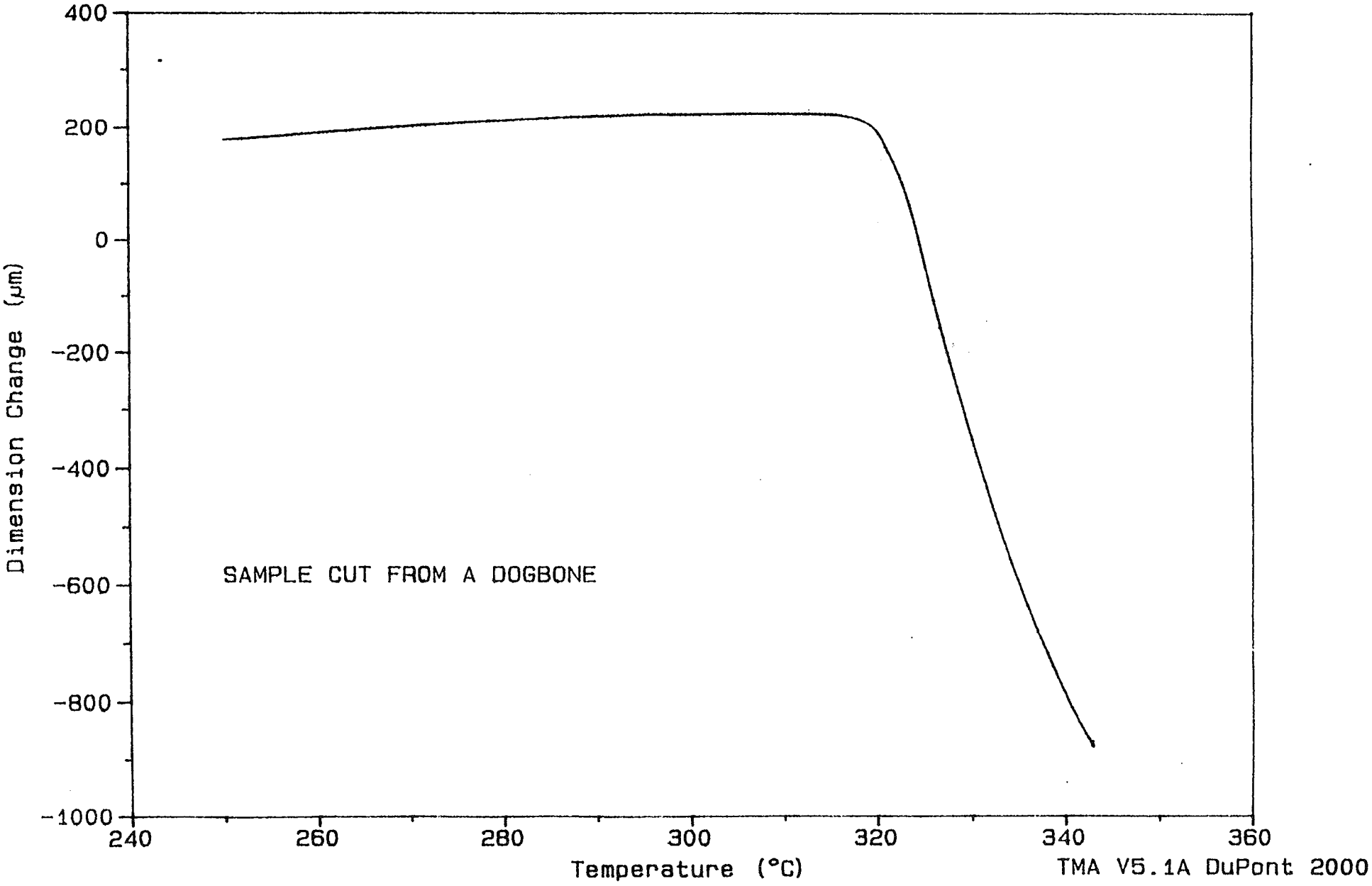

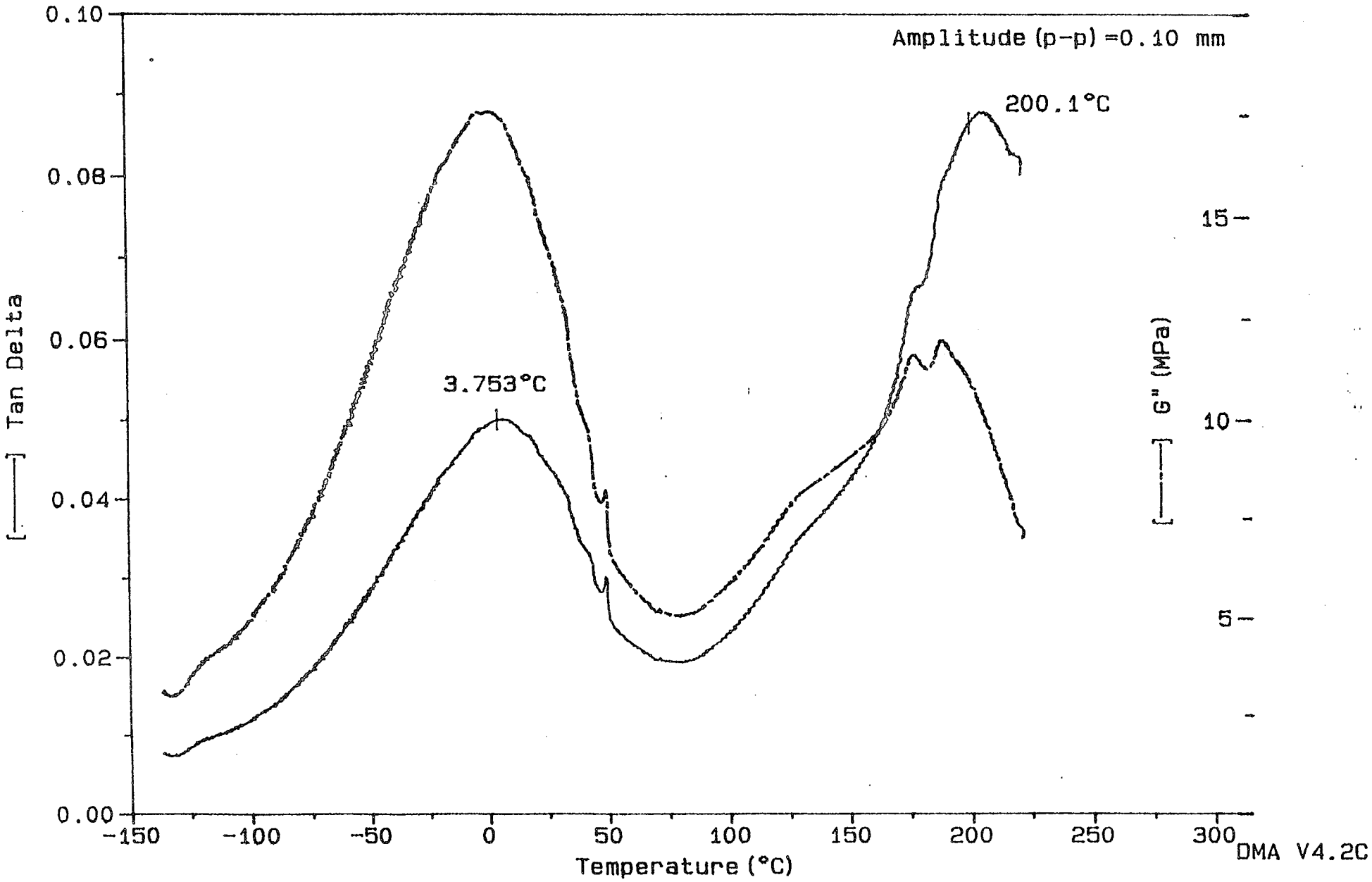
Sample : HX4000 UNANNEALED
Size : 34.3000 x 3.0000 x 12.8000 mm
Method : DMA LCP
Comment: RATE 3.0°C/MIN, NITROGEN ATMOSPHERE, SANDWICH APPARENCE IN SAMPL
DMA
File : A:DMALCP.17
Operator: PAUL JONES
Run Date: 30-Jul-91 12:22
Amplitude (p-p) =0.10 mm
200.1°C
3.753°C
Tan Delta
G" (MPa)
0.10
0.08
0.06
0.04
0.02
0.00
15
10
5
-150
-100
-50
0
50
100
150
200
250
300
Temperature (°C)
DMA V4.2C

Sample : HX 4000 320°C 1.9 HOURS
Size : 34.3000 x 3.4500 x 7.0000 mm
Method : DMA LCP
Comment: RATE 3.0°C/MIN, NITROGEN ATMOSPHERE, SAMPLE HAD TO BE CUT IN HALF

DMA

File : A:DSCLCP.22
Operator: PAUL JONES
Run Date: 2-Aug-91 08:15

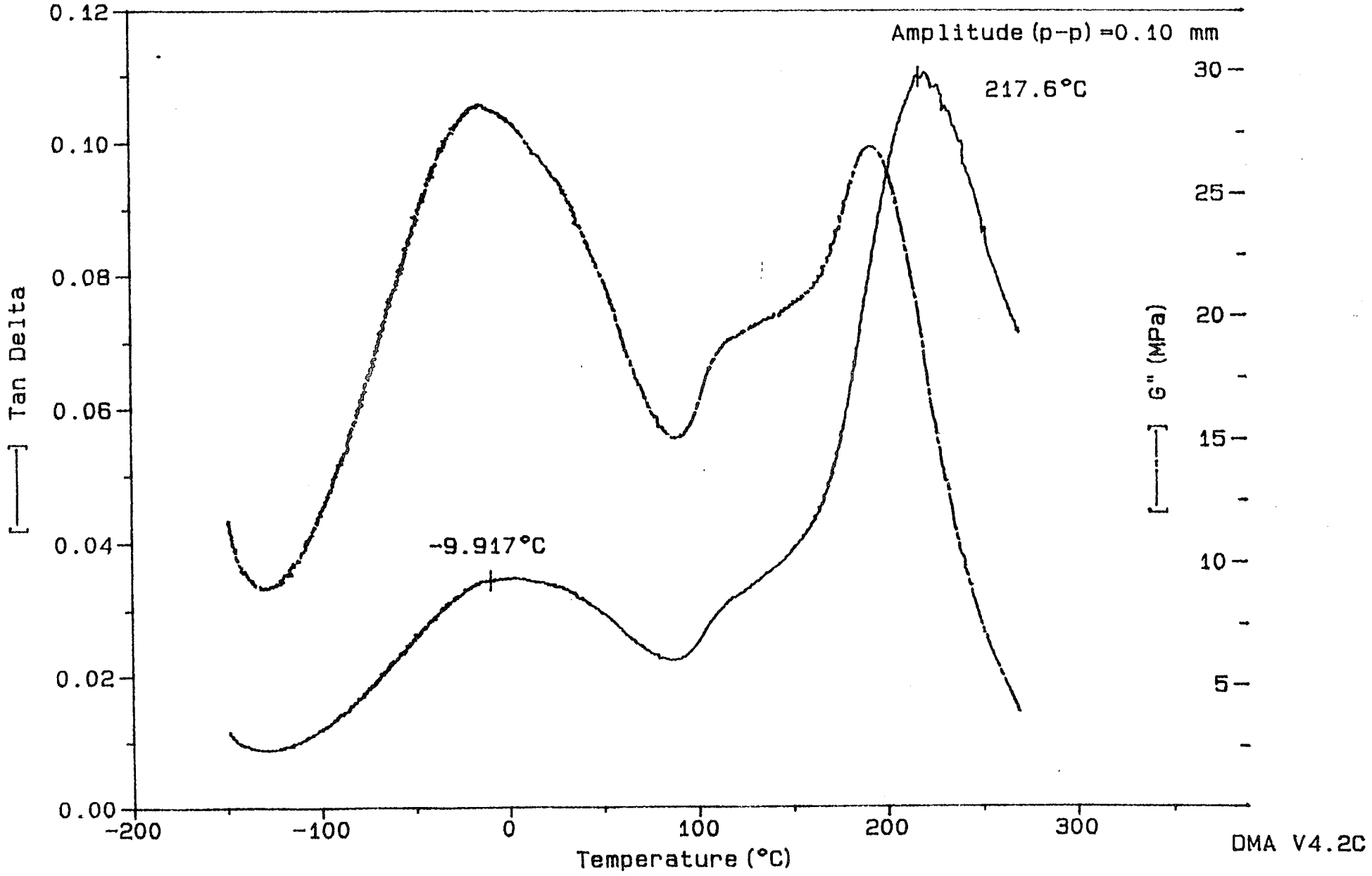

SYN SYSTEM

In March, following the "Annual Review" meeting in Indianapolis, you sent us 5 systems; SYN 1, 3, 5, 9, and 10. The data sheets describing the resin composition list the composition of each system as

SYN 1	MHQ, PHQ, CHQ with TCL, MC, and PY
SYN 3	PHQ with TCL, MC and PY
SYN 5	CHQ with TCL, MC and PY
SYN 9	PHQ, PEHQ with TCL, MC and PY
SYN 10	PEHQ with TC, MC and PY

where

MHQ is methylhydroquinone
PHQ is phenylhydroquinone
CHQ is chlorohydroquinone
PEHQ is phenylethylhydroquinone
TCl is trichloroethane
MC is methylenechloride
PY is pyridene

Based on conversations with the synthetic polymer chemist in my department, we suppose the dominant product is a linear CH_2 ether linkage Ar_1-O-CH_2-O-AR_2-O-CH_2-O- which bridges the aromatic hydroquinone units. My colleague, Bill Starnes, formerly of Bell Laboratories, where he studied PVC degradation mechanisms, also suggested that some trifunctional crosslinking at the hydroquinone might occur.

During the past six months we have conducted a full series of time-temperature ramps and holds on these systems to study the effects of their thermal processing history on their properties. We have monitored changes in the systems using FDEMS sensing where the resin has been pressed into plates in a press, using DSC on small mg samples and using a Schmadzu thermal mechanical analyzer.

A report of the results of these runs might best be presented by starting with samples SYN-9 and SYN-10, the PHQ/PEHQ and PEHQ systems. Figures 14 and 15 show the FDEMS output for two sequential up down ramps to 380°C. Flow occurs about 300° on the first ramp up and dipolar peaks in the log $\varepsilon''x\omega$ plot occur in the 150°-220° temperature region on cool down. The ε' output shows a drop in the 150° to 220° region as expected in conjunction with the dipolar loss peaks. Figures 15 and 16 show FDEMS output for a new sample given an up-down ramp to 380° followed by a ramp and hold at 340°C for 1 hour. The dipolar peaks are prominent in the 150°-220°C cool down temperature region. The value of ε'' drops strongly during the 340° hold indicating a cure process is occurring at 340° which is clearly still continuing after 1 hour. The ε' data, Figure 16, shows the expected drop in the 150°-220° region. What is also observed is a small drop in ε' during the 340° hold.

FDEMS output for a similar run both with a 3 hour hold temperature at 380° showed even stronger behavior of cure at the high temperature hold, Figures 17 and 18. The value of ε" drops strongly during the hold in this cure beginning to level out after 3 hours. Further, the value of ε' is also steadily dropping. Equally interesting is the observation that the dipolar peaks on cool down after the 380° hold disappear. The dipolar mobility has either dropped to much lower values and/or the relaxation spectrum is coupled to much longer range motions, thereby spreading out over many decades.

DSC output for two sequential up-down ramps to 380° are shown in Figure 19. The up ramp melt peak shifts from 313° to 323° on the second ramp, the down peak shifts from 273 to 260° and becomes broader. On one occasion the up ramp, Figure 20, actually broke into two peaks near 310° and 320°. Next, a sample was ramped to 380°, held for 10 minutes, and then cooled, Figure 21. The down ramp cooling exotherm moved to 249° where on a fresh sample it was 270°. Figure 22 shows the DSC output for this same sample ramped to 380° and held another 10 minutes. In this case the cooling exotherm is spread out over 230° to 240°.

Finally, we report % impregnation data from the thermal mechanical analyzer on a fresh sample of SYN-9 which had been ramped up-down to 380° in Figure 23. The fresh material allowed penetration up to 100% over the 135° to 240°C range. Figures 24 and 25 show results on samples of SYN 9 held at 380° for 1 hour. Only about 10% penetration occurs and at temperatures in the 300° to 400° range.

Conclusions: The FDEMS and DSC output shows a hold in the 340° to 380° region for 3 hours causes significant changes in the molecular structure and physical properties. The FDEMS data indicates during the high temperature holds the molecular mobility is decreasing either due to increased ordering and/or crosslinking of the polymer chains. This decrease in mobility results in a higher degree of super cooling in DSC ramps when the polymer is cooled. As a result, the exothermic peak shifts to lower temperatures on cooling. Decrease in mobility could also be related to the the increase in the endothermic melt temperature from 310° to 320°. Overall, it is difficult to see DSC evidence for a higher % order as this would show up as a larger area under the endothermic and/or exothermic heat up/cool down peaks. Rather, the FDEMS, DSC, and mechanical behaviors seem to point to a drop in molecular mobility which could arise from tighter packing, ordering over larger dimensions, or some additional polymerization. All three of these effects could increase mechanical properties and decrease molecular mobility without showing a significant increase in the area under endothermic melting peak.

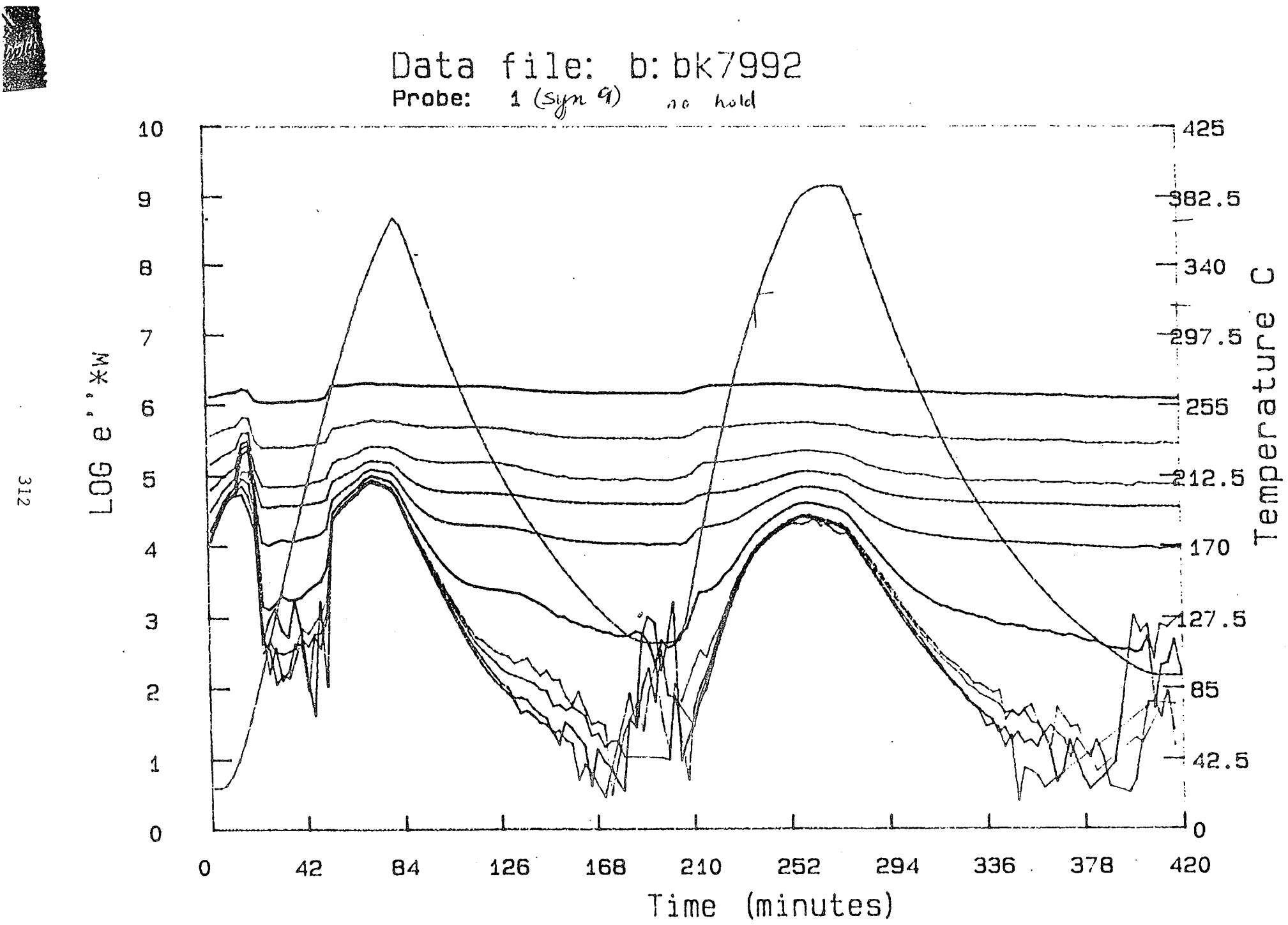
Data file: b:bk7992
Probe: 1 (sym 9) no hold
LOG e''*w
Temperature C
Time (minutes)
10
9
8
7
6
5
4
3
2
1
0
425
382.5
340
297.5
255
212.5
170
127.5
85
42.5
0
0
42
84
126
168
210
252
294
336
378
420

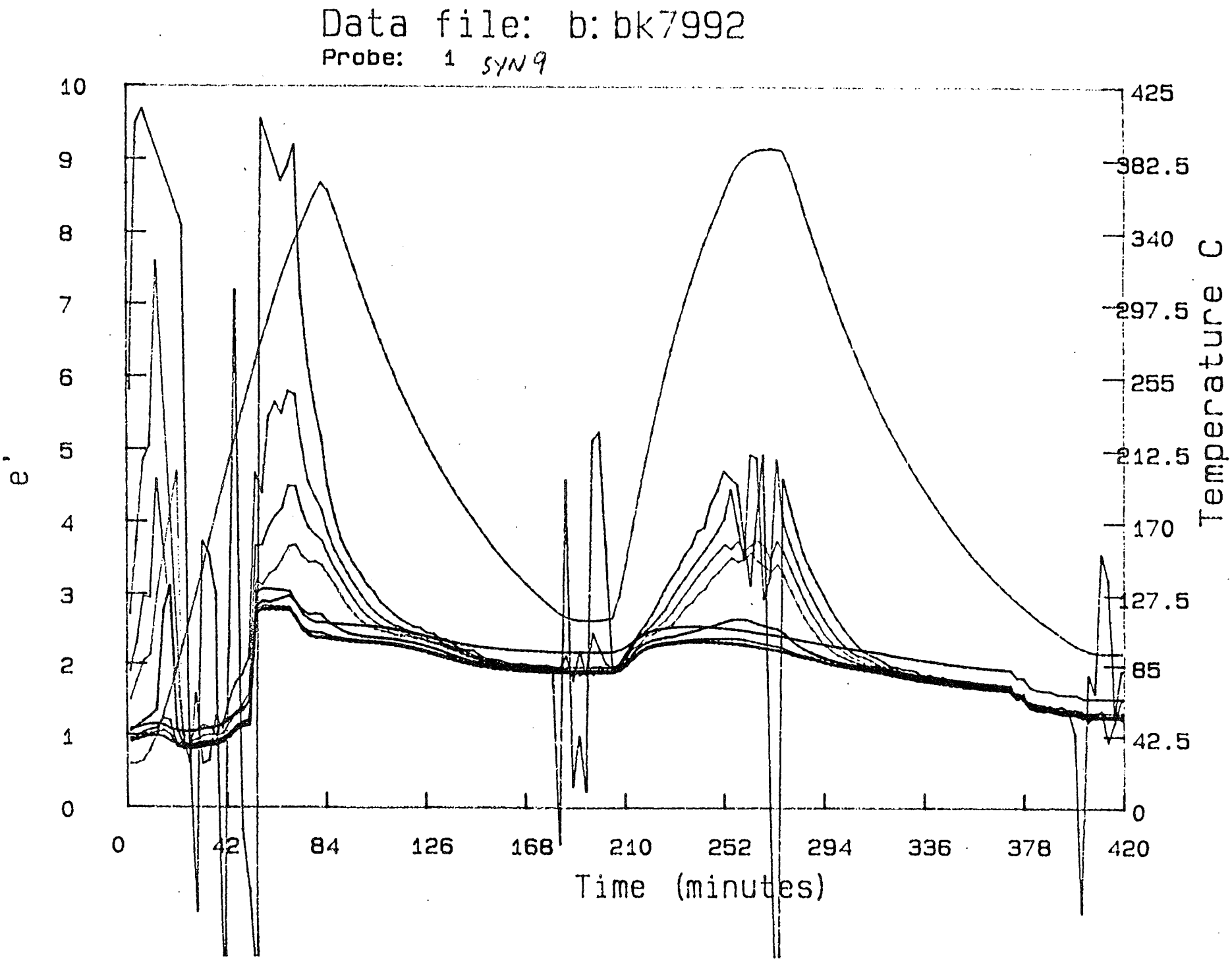
Data file: b:bk7992
Probe: 1 SYN9
e'
Temperature C
Time (minutes)
0
1
2
3
4
5
6
7
8
9
10
0
42.5
85
127.5
170
212.5
255
297.5
340
382.5
425
0
42
84
126
168
210
252
294
336
378
420

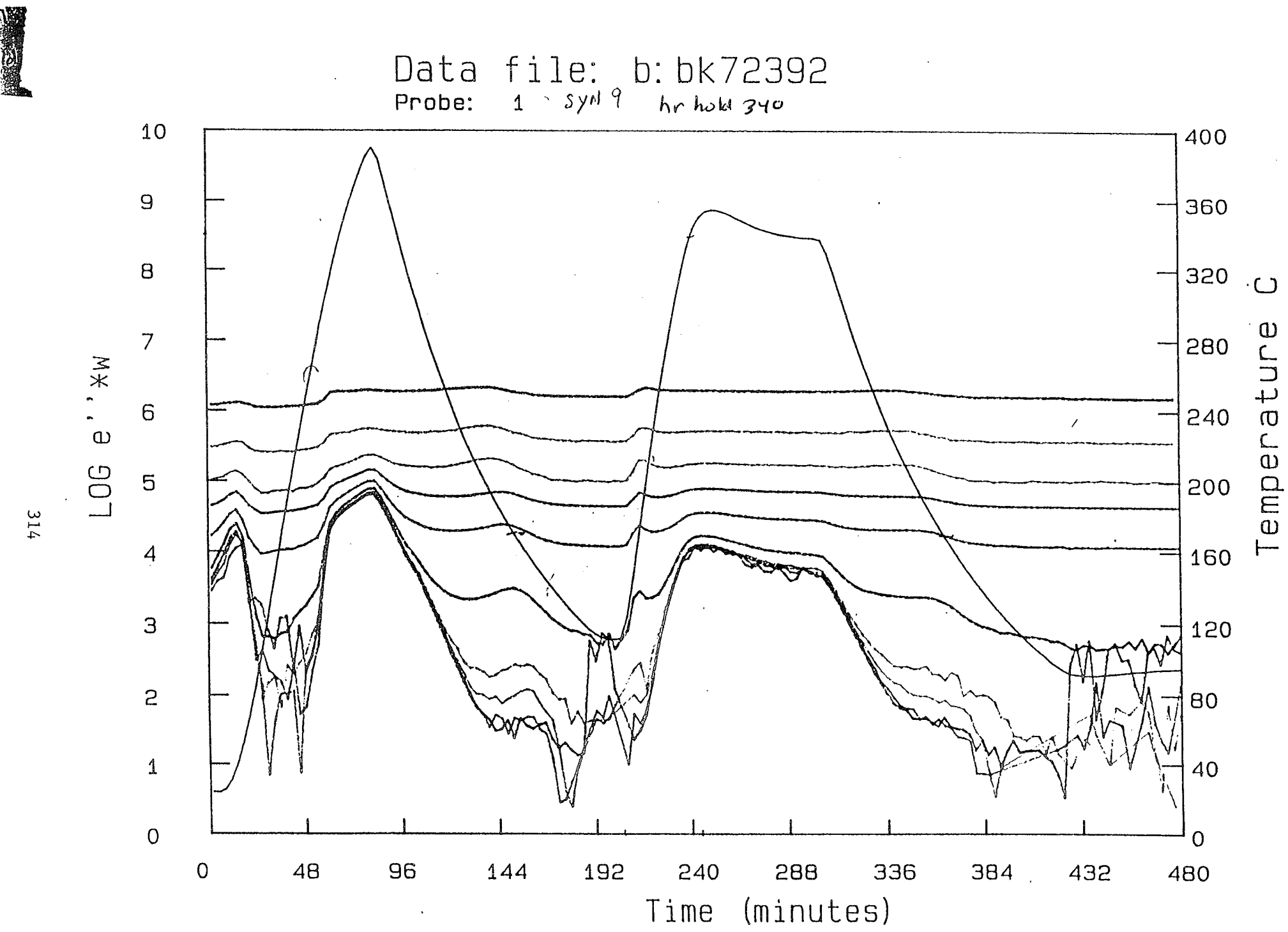
Data file: b:bk72392
Probe: 1 syn 9 hr hold 340
LOG e''*w
Temperature C
Time (minutes)
0
1
2
3
4
5
6
7
8
9
10
0
40
80
120
160
200
240
280
320
360
400
0
48
96
144
192
240
288
336
384
432
480

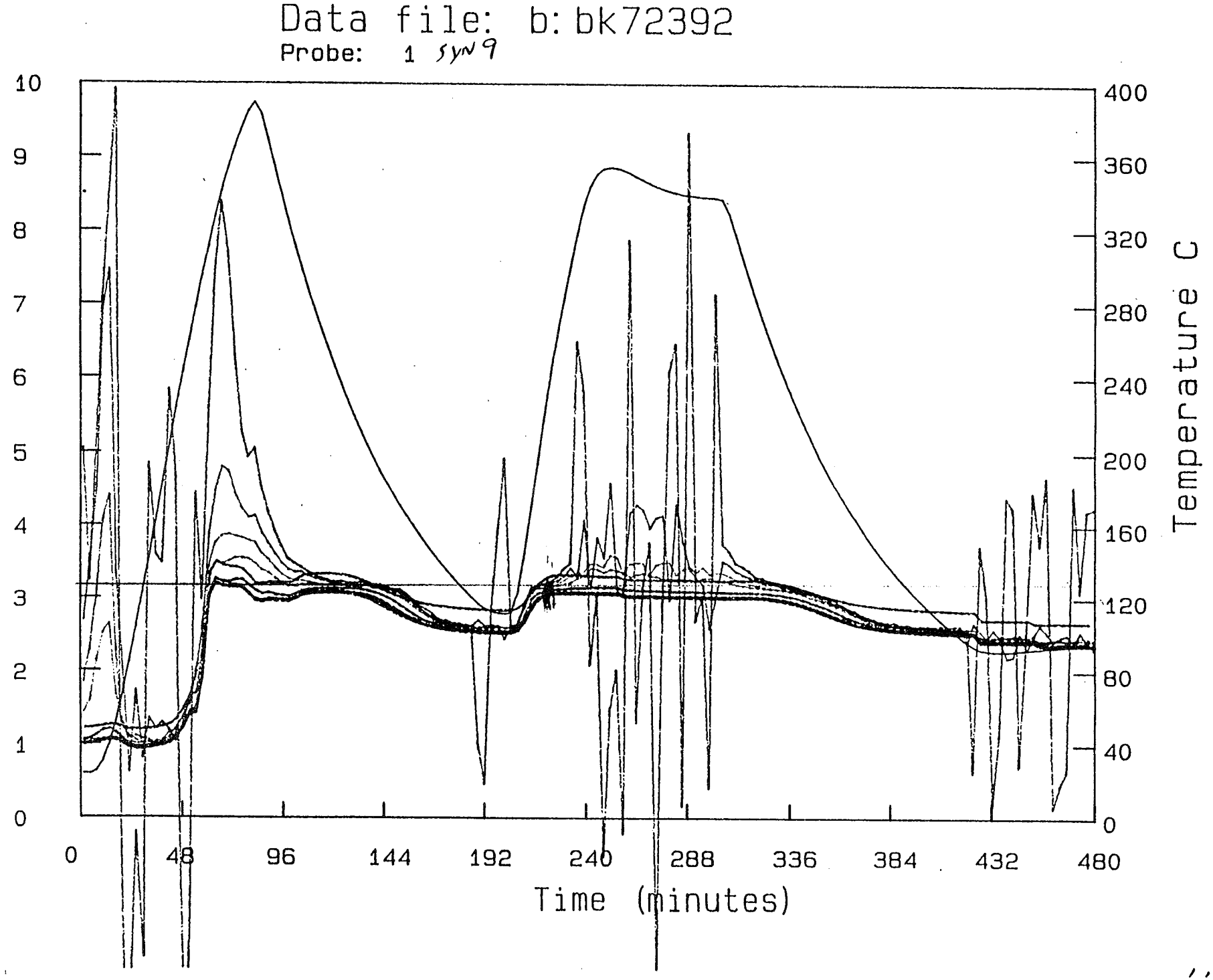
Data file: b:bk72392
Probe: 1 syn9
e'
Temperature C
Time (minutes)
0
1
2
3
4
5
6
7
8
9
10
0
40
80
120
160
200
240
280
320
360
400
0
48
96
144
192
240
288
336
384
432
480

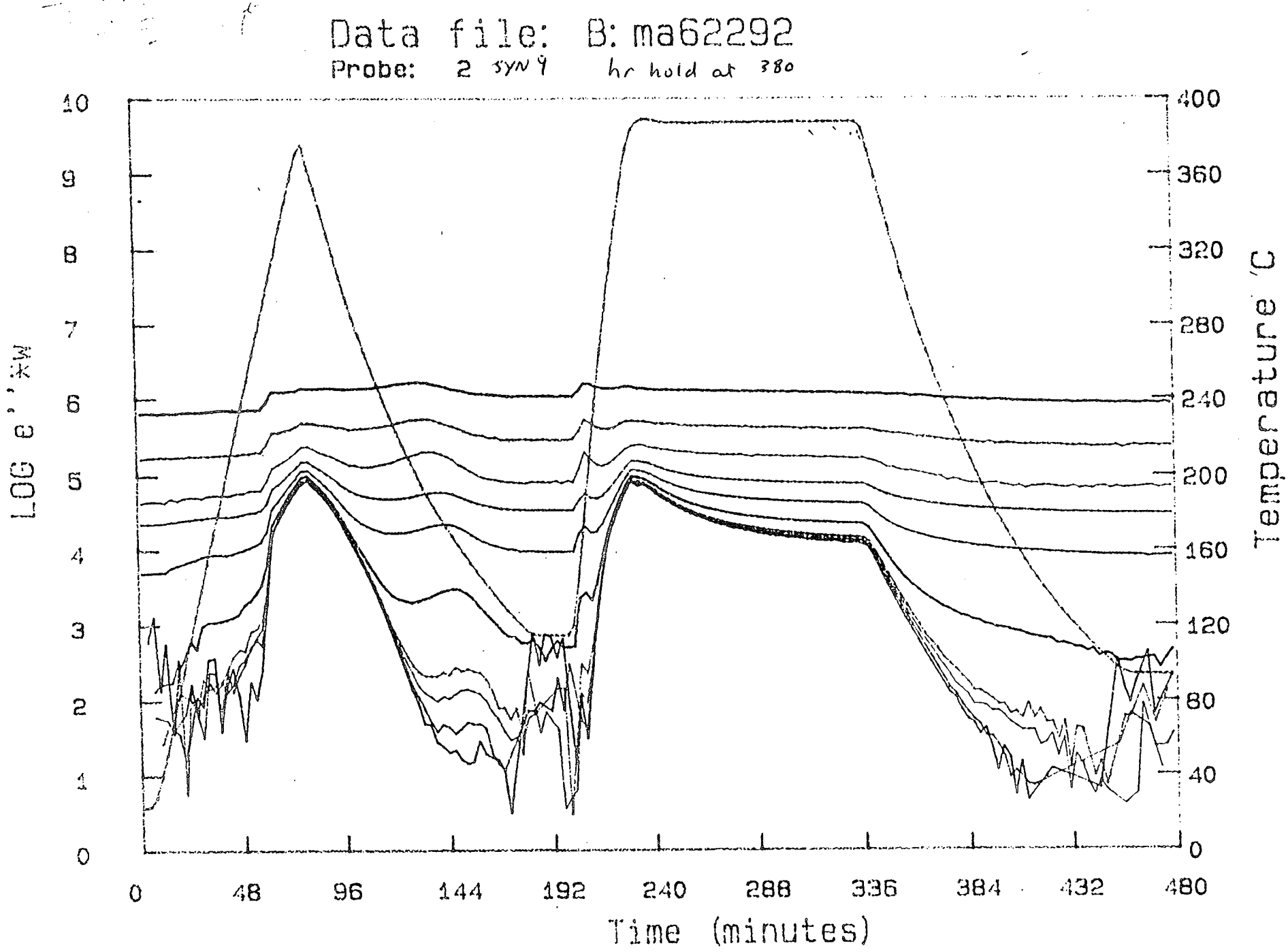
Data file: B:ma62292
Probe: 2 syn 9 hr hold at 380
LOG e''*w
Temperature C
Time (minutes)
0
1
2
3
4
5
6
7
8
9
10
0
40
80
120
160
200
240
280
320
360
400
0
48
96
144
192
240
288
336
384
432
480

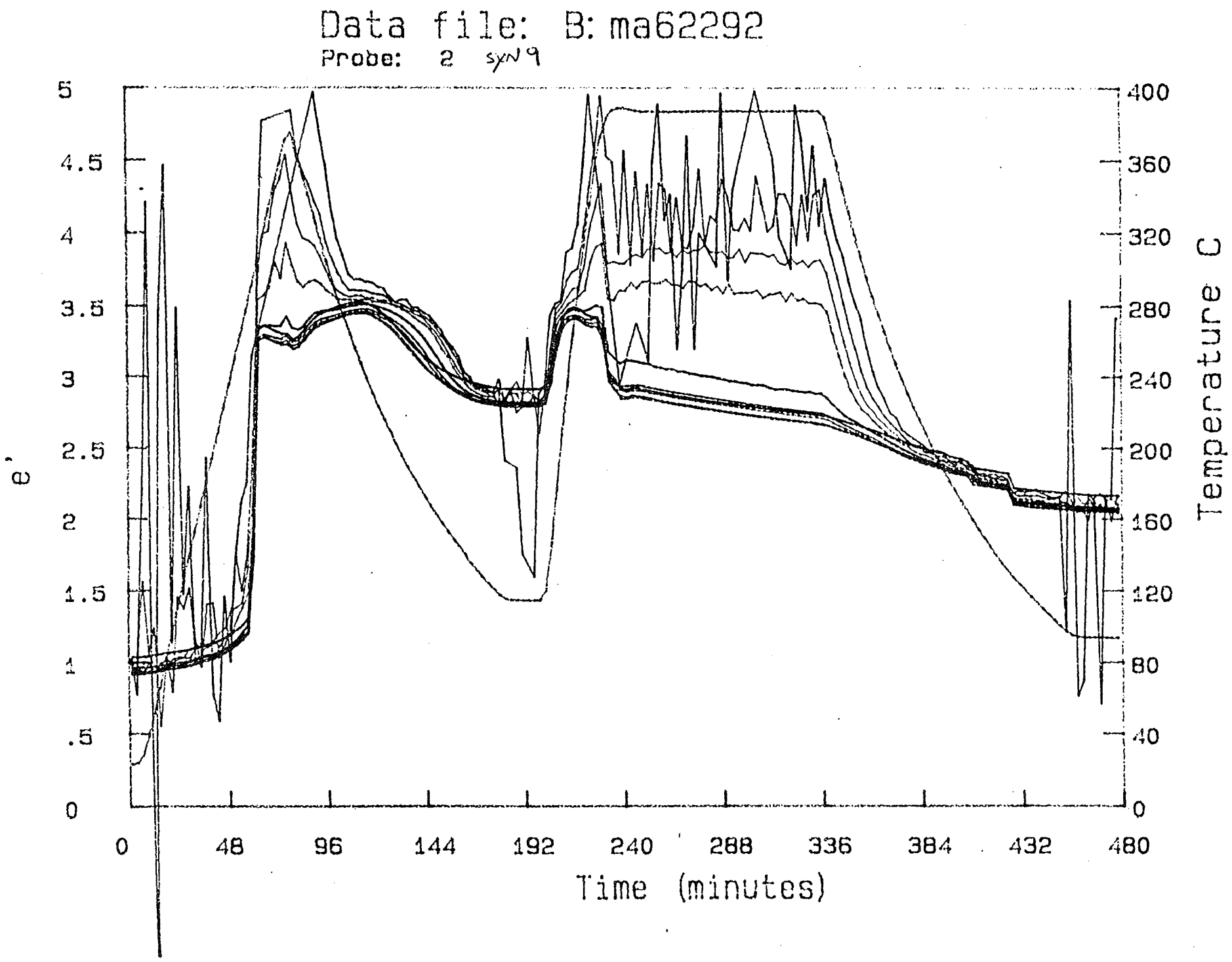
Data file: B:ma62292
Probe: 2 syn9
e'
Temperature C
Time (minutes)
0
.5
1
1.5
2
2.5
3
3.5
4
4.5
5
40
80
120
160
200
240
280
320
360
400
0
48
96
144
192
240
288
336
384
432
480

DSC Data File: ey903
Sample Weight: 5.300 mg
Sat Jul 25 12:32:55 1992
SYN-9 (fresh) empty ref

PERKIN-ELMER
7 Series Thermal Analysis System

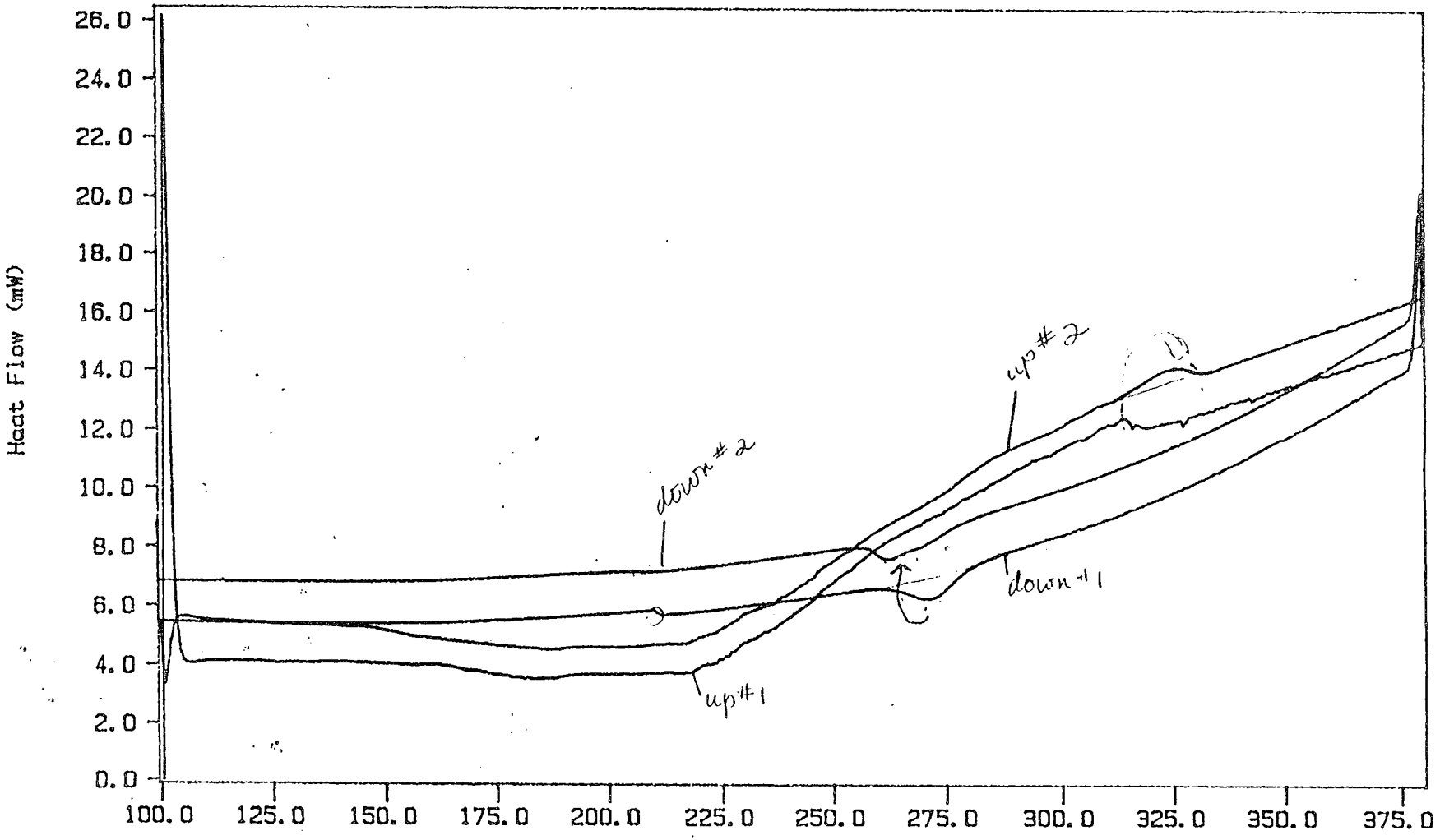

Ramp 100-380-100-380-100C 10C/min

TEMP 1: 100.0 C TIME 1: 0.0 min RATE 1: 10.0 C/min
TEMP 2: 380.0 C TIME 2: 0.0 min RATE 2: 10.0 C/min
TEMP 3: 100.0 C TIME 3: 0.0 min RATE 3: 10.0 C/min
TEMP 4: 380.0 C TIME 4: 0.0 min RATE 4: 10.0 C/min
TEMP 5: 100.0 C

DSC Data File: sy906
Sample Weight: 5.400 mg
Fri Jul 31 22:09:27 1992
Syn 9 (sy904) Ramp 100-380-100C

PERKIN-ELMER
7 Series Thermal Analysis System

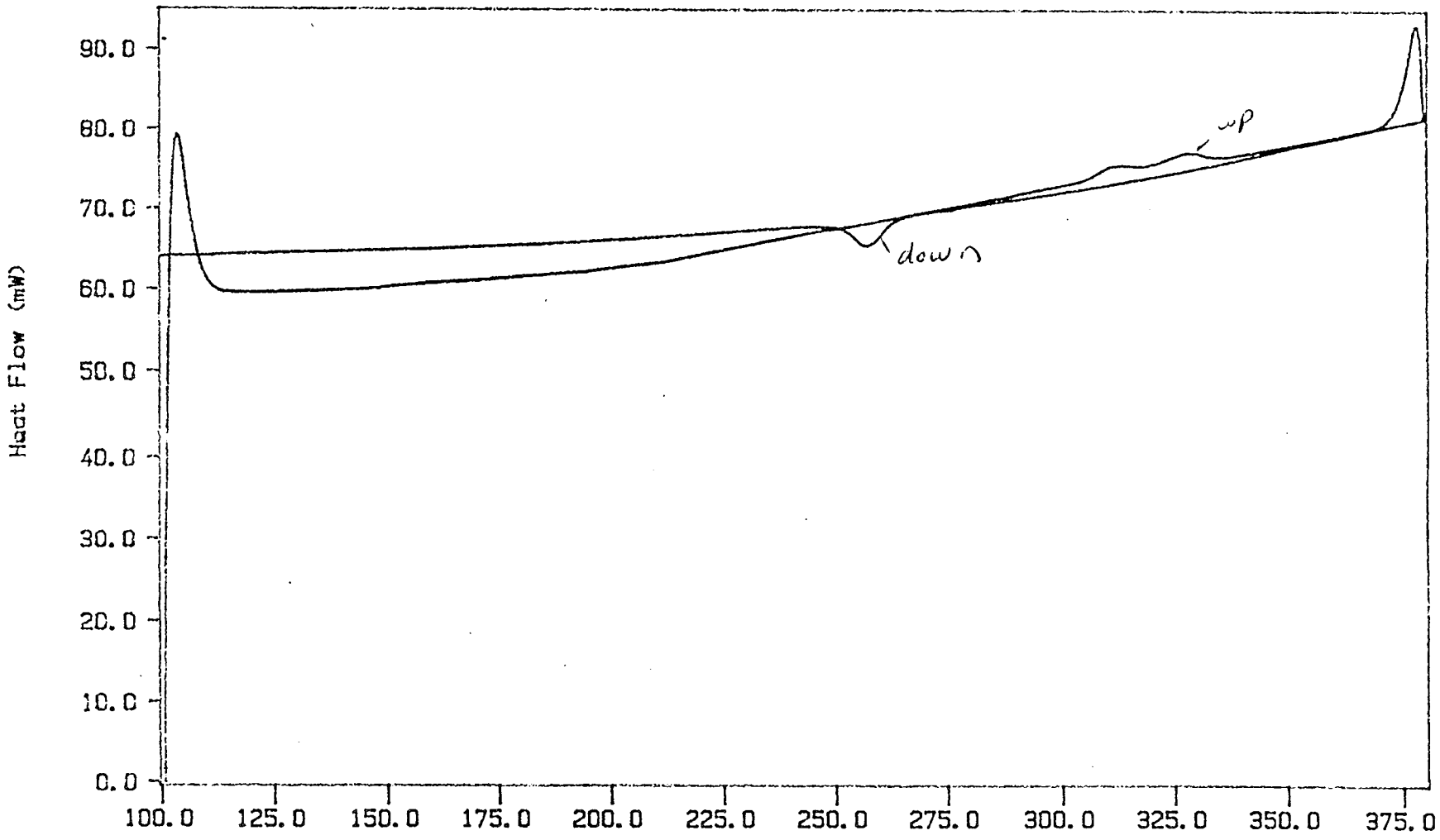

30C/min empty ref Jar/dmc

TEMP 1: 100.0 C TIME 1: 0.0 min RATE 1: 80.0 C/min
TEMP 2: 380.0 C TIME 2: 0.0 min RATE 2: 90.0 C/min
TEMP 3: 100.0 C

DSC Data File: ey907
Sample Weight: 4.800 mg
Sat Aug 01 01:56:16 1992
Syn9 (ey903) Empty ref

PERKIN-ELMER
7 Series Thermal Analysis System

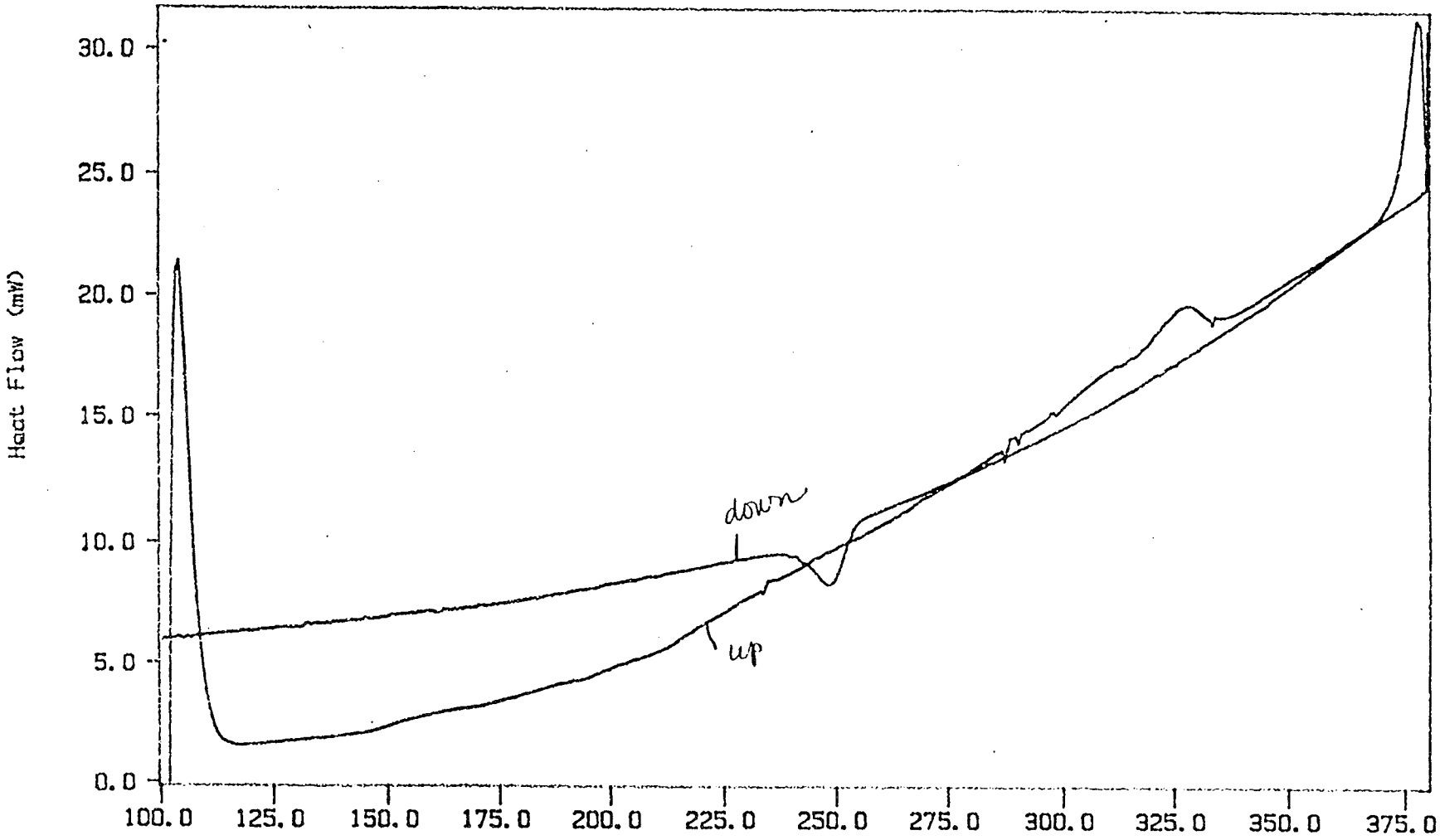

Ramp 100-380(10min hold)-100C 30C/min Jar/dmc

TEMP 1: 100.0 C TIME 1: 0.0 min RATE 1: 30.0 C/min
TEMP 2: 380.0 C TIME 2: 10.0 min RATE 2: 90.0 C/min
TEMP 3: 100.0 C

DSC Data File: sy908
Sample Weight: 4.800 mg
Sat Aug 01 04:28:21 1992
Syn9 (sy903) empty ref

PERKIN-ELMER #2
7 Series Thermal Analysis System

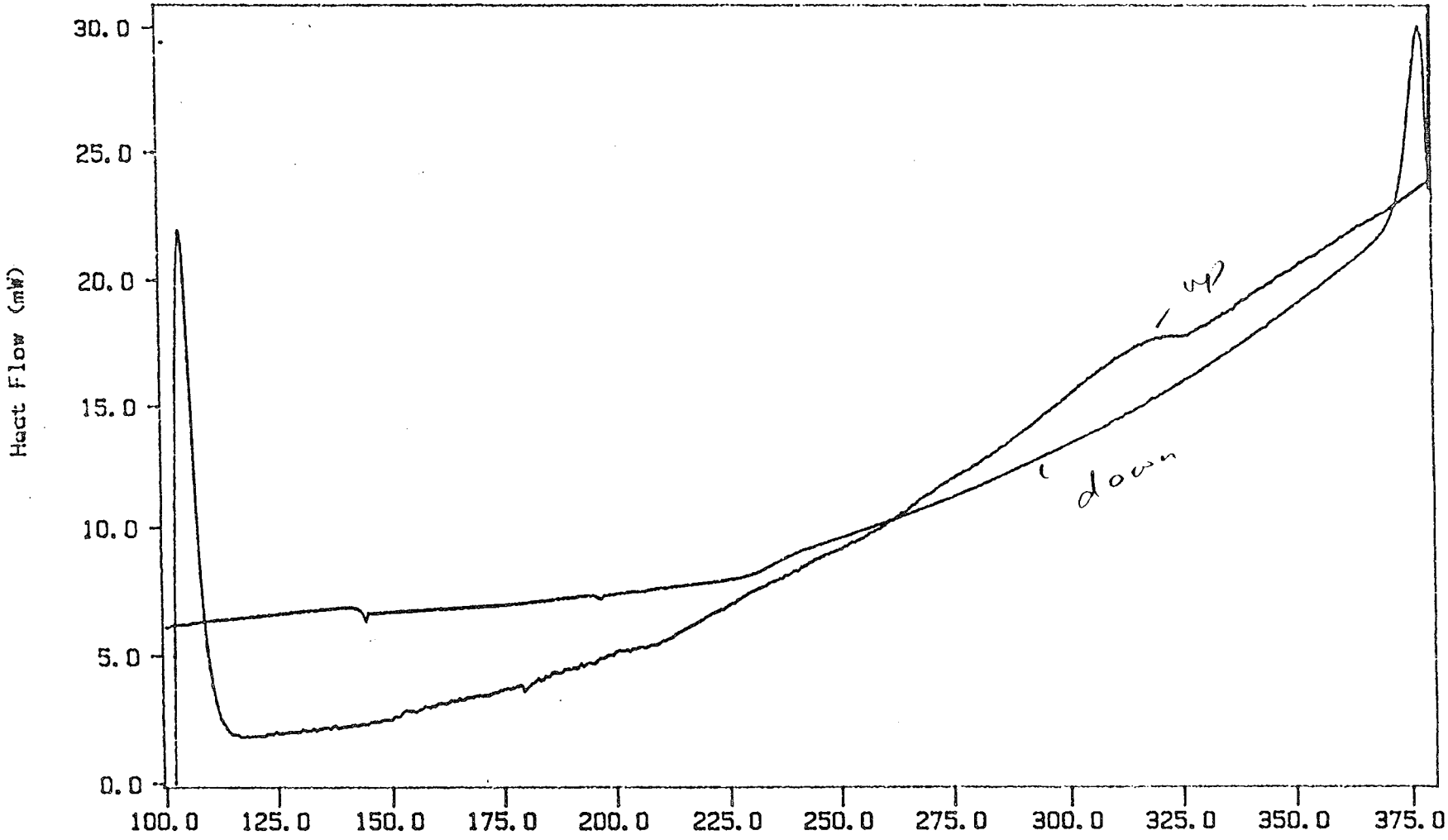

Ramp 100-380(10min hold)-100C 30C/min Temperature (°C) jar/dmc

TEMP 1: 100.0 C TIME 1: 0.0 min RATE 1: 30.0 C/min
TEMP 2: 380.0 C TIME 2: 10.0 min RATE 2: 80.0 C/min
TEMP 3: 100.0 C

THERMAL ANALYSIS DATA

DATE 92/08/04

FILE NAME A804K13.000 [TMA]

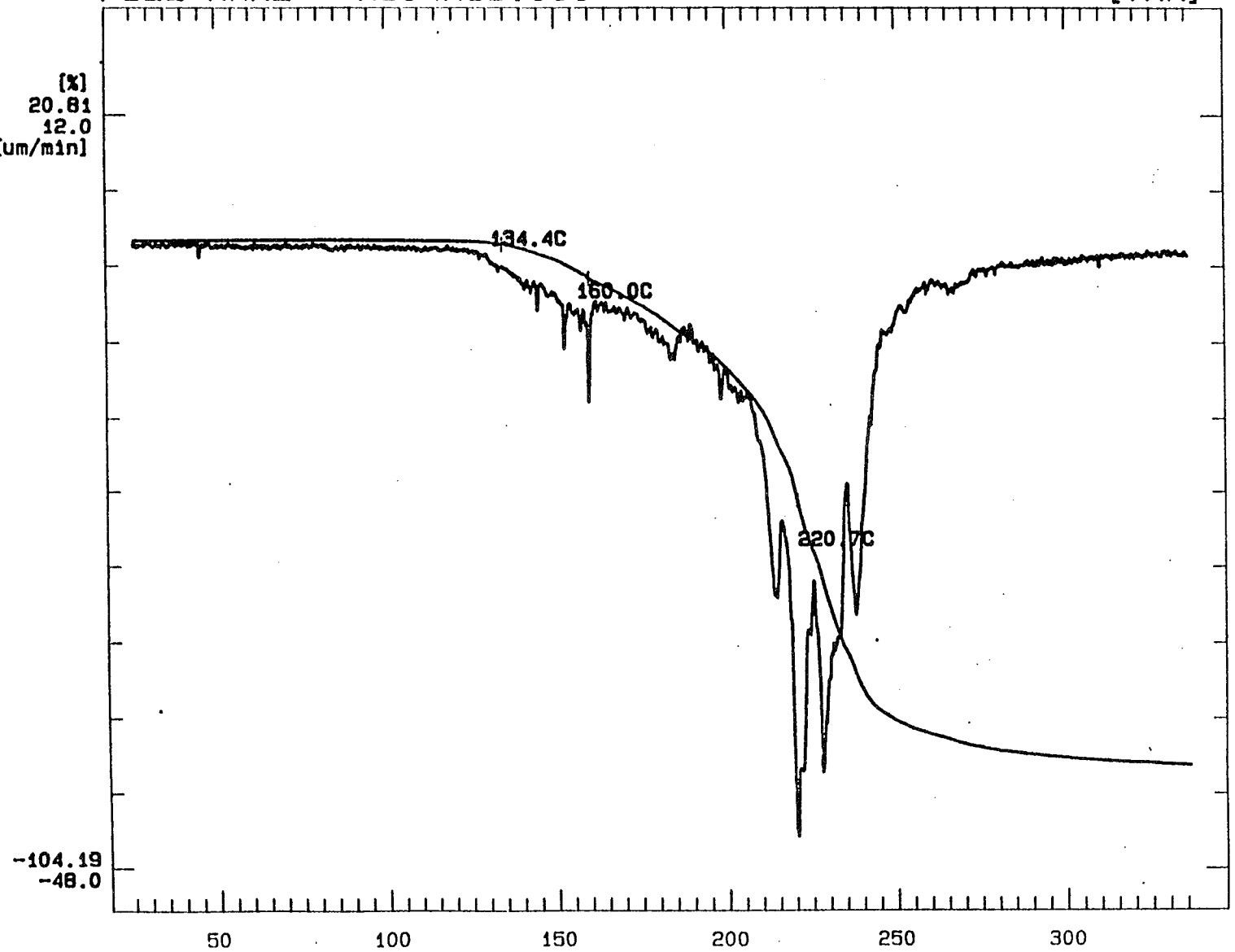

MEASURING CONDITIONS

SAMPLE NAME	Syn9up
SAMPLE SIZE	0.480
SAMPLING INT	1.0
ACQ. DATE	92/08/

COMMENT

ramp rt-450 5C/min

HEATING PROGRAM

	RATE	TEMP	TIM
1	5.0	450.0	

syn 9 - previously ramped to 380 and back down

Brian Kipp
Dr. D. Kranbuehl

Dave Olmeijer

SHIMADZU

321

2

THERMAL ANALYSIS DATA

DATE 92/08/03

FILE NAME A803L49.000 [TMA]

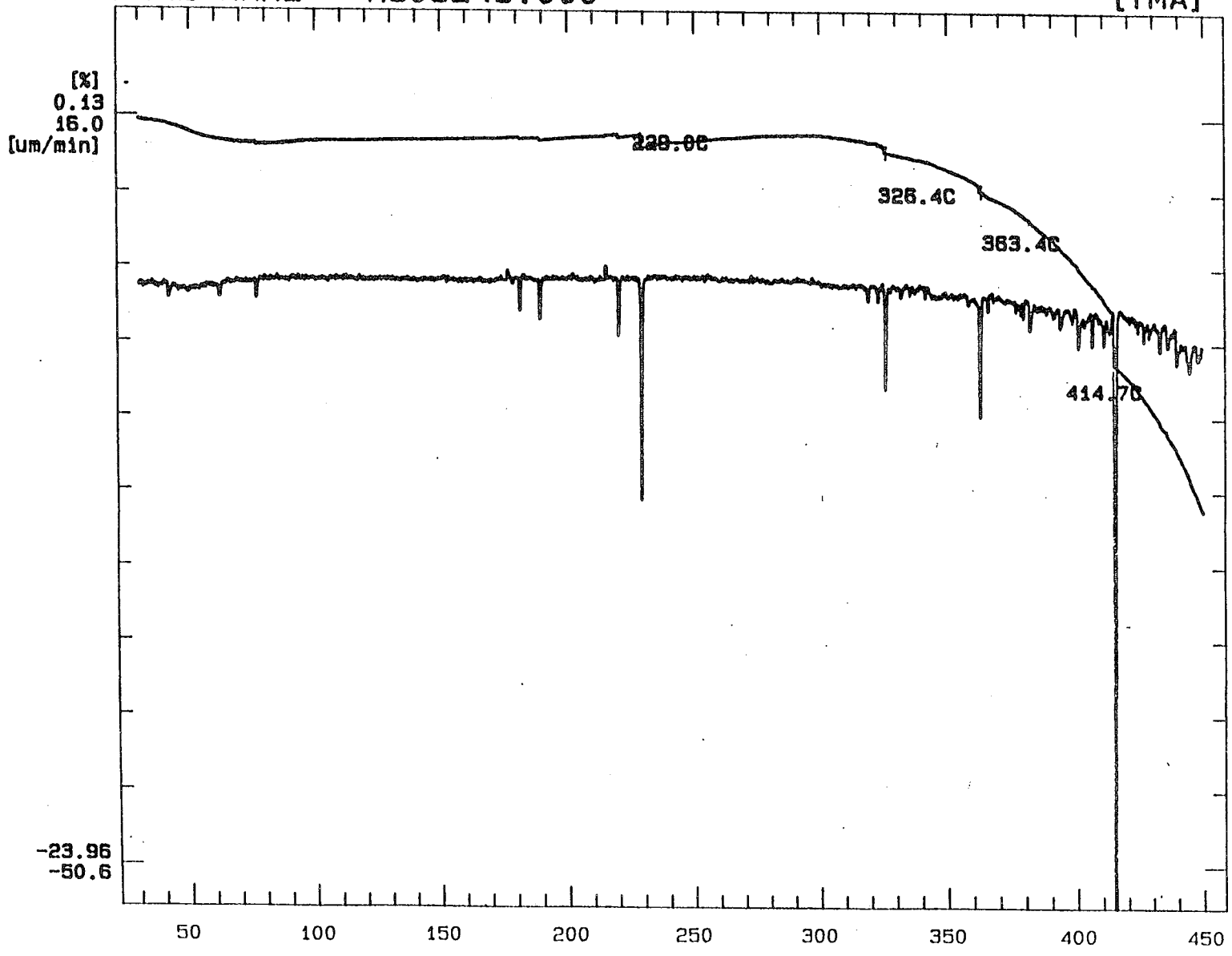

MEASURING CONDITIONS

SAMPLE NAME	syn9
SAMPLE SIZE	0.830
SAMPLING INT	1.0
ACQ. DATE	92/08/

COMMENT

syn9 remprt-450cured

HEATING PROGRAM

	RATE	TEMP	TIM
1	5.0	450.0	

Syn 9 - previously held for 1 hr at 380

THERMAL ANALYSIS DATA

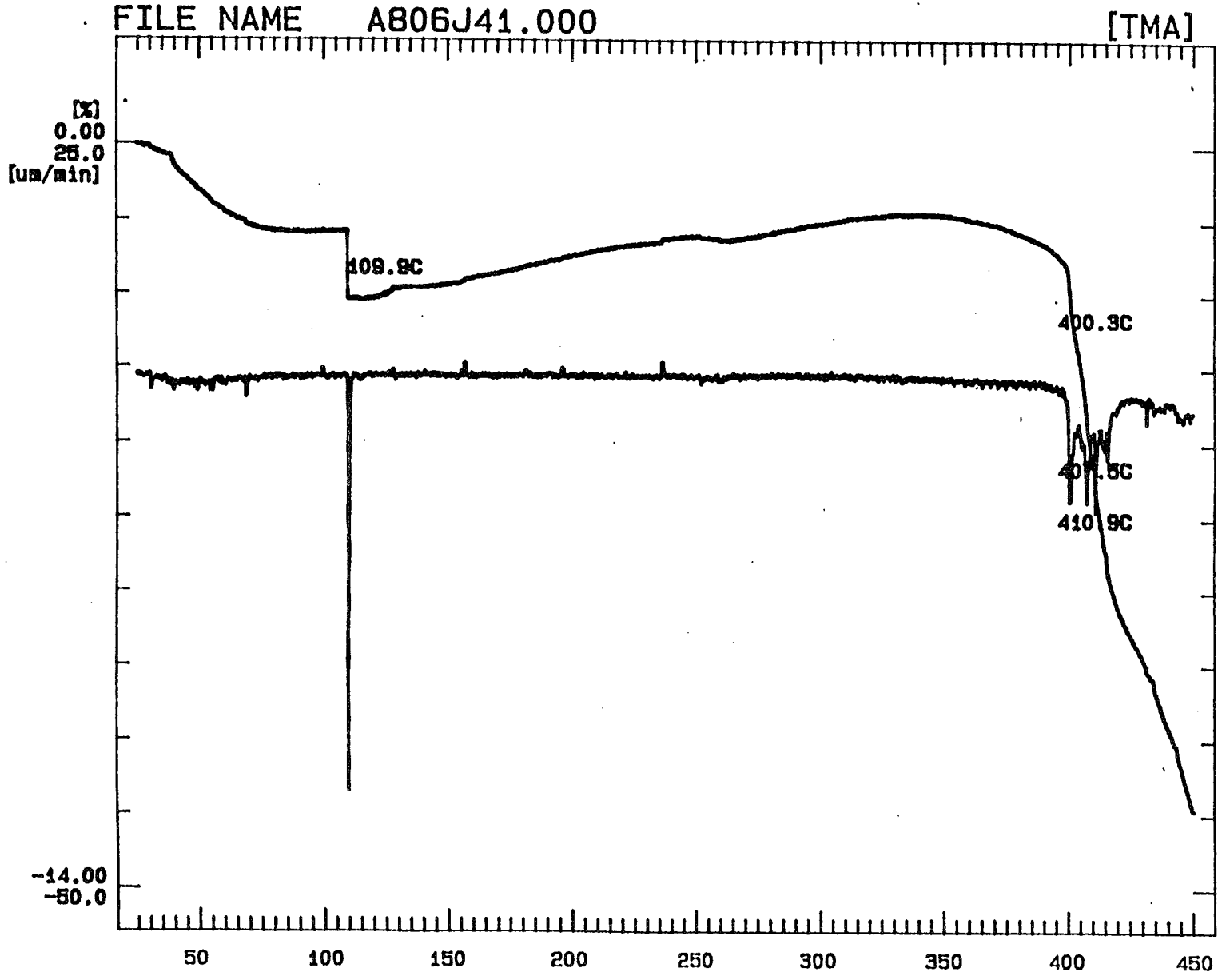

DATE 92/08/06

MEASURING CONDITIONS

SAMPLE NAME	synSh1
SAMPLE SIZE	0.520
SAMPLING INT	1.0
ACQ. DATE	92/08/

COMMENT

ramp rt-450, 5C/min

HEATING PROGRAM

	RATE	TEMP	TIM
1	5.0	450.0	

SYN9
hr hold @
380°C

WILLIAM

SYN 10

The FDEMS results and DSC results for SYN-10 are similar to SYN-9. Of particular importance are Figures 26 and 27. Again, the 380° hold shows a sharp drop in ionic mobility as shown by the drop in ε" during the hold. further, the dipolar peaks in the 150°-220° range on cool down disappear. Further, the value of ε' has dropped.

FDEMS output for the double up-down ramp sequence and the 340° hold are shown in Figures 28-31. The DSC output for a double up-down ramp is shown in Figure 32. The upward shift in the melt endotherm and the downward shift in the crystallizing exotherm are similar to the SYN-9 system. Figures 33, 35, and 35 emphasize this point even more as the sample is held at 380° for 10 minutes between 33 and 34 and another 10 minutes between 34 and 35. The exothermic crystallization peak drops from 303° to 250°.

Similar to SYN-9, the mechanical properties of the fresh SYN-10 show a 100% penetration between 150° and 200°. A 1 hour hold at 380° decreases the penetration to 10% and increases the softening region to 240° to 310°, Figures 36 and 37.

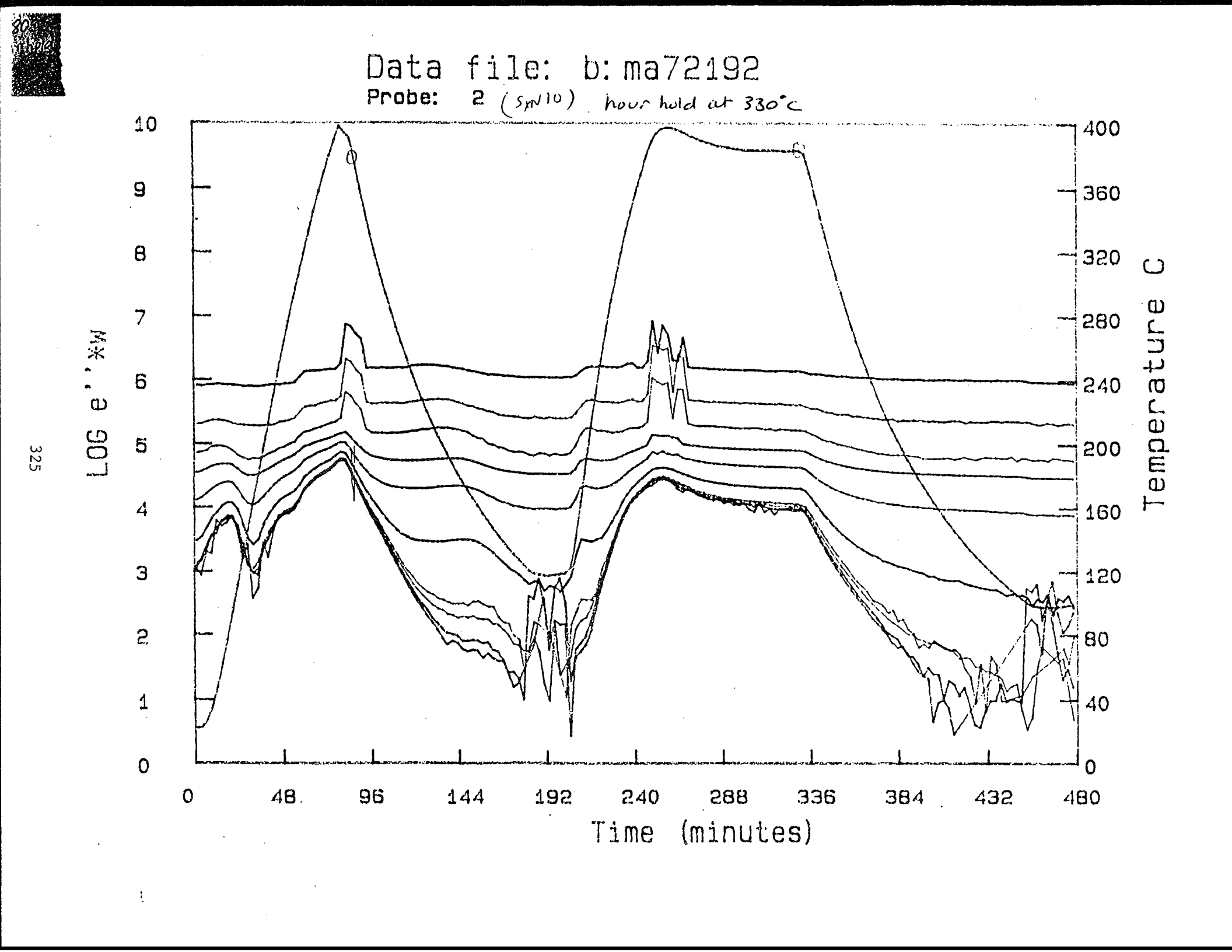
Data file: b:ma72192
Probe: 2 (SM10) hour hold at 330°C
LOG e''*W
Temperature C
Time (minutes)
0
1
2
3
4
5
6
7
8
9
10
0
40
80
120
160
200
240
280
320
360
400
0
48
96
144
192
240
288
336
384
432
480

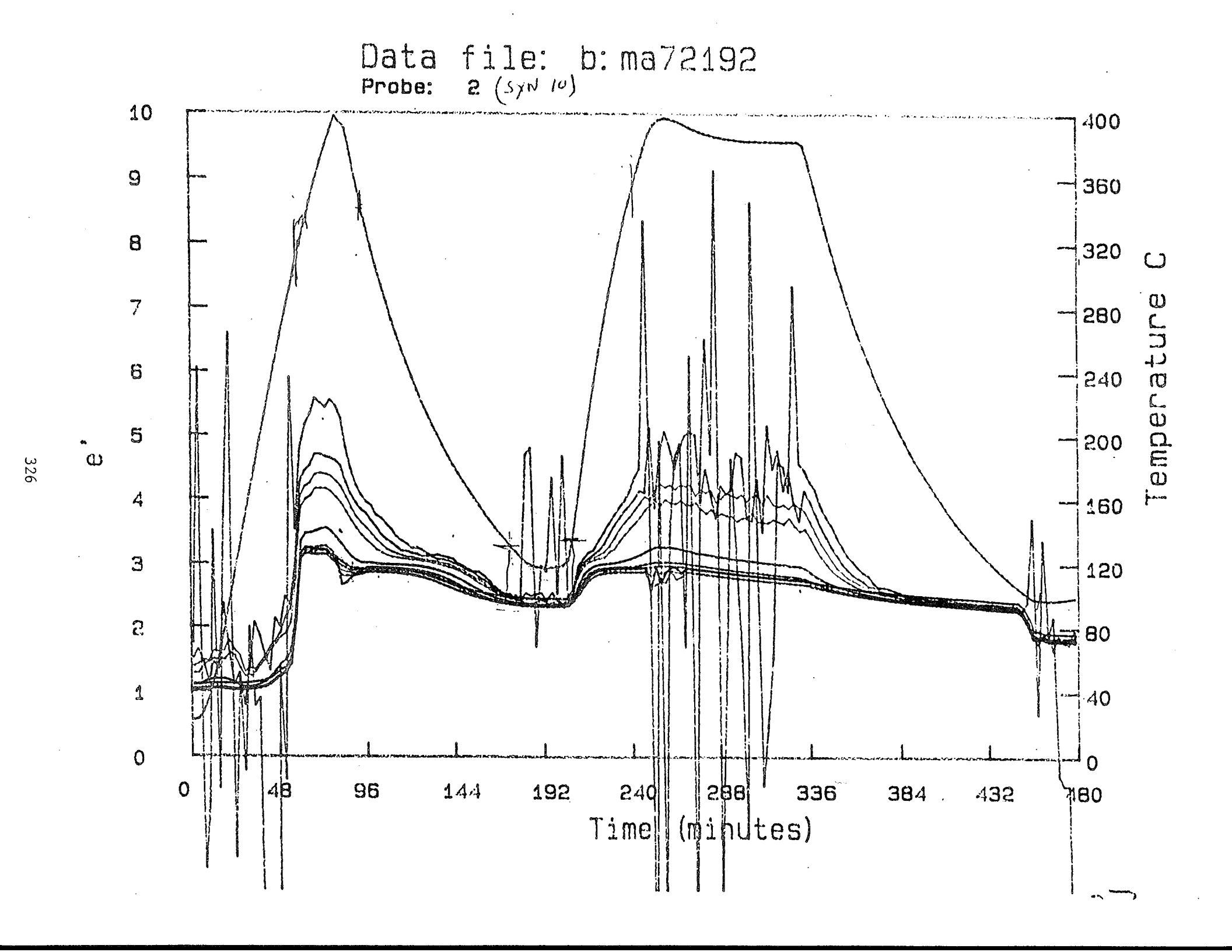
Data file: b:ma72192
Probe: 2 (SYN 10)
e'
Temperature C
Time (minutes)
0
1
2
3
4
5
6
7
8
9
10
0
40
80
120
160
200
240
280
320
360
400
0
48
96
144
192
240
288
336
384
432
480

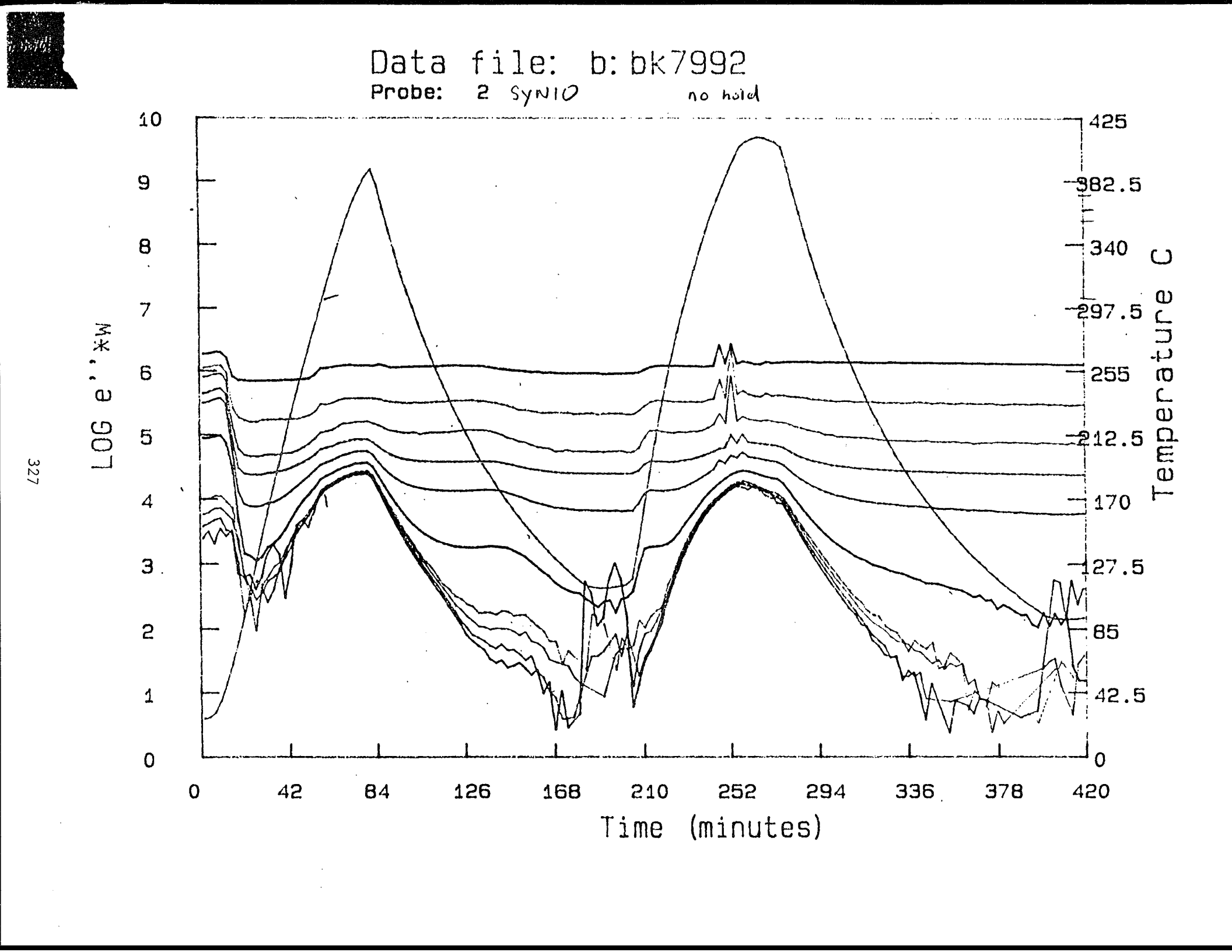
Data file: b:bk7992
Probe: 2 SyN10
no hold
LOG e''*W
Temperature C
Time (minutes)
10
9
8
7
6
5
4
3
2
1
0
425
382.5
340
297.5
255
212.5
170
127.5
85
42.5
0
0
42
84
126
168
210
252
294
336
378
420

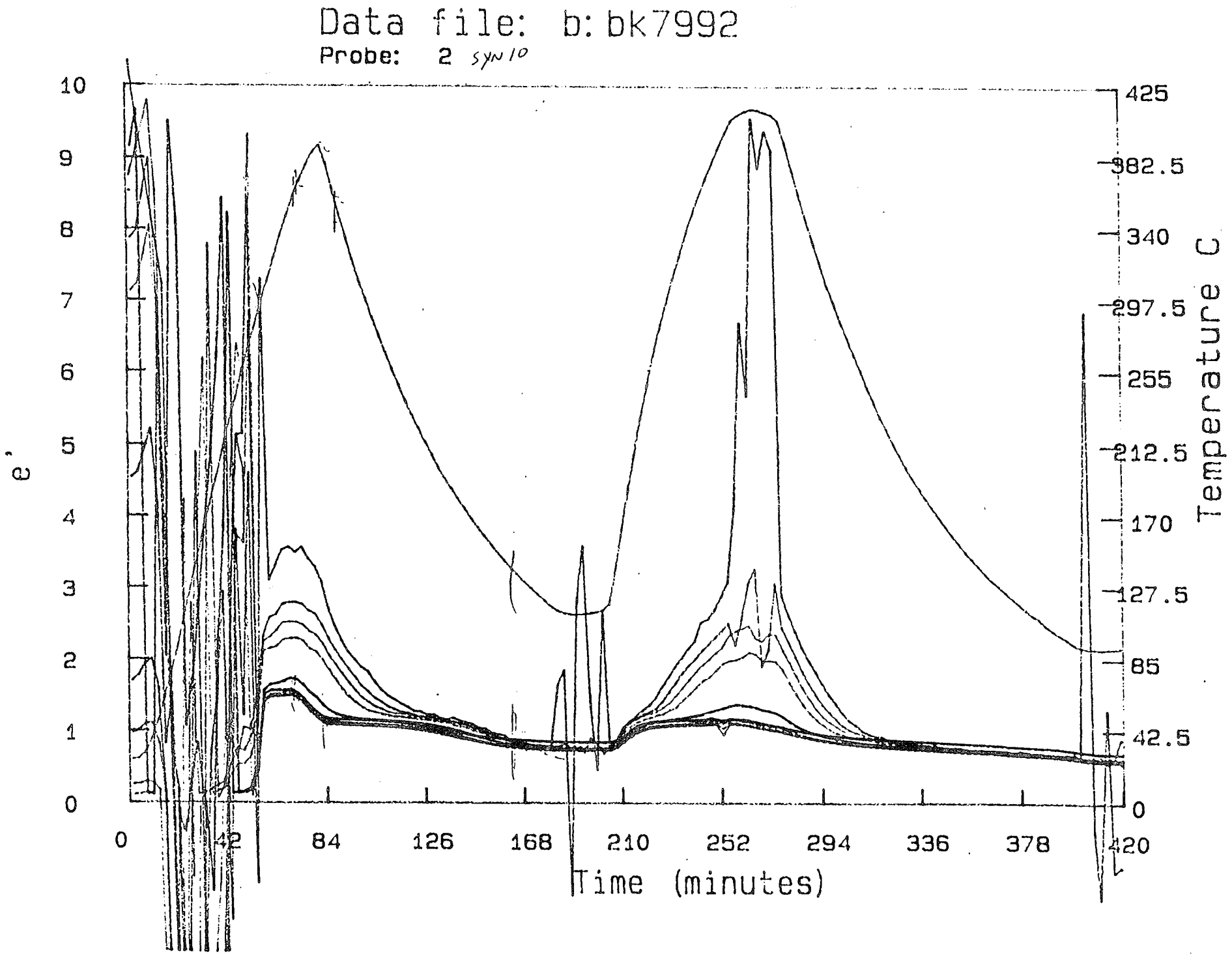
Data file: b:bk7992
Probe: 2 syn 10
10
9
8
7
6
5
4
3
2
1
0
e'
0
42
84
126
168
210
252
294
336
378
420
Time (minutes)
425
382.5
340
297.5
255
212.5
170
127.5
85
42.5
0
Temperature C

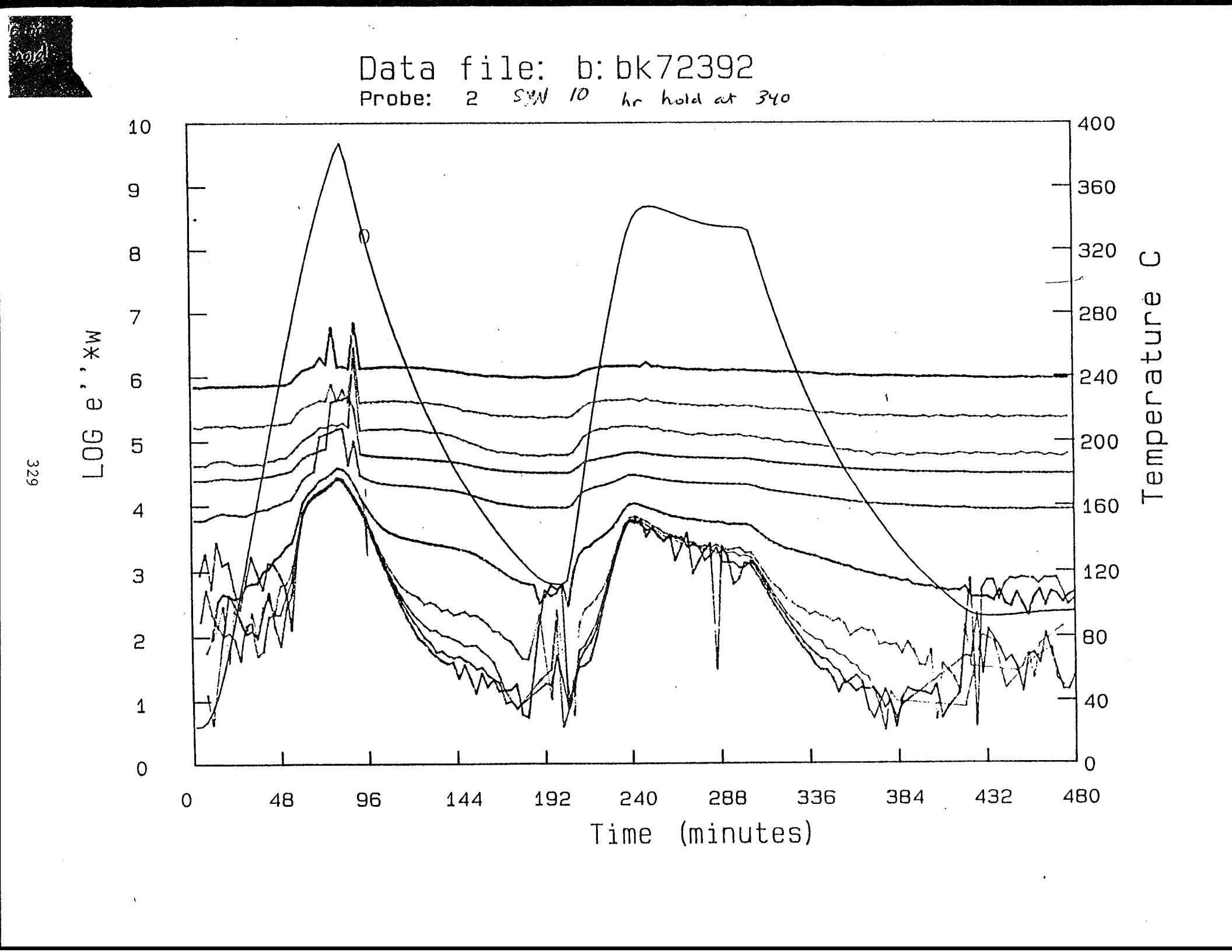
Data file: b:bk72392
Probe: 2 SYN 10 hr hold at 340
LOG e''*W
Temperature C
Time (minutes)
0
1
2
3
4
5
6
7
8
9
10
0
40
80
120
160
200
240
280
320
360
400
0
48
96
144
192
240
288
336
384
432
480

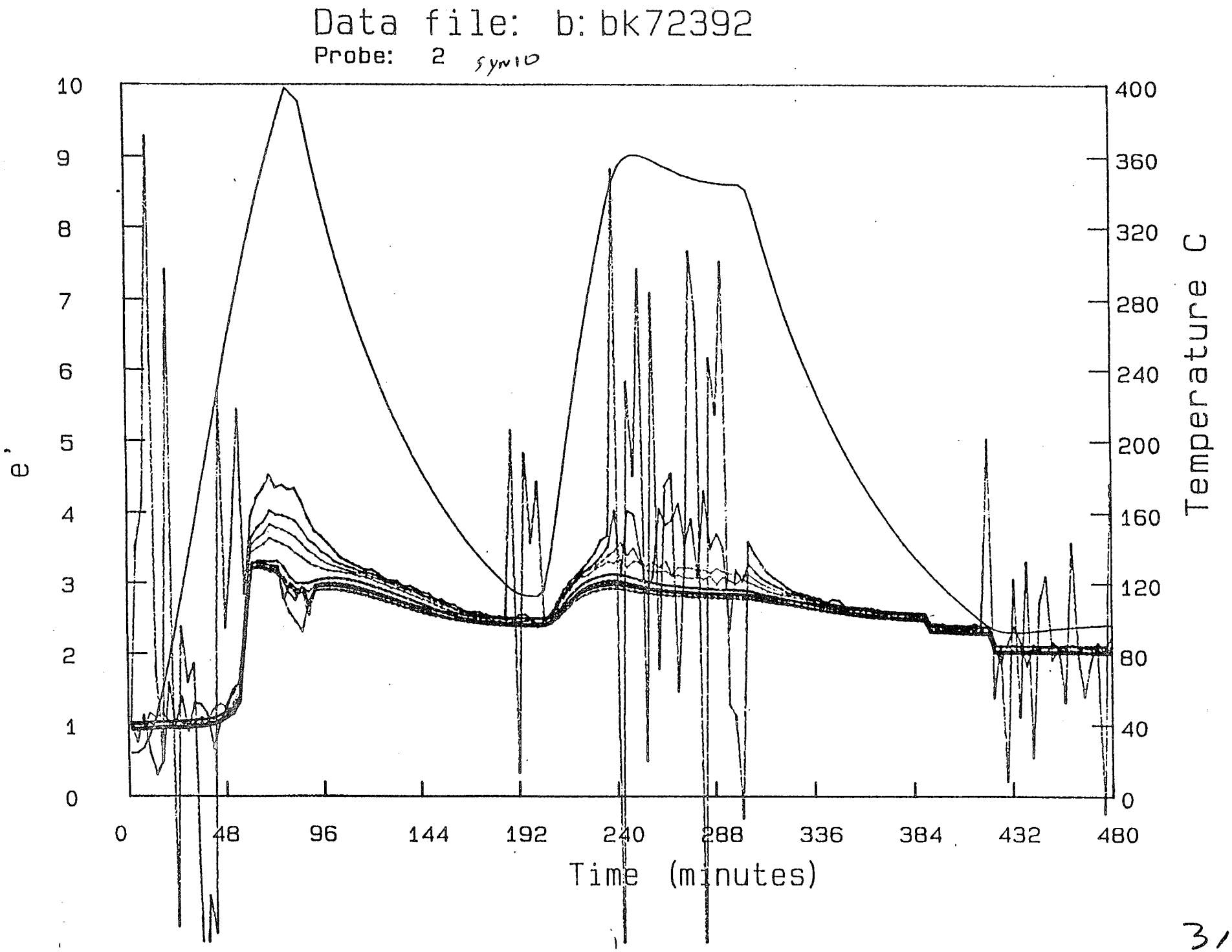
Data file: b:bk72392
Probe: 2 sym10
e'
Temperature C
Time (minutes)
0
1
2
3
4
5
6
7
8
9
10
0
40
80
120
160
200
240
280
320
360
400
0
48
96
144
192
240
288
336
384
432
480

3/

DSC Data File: syn03
Sample Weight: 5.400 mg
Sun Jul 26 02:04:48 1992
syn10 fresh: Ramp 100-380-100-380-200C

PERKIN-ELMER
7 Series Thermal Analysis System

no holds

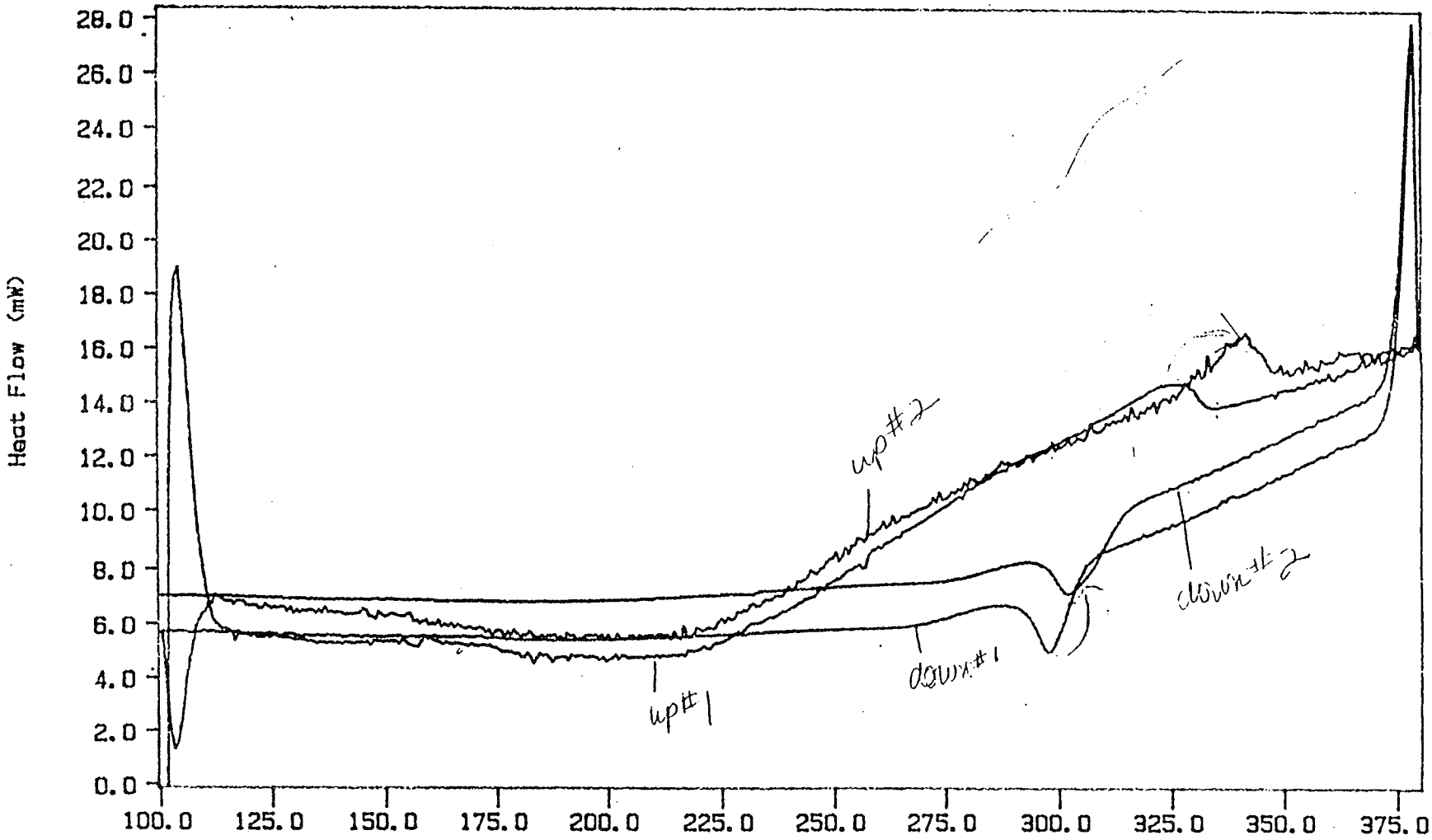

30C/min; empty ref Jar/dmc

TEMP 1:	100.0 C	TIME 1:	0.0 min	RATE 1:	90.0 C/min		
TEMP 2:	380.0 C	TIME 2:	0.0 min	RATE 2:	30.0 C/min		
TEMP 3:	100.0 C	TIME 3:	0.0 min	RATE 3:	90.0 C/min		
TEMP 4:	380.0 C	TIME 4:	0.0 min	RATE 4:	30.0 C/min		
TEMP 5:	100.0 C						

DSC Data File: syn08
Sample Weight: 5.300 mg
Fri Jul 31 22:51:52 1992
Syn10 (syn03) Ramp 100-380-100C

PERKIN-ELMER
7 Series Thermal Analysis System

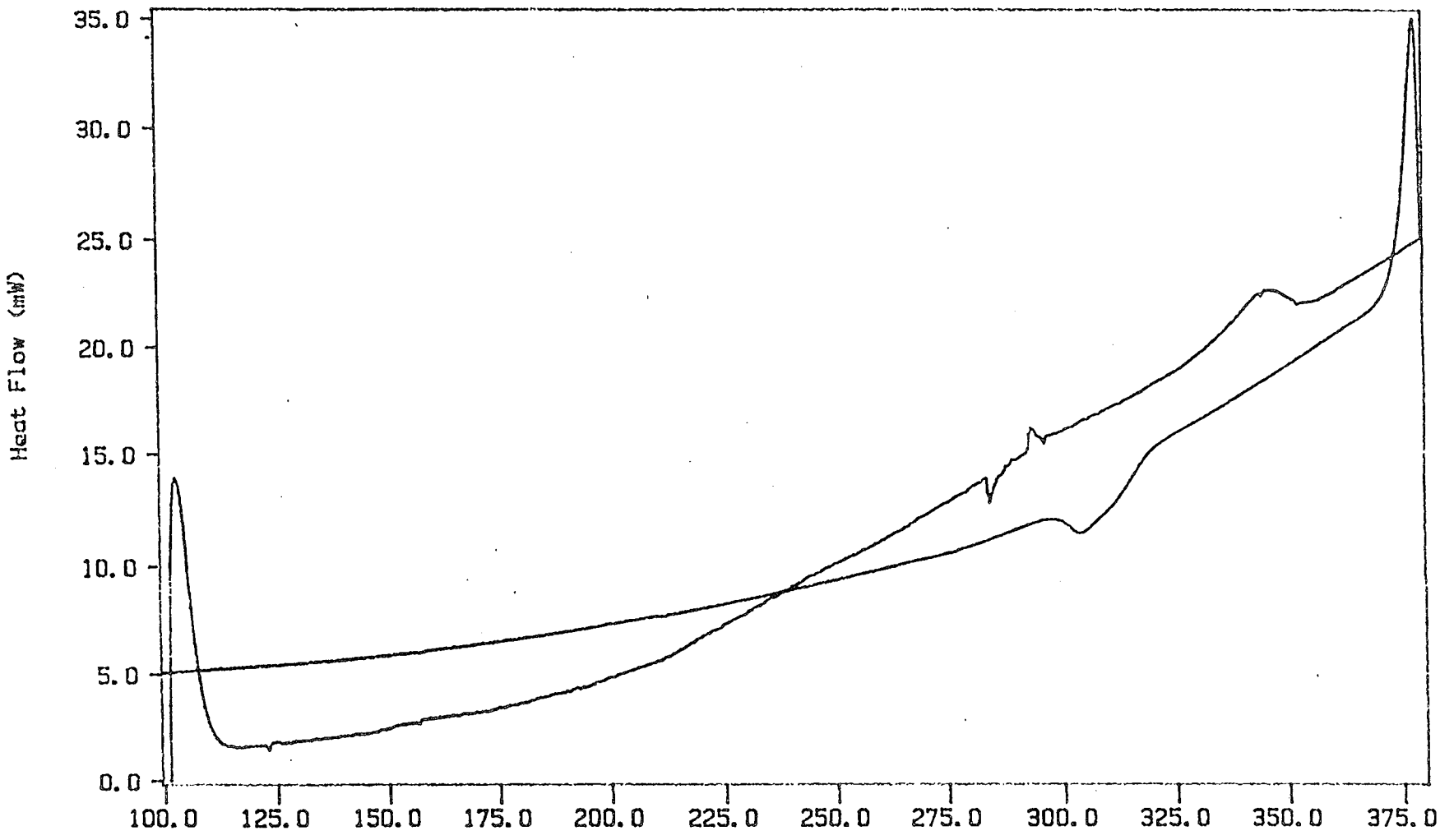

30C/min empty ref jar/dmc

TEMP 1: 100.0 C TIME 1: 0.0 min RATE 1: 80.0 C/min
TEMP 2: 380.0 C TIME 2: 0.0 min RATE 2: 80.0 C/min
TEMP 3: 100.0 C

DSC Data File: syn09
Sample Weight: 5.300 mg
Sat Aug 01 02:44:29 1992
Syn10 (syn03) empty ref

PERKIN-ELMER
7 Series Thermal Analysis System

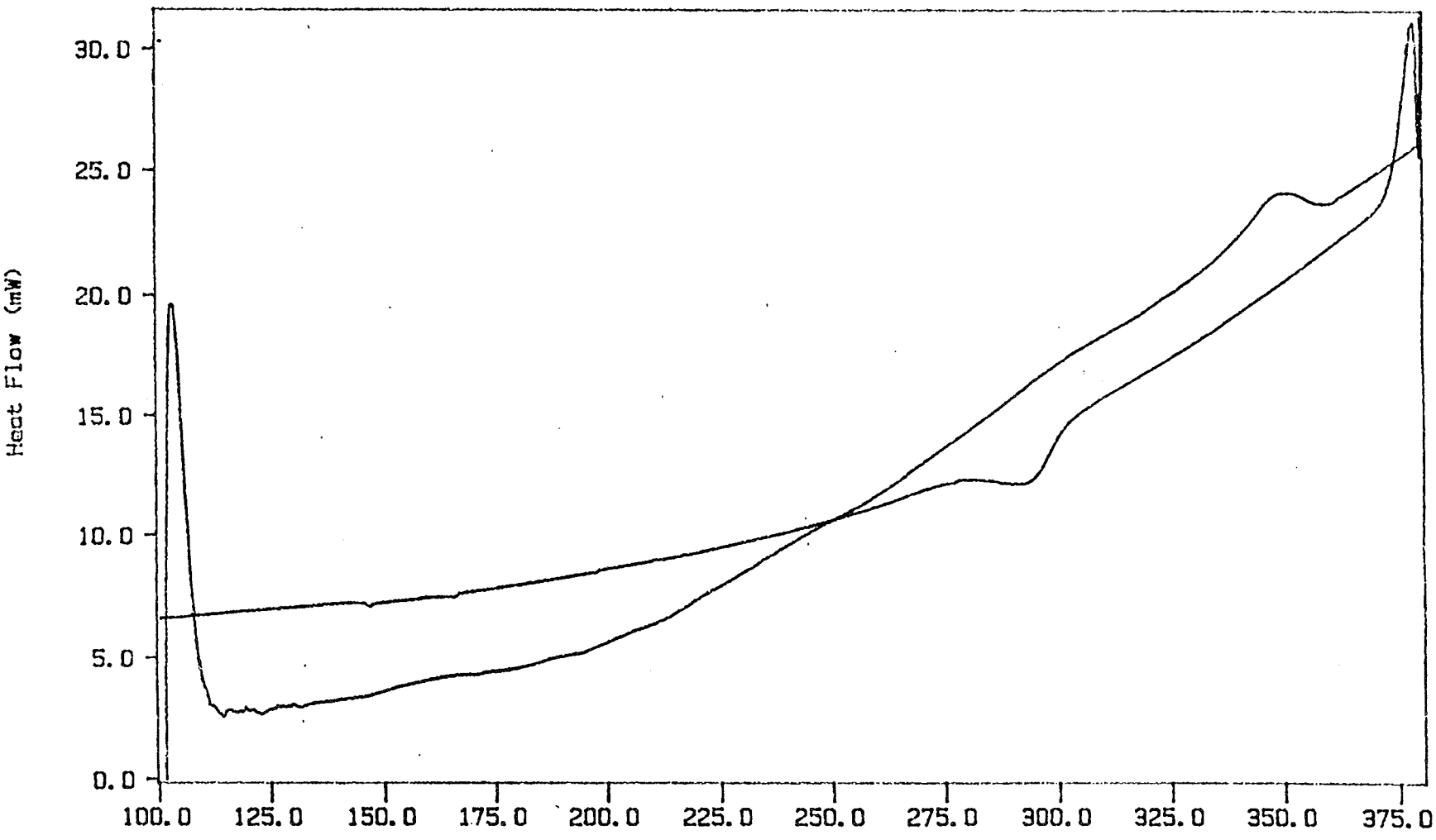

Ramp 100-380(10min hold)-100C 30C/min jar/dmc

TEMP 1: 100.0 C TIME 1: 0.0 min RATE 1: 30.0 C/min
TEMP 2: 380.0 C TIME 2: 10.0 min RATE 2: 30.0 C/min
TEMP 3: 100.0 C

DSC Data File: ey10n
Sample Weight: 5.300 mg
Sat Aug 01 03:43:43 1992
Syn10 (syn03) empty ref

#2

PERKIN-ELMER
7 Series Thermal Analysis System

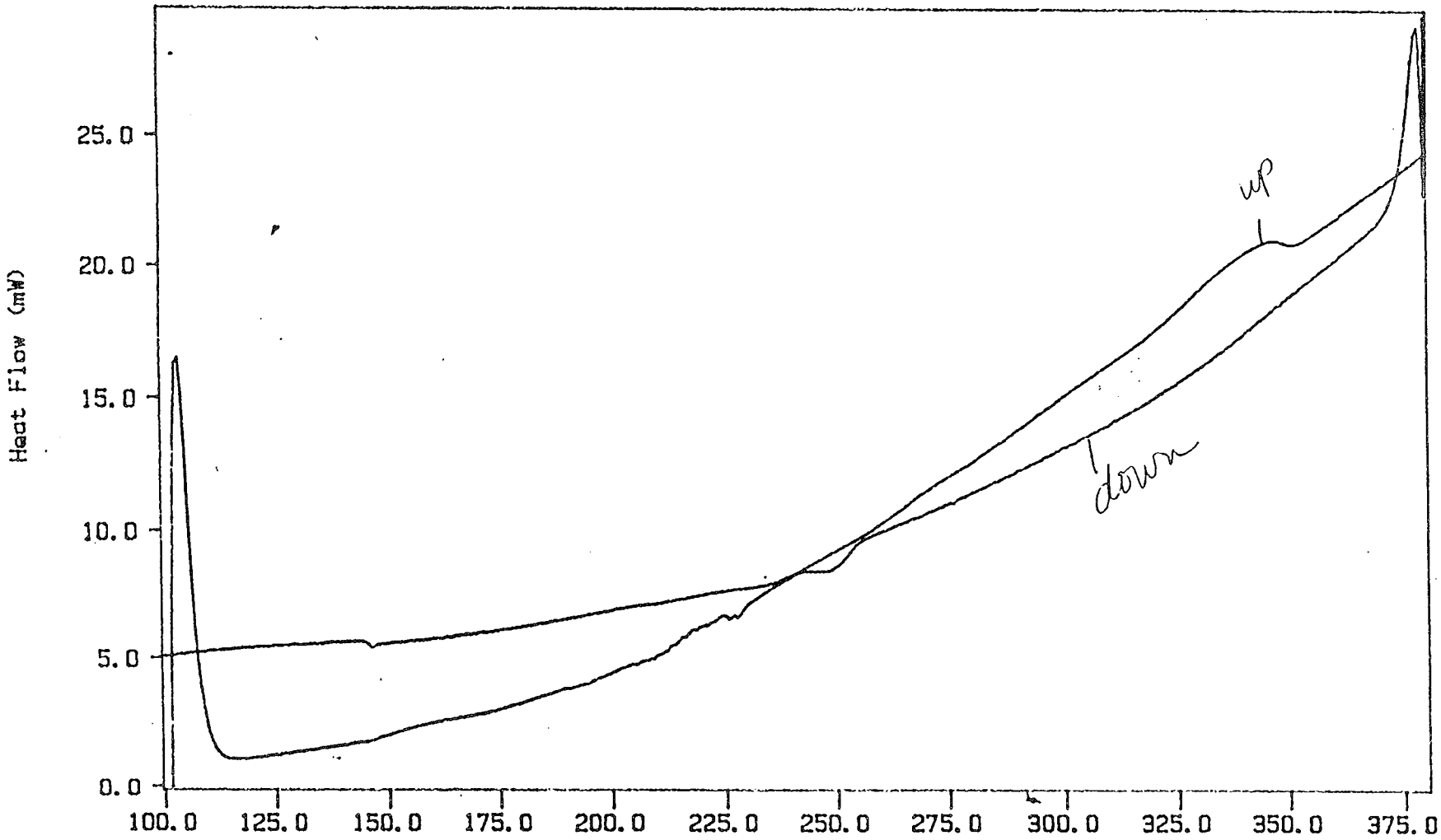

Ramp 100-380(10min hold)-100C 30C/min Temperature (°C) jar/dmc

TEMP 1: 100.0 C TIME 1: 0.0 min RATE 1: 30.0 C/min
TEMP 2: 380.0 C TIME 2: 10.0 min RATE 2: 30.0 C/min
TEMP 3: 100.0 C

THERMAL ANALYSIS DATA

DATE 92/08/05

FILE NAME A805J23.000 [TMA]

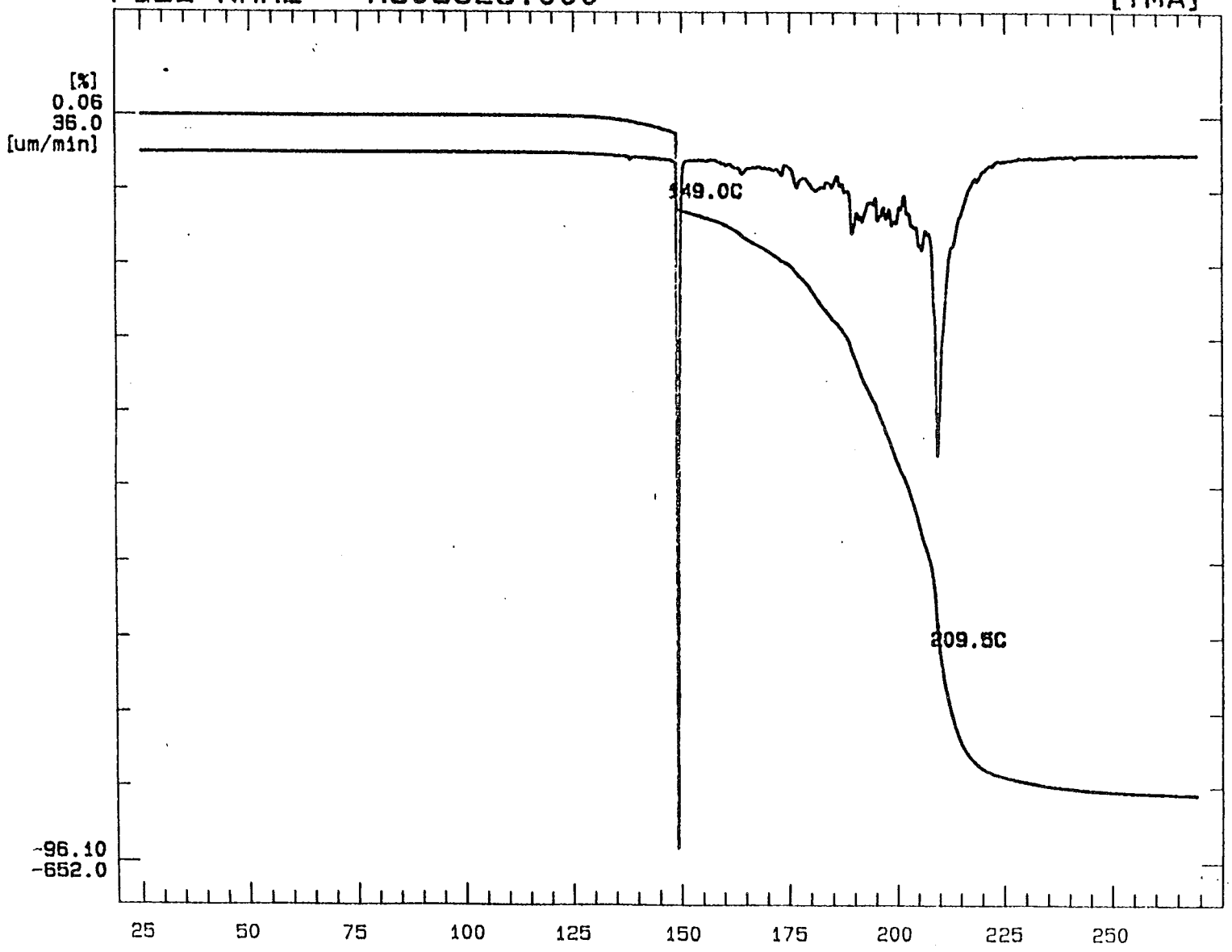

MEASURING CONDITIONS

SAMPLE NAME	syn10
SAMPLE SIZE	1.040
SAMPLING INT	1.0
ACQ. DATE	92/08/

COMMENT

ramp rt-450 5C/min

HEATING PROGRAM

	RATE	TEMP	TIM
1	5.0	450.0	

syn 10
ramped up and
down no hold

THERMAL ANALYSIS DATA

DATE 92/08/06

FILE NAME A806M31.000 [TMA]

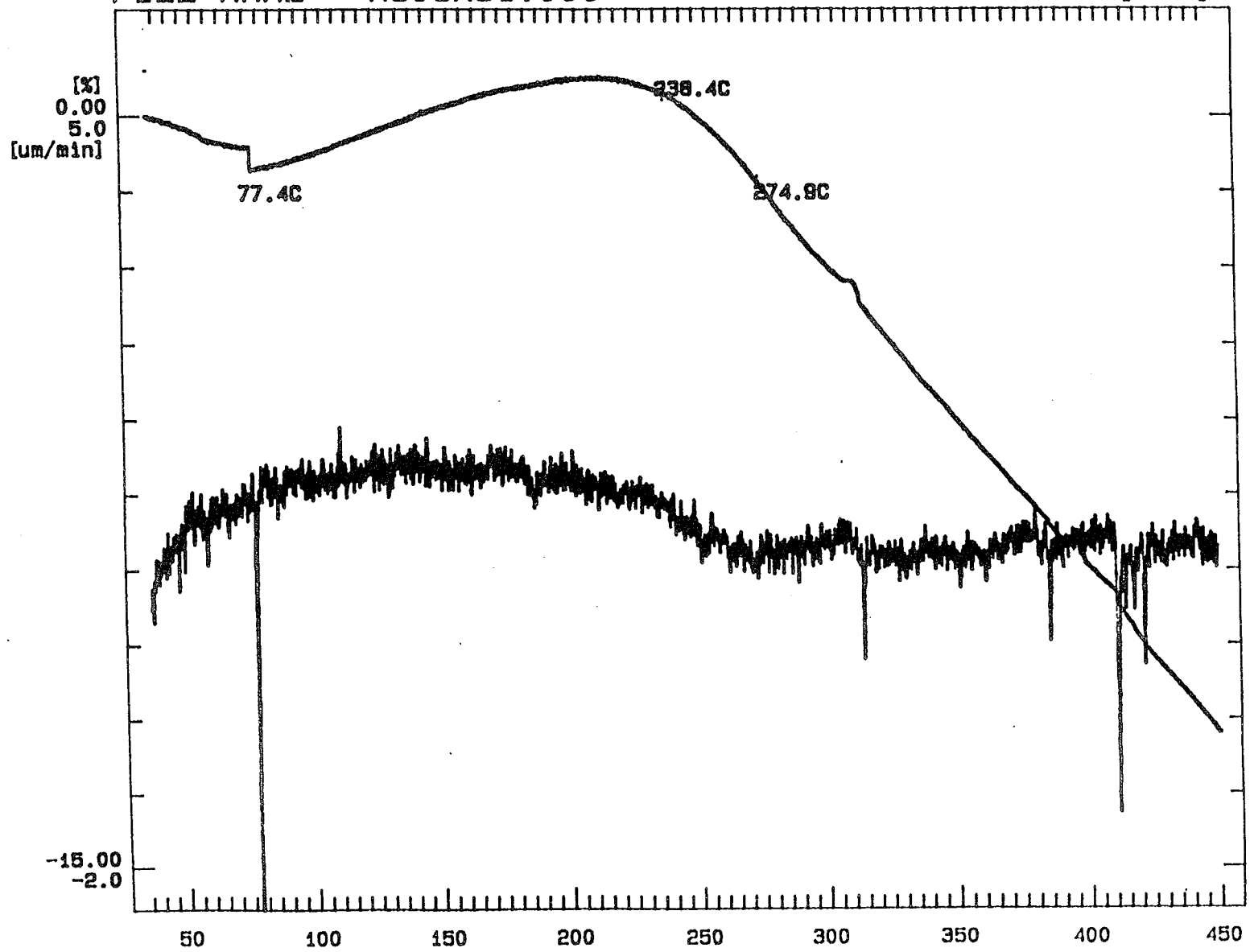

MEASURING CONDITIONS

SAMPLE NAME	syn10h
SAMPLE SIZE	0.245
SAMPLING INT	1.0
ACQ. DATE	92/08/

COMMENT

ramp rt-450 5c/min

HEATING PROGRAM

	RATE	TEMP	TIM
1	5.0	450.0	

Syn 10 hr hold @ 380°C

Brian Kipp
Dr. D. Kranbuehl

Dave Olmeijer

W & M

336

27

SYN 3

SYN 3 is the PHQ system. The FDEMS output for the up/down ramp followed by a ramp and 3 hour 380° hold is shown in Figures 38 and 39. As in the SYN 9 and 10 systems, there is over a decade drop in mobility at the 380° hold as seen by the trace of the low frequency ε" lines. Further, the intermediate frequency ε" dipolar peaks on cooling from the 380° hold are absent, where they are present after the simple up/down ramp to 380°. The lowering of ε' is also observed. The DSC trace figures also show a slightly different effect compared to SYN-9 and 10. Figure 40 shows the output of an up/down ramp (1); followed by a ramp to 380, a 10 minute hold and cool down (2), followed by a repeat of the ramp, 10 minute 380° hold cool down (3). In this case the ramp endotherm increases in temperature and the cool down exotherm also increases. This suggests a higher melting point, a less defined melting point, but not as much hindrance to ordering on cooling, *i.e.*, super cooling, in this system as in SYN-9 and 10. There may be less tendency to crosslink or less hinderance to motion with the phenyl group in PHQ as compared to the phenyl plus ethyl groups in PEHQ.

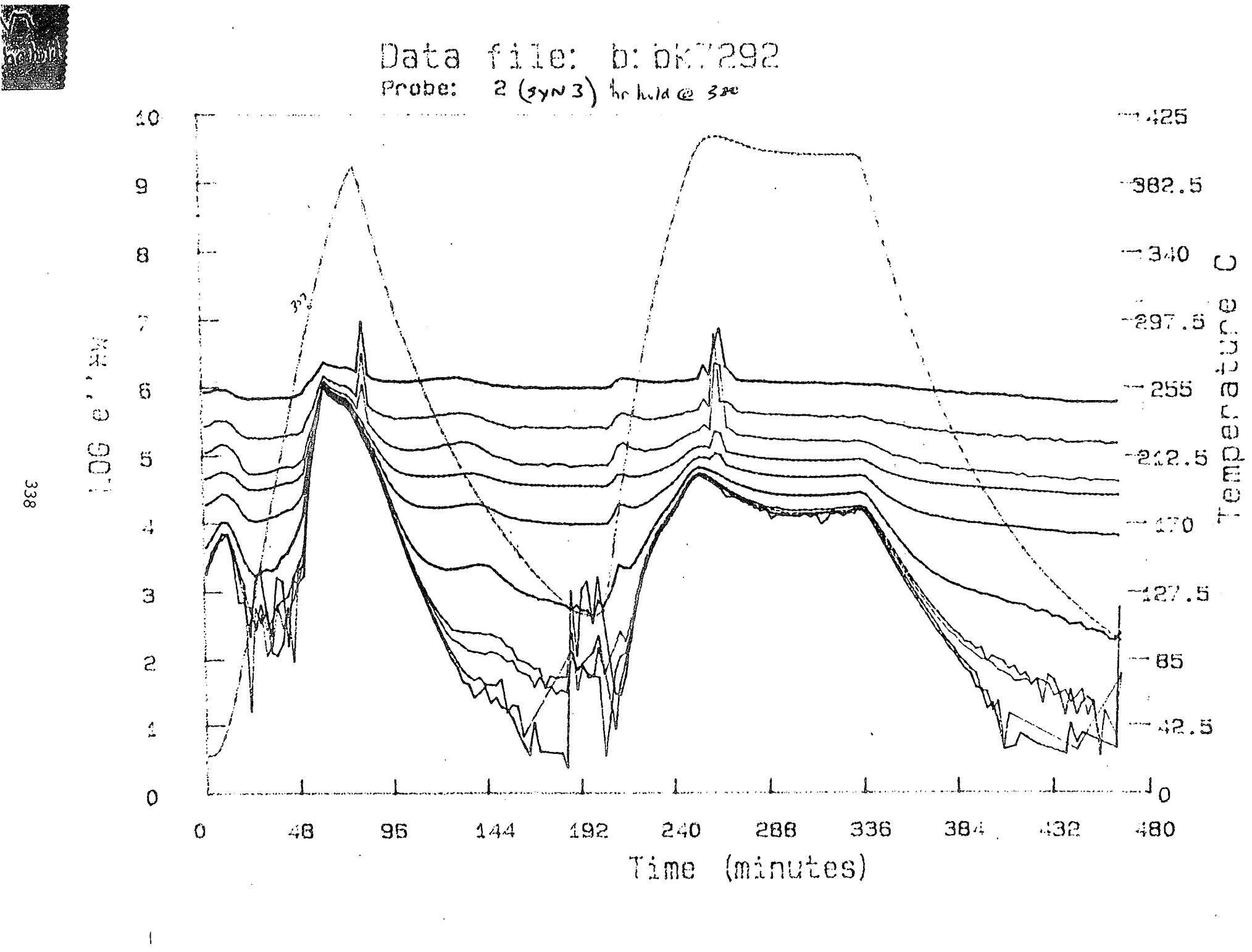
Data file: b:bk7292
Probe: 2 (syn 3) hr hold @ 350
10
9
8
7
6
5
4
3
2
1
0
425
382.5
340
297.5
255
212.5
170
127.5
85
42.5
0
0
48
96
144
192
240
288
336
384
432
480
Time (minutes)
Temperature C

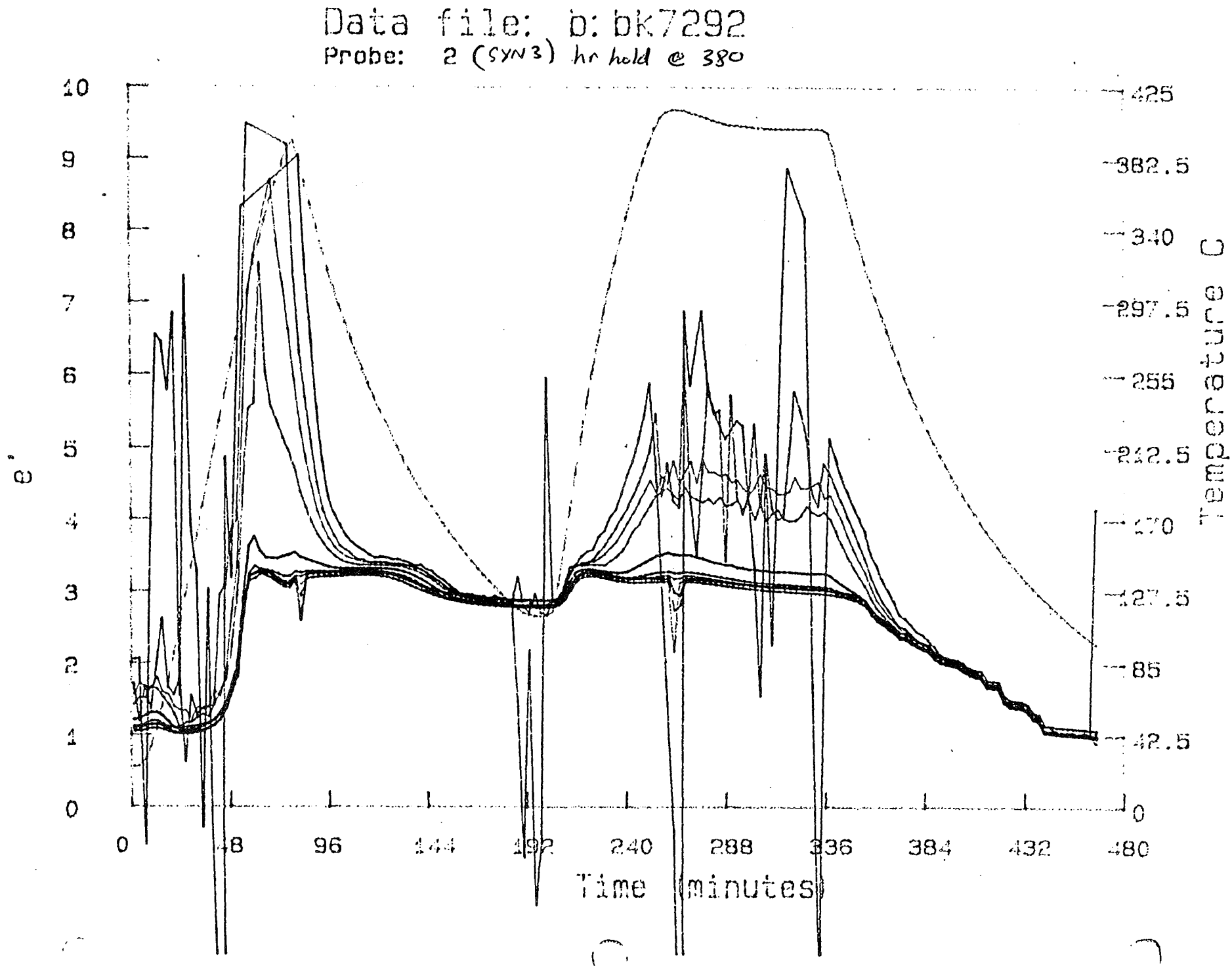
Data file: b:bk7292
Probe: 2 (SYN3) hr hold @ 380
ε'
Temperature C
Time (minutes)
0
1
2
3
4
5
6
7
8
9
10
0
48
96
144
192
240
288
336
384
432
480
42.5
85
127.5
170
212.5
255
297.5
340
382.5
425

DSC Data File: ay306
Sample Weight: 5.300 mg
Sat Aug 01 22:20:57 1992
SYN3 fresh: Ramp 30C/min: empty ref

PERKIN-ELMER
7 Series Thermal Analysis System

syn3 fresh sample
2 10mm holds at 380°C

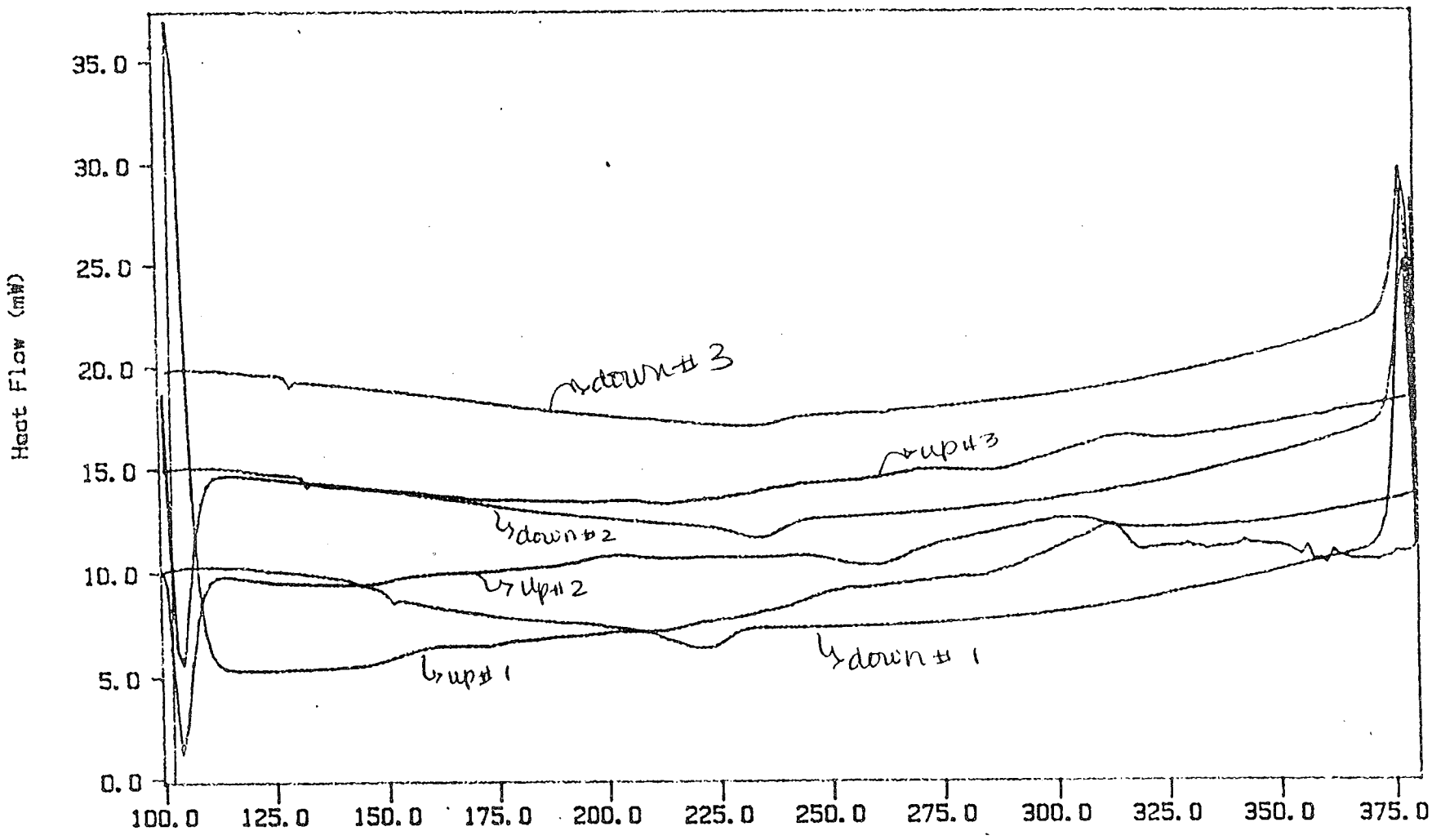

100-380-100-380(10mn)-100-380(10mn)-100C Temperature (°C) dmc/jar

TEMP 1:	100.0 C	TIME 1:	0.0 min	RATE 1:	30.0 C/min
TEMP 2:	380.0 C	TIME 2:	0.0 min	RATE 2:	30.0 C/min
TEMP 3:	100.0 C	TIME 3:	0.0 min	RATE 3:	30.0 C/min
TEMP 4:	380.0 C	TIME 4:	10.0 min	RATE 4:	30.0 C/min
TEMP 5:	100.0 C	TIME 5:	0.0 min	RATE 5:	30.0 C/min
TEMP 6:	380.0 C	TIME 6:	10.0 min	RATE 6:	30.0 C/min
TEMP 7:	100.0 C				

SYN 5

The SYN 5 system has the chloro substituted hydroquinone CHQ. Figures 41 and 42 show the FDEMS output for the up/down ramp followed by a ramp and 3 hour 380° hold and cool down. A drop in mobility is seen during the 380° hold as seen by the drop in ε''. The drop is less than in SYN 10. A similar drop in ε' is observed during the 380° hold. On the other hand, no dipolar peaks are seen in the initial cool down or the subsequent cool down. This was also observed in up down ramps done earlier but not described in this report. The lack of a dipolar peak is due, we believe, to the orientation of and electron withdrawing nature of the chloro group. It is competing with the -0- ether linkage. The result is a smaller dipole moment perpendicular to the chain backbone than in the phenyl and phenyl/ethyl substituted systems.

As seen in Figure 43, the CHQ system shows a considerably higher melting point 342° which increases upon thermal cycling with 380° 10 minute holds before the second and third cool downs. The melting endotherm peak on the DSC moves higher to 350° in this cycle. The cooling exotherm decreases from 320° to 310°.

The higher melting point could be due to the smaller side group volume of the Cl relative to the phenyl and phenyl/ethyl side groups. The FDEMS and DSC data on SYN-5 show a 380° hold decreases this mobility thereby both increasing Tm and increasing the extent of super cooling on the down ramp, for undoubtably similar reasons to that in SYN-9 and SYN-10.

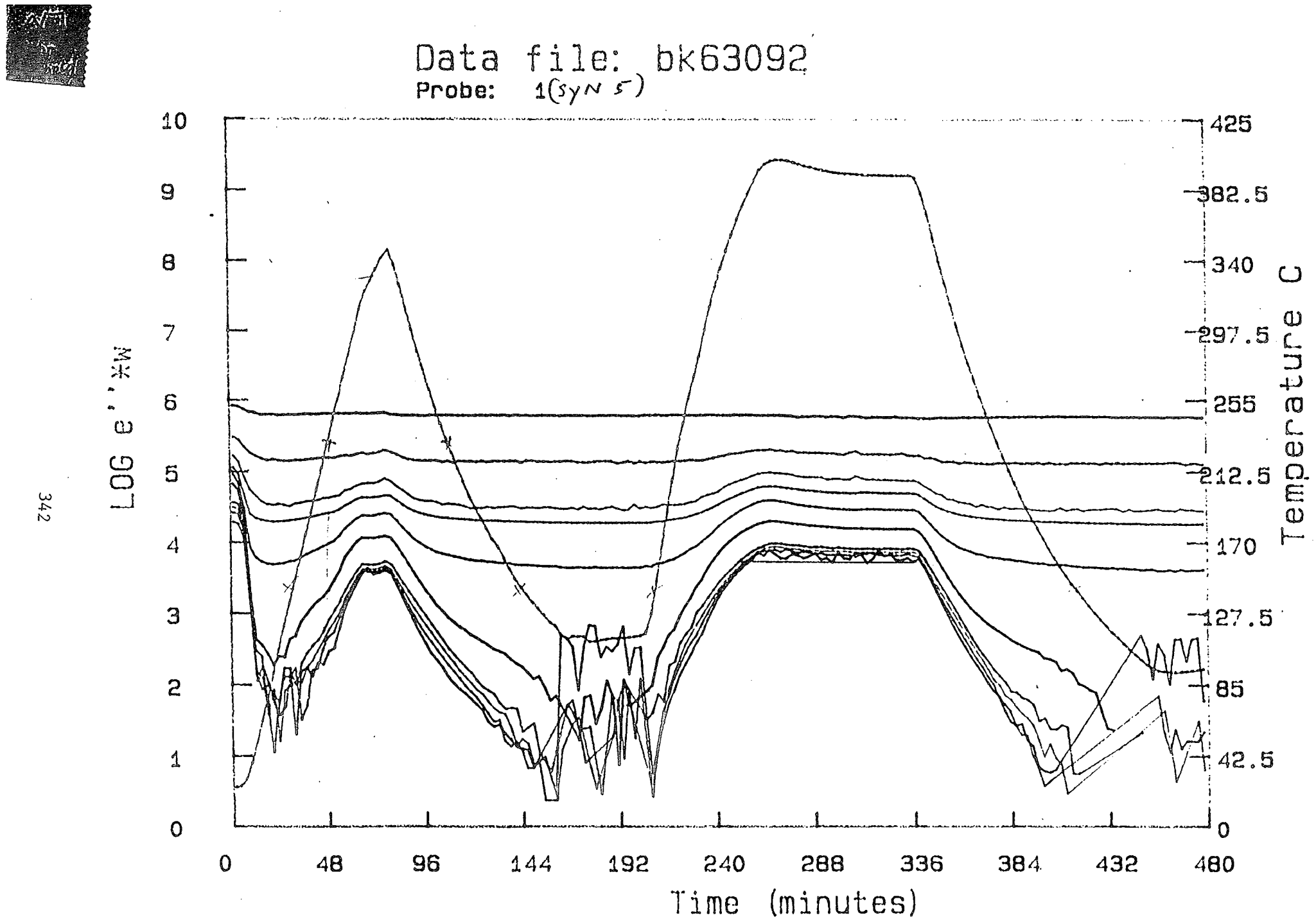
Data file: bk63092
Probe: 1(syN 5)
LOG e''*W
Temperature C
Time (minutes)
10
9
8
7
6
5
4
3
2
1
0
425
382.5
340
297.5
255
212.5
170
127.5
85
42.5
0
0
48
96
144
192
240
288
336
384
432
480

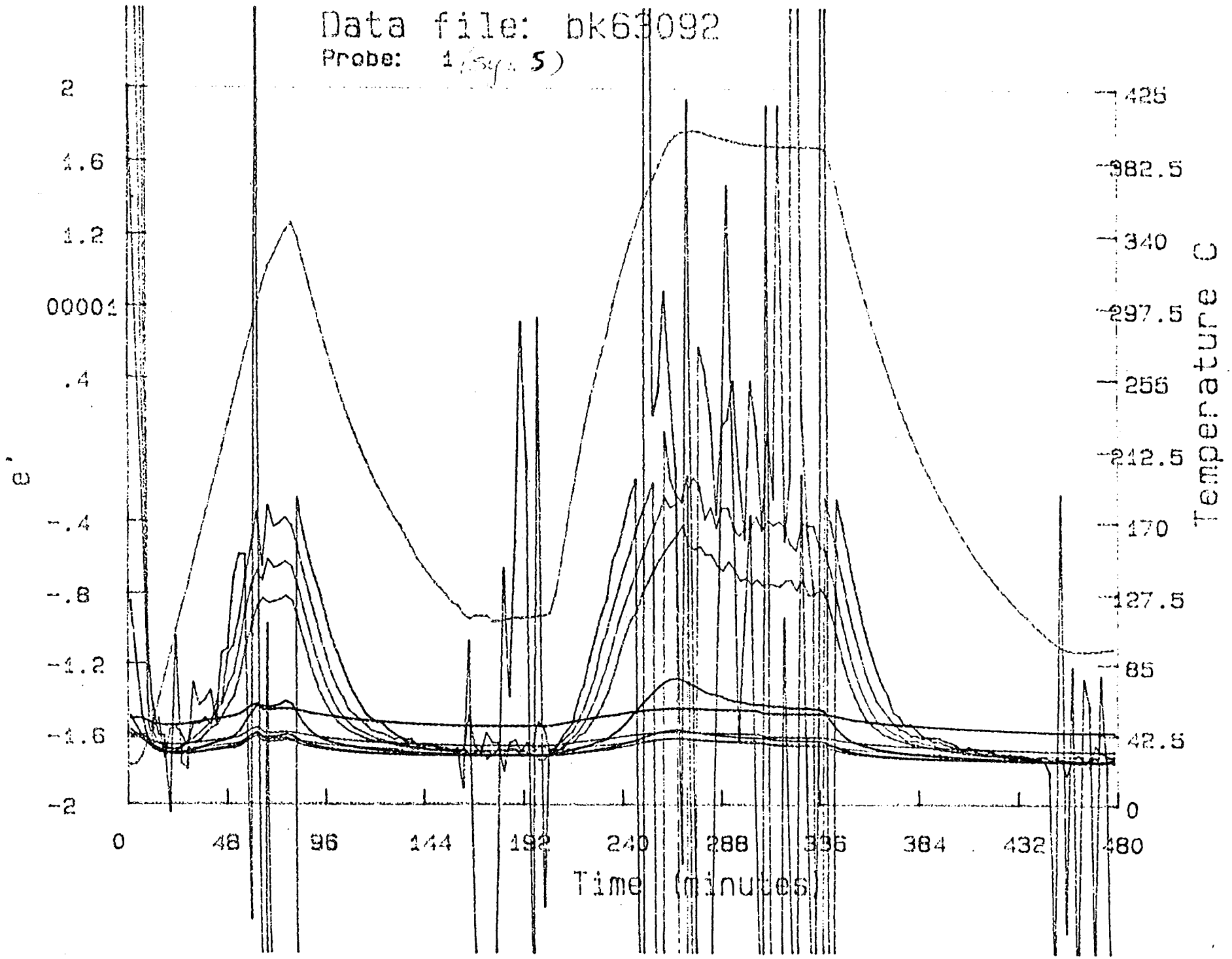
Data file: bk63092
Probe: 1 (Sig. 5)
2
1.6
1.2
00001
.4
-.4
-.8
-1.2
-1.6
-2
e'
425
382.5
340
297.5
255
212.5
170
127.5
85
42.5
0
Temperature C
0
48
96
144
192
240
288
336
384
432
480
Time (minutes)

DSC Data File: sy505
Sample Weight: 5.800 mg
Sat Aug 01 16:53:42 1992
SYN5 fresh: empty ref: Ramp 30C/min

PERKIN-ELMER
7 Series Thermal Analysis System

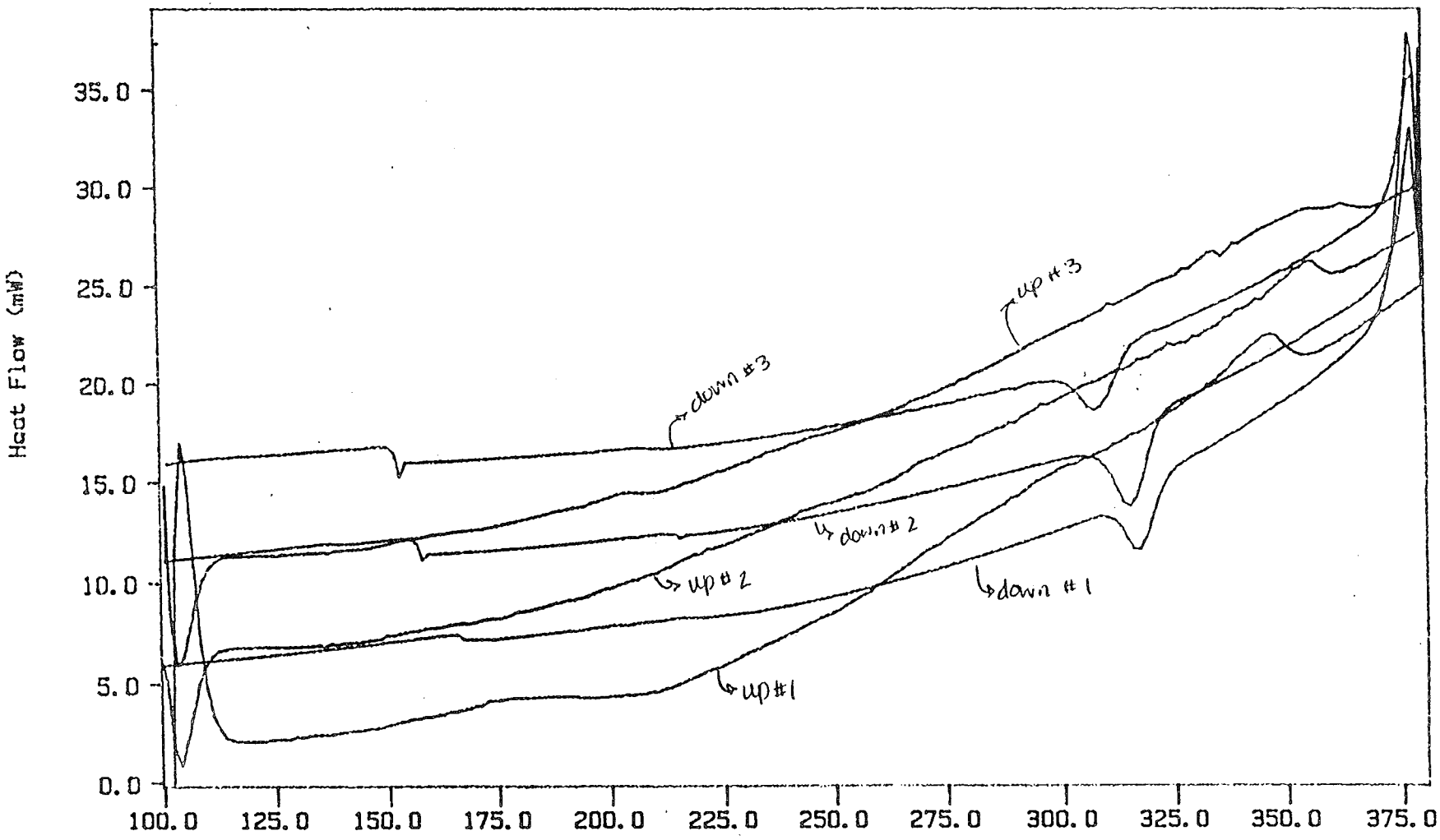

100-380-100-380(10mn)-100-380(10mn)-100C Temperature (°C) jar/dmc

TEMP 1:	100.0 C	TIME 1:	0.0 min	RATE 1:	30.0 C/min
TEMP 2:	380.0 C	TIME 2:	0.0 min	RATE 2:	30.0 C/min
TEMP 3:	100.0 C	TIME 3:	0.0 min	RATE 3:	30.0 C/min
TEMP 4:	380.0 C	TIME 4:	10.0 min	RATE 4:	30.0 C/min
TEMP 5:	100.0 C	TIME 5:	0.0 min	RATE 5:	30.0 C/min
TEMP 6:	380.0 C	TIME 6:	10.0 min	RATE 6:	30.0 C/min
TEMP 7:	100.0 C				

SYN-1

SYN-1 is treated last in this report as it is a mixture of MHQ methyl hydroquinone, phenyl hydroquinone PHQ and chlorohydroquinone CHQ. Figures 44 and 45 show the up/down ramp followed by the ramp to a 3 hour 380° hold. The FDEMS output shows similar behavior to the SYN-5 system. There is a definite drop in mobility during the 380° hold and a drop in ε'. As in the SYN-5 system, (1/3 of SYN-1 is composed of SYN-5) no dipolar peaks are observed, either in the first down cycle nor after the 380° hold.

Figure 46 shows the results of an up/down ramp followed by two ramps to 380°, a 10 minute hold and cool down. Figure 47 shows the results of an up/down ramp to 400°C on the sample after it has been exposed to the thermal cycle in Figure 46. Figures 48, 49, and 50 show the integral under the cooling endothermic peaks is 6 to 10 J/g. Values between 10 to 1 Joules per gram were measured for the other SYN systems. This value might be compared to the heat of fusion for various substituted phenyl ring systems, and 2 aromatic ring systems. These ΔH_f values range from 80 to 120 Joules/gram. It might also be compared to the heat of transition for simple liquid crystal systems which show melting transitions of ≈ 100 J/g and liquid crystal transitions around 1-10 J/g as shown in Figure 51. Together these literature facts and our experimental results do support the concept of a liquid crystal phase and/or the possibility of a partially crystalline and partially amorphous system.

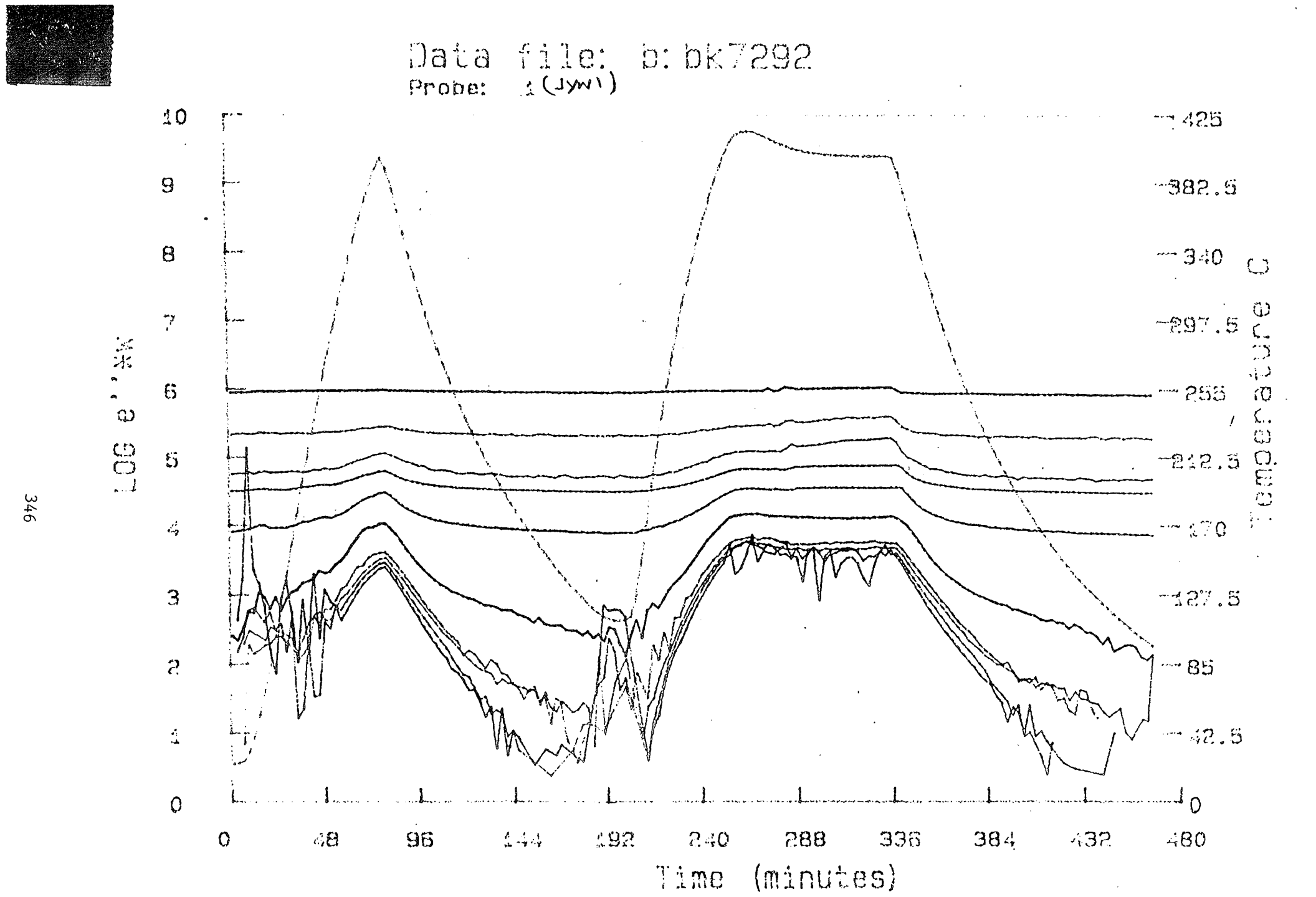
Data file: b:bk7292
Probe: 1(JYW1)
Log e''/K'
Temperature C
Time (minutes)
10
9
8
7
6
5
4
3
2
1
0
425
382.5
340
297.5
255
212.5
170
127.5
85
42.5
0
0
48
96
144
192
240
288
336
384
432
480

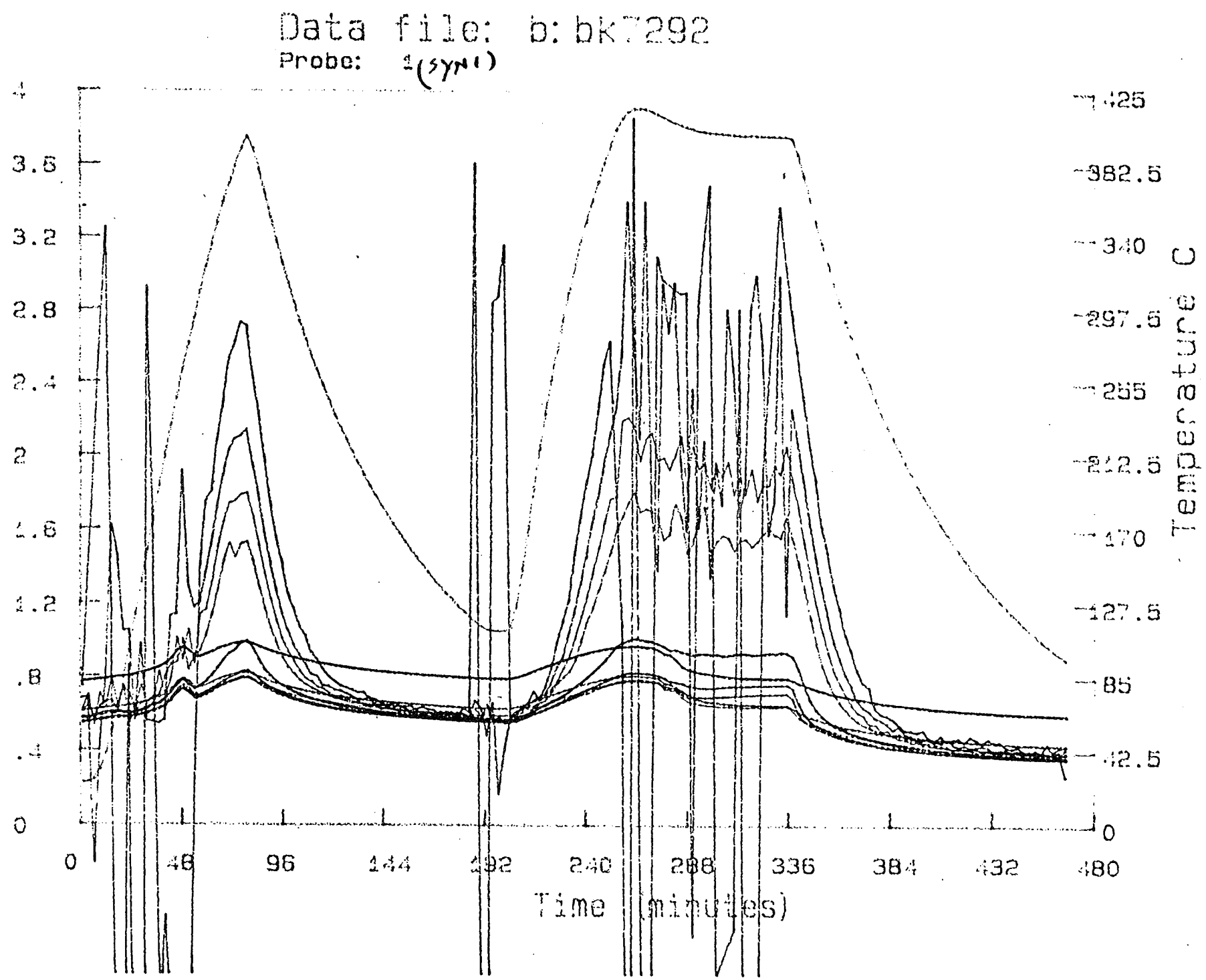
Data file: b:bk7292
Probe: 1(syn1)
4
3.6
3.2
2.8
2.4
2
1.6
1.2
.8
.4
0
ε'
425
382.5
340
297.5
255
212.5
170
127.5
85
42.5
0
Temperature C
0
48
96
144
192
240
288
336
384
432
480
Time (minutes)

DSC Data File: ey102
Sample Weight: 7.890 mg
Sun Sep 06 07:41:42 1992
syn1 empty ref 30C/min ramp

PERKIN-ELMER
7 Series Thermal Analysis System

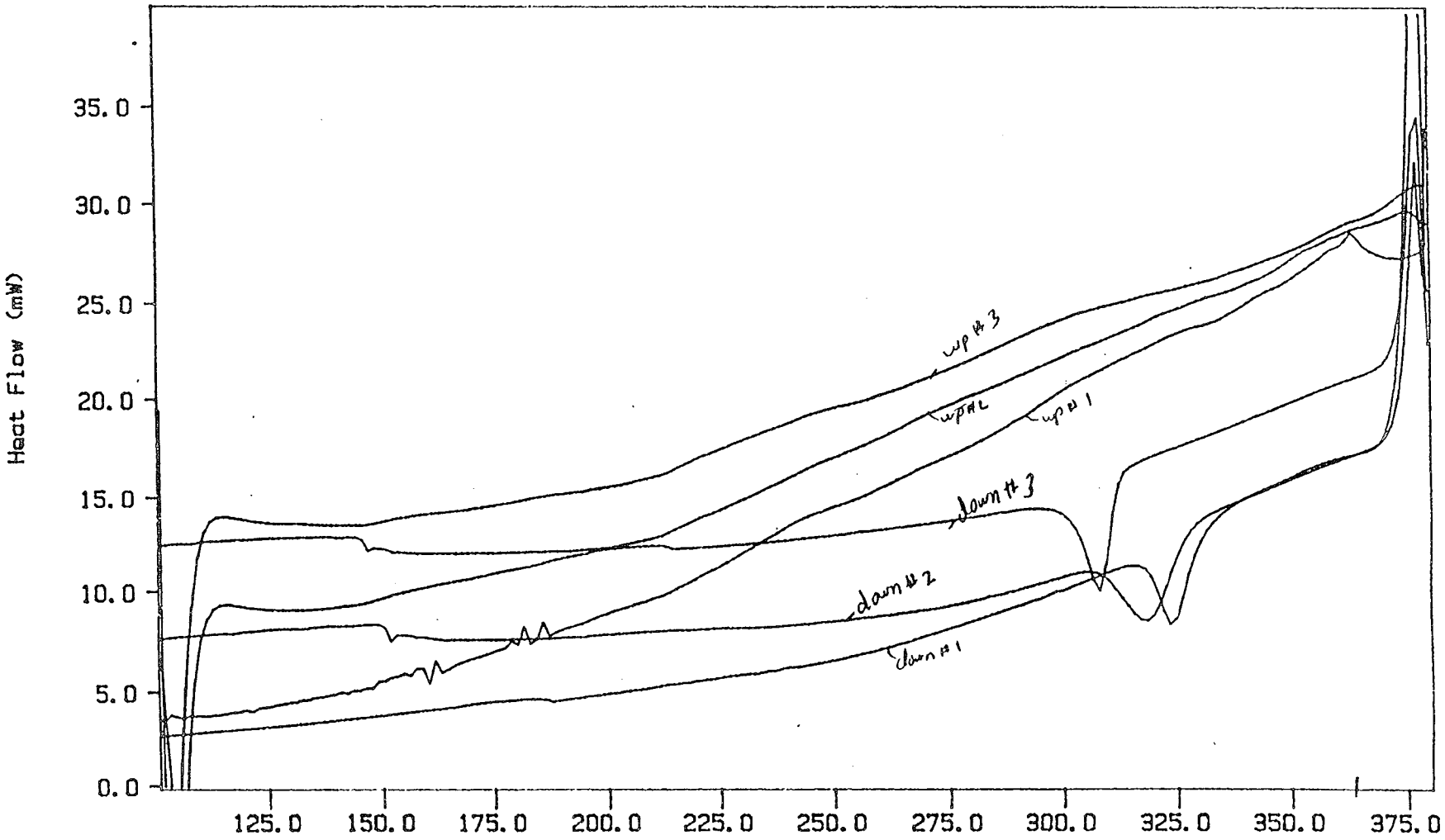

50-380-100-380(10)-100-380(10)-100

TEMP 1:	50.0 C	TIME 1:	0.0 min	RATE 1:	30.0 C/min
TEMP 2:	380.0 C	TIME 2:	0.0 min	RATE 2:	30.0 C/min
TEMP 3:	100.0 C	TIME 3:	0.0 min	RATE 3:	30.0 C/min
TEMP 4:	380.0 C	TIME 4:	10.0 min	RATE 4:	30.0 C/min
TEMP 5:	100.0 C	TIME 5:	0.0 min	RATE 5:	30.0 C/min
TEMP 6:	380.0 C	TIME 6:	10.0 min	RATE 6:	30.0 C/min
TEMP 7:	100.0 C				

DSC Data File: sy103
Sample Weight: 7.000 mg
Mon Sep 07 06:23:15 1992
syn1 reramp of sy102

PERKIN-ELMER
7 Series Thermal Analysis System

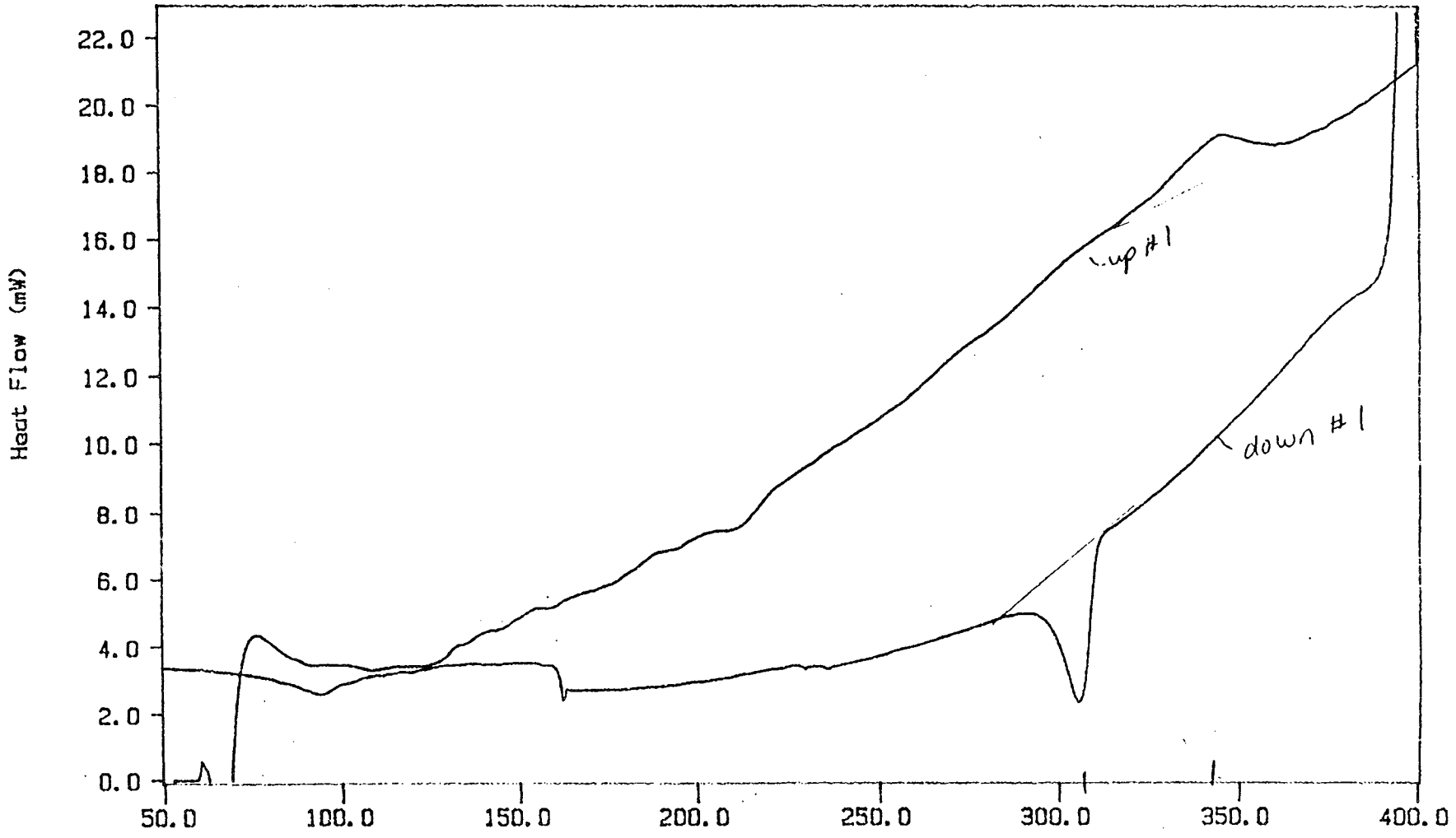

ramp 50-400-50 bek

TEMP 1: 50.0 C TIME 1: 0.0 min RATE 1: 30.0 C/min
TEMP 2: 400.0 C TIME 2: 0.0 min RATE 2: 30.0 C/min
TEMP 3: 50.0 C

DSC Data File: sy102
Sample Weight: 7.890 mg
Sun Sep 06 07:41:42 1992
syn1 empty ref 30C/min ramp

PERKIN-ELMER
7 Series Thermal Analysis System

down # 1

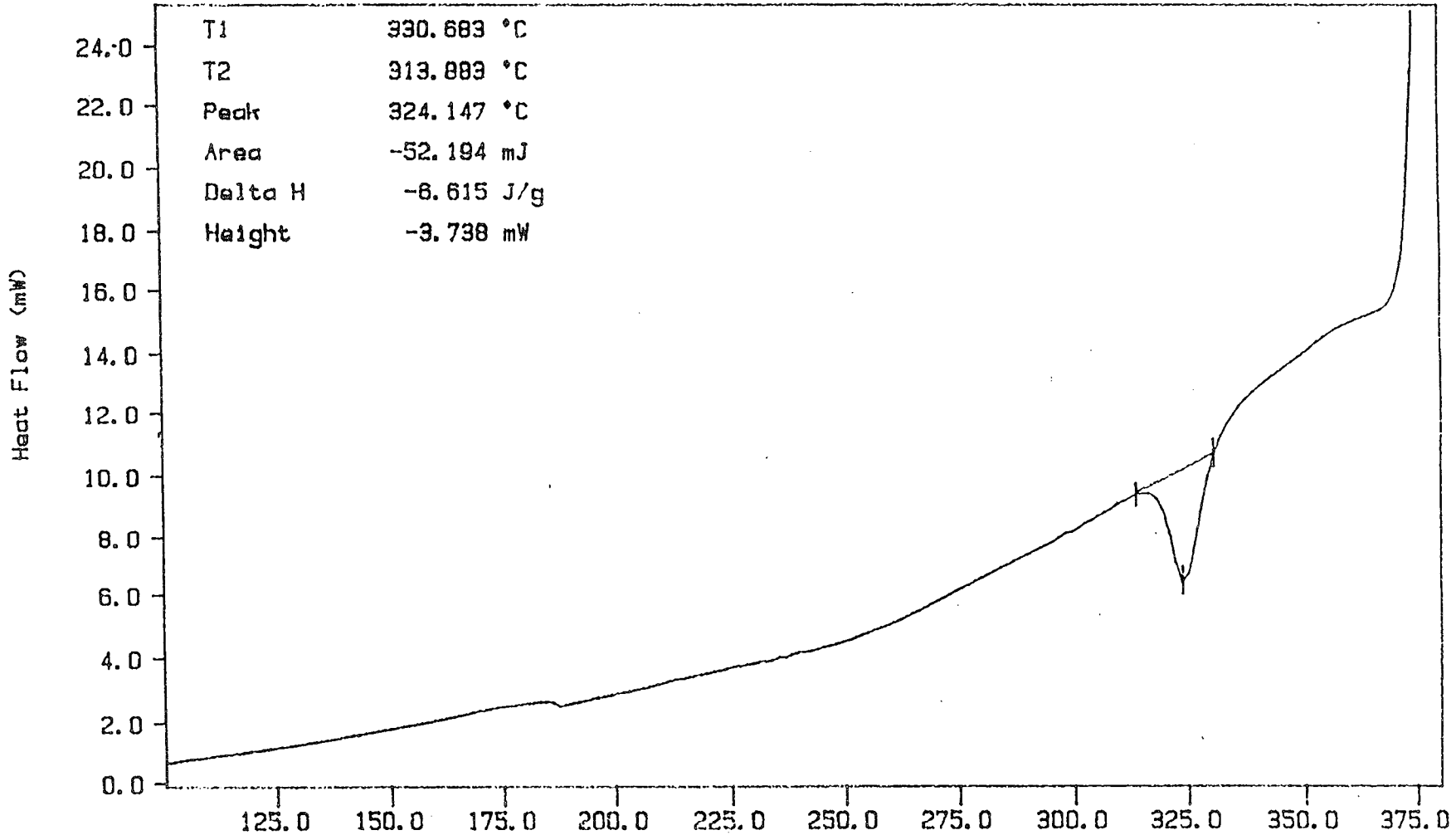

50-380-100-380(10)-100-380(10)-100
TEMP 1: 380.0 C TIME 1: 0.0 min RATE 1: 30.0 C/min
TEMP 2: 100.0 C TIME 2: 0.0 min

DSC Data File: sy102
Sample Weight: 7.890 mg
Sun Sep 06 07:41:42 1992
syn1 empty ref 30C/min ramp

PERKIN-ELMER
7 Series Thermal Analysis System

down # 2

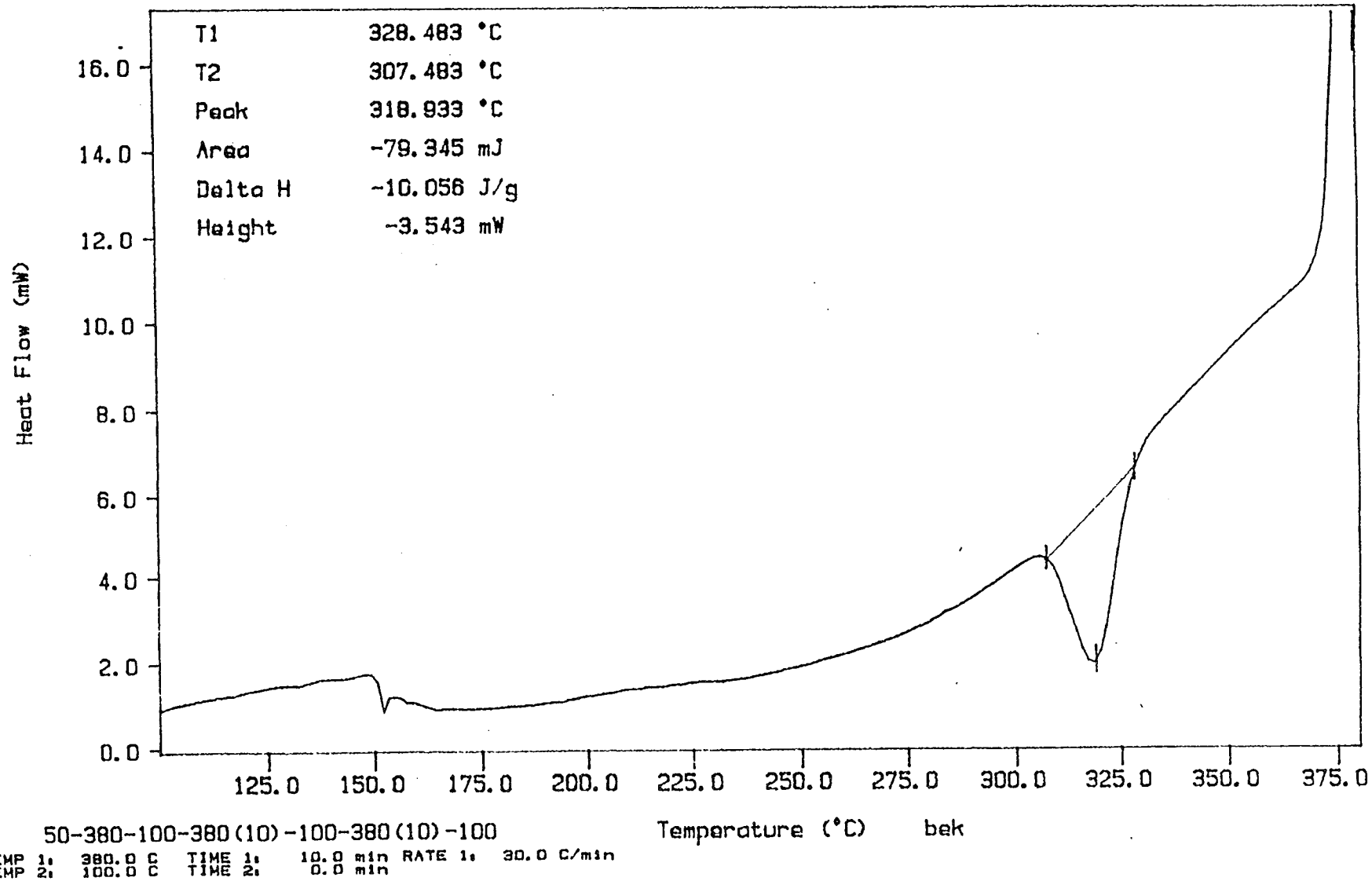

50-380-100-380(10)-100-380(10)-100

TEMP 1: 380.0 C TIME 1: 10.0 min RATE 1: 30.0 C/min
TEMP 2: 100.0 C TIME 2: 0.0 min

DSC Data File: sy102
Sample Weight: 7.890 mg
Sun Sep 06 07:41:42 1992
syn1 empty ref 30C/min ramp

PERKIN-ELMER
7 Series Thermal Analysis System

down A 3

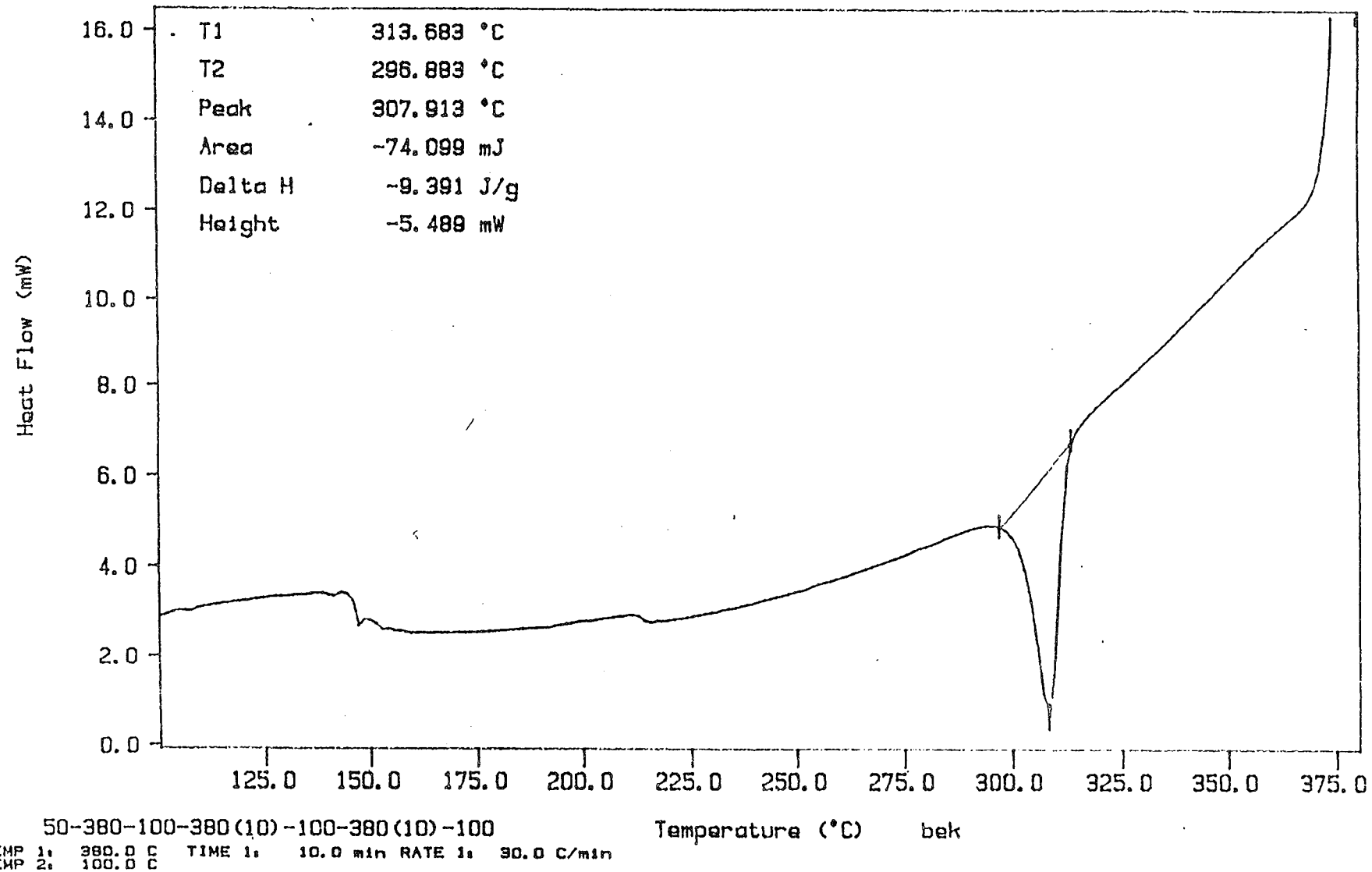

50-380-100-380(10)-100-380(10)-100 bek
TEMP 1: 380.0 C TIME 1: 10.0 min RATE 1: 30.0 C/min
TEMP 2: 100.0 C

DSC Data File: tlqc2
Sample Weight: 5.100 mg
Sat Jul 25 10:05:43 1992
True Liquid Crystal(tlqcr) empty ref

PERKIN-ELMER
7 Series Thermal Analysis System

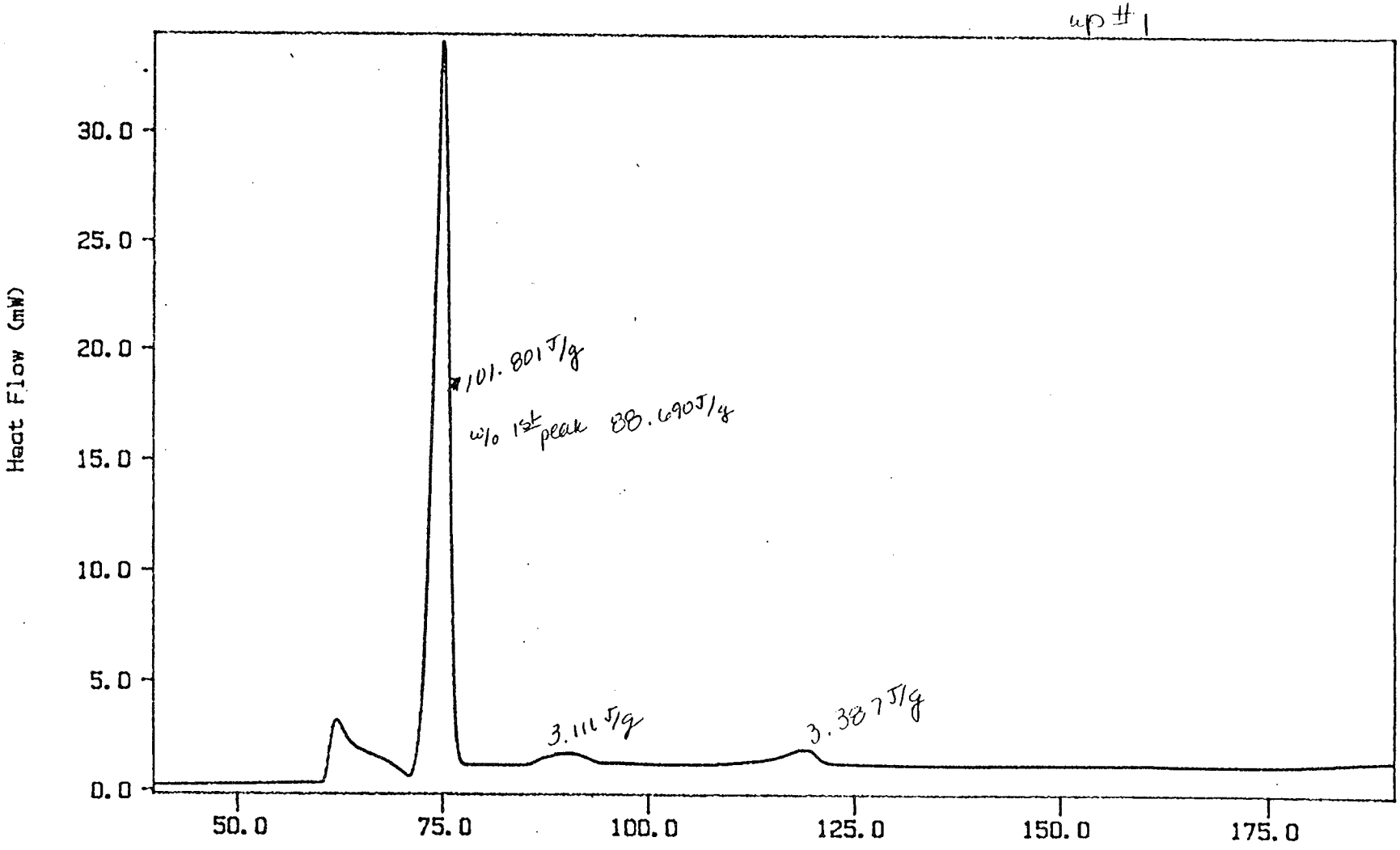

Ramp 40-190-40C 10C/min
TEMP 1: 40.0 C TIME 1: 0.0 min RATE 1: 10.0 C/min
TEMP 2: 190.0 C TIME 2: 0.0 min

JOURNAL OF MATERIALS SCIENCE 28 (1993) 225–238

The fibrillar hierarchy in liquid crystalline polymers

L. C. SAWYER, R. T. CHEN, M. G. JAMIESON
Hoechst Celanese Research Division, 86 Morris Avenue, Summit NJ 07901, USA

I.H. MUSSELMAN
Department of Chemistry, University of North Carolina, Chapel Hill, NC 27599, USA

P.E. RUSSELL
Department of Materials Science and Engineering and Precision Engineering Center, North Carolina State University, Raleigh, NC 27695, USA

It is well known that the structure of highly oriented liquid crystalline polymers (LCPs) can be characterized by a hierarchical fibrillar structural model. Structure models were first developed for the lyotropic aramid fibres in the late 1970s and a structural model was developed for the thermotropic copolyesters in the mid-1980s. Recently, imaging techniques with higher potential capability and resolution have been applied to assess the size, shape and organization of microfibrillar structures observed in LCPs. Field emission scanning electron microscopy and scanning tunnelling microscopy permit imaging of regions from 1 nm to many micrometres. As a result, the nature of the microfibrillar hierarchy has been further clarified and the macromolecular size has been shown to be less than 2 nm. The shape of the microfibrils has been shown to be tape-like. The LCP structural model, consisting of elongated well-ordered microfibrils continues to be consistent with measured properties: high anisotropy, very high tensile modulus and strength and poor compressive properties. A more detailed structural model is proposed to describe the macromolecular microfibril size, shape and organization for comparison with polymer composition and mechanical property evaluation.

1. Introduction

The last two decades have seen the vast growth of a new technology in high-performance polymeric materials owing to the invention and development of liquid crystalline polymers (LCPs) [1–10]. The concept of LCPs originated with Onsager [11], Isihara [12] and Flory [13, 14] who treated theories relating to the packing of rigid rod-like molecules. The processing of LCPs in elongational flow fields, in spinning, or in extrusion processes, results in a highly oriented extended chain structure in the solid state [1–6, 10]. These extended chain structures form owing to the flow characteristics of liquid crystals which are dominated by the nematic character in the melt or solution [15–23]. The long relaxation times for LCPs results in their orientation in the melt or solution being "frozen" into the solid state [24]. These highly oriented polymeric materials exhibit impressive mechanical and thermal properties compared to conventional polymers. Study of the complex interactions of liquid crystal chemical structure, in the nematic melt or solution, and their further development during processing to form oriented textures and outstanding physical properties, are currently being investigated in many materials science research laboratories.

Many hundreds of LCP compositions have been documented in review papers and patents [1–10, 25–27], the most commercially important of which fall into two categories.

(a) Lyotropic aramids such as poly(*p*-phenylene terephthalamide) (PPTA), also known as Kevlar, commercialized by duPont (i.e. 8–10, 25–28).

(b) Thermotropic aromatic copolyesters, such as the Eastman-modified polyesters [i.e. 29–33], and the Vectra family of LCP resins and Vectran fibres commercialized by Hoechst Celanese (i.e. [1, 15, 16, 34–40]).

Theoretical models of the LCP solid state structure, as well as those derived from experimental measurements, have value in permitting prediction of LCP structure–property relationships. The now well-known "hierarchies of structure" for LCPs were first described for aramids by Dobb *et al.* [41]. It is now known that the structure of highly oriented LCPs can be characterized by a hierarchical fibrillar microstructure [38–40]. Details of the aramid fibrillar structure have been published by Schaefgen and co-workers [26, 28], Dobb and co-workers [6, 41–45], Sotton [45] and Sawyer and co-workers [38–40]. In addition, documentation of the supramolecular structure of the

0022–2461

skin–core textures in moulded thermotropic articles has been provided by Ide and Ophir [15, 16], Thapar and Bevis [22], Baer *et al.* [47] and Sawyer and coworkers [38–40]. These models are useful for understanding the effect of various fabrication processes on the resulting structures. The models account for microstructures on a scale typically observed in light microscopy (LM) or scanning electron microscopy (SEM), although in our earlier paper [38] structures on a scale of about 10 nm were reported from a transmission electron microscopy (TEM) study. More recently, Sawyer and Jaffe [38] described the first general structural model that included both the aramids and the aromatic copolyesters, of major interest owing to the demonstrated similarities of the lyotropic and thermotropic LCP microstructures. Extensive TEM imaging by Donald and Windle [48–52] revealed banded textures and evidence for aperiodic crystallites (non-periodic layer crystallites, NPL) within oriented thermotropic LCPs formed by shearing on a glass slide [51, 53, 54]. Gutierrez *et al.*, in their X-ray diffraction studies, suggested that the thermotropic LCPs are random in nature although they observed evidence of crystallinity [55].

The elucidation of a hierarchical, microfibrillar structural model [38] included direct study of Vectra mouldings and extrudates as well as Vectran and Kevlar fibres. The model has been extended to other highly oriented materials and has been well accepted as depicting the morphology of the aramid and thermotropic aromatic polyester LCPs. The characterization utilized a broad range of microscopy techniques [38–40], including LM, SEM and TEM as well as X-ray diffraction studies [36, 48, 49, 55]. Although the model provided a description of three levels of fibrillar architecture, the finest such unit, the microfibril, was not observed in much detail. From this study, questions remained regarding the nature of structures less than 10 nm in size.

Recently, imaging techniques with higher spatial resolution have been applied to address questions regarding the size, shape and organization of microfibrillar structures [56, 57]. Field emission scanning electron microscopy (FESEM) at low voltages, and more importantly, scanning tunnelling microscopy (STM), are capable of imaging regions from 1 nm to many micrometres on the same specimen. The experimental observations obtained using these novel characterization techniques have been correlated and compared to results of prior studies and to observations from more traditional imaging methods, such as polarized light microscopy (PLM) and TEM, to aid in the interpretation of structures from the nanometre to the micrometre-size scale.

The present focus of LCP research is to develop a better understanding of the process–structure–property relationships controlling the thermotropic polymers and the aramids, especially in defining the relationships of polymer structure and properties (i.e. tensile modulus and tensile strength). Although it is well known that a higher molecular orientation favours a higher tensile modulus, it is unclear whether this molecular orientation is related to the microfibrillar structure (i.e. the microfibril size and organization of these microfibrils into fibrillar units) and whether such structural studies are useful in predicting mechanical properties.

Theories of LCP organization by Ward and coworkers [2, 58–61] have provided insight into the molecular arrangement of these polymers and the effect of such arrangements on mechanical properties, especially the various moduli. It is important to understand LCP organization and mechanical property relationship as the tensile modulus of the highly oriented LCP fibres approaches theoretical values [1, 38, 62]. The nature of the basic structural unit for the aggregate model, used as a descriptor of the properties in these theories, is not defined and is of major interest to materials science studies.

This paper further delineates the LCP structural model based on observations made using a range of complementary microscopes. The microstructural findings will be compared with the mechanical properties of the LCPs to aid in their development.

2. Experimental procedure

2.1. Materials

The LCPs investigated in this study consisted of highly oriented Vectran (tradename, Hoechst Celanese Corporation) fibres and thin extruded tapes typically composed of naphthalene moiety containing copolyesters [1, 38], i.e. copolyesters composed of 2, 6-naphthyl and 1, 4-phenyl units and other related thermotropic polymers. The aramid fibre, Kevlar (tradename, duPont), was also investigated to compare a lyotropic and thermotropic fibre. Fibres in this study had tensile moduli of about 200–300 GPa, shear moduli of 0.1–1.5 GPa and compressive strengths of approximately 0.35 GPa. The well-known unidirectionally oriented structures of Vectran and Kevlar fibres were revealed previously by X-ray diffraction (e.g. [6, 10, 29, 31, 48–50, 55]) and microscopy (e.g. [6, 22, 35, 38–54, 63]).

2.2. Sample preparation and instrumental methods

Surfaces and internal textures of the highly oriented, thin extruded tapes and fibres were examined by a range of techniques including polarized light microscopy (PLM), field emission scanning electron microscopy (FESEM), TEM and STM. For internal structure study, the LCP samples were prepared by the Scott peel-back technique and by ultrasonication, both of which have been previously described [38–40]. The peel-back method reveals internal structures within the fibres which can be observed by PLM, FESEM and STM. Ultrasonication was used to rupture fibres and tapes into finely textured fibrils and microfibrils for analysis by TEM, FESEM and STM. The fibrils mounted on copper TEM grids were shadowed with Au–Pd by vacuum evaporation to enhance topography and facilitate fibril thickness measurements [40, 56, 57]. Selected-area electron diffraction was also performed on the JEOL 100CX STEM

operated at 100 kV. As in the earlier studies [35, 38, 40], longitudinal ultrathin sections, prepared by ultramicrotomy, were coated with evaporated carbon prior to imaging. To our knowledge, this is the first STM study in which polymers have been prepared using the peel-back and sonication techniques.

LCP samples were mounted on silicon or highly oriented pyrolytic graphite (HOPG) substrates for FESEM and STM studies. The specimens were then coated with ~ 5 nm of platinum using ion-beam sputtering (Ion Tech., Ltd) in a turbo-pumped system, backfilled with ultrapure argon [40, 56, 57, 64]. Ion-beam sputter coatings have been shown to introduce minimal topography to original surfaces as is evident from the measured root mean square surface roughness values of less than 1 nm for these fine-grain platinum coatings [57, 65].

FESEM imaging was conducted in a JEOL 840 field emission scanning electron microscope at an excitation energy of 2–5 kV [56, 57, 65]. All STM images were acquired in air using a Nanoscope II, Digital Instruments, Inc. scanning tunnelling microscope with a long-range tube scanner (D head) which was calibrated by the manufacturer. The software for data acquisition and image processing was also provided by Digital Instruments, Inc. Controlled geometry Pt/Ir tips, formed by a two-step electrochemical etching procedure [65], were used exclusively to acquire images from the LCP samples in order to minimize tip-related image artefacts. The images were acquired in the constant current mode, typically using a 1 nA set current with the sample biased positively 100 mV with respect to the tip. Width and thickness measurements were made of the smallest microfibrils using the software package [56, 57].

3. Results

3.1. Liquid crystal "domains"

Liquid crystal "domains" are regions of local order in which there is correlative nematic order bounded by walls or disclinations [67–70]. The domains have a defined orientation described by a director. Models for the "domain" flow of liquid crystals have been described by Flory [13, 14], Wissbrun [17–19, 23, 24], Wong [20], Mackley [66, 67] and Asada [68]. These models help to explain the low shear-rate region of shear thinning of viscosity and the dependence of texture and rheology on shear history. Thus the nature of the polydomain fluid [68] is critical to an understanding of the solid state textures of LCPs. It is the long relaxation times of such LCPs [24] that provide fruitful research in the evaluation of the textures frozen into the solid state.

Observation of small molecule liquid crystals in polarized light is known to reveal textures which are useful for identification of phase structures [69, 70]. PLM is useful for observation of liquid crystal domain textures both in dynamic studies, using a hot stage, and in the solid state. Nematic domains, characteristic of highly oriented thermotropic LCPs, can be observed in a polarized light micrograph of a LCP thin section (Fig. 1). The PLM image, which is viewed orthogonal to the crossed polarizers, reveals incomplete extinction and an elongated domain texture. Incomplete extinction is unexpected for a material such as a LCP, which is well oriented parallel to either polarization direction [38]. Furthermore, incomplete extinction is also observed for the aramid fibres [38] in which the textures observed are thought to be due to their sharp pleated sheet structure [71].

Nematic domains (Fig. 1) were observed in the solid state to be oriented with the fibre axis and exhibited polarization colours in the same order due to their similar orientation. Slight variations in colour suggested the presence of small orientation differences within the plane of the 1 μm thick section, accounted for by a serpentine trajectory or meander of the molecules [38]. A lateral banded texture was also observed in the solid state core of poorly oriented extrudates [38] and for many model studies in which the LCPs were sheared for sample preparation [49, 72, 73]. This banded texture, probably analogous to the pleated structure of the aramids, was interpreted by Donald and Windle [49, 72, 73] as being associated with a serpentine path of the molecules about the shear direction. The analogy to the meander reported for poly(*p*-phenylene benzobisthiazole) (PBZT) [31] and the sharp path caused by the pleated sheet structures of some Kevlar fibres [42] are all consistent. According to Zachariades *et al.* [71] the optical banded textures form in sheared LCPs by ordering of domains. Recent studies have confirmed the serpentine meander of the molecules and it is likely that the diffuse dark zones outlining the domains as shown by TEM are domain walls [49, 50]. Anwer *et al.* [53] suggested that these boundaries are analogous to the walls observed for small-molecule liquid crystals [69, 70].

A periodicity of about 500 nm has been reported for the banding and pleated textures observed for the aramids and copolyesters [6, 38, 42, 45, 48, 72, 73]. This dimension is consistent with the approximate 500 nm domain size observed in highly oriented thermotropic LCPs, as illustrated in Fig. 1. The lateral

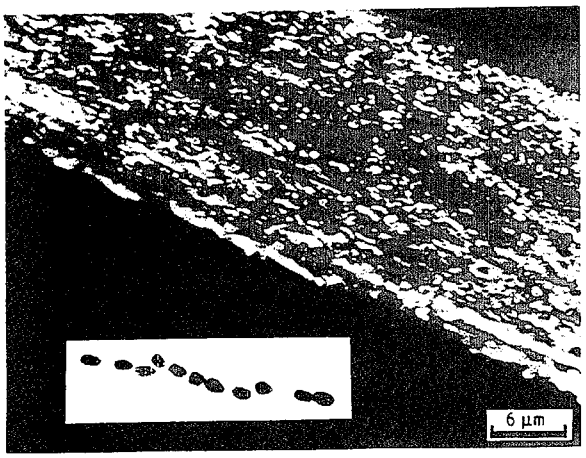

Figure 1 Polarized light micrograph, taken in the orthogonal view, of a thin section of a highly oriented Vectran tape showing domains elongated with the extrusion axis. The inset is a schematic drawing of the domains in the box suggesting they are a fibril meandering in and out of the plane of the section.

banded textures exhibited by some of the thermotropes and the pleated sheet textures exhibited by some of the aramids, as discussed above, are observed for those materials which have a poorer degree of molecular orientation. In fact, the more highly oriented thermotropic and lyotropic fibres do not exhibit these textures. For instance, in the case of the thermotropic copolyesters, the highly oriented heat-treated fibres do not exhibit any lateral banding. Likewise, Kevlar 149 exhibits higher modulus than Kevlar 49 [74], which is consistent for a material with increased crystallinity and crystallite size, and without a pleated sheet structure. The relationship of the domains to the fibrillar textures is also important. The inset in Fig. 1 is a magnified view of the polarized light micrograph of the Vectran tape on which is sketched the domains that appear to be aligned along the fibre axis. The schematic drawing shows that the worm-like domains consist of fibrils which meander in and out of the plane of the section, parallel to the director or fibre axis. The wall boundaries result, in part, from their homeotropic alignment.

3.2. Liquid crystal polymer fibrils

To interpret images obtained from new imaging techniques, similar materials must be explored using imaging methods that are well understood. Therefore, the LCPs were examined by SEM, FESEM and TEM for surface and bulk or internal detail prior to evaluation by STM. Representative complementary images are given in this paper and elsewhere [56, 57].

A fibrillar texture is observed for many LCPs including the thermotropes [38–40], aramids [6, 9, 38], and the "rigid-rod" polymers [25, 29, 31]. SEM images, acquired from Vectran fibres are presented in Fig. 2. The fibrils for less well oriented, large extrudates, can be highly woody in texture (Fig. 2a). A finer texture is exhibited for fibres with smaller micrometre-sized diameters (Fig. 2b, c). The peel-back technique clearly reveals the fibrillar nature of the fibre core (Fig. 2b, c). In contrast, the fibre surface tends to be smooth in texture (Fig. 2d). A common manifestation of this highly oriented texture is poor compressive properties, demonstrated by the kink bands in the SEM images acquired from the surface (Fig. 2d) and internal structure (Fig. 2e) of a fibre. The fracture mechanism in fatigue also reflects poor compressive properties [75–79]. Kink bands have been studied by Dobb *et al.* [79] for the aramids and a mechanism for their formation, consistent with tensile loss, was proposed. However, only conjecture has been made as to the primary cause of compressive failure. It is clear

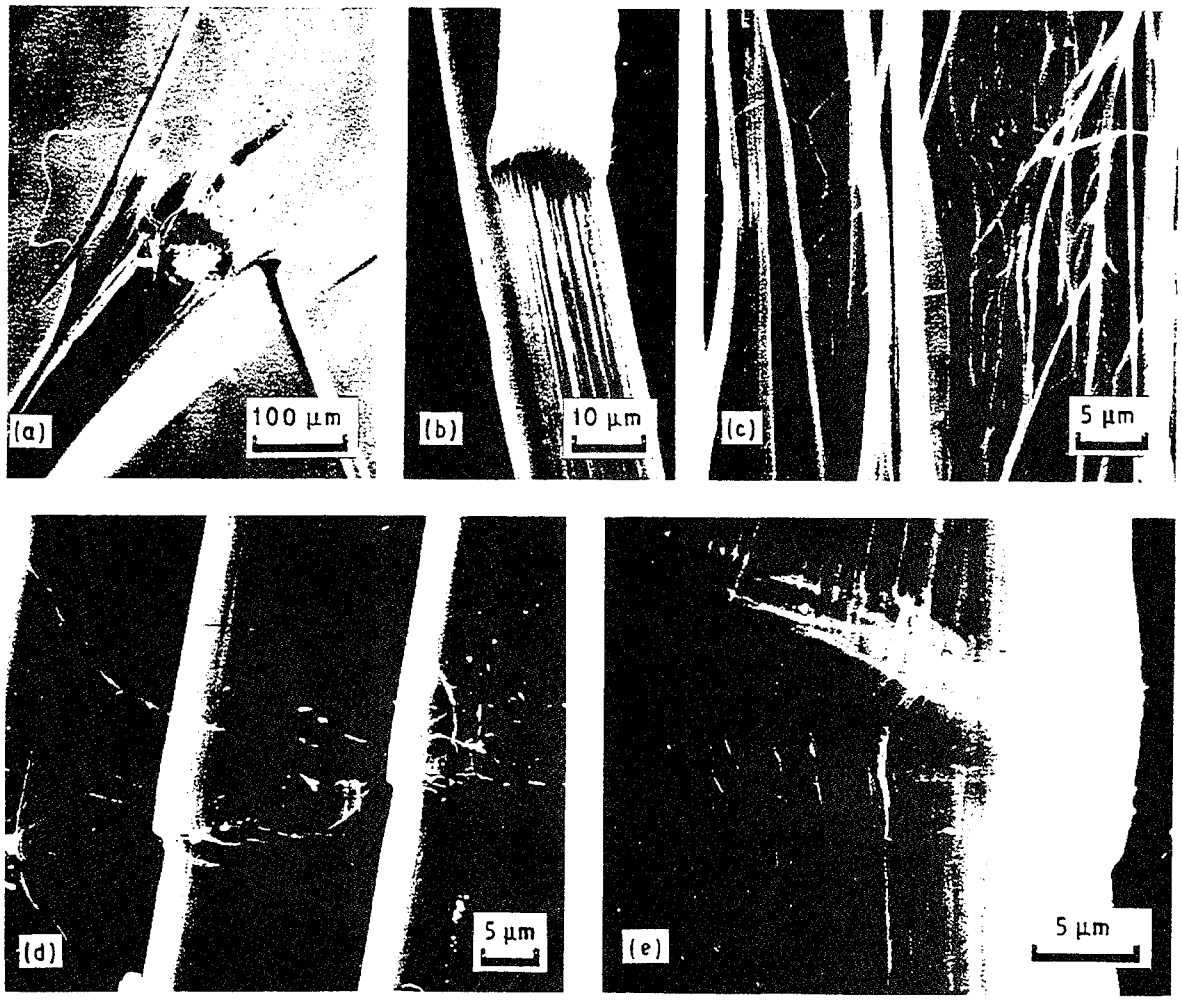

Figure 2 (a) Scanning electron micrographs reveal the woody nature of Vectra extrudates. (b, c) Images of peel back Vectran fibres show a fibrillar texture (d, e). The surface of the fibres is smooth with some discontinuities due to kink bands.

that kink bands are related to the deformation process but the size scale of its origin (fibre, fibril or microfibril) is uncertain. This topic will be discussed below.

FESEM images were acquired from highly oriented Vectran fibre which was peeled to reveal kinked regions (Fig. 3a). The highly ordered Vectran fibrillar structure also shows local deformation in the region of a kink band. A more ordered fibrillar organization is apparent for fibres after heat treatment (Fig. 3b) and for a Kevlar fibre (Fig. 3c) which also exhibits a fibrillar internal texture.

Peeled-back, highly oriented Vectran fibres and tapes were also imaged in the STM to explore details of the fibrillar and kink-band textures [56, 57]. Three-dimensional views are shown in the centre of Fig. 4a and b and top down views are shown in the lower right corners and in Fig. 4c and d. In the figure, the region scanned was 500 nm, along both the x and y axes, while the maximum z-axis range was about 50 nm. The organization of the fibrils and microfibrils is clearly detailed (Fig. 4) and local order can be compared to the typical bulk average order or orientation provided by X-ray analysis. The alignment of the microfibrils to the fibre axis is seen to be very good over all. Two types of local disorder are evident, however, especially in the top down views (Fig. 4c, d). The first type of disorder observed is the kink band in which there are clear discontinuities across the individual microfibrils (Fig. 4c, d) as well as damage to individual microfibrils (Fig. 4b, d). The STM images definitively revealed that damaged microfibrils are observed in shear bands which result from compressive damage and thus result in tensile strength loss. The second type of disorder observed is the "Y" shaped regions, where microfibril contours disappear beneath the surface (Fig. 4b). Although such structures were implied in the two-dimensional sections imaged by TEM (e.g. [35, 38]), the STM images provide important three-dimensional confirmation of microfibril organization. From STM images, direct measurements can be made of the fibril width and thickness. Therefore, their organization can be directly measured instead of inferring the third dimension from two-dimensional images.

Although X-ray analysis demonstrates a high average orientation for LCP materials, microanalysis imaging techniques reveal that the local order is not uniform. Further observations of microstructure may provide a better understanding of process histories and mechanical properties.

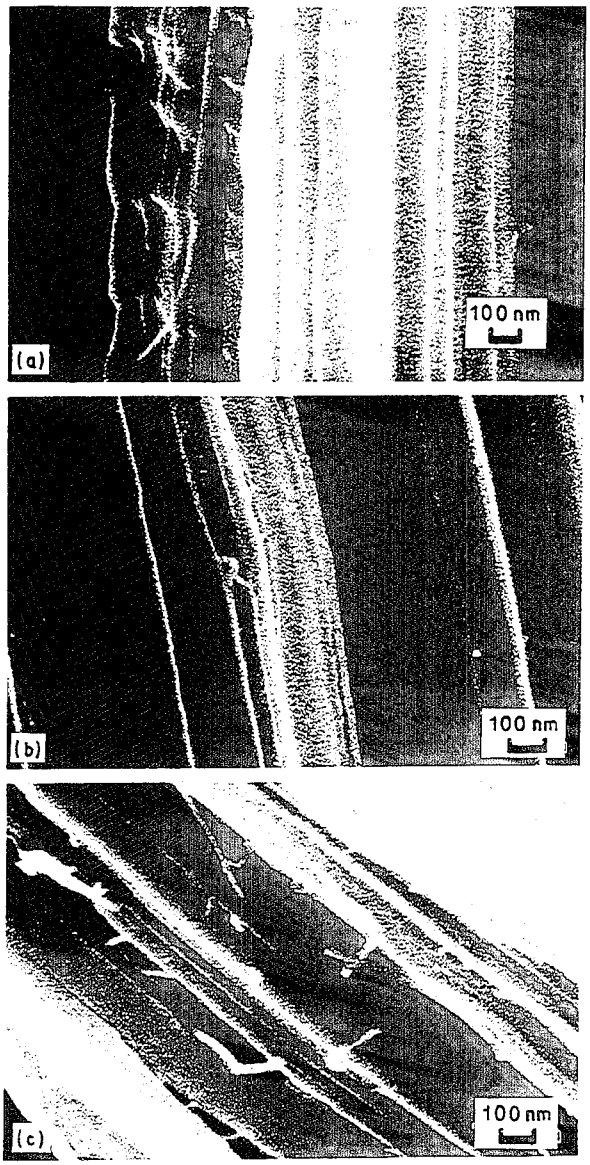

Figure 3 FESEM micrographs showing the internal texture in peeled-back highly oriented (a) Vectran as-spun, (b) Vectran heat-treated and (c) Kevlar fibres.

3.3 Microfibrillar textures in LCPs

The three-tiered fibrillar hierarchy is a well-accepted LCP model with predictive import [38–40]. The current work using new high-resolution instruments permitted the observation of all the various size scales in one imaging device and led to our reconsideration of the hierarchy. There has always been some question whether microfibrils originated because of deformation during sample preparation, or whether they are an original form of structure within the nematic domains in the melt. Additionally, a question remains regarding the interaction of microfibrils within the LCPs and the effect on mechanical properties. It is these issues that are being investigated once again in the present study.

The sonication procedure, originally developed by Dobb *et al.* [41], and adapted by us [38], was used to prepare samples of Kevlar, and various Vectran fibres and highly oriented tapes for TEM imaging. TEM images of the sonicated materials (Fig. 5) clearly show a range of fibrillar sizes resulting from this preparation method. The fibrils are very long and tend to fibrillate into ever smaller units. However, no clear interfibril tie fibrils were observed by the high-resolution imaging methods. Twisting of the microfibrils is clearly shown in the three-dimensional images and in TEM (Fig. 5a) where the twist in a tape-like fibril is reminiscent of cellulosic fibres. In Fig. 5b, Kevlar is shown to fibrillate into units less than 10 nm wide. Similar-sized microfibrils are also observed within these fibrils. Fibril width and/or thickness measurements were

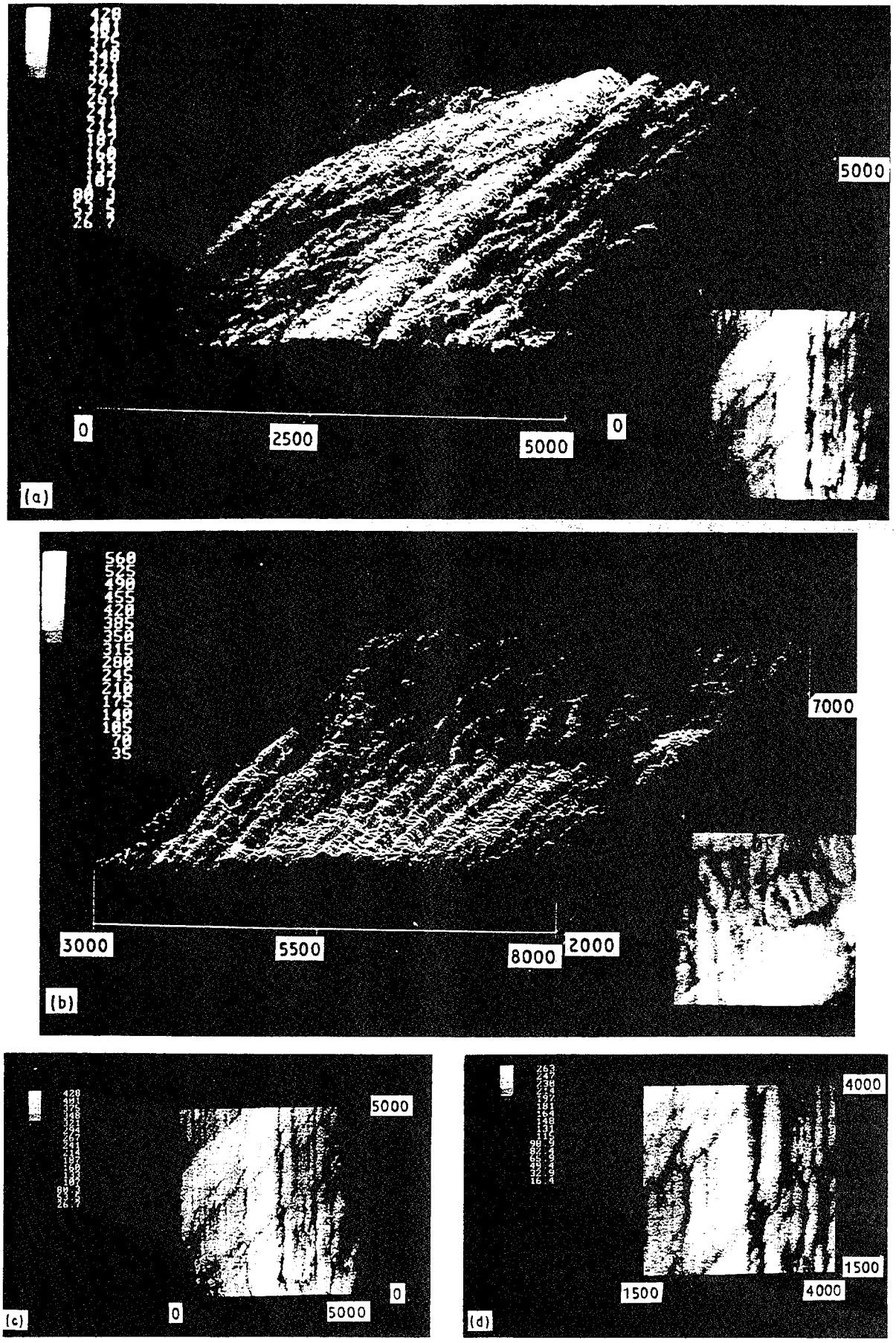

Figure 4 (a, b) STM micrographs of peel-back Vectran fibres in which fibre and microfibril orientation is vertical. Three-dimensional views (centre) accentuate z-height details; maximum z-height ($\sim$ 50 nm) divided into 15 grey levels. Top down views in lower right-hand corner (a, b) are shown in more detail in (c, d). Kink bands at an angle to the fibre axis are observed in all the images; individual broken microfibrils are observed in the region of the kink bands (b). Numerical values for scanned regions are in Ångstroms.

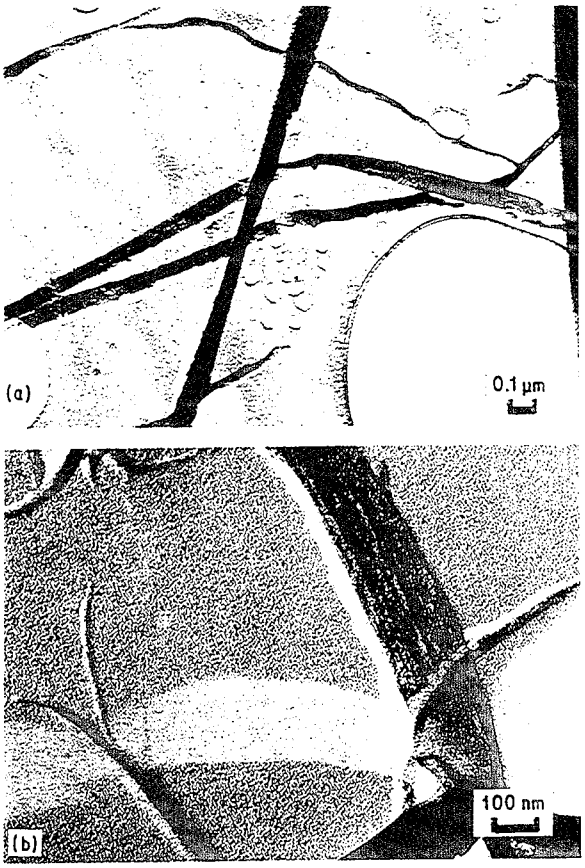

Figure 5 Transmission electron micrographs of sonicated fibrils of (a) Vectran and (b) Kevlar illustrating tape-like structure. Finer structures are observed to form due to fibrillation (a, b) but the fact that they are present within the larger fibrils (b) shows they exist within the spun fibres.

made using shadowing techniques [40] carefully controlling distances and angles in the vacuum evaporator. This tape-like structure is consistently observed in TEM studies of fibrils and microfibrils in all the LCPs studied.

Sonicated LCP samples were also imaged by STM to determine the dimensions of the smallest fibrils present in Vectran and Kevlar fibres with differing tensile modulus properties. In addition, evidence was sought related to the hierarchy and the genesis of the microfibrils. Early STM images, taken using the Nanoscope I, are shown in Fig. 6 [56] and recent STM images taken using the Nanoscope II are shown in Figs 7 and 8.

An overview of the sonicated fibrils (Fig. 6a) which shows large and small layered structures in three dimensions, looks remarkably similar to the TEM and FESEM views of the same sample. A more detailed view of the finer microfibrils in the Vectran sample (Fig. 6b) reveals two individual microfibrils. The width of the microfibrils is about 10 nm; the "thickness" (z height) of the microfibrils is about 3 nm. These measurements correspond to a tape-like structure, 3 nm by 10 nm, rather than a round fibrous shape.

STM images, taken with the Nanoscope II, of Vectran (Fig. 7) and Kevlar (Fig. 8) are more revealing. Each image series was acquired from the same area of the specimen, although smaller and smaller regions within each area were consecutively scanned, resulting in a series of images at successively higher magnifications. Fig. 7a and b show the nature of the coarser fibrils and reveals the microfibrils within these larger units. The microfibrils can be observed within the larger fibrils in the STM images acquired from both the as-spun Vectran (Fig. 7a) and heat-treated Vectran (Fig. 7b). Detailed views of the images in Fig. 7b are shown in more detail in Fig. 7c–e. A periodic texture is observed across a group of microfibrils arranged normal to the microfibril axis. It is very interesting to note that the periodicity of this texture is about 50 nm.

The series of STM images of Kevlar (Fig. 8) most clearly reveal the nature of the LCP hierarchy. Fig. 8a shows a bundle of uniform microfibrils, 10 nm wide within a larger aggregated fibrillar structure unit. The fine microfibrils can be observed more clearly in Fig. 8b–d. Finally, the on-line image analysis capability of the Nanoscope II permitted the measurement of the width and thickness of the smallest microfibrils (Fig. 8e). Many measurements were made of the finest microfibrils in Vectran and Kevlar fibres using this direct image measurement ability. The distribution of fibril width, thickness and the aspect ratio of width to thickness are shown in frequency histograms (Fig. 9) to reveal very similar dimensions for these very different fibre types, although the actual sizes are somewhat smaller for Kevlar than Vectran. Interestingly, the very smallest microfibril widths are on the order of 10 nm and the range is from 10–40 nm. The mean thickness of the microfibrils is about 3–5 nm and the smallest microfibrils are about 1 nm thick. It is clear from the measurements and the shape ratio considerations that the microfibrils are long and tape-like in shape as they are on the order of six to ten times as wide as they are thick.

3.5. LCP structure model

An extended structural model of the LCP hierarchy which is the culmination of these microscopy studies is presented in Fig. 10. This new model further elucidates the microfibrillar sizes and shapes first described in the earlier model [38–40] thereby providing a detailed description of the LCP structural features from the macromolecular to nanomolecular size scale. The model once again confirms the presence of a hierarchy, specific to the liquid crystalline polymers. The key microstructural element responsible for the properties of these thermotropic and lyotropic LCPs is the microfibril, the same microstructural unit basic to melt-spun and drawn flexible polymers. The tape-like shape of the microfibril and its size support the basic two-chain molecular organization that has been proposed by Ward and co-workers [61, 80] and Windle [81] in which the size of the smallest microfibrils are ~ 1 nm.

Important features of the original model that have been confirmed in the present work relate to the organization and size of the microfibrils. The orientation of the microfibrils and the bundles collected as

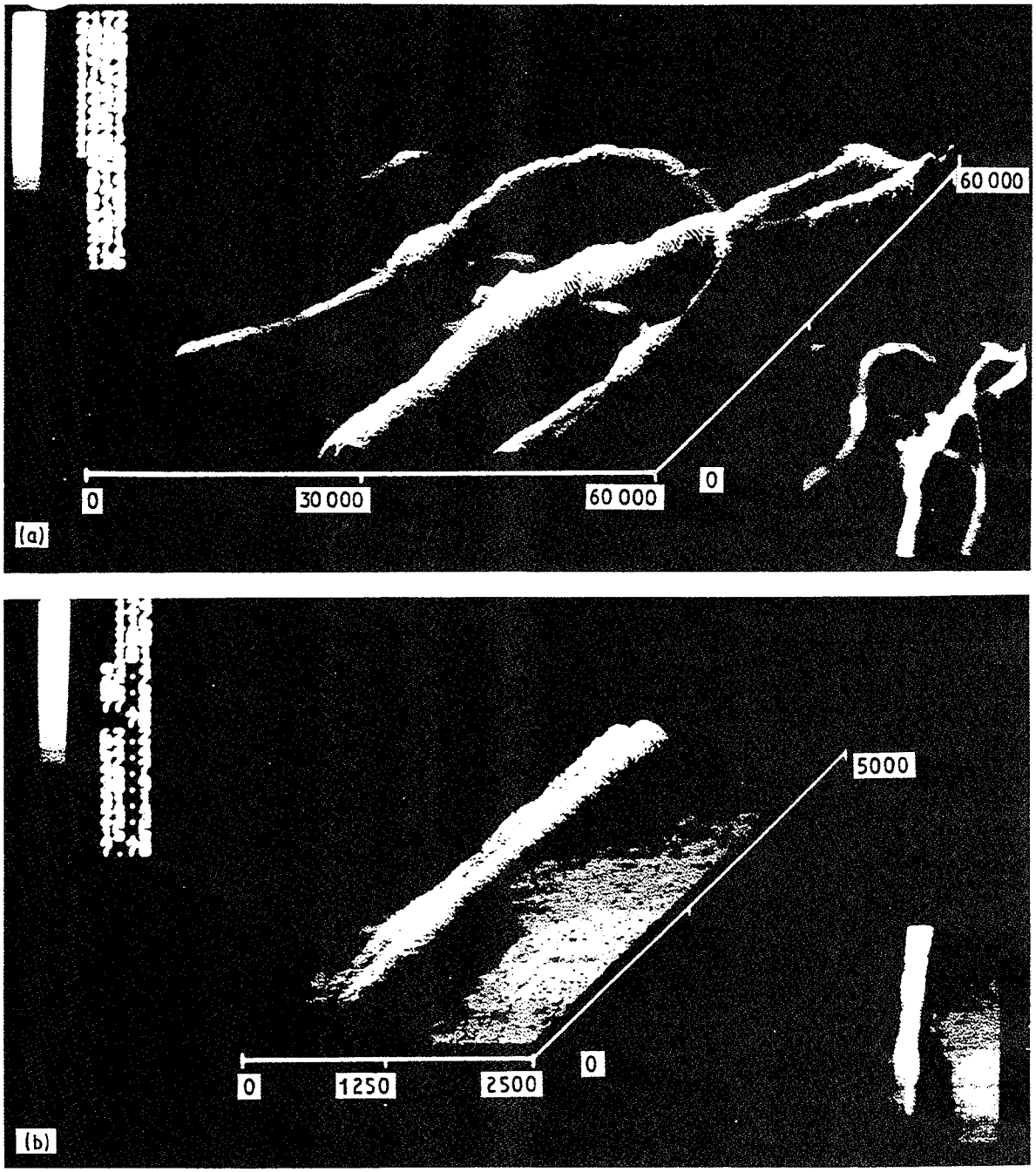

Figure 6 STM images of sonicated Vectran fibrils are observed in (a) a 6 μm × 6 μm overview image, and (b) in more detail in a 250 nm × 500 nm image. The detailed image (b) reveals two microfibrils ~ 10 nm wide and about 3 nm thick (z dimension). Numbers on the image are in Ångstroms.

fibrils is generally along the fibre or elongational axis. However, on a local scale it is clear that the microfibrils meander along the path of the director and are not best represented by a stick-like rigid-rod scheme, but rather are best characterized as worm-like in nature, somewhere between the random coil model of conventional polymers and the true rigid-rod structures. These worm-like microfibrils meander in and out of the plane of the director as shown by the "Y" shaped junctions in many of the images. The microfibrils are flat in shape and tend to layer readily without the need of tie fibrils. Although, there is a range of fibril and microfibril sizes, the smallest stable structures are shown in the model. A more complete discussion of the model and its implications is described below.

4. Discussion

In the last decade, major technological developments have occurred for the production of polymer fibres with high mechanical strength and stiffness. In concert with these efforts, studies have been directed towards a better understanding of the relationship between chemical composition, physical structure and mechanical properties. One goal is to develop a predictive structure–property model which can result in the development of improved marketable technologies.

For highly oriented thermotropic and lyotropic liquid crystalline fibres, there are a series of questions that must be answered to determine whether there is one consistent structural model. They are:

(a) What is the supramolecular nature of liquid crystalline polymers?

(b) Does a hierarchy of structures exist and what is its nature?

(c) Can such a hierarchy be generalized for both lyotropic and thermotropic liquid crystalline polymers?

(d) What is the three-dimensional size and shape of the microfibril?

(e) Does the size and/or the organization of the microfibril relate to the stiffness of the fibrous product?

Polarized light microscopy revealed domains of micrometre-sized structures in the thermotropic LCPs aligned along the fibre axis. The domains in the solid state were consistent with nematic domains thought to be discrete entities in the nematic melt or solution [11–13, 17–20, 23, 24]. The meander of the domains was shown (Fig. 1) to be consistent with their polarization colours. Fibrils pulled out of the same oriented specimen consisted of fibrils, oriented along the fibre axis, with the same width as the domains. Models have suggested that the organization is such that the domains consist of fibrils which are further composed of smaller microfibrils. The presence of domain walls appears to be consistent with the worm-like arrangement of the fibrils in and out of the plane of the section. This meander is further illustrated in the three-dimensional STM images. Highly aligned fibrils exhibit a shallow trajectory as they meander through highly oriented fibres and films. Thus the organization of the thermotropic LCPs appears to include microfibrils arranged within fibrils.

Sonicated fibres were presented in earlier TEM images [35, 38–40] ; however, the present study reveals for the first time that microfibrils definitely exist within the larger fibrillar units. The fibrils clearly pull apart and there is no indication of tie fibrils holding them together. Additionally, the shape of the fibrils and microfibrils appears to be flat or tape-like and some twisting of the fibrils is observed. The most definitive images, however, are those of sonicated Vectran and Kevlar fibrillar structures shown in the STM images (Figs 7 and 8). For the first time, all of the hierarchical structures are delineated clearly in the same region of the material. Large fibrils, ~ 0.5–1 μm across, are seen to consist of smaller and smaller microfibrils. Microfibrils about 10 nm across are shown to be well aligned within a larger fibril. Detailed images show that the smallest microfibrils range in size from 3–30 nm wide and from 2–5 nm thick. These numerical values suggest that the three-dimensional microfibril shape is tape-like. The image detail is of sufficient quality in the 1–10 nm range that histograms of the microfibrillar width and thickness provide comparison of the microfibril size for polymers of different compositions and heat treatments. Studies thus far suggest that the microfibril sizes and shapes are similar for lyotropic and thermotropic LCPs, as well as for as-spun and heat-treated fibres.

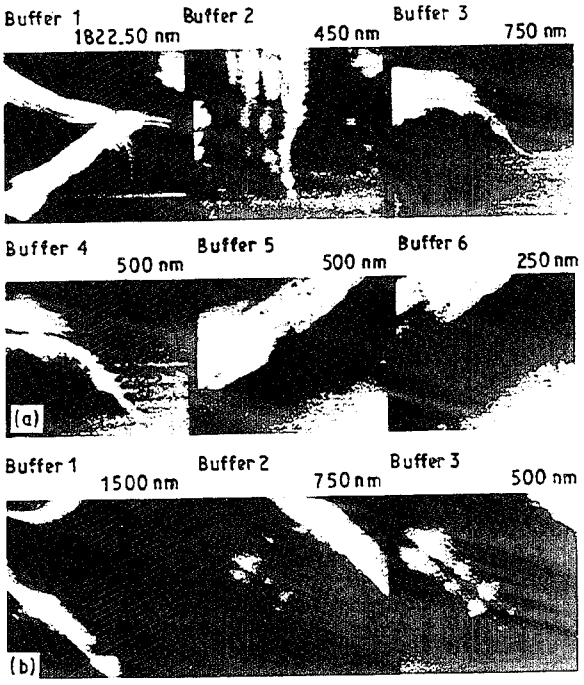

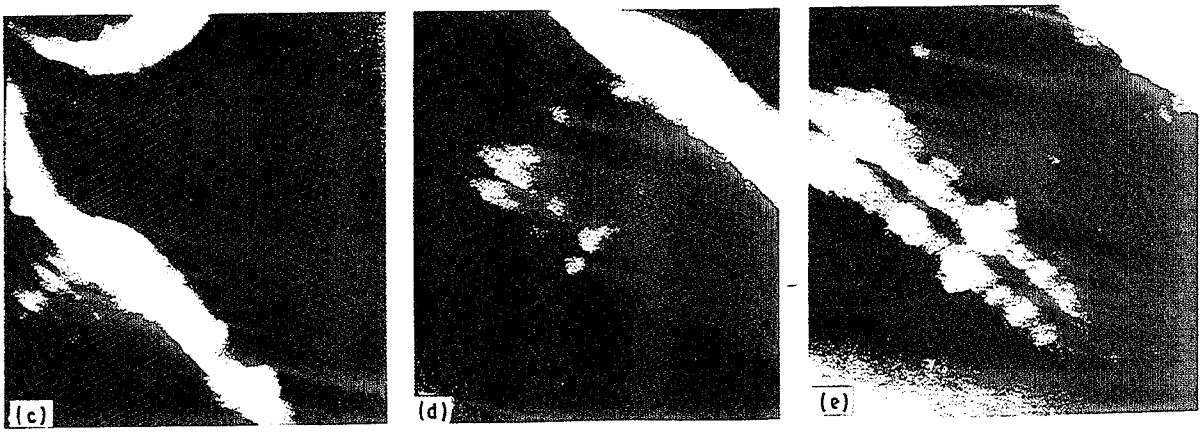

Figure 7 STM images of Vectran (a) as-spun and (b) heat-treated reveal a range of fibrillar sizes in images scanned at successively higher magnifications. The images in (b) are shown in more detail (c–e) to consist of finer microfibrils within larger fibrils. Lateral banded textures (c–e) reveal a 50 nm periodicity.

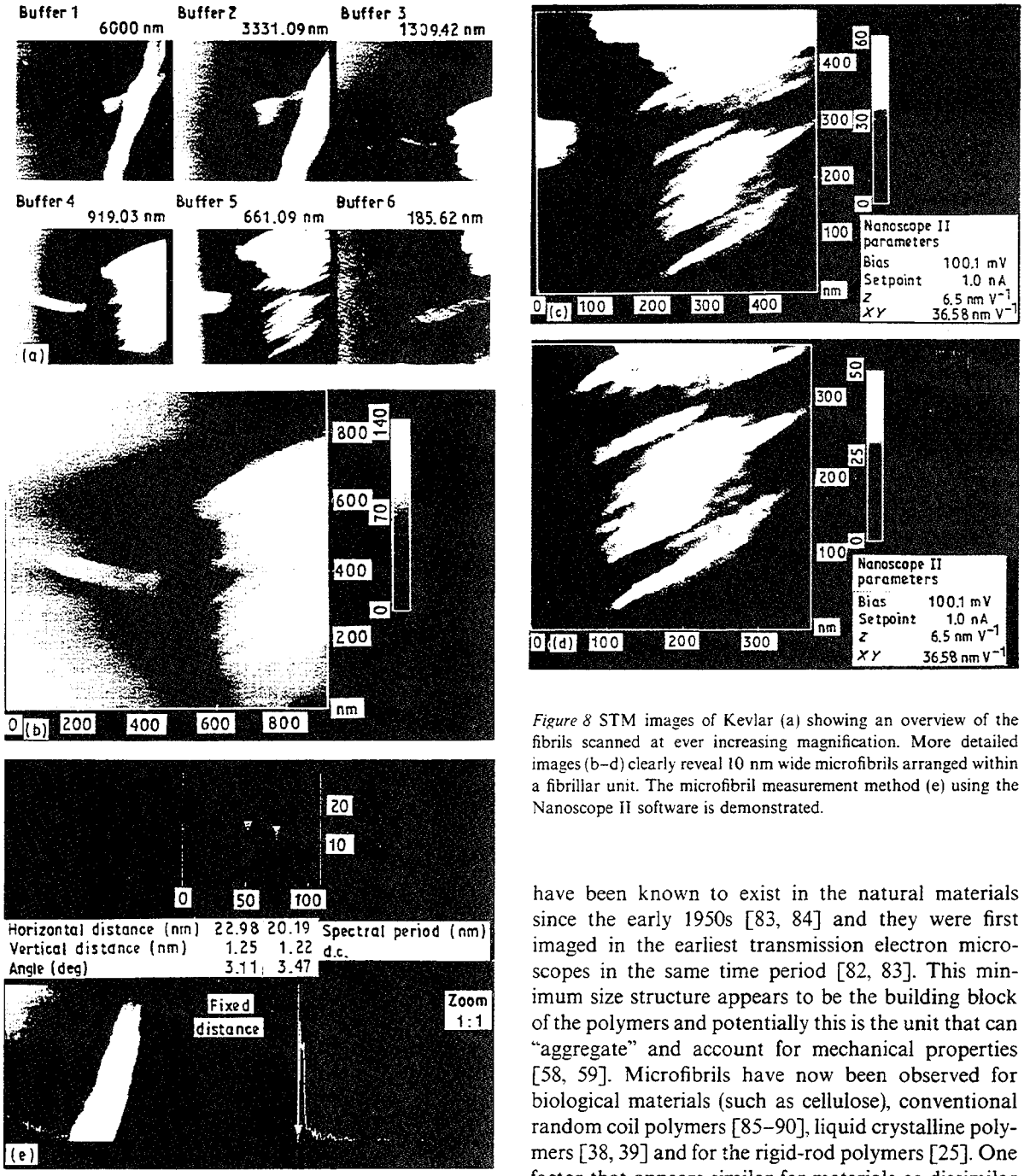

Figure 8 STM images of Kevlar (a) showing an overview of the fibrils scanned at ever increasing magnification. More detailed images (b–d) clearly reveal 10 nm wide microfibrils arranged within a fibrillar unit. The microfibril measurement method (e) using the Nanoscope II software is demonstrated.

Although the microfibrils and fibrils are, on average, oriented with the fibre axis, in agreement with X-ray diffraction studies (e.g., [25, 36, 48–55]), they are not perfectly uniform and oriented on a local scale. In fact, the STM, TEM and FESEM images obtained from the *in situ* structures suggest that the fibrils weave or meander in and out of the longitudinal plane and exhibit a worm-like trajectory rather than a "rigid-rod" structure, as generally portrayed for the nematic LCPs.

One general concept that has received much attention is the notion that the microfibril is the fundamental building block in polymers made from flexible linear molecules. A decade ago Sawyer and George [82] proposed a basic microfibrillar building block for both natural and synthetic materials. The microfibrils have been known to exist in the natural materials since the early 1950s [83, 84] and they were first imaged in the earliest transmission electron microscopes in the same time period [82, 83]. This minimum size structure appears to be the building block of the polymers and potentially this is the unit that can "aggregate" and account for mechanical properties [58, 59]. Microfibrils have now been observed for biological materials (such as cellulose), conventional random coil polymers [85–90], liquid crystalline polymers [38, 39] and for the rigid-rod polymers [25]. One factor that appears similar for materials as dissimilar as cellulose, polyesters, lyotropic aramids and thermotropic liquid crystalline polymers is that the general shape of the molecular chain is rather long compared to its width and thickness. Thus it is possible that the microfibril is simply a replication of the molecular chain. This replication, and the straightness of the chain, is dependent upon the specific chemical composition. The association of chains into microfibrils and the aggregation of microfibrils into fibrils suggests that the microfibril might be the smallest structure associated with mechanical properties.

The extended, worm-like nature of the microfibrils is consistent with the generally high orientation values calculated from X-ray diffraction results. However, these orientation values are very high and they do not exhibit significant variations even for fibres with quite different tensile modulus. Ward [80] has stated that

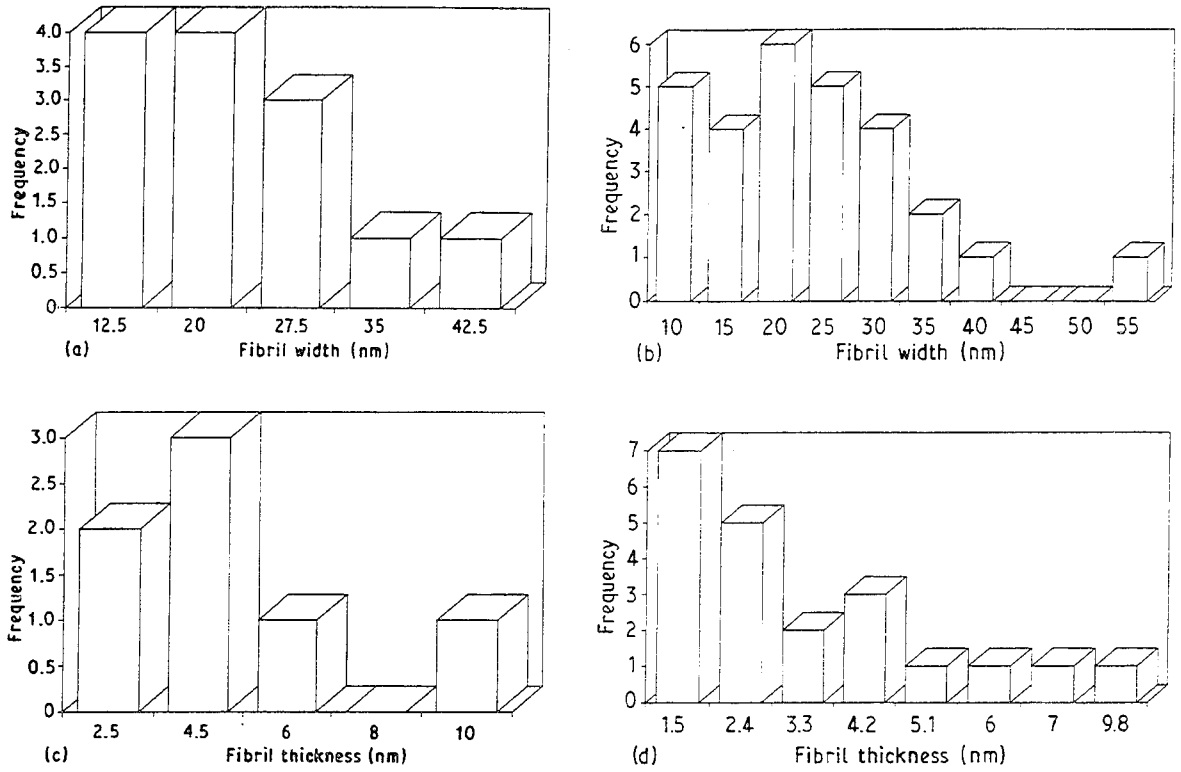

Figure 9 The distribution of the width and thickness of microfibrils in Vectran and Kevlar shown in histogram format; measurements were made directly from STM images. The mean of the fibril widths for (a) Vectran and (b) Kevlar are about 22 nm, with a standard deviation (breadth of the distribution) of about 10 nm. The mean of the fibril thickness for (c) Vectran and (d) Kevlar are about 5 and 3 nm, respectively, with standard deviations about 2.5 nm. Thus the thickness values are very similar, as are the fibril widths. The width to thickness ratios are about 6–8 for both fibre types.

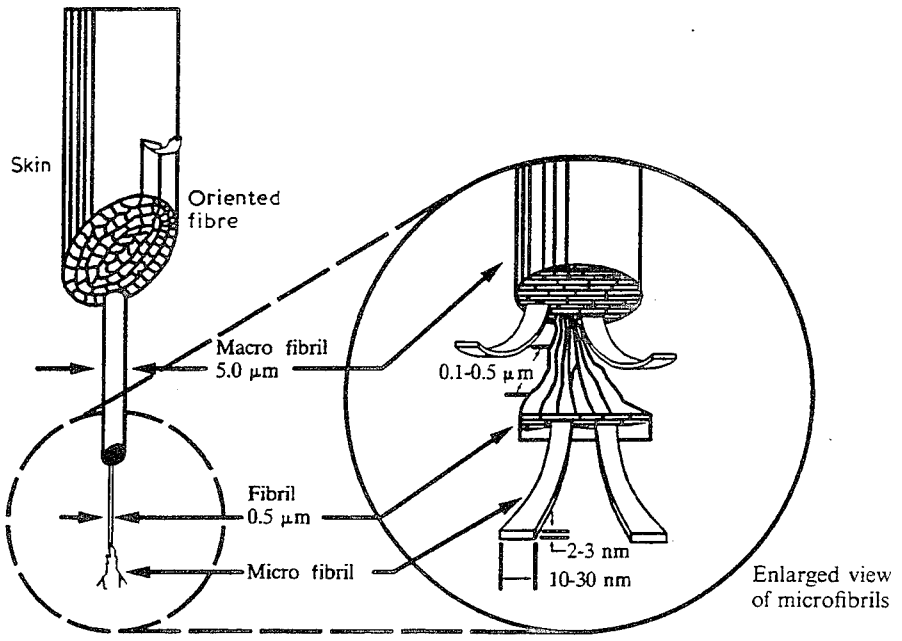

Figure 10 An expanded structural model is shown for the thermotropic and lyotropic LCPs, with more detail of the microfibril sizes, shapes and order.

X-ray diffraction does not provide the complete answer for understanding the tensile modulus properties of the LCPs. In the case of the aramids, with a true three-dimensional structure, the X-ray results, combined with the presence or absence of the pleated sheet structure, are consistent with lower and higher tensile modulus or stiffness values, respectively. In fact, the higher modulus-aramid variants exhibit about 80% –90% of theoretical tensile modulus values [74] when there is no pleated structure. Chain rigidity and strong intermolecular cohesive forces in the solid state, owing to hydrogen bonding [91] are responsible for these

properties. Thus the "straightness" of the extended-chain structure imposed by the chemical composition and the processing are related to the range of tensile moduli observed. It is interesting to note that two polymorphs have been observed for the aramids [92, 93] with the pseudo-orthorhombic structure exhibiting two chains per unit cell. This is similar to the work of both Ward and co-workers [61, 80] and Windle [81] who suggest the same two-chain structure for the thermotropes. In both cases, the size of the two-chain fundamental unit is $\sim$ 1 nm, the size of the smallest microfibril.

The final mechanical parameter of interest, although one which is known to be poor for these highly oriented materials, is compressive strength. Intuitively, low compressive strength seems consistent with a highly oriented texture, although the mechanism of compressive failure is not fully known. What is known is that kink bands form in the thermotropes and the aramids, as was shown in Figs 2 and 3. It has not been shown previously whether failure at these kink bands is macroscopic in natûre or occurs on a smaller scale. The figures in this study reveal, for the first time, that the early onset of compressive failure, associated with kink band formation, results in failure on the microfibril size (2–10 nm) scale. When a significant number of these microfibrils are severed the kink band must open up, resulting in failure. More work is needed to understand fully the stress transfer method implied by these observations, but the results strongly suggest that the mechanical building block is the microfibril and that they can fail individually.

Rigid-chain polymers, i.e. all LCPs, follow the aggregate model [2, 4, 58–61] whereas a composite model with tie molecules, crystalline bridges and long crystals is better for highly oriented flexible polymers such as polyethylene [80]. The high mechanical properties of the aramids are thought to be associated with chains in crystallographic registry, i.e. the persistence length of the molecular chain is greater than the average axial distance between the crystallites. The best mechanical properties are associated with aramids which do not exhibit the axially periodic defect layer. In a consistent manner, the thermotropes with the best mechanical properties do not exhibit the lateral banded texture, suggesting that better molecular chain registry is associated with improved properties. However, the lack of three-dimensional crystallographic registry in the Vectran fibres does not preclude similar overall properties compared to the aramids. Thus three-dimensional crystallinity, and the tie molecules associated with the extended-chain polyethylenes and aramids, are not required for high performance.

The question of interfibrillar stress transfer has not been fully resolved. There were five possible mechanisms proposed earlier [38] for interfibrillar stress transfer, of which only three now still appear to be possible and consistent with the current observations. The possible mechanisms appear to include:

1. A fibrillar network, as hypothesized by Allen *et al.* in PBZT [29] ;
2. Interfibrillar friction due to the tortuosity and proximity of fibrillar units, as hypothesized by Sawyer and Jaffe [38] ;
3. Interchain interactions–strong evidence points to chain slippage as the ultimate failure mechanism (see Yoon [37]).

The expanded structural model presented appears to be consistent with interactions among the microfibrils due to their tortuosity and proximity. These local interactions and the variation of the tortuosity or organization of the microfibrils among samples with different tensile properties is likely to be important in understanding the mechanism of mechanical property limitations. Further study is required to understand how the size and organization of the microfibrils and the entire hierarchy relate to the tensile strength and tensile modulus of these high-performance LCPs.

5. Conclusions

The conclusions of this work confirm and expand on those ideas in earlier papers by Sawyer and Jaffe [38, 39], and Sawyer *et al.* [40, 56, 57]. All LCPs studied to date are composed of the same fibrillar building blocks arranged in a hierarchy reminiscent of biological systems such as collagen and cellulose. The microfibrils are tape-like in shape and this is hypothesized to be due to a replication of the rod-like molecular chain. Comparison of the molecular and microfibrillar sizes suggest that the microfibrils are composed of a minimum of two molecules, in the smallest dimension, and thus they represent the finest nanostructural element in the LCPs. An extended LCP structural model, consisting of well-ordered, elongated fibrils, continues to be consistent with measured properties: high anisotropy, very high tensile modulus and tensile strength, and poor shear and compressive properties in the lateral dimension.

For the first time, evidence has been shown which suggests that the microfibril is the finest unit which mediates mechanical properties, including compressive strength and tensile modulus. A major conclusion of this work is that the sizes of the microfibrils appear similar for all the lyotropic and thermotropic LCPs studied. Thus, the microfibrillar sizes are not very different for fibres with different tensile strength values, such as before and after heat treatment, or for fibres with different tensile modulus values. However, the organization of the microfibrils does appear to differ with tensile modulus, as the higher degree of local order, improvements in lateral arrangement and orientation all reflect higher tensile modulus values. The nature of the nanostructural, microfibrillar units, meandering through otherwise highly oriented LCPs, is being used to understand further the origin of mechanical properties.

Questions remain regarding the nature of the transformations occurring during heat treatment and the nature of the tensile strength failure mechanism. In addition, the interfibrillar stress transfer mechanism is still not known.

Acknowledgements

The present work was initiated as a result of stimulating discussions and collaboration with Michael Jaffe and Larry Charbonneau of Hoechst Celanese. The study was made possible by the on-going collaboration between Hoechst Celanese and North Carolina State University. Extremely helpful discussions with Ian Ward (Leeds University), Alan Windle (Cambridge University) and colleagues in Hoechst Celanese, notably Michael Jaffe, Gerry Farrow and Hyun-Nam Yoon, are all gratefully acknowledged. The authors would like to acknowledge Howard Furst and Greg Nelson for computer generation of the model, the X-ray diffraction studies of Paul J. Harget and Cheng K. Saw and to thank Tom Bruno for the sample preparation. Finally, thanks to the management of Hoechst Celanese for support of our research. The support of Hoechst Celanese is gratefully acknowledged (I.H.M., P.E.R.) for their sponsorship as part of the NSF PYI program (P.E.R.), and to N.S.F for support (P.E.R., I.H.M.) under contract DMR-8657813.

References

1. G. CALUNDANN and M. JAFFE, in "Proceedings of The Robert A. Welch Conferences on Chemical Research XXVI", Synthetic Polymers, Houston, Texas, 15-17 November 1982, p. 247.
2. G. R. DAVIES and I. M. WARD, in "High Modulus Polymers", edited by A. Zachariades and R.S. Porter (Marcel Dekker, New York, 1988).
3. A. ZACHARIADES and R. S. PORTER (eds), "The Strength and Stiffness of Polymers" (Marcel Dekker, New York, 1983).
4. *Idem*, "High Modulus Polymers" (Marcel Dekker, New York, 1988).
5. A. CIFERRI, W. R. KRIGBAUM and R. B. MEYER (eds), "Polymer Liquid Crystals" (Academic Press, New York, 1982).
6. M. G. DOBB and J. E. MCINTYRE, in "Advances in Polymer Science 60/61" (Springer-Verlag, Berlin, 1984).
7. S. L. KWOLEK, US Pats 3600 350 (1971) and 3671 542 (1972).
8. H. BLADES, U S Pat. 3767 756 (1973).
9. M. PANAR, P. AVAKIAN, R. C. BLUME, K. H. GARDNER, T. D. GIERKE and H. H. YANG, *J. Polym. Sci. Polym. Phys. Ed.* **21** (1983) 1955.
10. M. JAFFE and R. S. JONES, in "High Technology Fibers", Part A, "Handbook of Fiber Science and Technology", Vol. III, edited by M. Lewin and J. Preston (Marcel Dekker, New York, 1985).
11. L. ONSAGER, *N.Y. Acad. Sci.* **51** (1949) 627.
12. A. ISIHARA, *J. Chem. Phys.* **19** (1951) 1142.
13. P. J. FLORY, *Proc. Roy. Soc.* **A234** (1956) 73.
14. *Idem*, in "Polymer Liquid Crystals", edited by A. Ciferri, W.R. Krigbaum and R.B. Meyer (Academic Press, New York, 1982).
15. Y. IDE and Z. OPHIR, *Polym. Engng Sci.* **23** (1983) 261.
16. Z. OPHIR and Y. IDE, *ibid.* **23** (1983) 792.
17. K. F. WISSBRUN, *Brit. Polym. J.* **12** (1980) 163.
18. *Idem*, *J. Rheol.* **25** (1981) 619.
19. K. F. WISSBRUN and A. C. GRIFFEN, *J. Polym. Sci. Polym. Phys. Ed.* **20** (1982) 1835.
20. C. P. WONG, H. OHNUMA and G. C. BERRY, *J. Polym. Sci. Polym. Symp.* **65** (1978) 173.
21. Z. TADMOR and C. G. GOGOS, "Principles of Polymer Processing" (Wiley Interscience, New York, 1979).
22. H. THAPAR and M. BEVIS, *J. Mater. Sci. Lett.* **2** (1983) 733.
23. K. F. WISSBRUN, *Farad. Discuss. Chem. Soc.* **79** (1985) 161.
24. K. F. WISSBRUN, G. KISS and F. N. COGSWELL, *Chem. Engng Commun.* **53** (1987) 149.
25. E. J. ROCHE, T. TAKAHASHI and E. L. THOMAS, in "Fiber Diffraction Methods", edited by A.D. French and K. H. Gardner, A. C. S. Symposium Series No. 141 (1980) p. 303.
26. J. R. SCHAEFGEN, T. I. BAIR, J. W. BALLOU, S. L. KWOLEK, P. W. MORGAN, M. PANAR and J. ZIMMERMAN, in "Ultra-high Modulus Polymers", edited by A. Ciferri and I. M. Ward (Applied Science, London, 1979) p. 173.
27. M. G. NORTHOLT, *Polymer* **21** (1980) 1199.
28. J. R. SCHAEFGEN, in "The Strength and Stiffness of Polymers", edited by A. Zachariades and R. S. Porter, (Marcel Dekker, New York, 1984) p. 327.
29. S. R. ALLEN, A. G. FILLIPPOV, R. J. FARRIS and E. L. THOMAS, *ibid.*, p. 357.
30. W. C. WOOTEN, Jr, F. E. McFARLANE, T. F. GRAY, Jr, and W. J. JACKSON Jr, in "Ultra-high Modulus Polymers", edited by A. Ciferri and I. M. Ward (Applied Science, London, 1979) p. 227.
31. E. J. ROCHE, R. S. STEIN and E. L. THOMAS, *J. Polym. Sci. Polym. Phys. Ed.* **18** (1980) 1145.
32. W. J. JACKSON Jr, and H. F. KUHFUSS, *J. Polym. Sci. Polym. Chem. Ed.* **14** (1976) 2043.
33. J. ECONOMY and W. VOLKSEN, in "The Strength and Stiffness of Polymers", edited by A. Zachariades and R. S. Porter (Marcel Dekker, New York, 1983) p. 293.
34. R. N. DeMARTINO, *J. Appl. Polym. Sci.* **28** (1983) 1805.
35. L. C. SAWYER, *J. Polym. Sci. Polym. Lett. Ed.* **22** (1984) 347.
36. J. B. STAMATOFF, *Molec. Cryst. Liq. Cryst.* **110** (1984) 75.
37. H. Y. YOON, *Colloid and Poly. Sci.* **268** (1990) 230.
38. L. C. SAWYER and M. JAFFE, *J. Mater. Sci.* **21** (1986) 1897.
39. *Idem*, in "High Performance Polymers", edited by E. Baer and A. Moet (Carl Hanser, Germany, 1991) p. 56.
40. L. C. SAWYER and D. T. GRUBB, "Polymer Microscopy" (Chapman and Hall, London, 1987).
41. M. G. DOBB, D. J. JOHNSON and B. P. SAVILLE, *J. Polym. Sci. Polymer Symp.* **58** (1977) 237.
42. *Idem*, *J. Polym. Sci.* **15** (1977) 2201.
43. M. G. DOBB, A. M. HENDELEH, D. J. JOHNSON and B. P. SAVILLE, *Nature* **253** (1975) 189.
44. S. C. BENNETT, M. G. DOBB, D. J. JOHNSON, R. MURRAY and B. P. SAVILLE, in "Proceedings EMAG 75" (Academic Press, Bristol, London, 1976) p.329.
45. M. G. DOBB, D. J. JOHNSON and B. P. SAVILLE, *Polymer* **22** (1981) 961.
46. R. HAGEGE, M. JARRIN and M. J. SOTTON, *J. Microsc.* **115** (1979) 65.
47. T. WENG, A. HILTNER and E. BAER, *J. Mater. Sci.* **21** (1986) 744.
48. C. VINEY, A. M. DONALD and A. H. WINDLE, *ibid.* **18** (1983) 1136.
49. A. M. DONALD and A. H. WINDLE, *ibid.* **18** (1983) 1143.
50. A. M. DONALD, *Phil. Mag.* **A47** (1983) L13.
51. A. M. DONALD and A. H. WINDLE, *J. Mater. Sci. Lett.* **4** (1985) 58.
52. *Idem*, *Polymer* **25** (1984) 1235.
53. A. ANWER, R. J. SPONTAK and A. H. WINDLE, *J. Mater. Sci. Lett.* **9** (1990) 935.
54. A. H. WINDLE, C. VINEY, R. GOLOMBOK and G. R. MITCHELL, *Farad. Discuss. Chem. Soc.* **79** (1985) 55.
55. G. A. GUTIERREZ, R. A. CHIVERS, J. BLACKWELL, J. B. STAMATOFF and H. N. YOON, *Polymer* **24** (1983) 937.
56. I. H. MUSSELMAN, P. E. RUSSELL, R. T. CHEN, M. G. JAMIESON and L. C. SAWYER, in "Proceedings of the XIIth International Congress for Electron Microscopy", Seattle, August 1990, edited by W. Bailey (San Francisco Press, San Francisco, 1990) p. 866.
57. L. C. SAWYER, R. T. CHEN, M. JAMIESON, I. H. MUSSELMAN and P. E. RUSSELL, *J. Mater. Sci. Lett.* **11** (1992) 69.
58. M. J. TROUGHTEN, A. P. UNWIN, G. R. DAVIES and I. M. WARD, *Polymer* **29** (1988) 1389.
59. D. I. GREEN, A. P. UNWIN, G. R. DAVIES and I. M. WARD, *ibid.* **31** (1990) 579.
60. D. I. GREEN, G. R. DAVIES, I. M. WARD, M. H. ALHAJMOHAMMED and S. ABSUL JOWAD, *Polym. Adv. Technol.* **1** (1990) 41.

61. R. A. ALLEN and I. M. WARD, *Polymer* **32** (1991) 203.
62. A. CIFERRI and B. VALENTI, in "Ultra-high Modulus Polymers" edited by A. Ciferri and I.M. Ward (Applied Science, London, 1979) p. 1.
63. D. J. BLUNDELL, *Polymer* **23** (1982) 359.
64. L. C. SAWYER, in "Proceedings of the 39th Annual Meeting of the EMSA", edited by G.W. Bailey (Claitors, Baton Rouge, 1981) p. 334.
65. I. H. MUSSELMAN and P. E. RUSSELL, in "Microbeam Analysis" edited by P. E. Russell, (San Francisco Press, San Francisco, CA, 1989) p. 535.
66. M. R. MACKLEY, F. PINAUD and G. SIEKMANN, *Polymer* **22** (1981) 437.
67. D. J. GRAZIANO and M. R. MACKLEY, *Molec. Cryst. Liq. Cryst.* **106** (1984) 73.
68. T. ASADA, in "Polymer Liquid Crystals", edited by A. Ciferri, W. R. Krigbaum, and R. B. Meyer (Academic Press, New York, 1982) p. 247.
69. P. G. de GENNES, "The Physics of Liquid Crystals" (Oxford University Press, 1979).
70. D. DEMUS and L. RICHTER, "Textures of Liquid Crystals" (Verlag Chemie, New York, 1978).
71. A. ZACHARIADES, P. NAVARD and J. A. LOGAN, *Molec. Cryst. Liq. Cryst.* **110** (1984) 93.
72. A. M. DONALD and A. H. WINDLE, *Coll. Polym. Sci.* **261** (1983) 793.
73. *Idem, J. Mater. Sci.* **19** (1984) 2085.
74. S. J. KRAUSE, D. L. VEZIE and W. W. ADAMS, *Polym. Commun.* **30** (1989) 10.
75. C. O. PRUNEDA, R. J. MORGAN, F. M. KONG, J. A. HODSON, R. P. KERSHAW and A. W. CASEY, in "Proceedings of the 29th National SAMPE Symposium", (1984) p. 1213.
76. J. H. GREENWOOD and P. G. ROSE, *J. Mater. Sci.* **9** (1974) 1804.
77. A. R. BUNSELL, *ibid.* **10** (1975) 1300.
78. M. H. LAFITE and A. R. BUNSELL, *ibid.* **17** (1982) 2391.
79. M. G. DOBB, D. J. JOHNSON and B. P. SAVILLE, *Polymer* **22** (1981) 1960.
80. I. M. WARD, private discussions.
81. A. H. WINDLE, private discussions.
82. L. H. SAWYER and W. GEORGE, in "Cellulose and Other Natural Polymer Systems: Biogensis, Structure, and Degradation", edited by R. Malcolm Brown Jr, (Plenum, New York, 1982) p. 429.
83. E. BAER and A. MOET (eds), "High Performance Polymers" (Hanser, New York, 1991).
84. A. FREY-WYSSLING, *Science* **119** (1954) 80.
85. A. PETERLIN, *J. Mater. Sci.* **6** (1971) 490.
86. *Idem, Polym. Engng Sci.* **18** (1978) 277.
87. *Idem*, in "Ultra-high Modulus Polymers", edited by A. Ciferri and I.M. Ward (Applied Science, London, 1979) p. 279.
88. B. KALB and A. J. PENNINGS, *J. Mater. Sci.* **15** (1980) 2584.
89. J. SMOOK, M. FLINTEMAN and A. J. PENNINGS, *Polym. Bull.* **2** (1980) 775.
90. *Idem, J. Mater. Sci.* **19** (1984) 31.
91. S. KWOLEK, W. MEMGER and J. E. VAN TROMP, in "International Symposium on Polymers for Advanced Technology", edited by M. Lewin, (International Union of Pure and Applied Chemistry, 1987) p. 421.
92. M. G. NORTHOLT, *Eur. Polym. J.* **10** (1974) 799.
93. K. HARAGUCHI, T. KAJIYAMA and M. TAKAYANAGI, *J. Appl. Polym. Sci.* **23** (1979) 915.

Received 3 February
and accepted 17 February 1992

INDEX
AUTHORS